Source, facies, and sedimentary environments of the Middle to Upper Jurassic strata in the Kerman and Tabas areas, east-central Iran

Dissertation zur Erlangung des
Naturwissenschaftlichen Doktorgrades
der Bayerischen Julius-Maximilians-Universität Würzburg

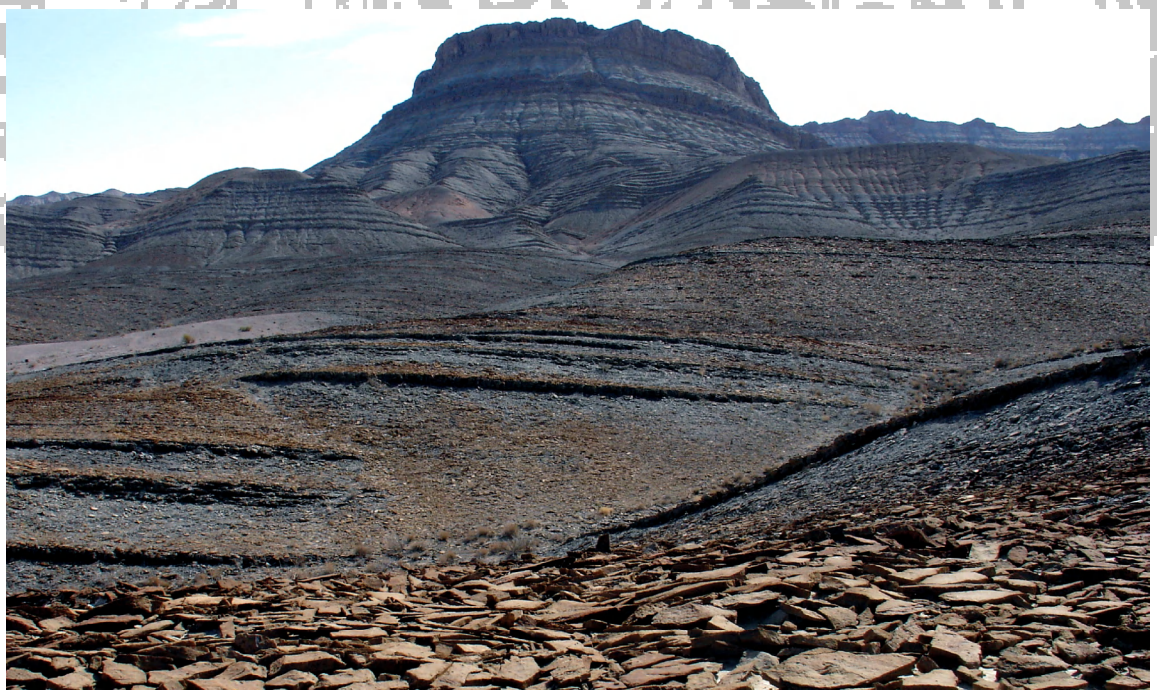

Vorgelegt von
Masoud Zamani Pedram
aus
Tehran in Iran

Würzburg 2011

Eingereicht am: ……

1. Gutachter: Prof. Dr. F. T. FÜRSICH

2. Gutachter der Dissertation: Prof. Dr. M. WILMSEN

1. Prüfer: Prof. Dr. F. T. Fürsich……

2. Prüfer: Prof. Dr. H. De Wall ……

der mündlichen Prüfung

Tag der mündlichen Prüfung: ……..

Doktorurkunde ausgehändigt am: ……

Contents

1 INTRODUCTION

Middle to Upper Jurassic rocks are widely distributed and superbly exposed on the western Tabas Block of the central-east Iranian Microplate (CEIM). Based on AGHANABATI (1977, 1998), the Upper Triassic-Jurassic succession can be subdivided into a numbers of formations, which can be combined into two groups separated by unconformities related to tectonic events. The Shemshak Group is intercalated between the Early and the Mid Cimmerian tectonic event (see also FÜRSICH et al. 2009) and the Magu Group is sandwiched between the Mid to Late Cimmerian tectonic event. In the new lithostratigraphic scheme of WILMSEN et al. (2003, 2009), the Magu Group in the northern part of the Tabas Block is subdivided into three subgroups, i.e. the Baghamshah, Esfandiar and Garedu subgroups. In the Zarand-Kerman area, the Magu Group laterally turns into the Bidou Formation. Earlier on, HUBER & STÖCKLIN (1954) had introduced the Bidou Series for the Middle-Upper Jurassic rocks north of Kerman, close to the Hojedk Coal Mine. According to SEYED-EMAMI (1999), the Bidou Series is composed of the Bidou Formation (Bathonian-Callovian), Pectinid Limestone (Upper Callovian to Oxfordian and Kimmeridgian) and Ravar Formation (Kimmeridgian and probably Tithonian). He suggested to use the Bidou Group just for the non-separated Bidou Series. AGHANABATI (2004, 257) believed the Bidou Group ("Bidou Series") to be equivalent of the Magu Group (see also WILMSEN et al. 2009). The aim of this study is to analyse the facies and to reconstruct the palaeoenvironments of the Middle to Upper Jurassic strata (Magu Group and Bidou Formation) of the western and southern Tabas Block, combining sedimentary petrography, sedimentology, lithostratigraphy, trace fossils, macrofossil and heavy mineral analysis in order to trace the evolution of the sedimentary basin and to elucidate any synsedimentary tectonic events. This approach is used to test the hypothesis that during the Jurassic, the Tabas Block was a tilted fault block, more or less in its present position between the neighbouring Yazd and Lut blocks and adjacent to the Neotethys. Previous studies of the Middle to Upper Jurassic strata were mainly concerned with mapping (e.g., HUCKRIEDE et al. 1962; STÖCKLIN et al. 1965; RUTTNER et al. 1968; SAHANDI et al. 1990; HAJ MOLA ALI 1995; VAHDATI 1995; SHAIKHOLESLAMI, M.R. 1999; KARIMI-BAVANDPUR et al. 2002; AZHDARI 2004). During last few years, some papers on the lithostratigraphy attempted to improve and define more precisely a number of formations of the Magu Group mainly on the northern Tabas Block (Qaleh Dokhtar Formation: SCHAIRER et al. 2000, FÜRSICH et al. 2003a; Kamar-e-Mehdi Formation: WILMSEN et al. 2003, 2009; Korond Formation:

SCHAIRER et al. 2003; Sikhor Formation: FÜRSICH et al. 2003b; general review of the Middle Jurassic lithostratigraphy of Iran: SEYED-EMAMI et al. 2001; new evidence on the lithostratigraphy of the Jurassic system on the northern Tabas Block: SEYED-EMAMI et al. 2005).

2 METHODS AND MATERIAL

Nine sections of the Middle to Upper Jurassic strata were measured bed-by-bed in the western and southern Tabas Block (Fig. 1) using a modified Jacob Staff (SDZUY & MONNINGER, 1985). Over 400 outcrop samples were collected. Siliciclastic rocks were studied by petrographically evaluating mineral composition, texture and diagenetic characteristics (see Chapter 9). The textural maturity was determined by the grain shape (TUCKER 1981), roundness of sediment grains (PETTIJOHN et al. 1987; TUCKER 1991), and the degree of sorting (FOLK 1951; COMPTON 1962). Siliciclastic arenaceous rocks were classified according to composition (PETTIJOHN et al. 1987). For determination of the grain-size, the scheme of WENTWORTH (1922) was used. Several samples were collected to determine the heavy mineral composition as index of the composition of rocks in the source area (BOSWELL 1933). Detrital heavy minerals were studied under a polarized (MANGE & MAURER 1992) and binocular microscope (DEVISMES 1978). Several samples of fine-grained siliciclastic rocks (marl, mudstones and shales) were taken in order to analyse the clay-mineral assemblages. The study of clay-mineral assemblages was carried out by means of X-ray diffraction (XRD) analysis. To characterize carbonate rocks based on their depositional, biogenic or diagenetic texture, the classification schemes of DUNHAM (1962), EMBRY & KLOVAN (1972), and Khosro-Tehrani (2007) were used. To describe skeletal and non-skeletal particles in thin-sections, ADAMS et al. (1984), ADAMS & MACKENZIE (1998), and FLÜGEL (2004) were used. The benthic macrofauna was identified by HOLZAPFEL, 1998, FÜRSICH (pers. comm. 2007). Determination of trace fossils was based, for example, on FÜRSICH (1974), HÄNTZSCHEL (1975), and FREY (1975). The rich literature on sedimentary structures (e.g. REINECK & SINGH 1973; POTTER & PETTIJOHN 1977; ALLEN 1984; STOW 2005) has been applied in the field.

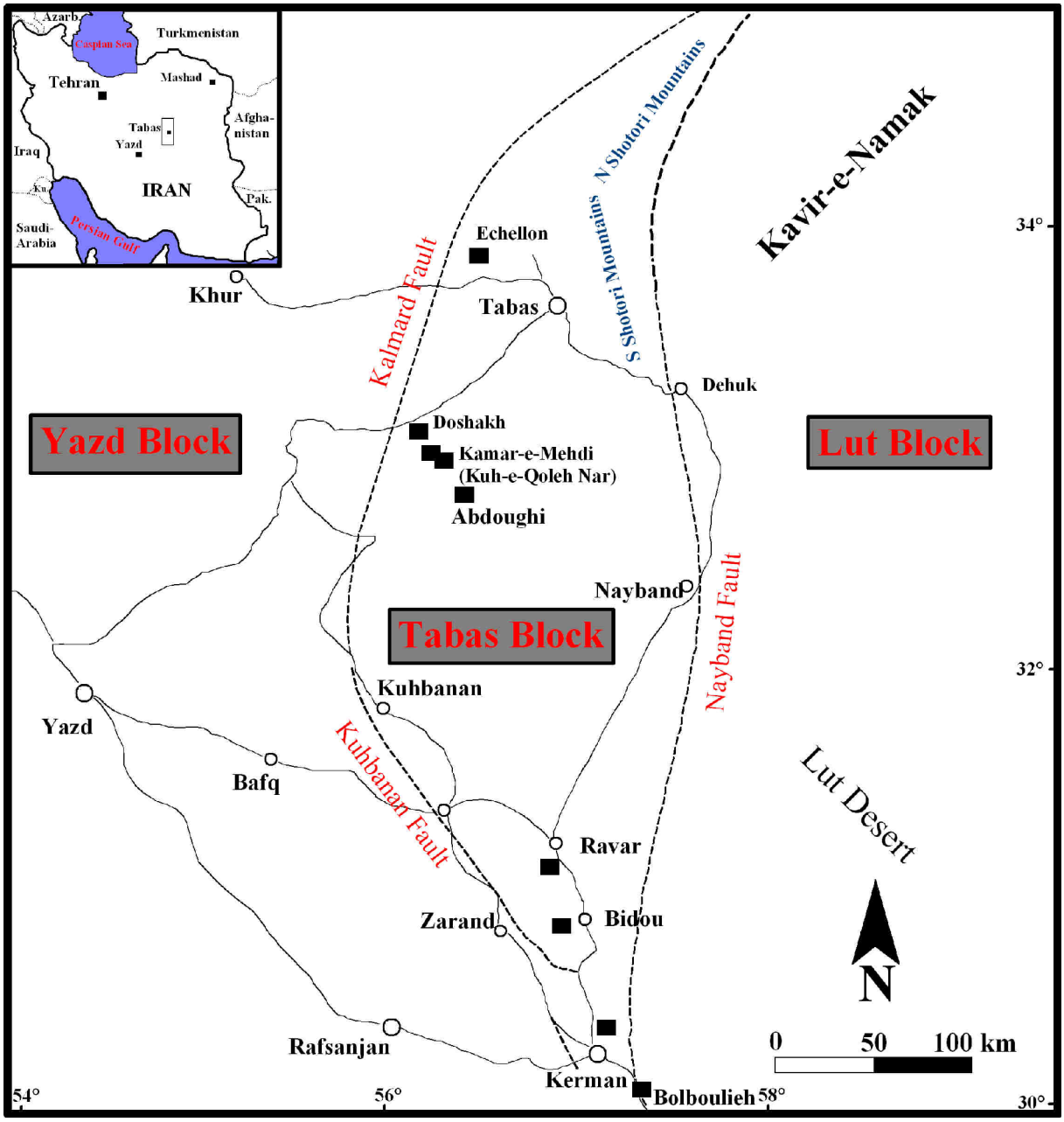

Fig. 2.1. Locality map of measured sections indicated by black squares and major structural units (blocks and block-bounding faults) of east-central Iran.

3 GEOLOGICAL SETTING

The concept of a distinct fault-bounded Central-East Iranian Microcontinent, which consists of three major crustal domains: the Lut Block, Tabas Block and the Yazd Block (e.g., ALAVI 1991; FÜRSICH et al. 2009), was first introduced by TAKIN (1972; Fig. 2). These blocks, now adjoined from east (Lut Block) to west (Yazd Block), are separated by a series of intersecting regional-scale faults. Each block features a particular overall deformation style and pattern of Recent seismicity, distinguishable from those in the adjacent domains (BERBERIAN 1981). The overall uniformity of the Eocambrian (Late Neo-Proterozoic) and Palaeozoic platform strata that covered the Zagros, Central Iran and the Main Alborz provinces led to the predominant notion that all these regions were once part of the undivided Palaeozoic Arabian-Iranian platform of Gondwanaland (STÖCKLIN 1968, 1974). The Iran Plate as a part of the Cimmerian continent collage collided with the Turan Plate during the Late Triassic (Early Cimmerian Orogeny), either at the Ladinian-Carnian boundary (SAIDI et al. 1997) or around the Carnian-Norian boundary (SEYED-EMAMI 1971a, b; SENGÖR 1990; ALAVI et al. 1997). The development and evolution of Late Triassic-Jurassic sedimentary basins of east-central Iran was largely governed by the Late Triassic collision of the Lut, Tabas, and Yazd blocks, parts of the Cimmerian microplate assemblage (SENGÖR et al. 1988; SENGÖR 1990), with the Turan Plate (Eurasia) and by subsequent rotational movements of the three blocks of about 135° with respect to Eurasia (e.g., SOFFEL & FORSTER 1984; ALAVI et al. 1997). The thick post-collisional molasse sedimentation of the Upper Triassic to Lower Middle Jurassic Shemshak Group and its widespread occurrence across the Cimmerian Continent indicates that during this time it represented a coherent tectonic unit (WILMSEN et al. 2003). Based on FÜRSICH et al. (2003), the Shemshak Group (Norian-Lower Bajocian) consists of sediments eroding from the rising Cimmerian mountains in the area of the present-day Caspian sea (AGHANABATI 1998; SEYED-EMAMI et al. 2001). These sediments are widespread throughout central and northern Iran, but accumulated in different basins ranging from remnant basins of the Palaeotethys to foreland basins, and rift basins. The lower part of the Shemshak Group corresponds to Cimmerian flysch and molasse deposits, the upper part to the fill of an extensional basin (FÜRSICH et al. 2009). According to SEYED-EMAMI & ALAVI-NAINI (1990), facies differentiation and differential subsidence in several sedimentary and structural units such as the Lut, Tabas, and Yazd blocks, took place in connection with the Mid-Cimmerian tectonic movements in the mid-Bajocian. FÜRSICH et al. (2003) related the extensive anticlockwise rotational movements, which took place during the Jurassic-Tertiary

(e.g., SOFFEL & FÖRSTER 1984), with extensive strike-slip faults between the blocks. This complex tectonic regime largely governed the Middle to Upper Jurassic sedimentation pattern of the Magu Group in the northern part or of equivalent rocks, the Bidou Formation, in the southern part of the Tabas Block. According to FÜRSICH et al. (2003a) the Bajocian Mid-Cimmerian tectonic movements were followed, in the Bathonian to Callovian, by rapid subsidence and the deposition of the thick and uniform silty to sandy shelf sequence of the Baghamshah Formation. Renewed tectonic activities in the (Early) Callovian caused uplift, erosion and progradation at the base of the Callovian-Oxfordian/Kimmeridgian Kamar-e-Mehdi Formation and in the Late Oxfordian-Late Kimmeridgian/Tithonian siliciclastic-evaporatic rocks of the Garedu Group on the northern Tabas Block (see also SEYED-EMAMI et al. 2005). On the western and southern Tabas Block (Tabas-Kerman area), evidence of these tectonic movements can be observed at the base of the Kamare-e-Mehdi, and Magu Gypsum formations and in equivalent rocks of the Bidou Formation (Mixed Siliciclastic-Carbonate Member: Middle Callovian to Lower Kimmeridgian) and the Upper Siliciclastic Member (Upper Kimmeridgian to Upper Berriasian-?Valanginian). The latter member terminates the depositional cycle of the Bidou Formation.

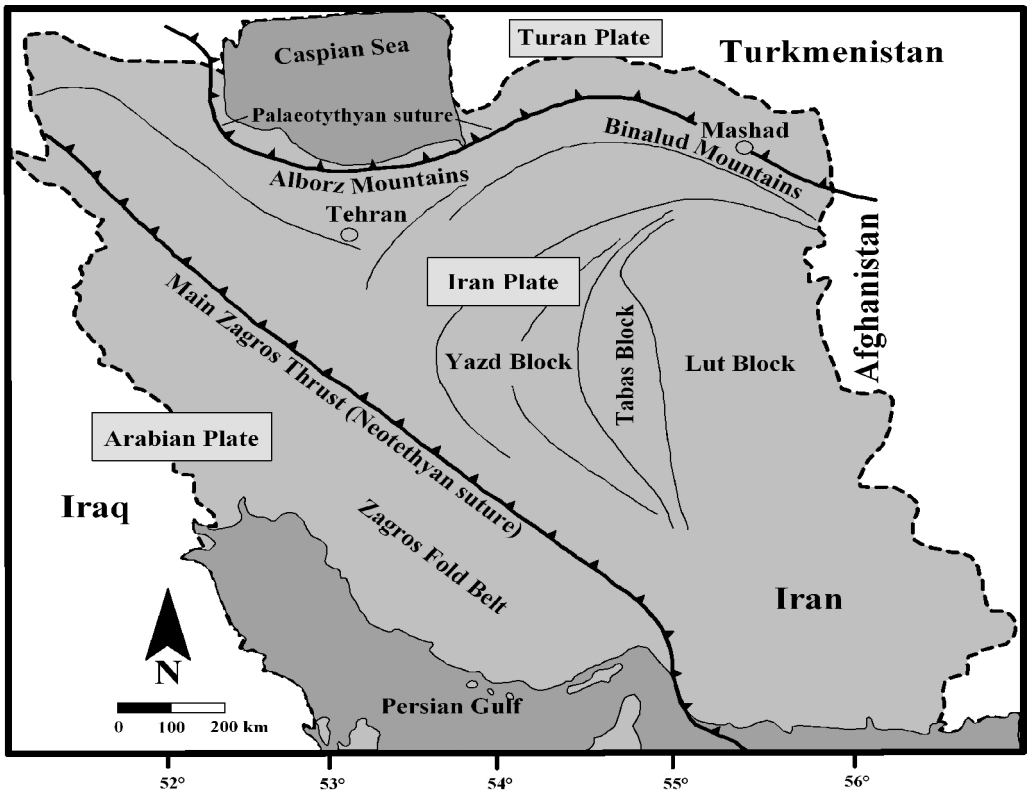

Fig. 3.1. Structural framework of Iran.

4 JURASSIC STRATIGRAPHY OF THE TABAS BLOCK

The Upper Triassic to Upper Jurassic sedimentary succession of the central-east Iranian Microcontinent starts with shales, sandstones and limestones of the Nayband Formation, which was introduced first time by DOUGLAS (1929) and modified by BRÖNNIMANN et al. (1971) in the Nayband area. Recently, it was investigated in detail by FÜRSICH et al. (2005). This unit is followed by the siliciclastic Ab-e-Haji Formation (Lower Jurassic), the Toarcian-Lower Bajocian Badamu Formation and the Upper Bajocian-Lower Bathonian Hojedk Formation, (SEYED-EMAMI et al. 2001). Based on AGHANABATI (1977, 1978, 2004, 241) the Upper Triassic to Upper Jurassic strata can be combined into two groups, which are separated by unconformities related to tectonic events; the Shemshak Group containing the above mentioned formations which are intercalated between the Early (Ladinian-Carnian) and the Mid-Cimmerian (Bajocian) tectonic event, and the Magu Group. The basal lithostratigraphic unit of the latter is the Upper Bajocian-Middle Bathonian Parvadeh Formation followed by the ?middle Late Bathonian to early Middle Callovian Baghamshah Formation, the Bathonian-Oxfordian Qaleh Dokhtar Formation, the Lower Callovian-Upper Oxfordian Esfandiar Limestone Formation, the Lower-Middle Callovian-Lower Kimmeridgian Kamar-e-Mehdi Formation, the Kimmeridgian-Tithonian Garedu Red Bed Formatiom and the Upper Kimmeridgian-Tithonian Magu Gypsum Formation (RUTNER et al. 1968; SEYED-EMAMI et al. 1997, 1998, 2001, 2002, 2005; SCHAIRER et al. 2003). These formations are sandwiched between the Mid and Late Cimmerian (latest Jurassic) tectonic events. During the last few years, several studies on the lithostratigraphy attempted to improve and define more precisely a number of formations of the Magu Group (Qaleh Dokhtar Formation: SCHAIRER et al. 2000; FÜRSICH et al. 2003a; Kamar-e-Mehdi Formation: WILMSEN et al. 2003, 2009; Korond Formation: SCHAIRER et al. 2003; Sikhor Formation: FÜRSICH et al. 2003b; general review of the Middle Jurassic lithostratigraphy of Iran: SEYED-EMAMI et al. 2001). Based on FÜRSICH et al. (2003a), the lithostratigraphic framework of the Esfandiar Subgroup of the Shotori Range (Tabas area) from east to west comprises the Korond, Qaleh Dokhtar, Esfandiar, and Kamar-e-Mehdi formations (Fig. 3). The latter formation is characterized by the basal Echellon Limestone Member and is, superbly exposed in the northern Tabas Block. It can be traced for a great distance, being widespread also in Ravar area. However, in the Zarand-Kerman area (Bidou, Mohamadshah and Bolboulieh sections) it changes into the Mixed Siliciclastic-Carbonate Member of the Bidou Formation. In total, the Baghamshah Formation is unconformably followed by the Kamar-e-Mehdi Formation (Gypsum-Pecten Limestone of

HUCKRIEDE et al., 1962). The upper part of the Kamar-e-Mehdi Formation is formed by the Nar Limestone Member (WILMSEN et al. 2003, 2009), earlier on regarded by AGHANABATI (1977) as a separate formation. The Kamar-e-Mehdi Formation is followed with erosional contact by the Magu Gypsum Formation in the Echellon and Qoleh Nar area. In the latter area, this formation is followed with unconformable contact by siliciclastic rocks of the Lower Cretaceous. AGHANABATI (1977) had called this facies ``Magu Gypsum`` in the Qoleh Nar area. In the Zarand-Kerman area, the Magu Group laterally grades into siliciclastic-carbonate rocks of the Bidou Formation. Earlier on, Huber & Stöcklin (1954) had introduced the Bidou Series for the rock succession north of Kerman, close to the Hojedk Coal Mine. They believed this series to consist of a basal conglomerate, followed by green to red marl and sandstone in the middle and by limestone at the top. The latter has been subdivided into two parts, the lower part consisting of three, very thick to massive limestone units, which are separated by two intercalations of gypsiferous-sandy marl and marly limestone, whereas the upper part consists of red marl and sandstone. According to HUBER & STÖCKLIN (1954), the Bidou Limestone member indicates a early to middle Cretaceous age, but HUCKRIEDE et al. (1962) suggested an Oxfordian to Kimmeridgian age and believed that the Bidou Series ranges from the upper red part of the middle unit up to the upper unit. SEYED-EMAMI (1999) proposed that the Bidou Series is composed of the Bidou Formation (Bathonian-Callovian), Pectinid Limestone (upper Callovian-Kimmeridgian), and Ravar Formation (Kimmeridgian and probably Tithonian). He suggested that the name Bidou Group should be restricted to the non-separated Bidou Series. AGHANABATI (2004: 257) argued that the "Bidou Series" is equivalent of the Magu Group. In the Kerman area, also the Asad-Abad formation has been introduced for the Upper Jurassic siliciclastic rocks (quoted from AGHANABATI 1998). It has been subdivided into three parts ranging in age from the Callovian-Oxfordian to the Kimmeridgian. South-east of Kerman, the middle part of the Asad-Abad Formation indicates an Oxfordian to ?Kimmeridgian age (POLYANSKII 1984) and its upper part probably a Kimmeridgian age. HUCKRIEDE et al. (1962) believed the Hojedk Formation of the Ravar-Kerman Basin to be discontinuously followed by the Bidou Formation. The thickness of latter varies from 500 m to more than 1000 m and ranges from the Upper Jurassic to the Lower Cretaceous (Neocomian).

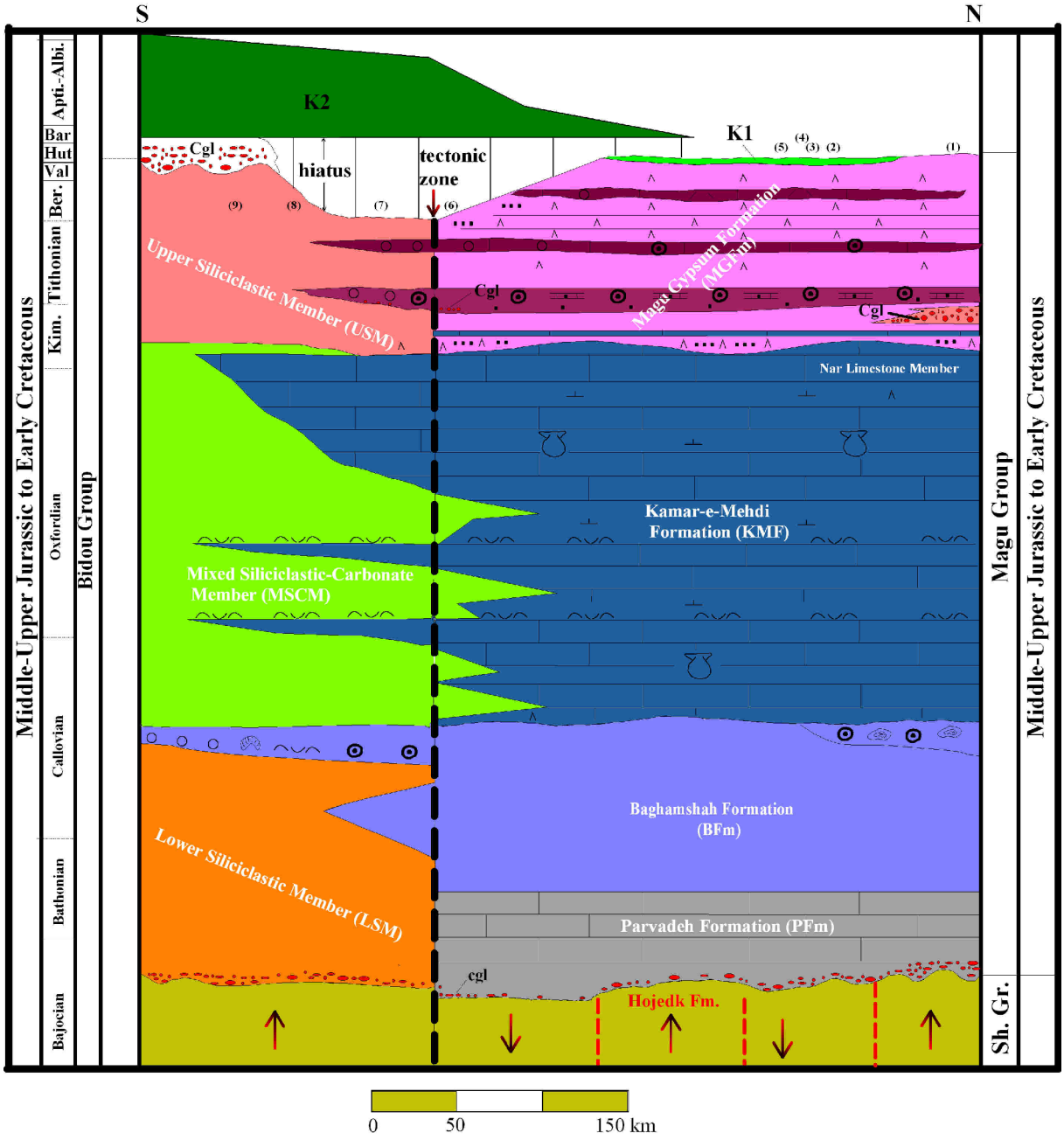

Fig. 4.1 Lithostratigraphic correlation of the Middle-Upper Jurassic and Lower Cretaceous rocks of the Tabas Block, east-central Iran, from the Kerman-Ravar area in the south and the Tabas area in the north. 1 to 9 refer to the Echellon, Doshakh, Kamar-e-Mehdi, Qoleh Nar, Abdoughi, Ravar, Bidou, Mohamadshah and Bolboulieh areas, respectively. Sh. Gr: Shemshak Group, Cgl: conglomerate, Kim: Kimmeridgian, Ber: Berriasian, Val: Valanginian, Hut: Hauterivian, Bar: Barremian, Apti: Aptian, Albi: Albian, K1: Berriasian-?Valanginian, Hojedk Fm: sandstone, siltstone and intercalated limestone, LSM: basal conglomerate, sandstone, siltstone/shale, and intercalated limestone, MSCM: sandstone, siltstone/shale, silty clay, and limestone, USM: siltstone/shale, sandstone, gypsiferous silty clay, limestone, and gypsum, PFm: limestone, silty marl, sandstone, and basal conglomerate, BF: silty shale, sandstone and intercalated limestone, KMF: marl, limestone, gypsum and sandstone, MGF: gypsiferous silty clay, gypsum, sandstone, and limestone, N: north, S: south. Arrows display uplift and subsidence during "mid"-Bajocian Mid-Cimmerian tectonic movements. For key of symbols see Fig. 5.8.16.

5 SECTIONS

In order to analyse the Middle to Upper Jurassic strata of the Magu Group/Bidou Formation of the western and southern Tabas Block, nine sections were measured. Each formation was sampled and their lithology, sedimentary structures, trace fossils, and macrofauna was recorded. These features are briefly characterized in this chapter. Detailed information of the formations will be found in subsequent chapters. Locations of the investigated sections are indicated in Fig. 2.1.

5.1. Echellon section (co-ordinates: 33° 49´ 53.1´´ N/56° 35´ 05.3 E)

The section in the Echellon area (Fig. 5.1.1) exposes the uppermost part of the Kamar-e-Mehdi Formation and its transition into the overlying Magu Gypsum Formation of the Garedu Subgroup. It was measured approximately 3.5 km north of Kuh-e-Echellon and has a thickness of 521 m. For more detailed information, the uppermost 63 m of the Kamar-e-Mehdi Formation were also measured.

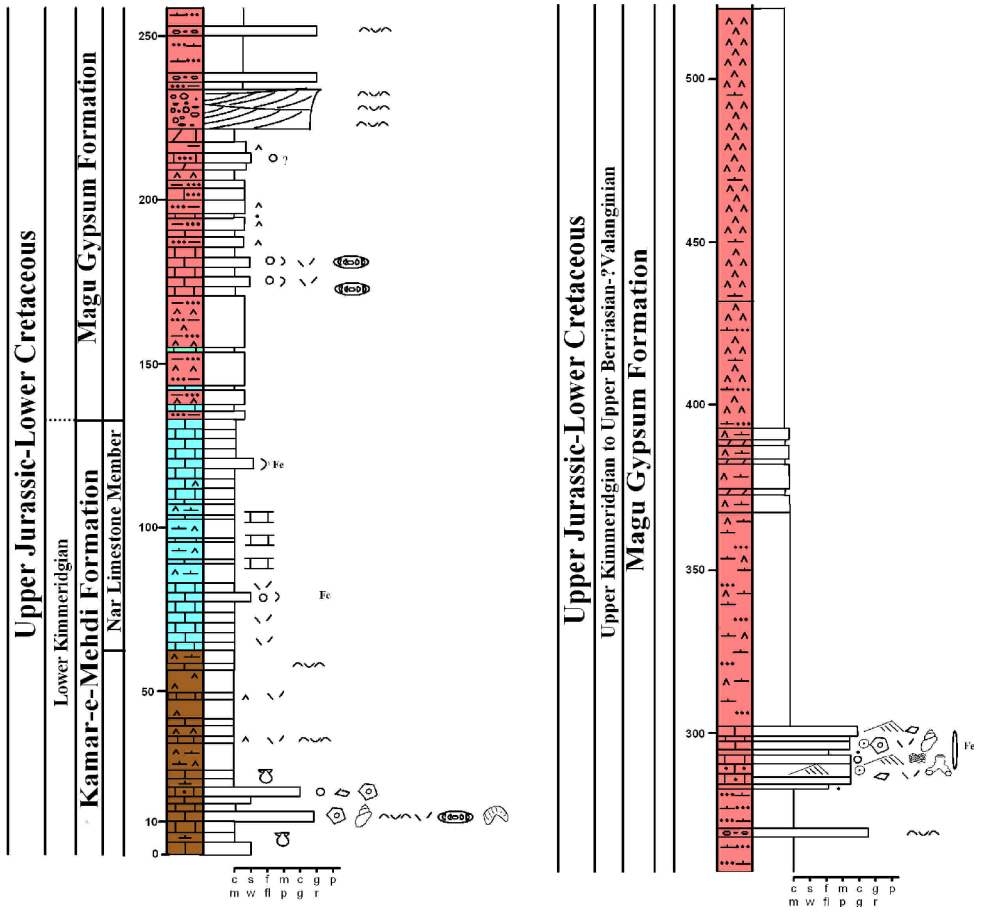

Fig. 5.1.1. Section of uppermost part of the Kamar-e-Mehdi Formation, the Nar Limestone Member and the Magu Gypsum Formation in the Echellon area. For key of symbols see Fig. 5.8.16.

The succession starts with 22 m thick of mudstones, wackestones and marl with intercalations of grainstones, rudstones and thin-bedded shell layers. The succession continues with a gypsiferous marl containing layers of mudstone and shell beds which is conformably overlain by the Nar Limestone Member (between 62 and 131 m). The latter is characterized by mudstones with intercalated wackestone in the base. Alternations of mudstone and green gypsiferous marl occur in the middle and mudstone in the upper part. The Nar Limestone Member has a erosional contact with the Magu Gypsum Formation (131-521 m). The latter formation consists of red to brown gypsiferous silty clay with intercalated carbonate mudstones at the base, followed by alternations of gypsiferous silty clay and carbonate mudstone containing intercalations of gypsum beds. Higher up, the latter turn into a calcareous conglomerate which is followed by silty clay to silty marl with some intercalated calcareous conglomerate, calcareous sandstone and grainstone. Higher up, these facies turn with conformable contact into gypsiferous silty marl and alternations of red gypsiferous silty marl and gypsum beds. Up-section, the thickness of massive gypsum beds increases. Lithostratigraphically the Magu Gypsum Formation of the Echelon section resembles that at the Kuh-e-Qoleh Nar type locality.

Field photographs and thin-sections of the Upper Jurassic rocks in the Echellon area are shown in Figs. 5.1.2-5.1.5.

Fig. 5.1.2. Echellon section. (A) Upper part of the Kamar-e-Mehdi Formation (right) and its transition into the Nar Limestone Member (left). (B) Disconformable contact (arrowed) between the Nar Limestone Member (right) and red gypsiferous silty clay of the Magu Gypsum Formation (left). (C) Alternations of gypsiferous silty clay with thin- to thick-bedded mudstone of the Magu Gypsum Formation. (D) Gypsiferous silty clay containing intercalation of lenticular thin- to thick-bedded gypsum beds (between two dashed lines). (E) Aspect of the Magu Gypsum Formation. Msc: Alternations of mudstone with silty clay; Cgl: conglomerate; Msm: monotonous silty marl to silty clay; O: Calcareous sandstone to grainstone; Gsc: Alternations of red gypsiferous silty marl with gypsum beds; G: Thick-bedded gypsum beds. (F, G) Coarsening-upward calcareous conglomerate (Cgl), which overlies alternations of mudstone and silty clay (Msc).

Fig. 5.1.3. Echellon section. (A) Upper part of the crudely bedded coarsening-upward monomict calcareous conglomerate with clast imbrication (black arrow); clasts are mainly subrounded to rounded, lower part of the Magu Gypsum Formation. (B) Lower part of the coarsening-upward calcareous conglomerate; clasts are mainly subangular to subrounded. Lower part of the Magu Gypsum Formation. (C) Contact (at hammer) between monomict calcareous conglomerate with overlying red silty clay to silty marl. Lower part of the Magu Gypsum Formation. (D) Lenticular calcareous conglomerate beds (channel fill) in red silty clay to silty marl. Lower to middle part of the Magu Gypsum Formation. (E) Conformable contact (white arrow) between red silty clay to silty marl and overlying calcareous sandstone. Middle part of the Magu Gypsum Formation. (F-H) Herringbone

cross-bedded fine- to medium-grained calcareous sandstone beds with the trace fossils *Ophiomorpha* (G) and *Skolithos* (H). Middle part of the Magu Gypsum Formation. Diameter of marker pen: 1.80 cm.

Fig. 5.1.4. Echellon section. Thin-sections of microfacies. (A) Mudstone with gypsum needles. Upper part of the Kamar-e-Mehdi Formation (sample m-123; width of photomicrograph: 2.5 mm). (B) Pure very fine-grained carbonate mudstone with rare shell fragments. Upper part of the Kamar-e-Mehdi Formation (sample m-124; width of photomicrograph: 2.5 mm). (C) Bio-pel-grainstone, Note abundant peloids (P) crinoids (black arrow), shell fragments (B) and agglutinating foraminifer (white arrow). Upper part of the Kamar-e-Mehdi Formation (sample p-127; width of photomicrograph: 2.5 mm). (D) Bio-rudstone in the upper part of the Kamar-e-Mehdi Formation. Note crinoid ossicle (Cr), shell fragment (B), intraclast (In) and agglutinating foraminifer (white arrow) (sample p-131; width of photomicrograph: 10 mm). (E) Laminated bindstone from the lower part of the Nar Limestone Mb. Note some ostracod shells (black arrow) (sample p-132; width of photomicrograph: 10 mm). (F) Pure carbonate mudstone, containing relicts of foraminifera (black arrow). Lower part of the Nar Limestone Mb (sample p-133; width of photomicrograph: 2.5 mm). (G) Very faintly laminated mudstone from the upper part of the Nar Limestone Mb (sample p-135; width of photomicrograph: 10 mm). (H) Bio-wackestone from the lower part of the Magu Gypsum Formation. Note agglutinating foraminifer (black arrow) and some peloids or intraclasts (white arrow) (sample p-140; width of photomicrograph: 2.5 mm).

Fig. 5.1.5. Echellon section. Thin-sections of various types of microfacies of lower to middle part of the Magu Gypsum Formation. (A) Calcareous conglomerate. Note shell fragments of mostly bivalves both as clasts (black arrow) and matrix debris (white arrow) (sample m-11; width of photomicrograph: 2.5 mm). (B) Silty carbonate mudstone (sample p-141; width of photomicrograph: 10 mm). (C) Bioclastic calcareous sandstone. Note bioclast fragment (white arrow) (sample m-13; width of photomicrograph: 0.8 mm). (D) Sandy oo-grainstone. Note superficial ooids with a thin cortex and large nucleus and a ostracod? (sample m-60; width of photomicrograph: 1.5 mm). (E) Sandy bio-oo-grainstone. Note spherical and or ellipsoidal ooids (O) with radial structures (white arrow), thin cortex and large nucleus, intraclasts (In) and shell fragments (B) (sample p-145; width of photomicrograph: 2.5 mm). (F) Sandy bio-oo-grainstone. Note micritized ooid (black arrow) and coralline algae (white arrow) (sample p-146; width of photomicrograph: 2.5 mm).

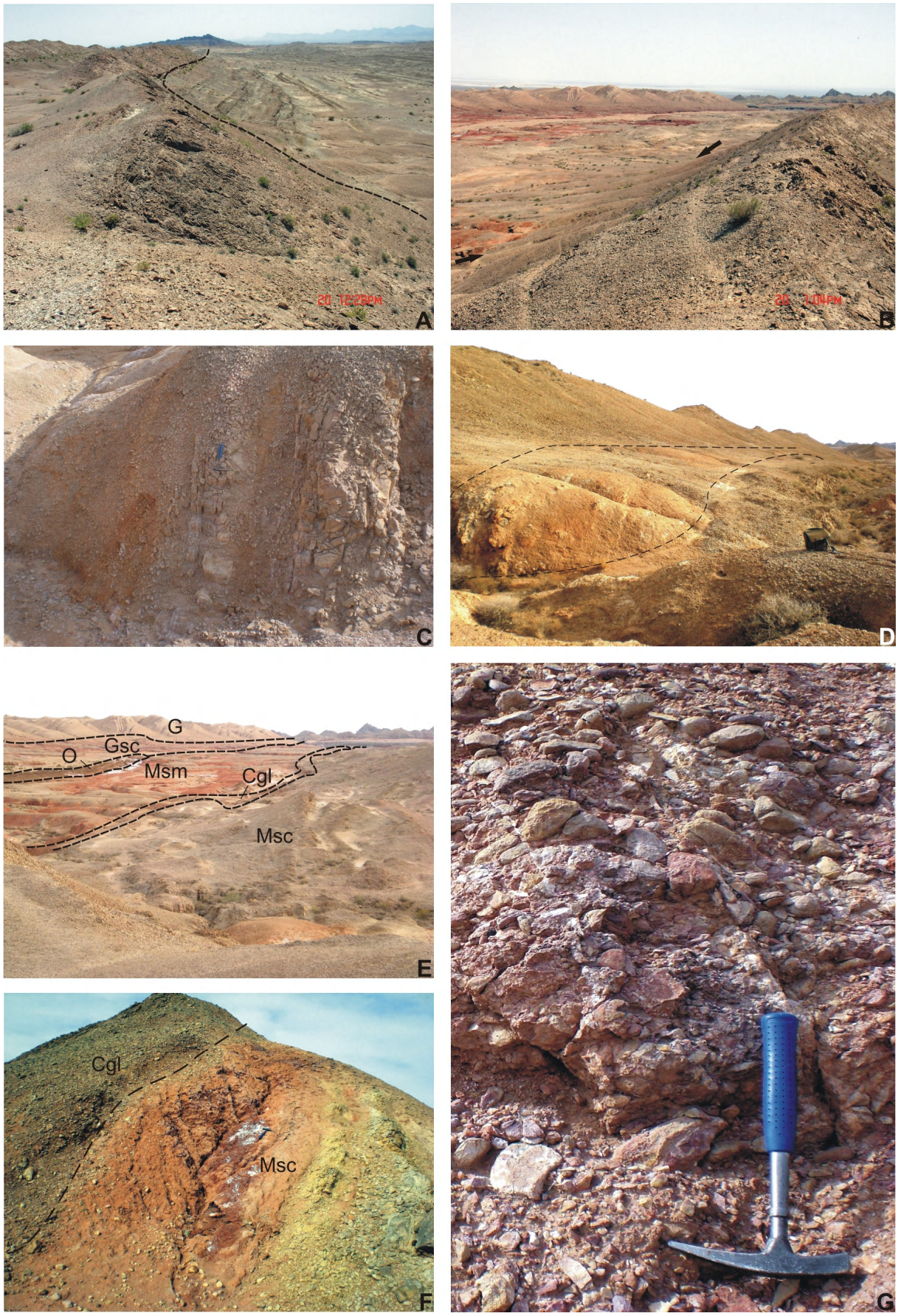

Fig. 5.1.2

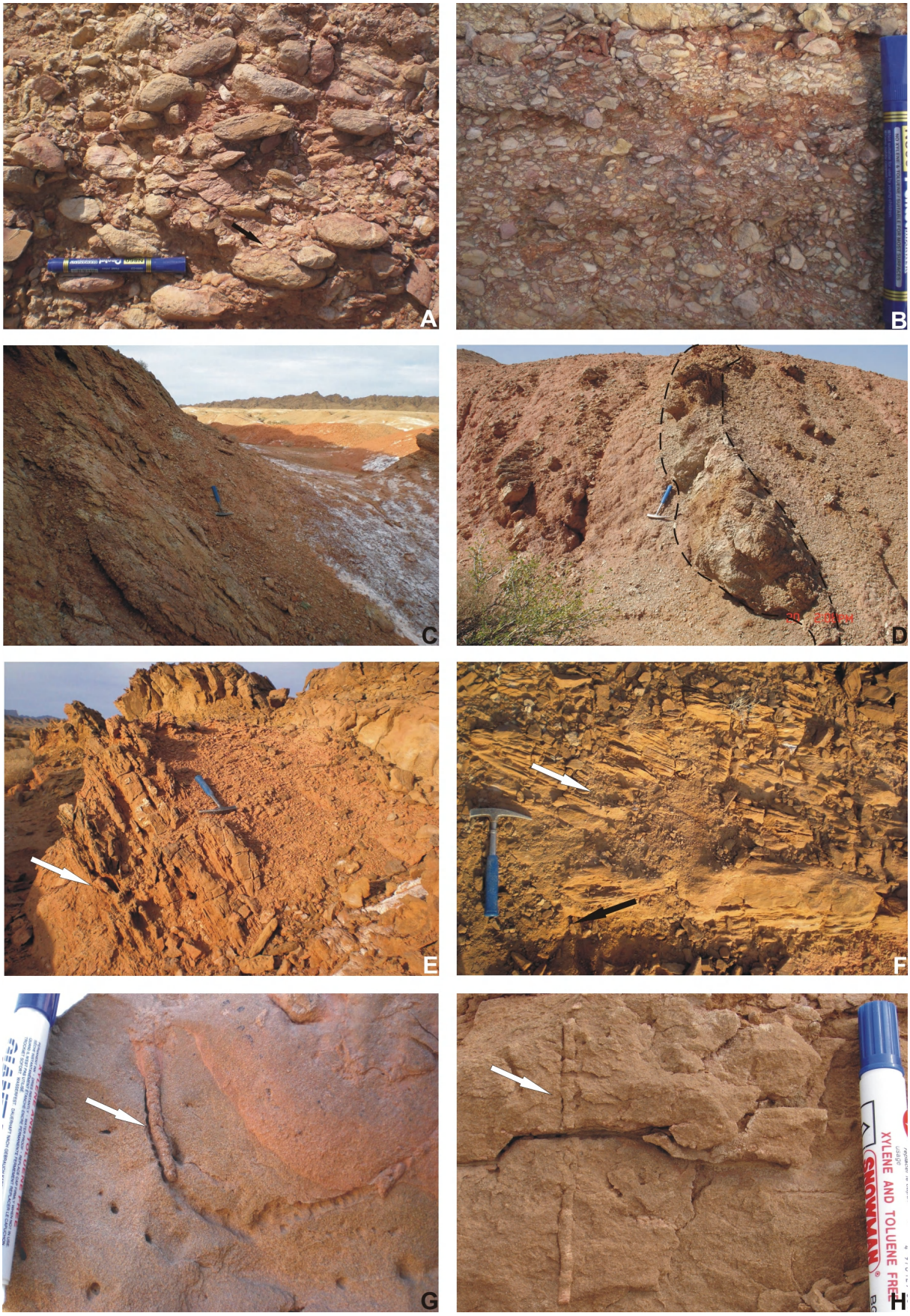

Fig. 5.1.3

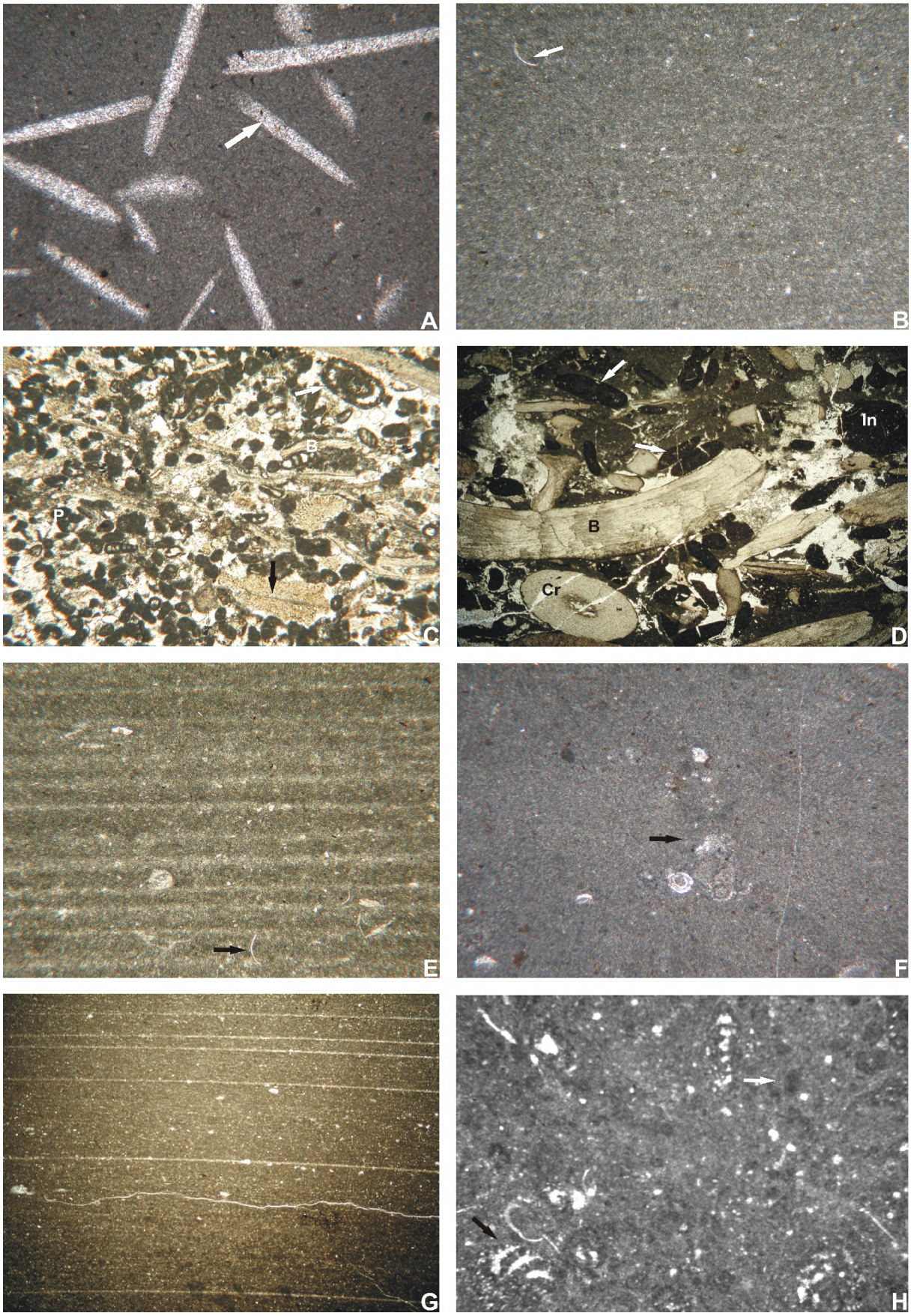

Fig. 5.1.4

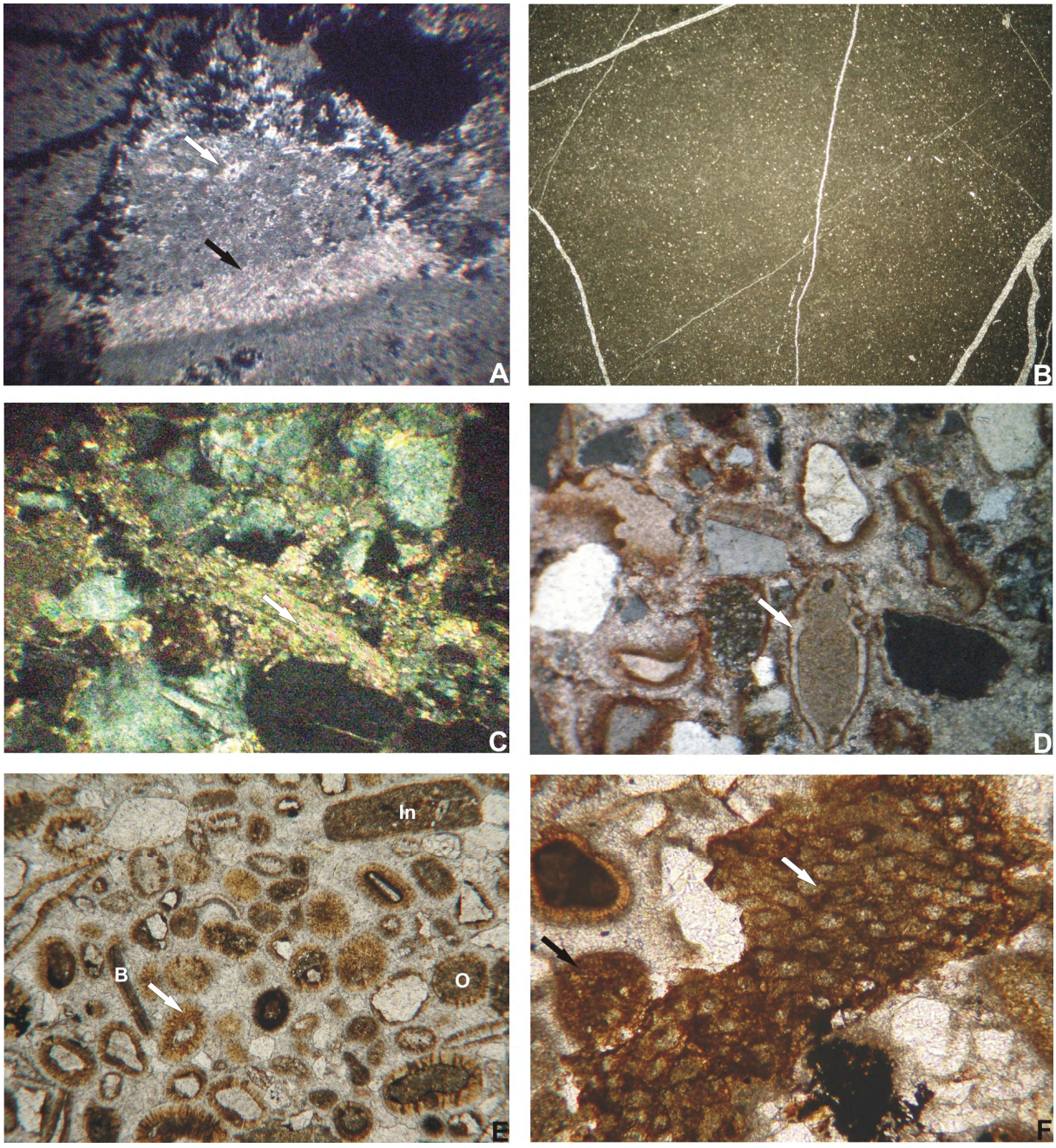

Fig. 5.1.5

5.2. Doshakh section (co-ordinates: 33° 08´ 36,8´´ N/56° 18´ 54.4 E)

The section in the Doshakh area (Fig. 5.2.1) exposes the uppermost part of the Baghamshah Formation (up to 109 m) and its transition into the overlying Kamar-e-Mehdi Formation. It was measured approximately 14 km NW of the Kamar-e-Mehdi area and has a thickness of 236 m. For more detailed information about the erosional contact between the Baghamshah Formation and the Kamar-e-Mehdi Formation, the uppermost 109 m of the Baghamshah Formation were measured. The latter consist of several coarsening-upward cycles of silty marl, siltstone and sandstone beds containing intercalations of grainstone,

onco-floatstone, wackestone and floatstone. At 109 m, the succession is followed by a 8.1 m thick of basal calcareous sandstone of the Kamar-e-Mehdi Formation, which turns into grainstone beds with intercalations of packstone, wackestone and floatstone. Higher up, alternations of silty marl and sandstone occur, which are overlain by floatstone. Up-section (at 172 m), the rocks are mostly marl, pure mudstones, and silty mudstones with irregular coarsening- and thickening-upward cycles, in which intercalations of wackestone and floatstone occur.

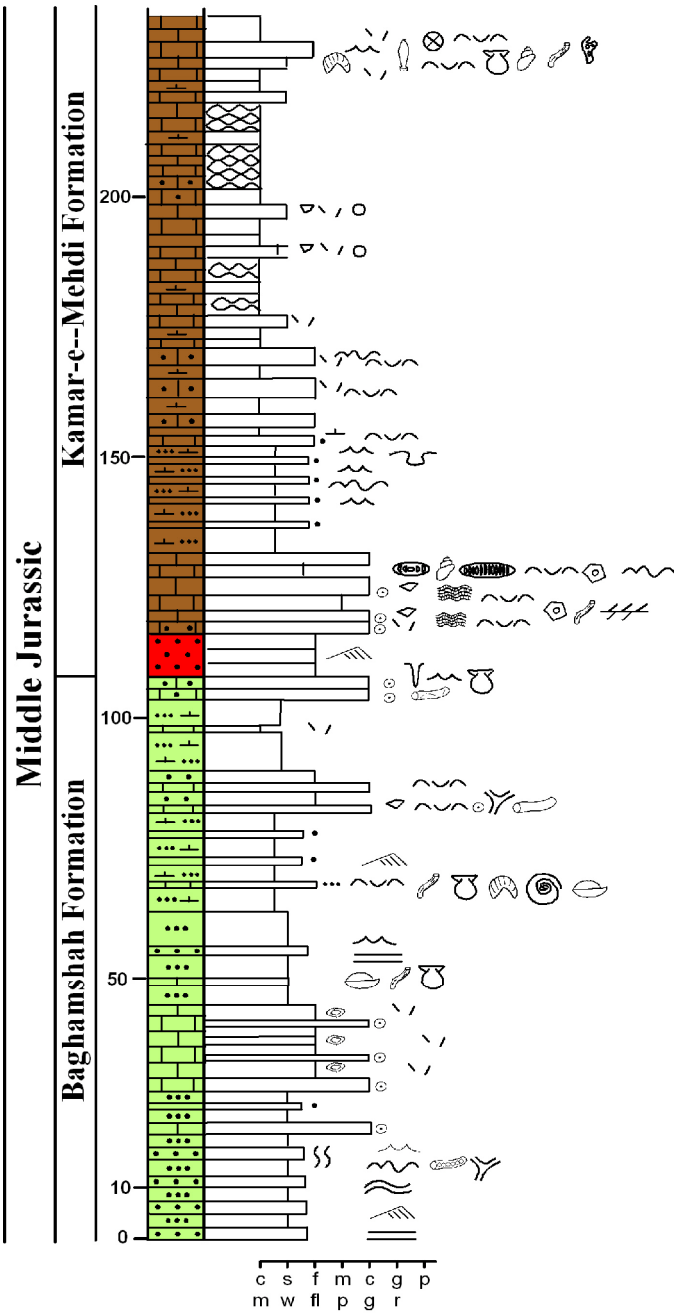

Fig. 5.2.1. Section of the uppermost part of the Baghamshah Formation and lower part of the Kamar-e-Mehdi Formation in the Doshakh area. For key of symbols see Fig. 5.8.16.

Field photographs and thin-sections of the Doshakh section are shown in the following figures.

Fig. 5.2.2. Features of the Doshakh section. (A) Coarsening-upward cycles of silty marl or siltstone at base and calcareous sandstone beds at top, upper part of the Baghamshah Formation. (B) Calcareous sandstone bed with an erosional base at 15 m of the measured section, upper part of the Baghamshah Formation. (C) Weathered oncoid limestones and marls (about 8 m thick) at 25 m of the measured section, upper part of the Baghamshah Formation, forming a marker bed. (D) Bioturbated sandstone intercalated within coarsening-upward cycles at 75 m of the measured section, upper part of the Baghamshah Formation. (E-G) Hummocky- (E: at 10 m), oscillation- (F: at 13 m) and sub-parallel-crested rippled beds (G: at 57 m) in sandstones, upper part of the Baghamshah Formation. (H) *Planolites* sp. (arrowed) at 79 m, upper part of the Baghamshah Formation.

Fig. 5.2.3. Features of the Doshakh section. (A) *Ophiomorpha* isp. (arrowed), upper part of the Baghamshah Formation. (B-D) *Palaeophycus* isp. (white arrows), with walls which are smooth or, rarely, exhibit faint longitudinal striae (B), paired openings of *Diplocraterion* or *Arenicolites* isp. (arrowed) on bedding plane (C), small bivalves of uniform size on bedding plane (D); uppermost part of the Baghamshah Formation. (E) Basal calcareous sandstone of the Kamar-e-Mehdi Formation. (F) Wave-ripples in the upper part of the basal siliciclastic-carbonate beds. (G) Planar cross-stratified calcareous sandstone at the base of the Kamar-e-Mehdi Formation. (H) Erosional surfaces (arrows) in calcareous sandstones, lowermost part of the Kamar-e-Mehdi Formation.

Fig. 5.2.4. Microfacies of the upper part of the Baghamshah Formation, Doshakh section. (A) Feldspathic sandstone with carbonate cement, partly impregnated by iron oxide (white arrow). Sample p-81; width of photomicrograph: 0.5 mm. (B) Oo-grainstone. Note spherical ooids with thick radial cortex and small nucleus (sample p-83; width of photomicrograph: 2.5 mm). (C) Oncoid floatstone forming a marker bed at the top of the Baghamshah Formation. Sample p-113; width of photomicrograph: 10 mm. (D, E1) Silty bio-floatstone/packstone**.** Note serpulid-encrusted shell fragment (white arrow). Sample p-87a; width of photomicrographs: 10 mm (D) and 5 mm (E1). (E2-E4) Bio-wackestone. Note serpulids (E2), articulated bivalve (E3), and articulated brachiopod (E4). Sample p-85; width of photomicrographs: 2 mm (E2), 2.5 mm (E3) and 3 mm (E4). (F) Silty bio-floatstone**.** Note serpulid-encrusted oyster shell (black arrow). Sample p-87b; width of photomicrograph: 10 mm. (G) Intra-oo-grainstone. Note a few cortoid (white arrows). Sample p-88; width of photomicrograph: 10 mm. (H) Mudstone. Sample p-90; width of photomicrograph: 10 mm.

Fig. 5.2.5 (A) Sandy oo-grainstone. Ooids with radial cortex some of which are completely micritized (black arrow), uppermost part of the Baghamshah Formation (sample p-92; width of photomicrograph: 1.5 mm). (B) Calcareous sandstone. Note microstructures which are very similar to ooids with a large nucleus and thin cortex (white arrows), base of the Kamar-e-Mehdi Formation (sample p-93; width of photomicrograph: 1.3 mm). (C) Bio-oo-packstone. Note bryozoan (Br)-encrusted shell fragment (B), ooid (O), and crinoid ossicle (Cr), Kamar-e-Mehdi Formation (sample p-96; width of photomicrograph: 10 mm). (D) Bio-oo-grainstone. Note intraclast (black arrow), Bryozoan (Br), shell fragment (B), and crinoid ossicle (Cr) in a syntaxial carbonate cement, Kamar-e-Mehdi Formation (sample p-97; width of photomicrograph: 2.5 mm). (E) Intra-pel-wackestone. Note

peloid (white arrowed) and intraclast (In), Kamar-e-Mehdi Formation (sample p-101; width of photomicrograph: 2.5 mm). (F-H) Intra-cortoid-bio-wacke- to floatstone. Note crinoid remains (Cr), gastropod (G), shell fragment (B), cortoid (Co), the hinge of a nuculid bivalve (black arrowed), serpulid (Se) and a foraminifer in an intraclast (white arrow) (sample p-88; width of photomicrographs: 2 mm).

Fig. 5.2.6 (A-D) Some parts of the intra-cortoid-bio-wacke- to floatstone of the uppermost part of the Baghamshah Formation (at 80 m). (A) Cross-sections of a blue-green alga, bryozoan (B), long branched tubes (black arrow) of a blue-green alga (C), thin-walled aligned tubes and prostrate growth of a blue-green algae encrusted by Dorsoserpula (D) (sample p-88; width of photomicrographs: 2.5 mm (A, B), 2 mm (C) and 3 mm (D)). (E) Calcareous sandstone, lower part of the Kamar-e-Mehdi Formation at 132 m (sample p-101; width of photomicrograph: 1.5 mm). (F) Silty to sandy bio-floatstone with some shell fragments, lower part of the Kamar-e-Mehdi Formation at 197 m (sample p-103; width of photomicrograph: 10 mm).

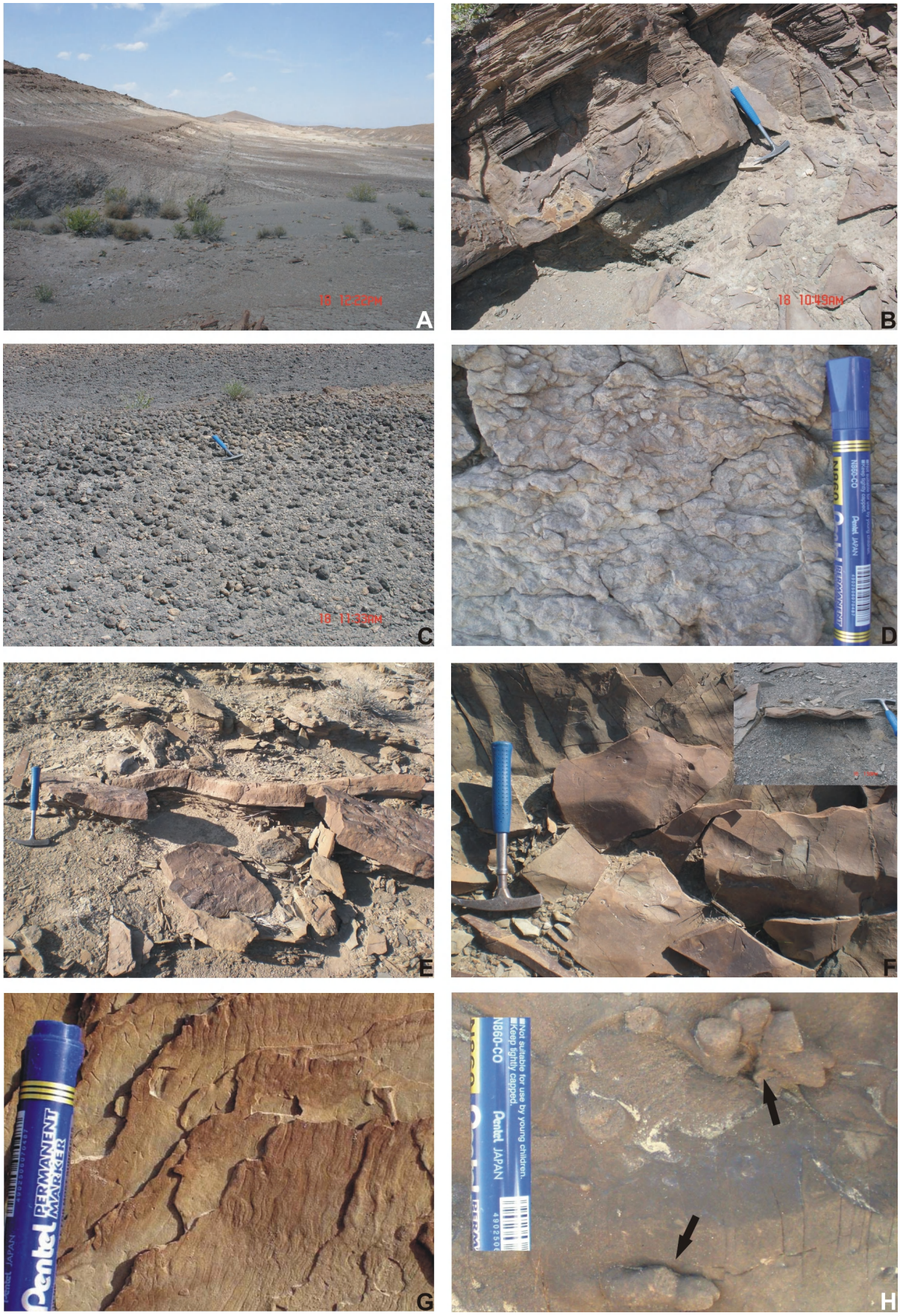

Fig. 5.2.2

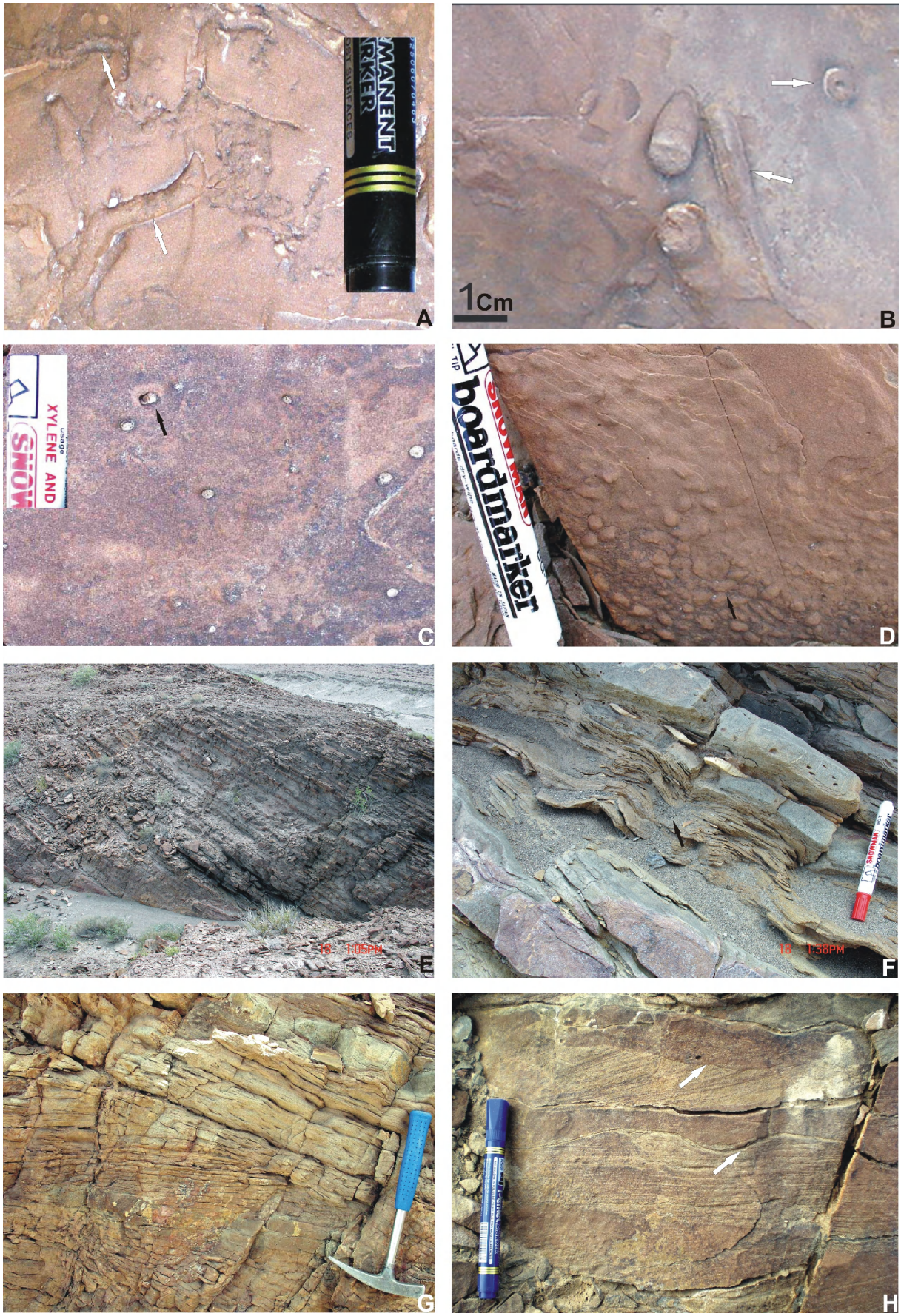

Fig. 5.2.3

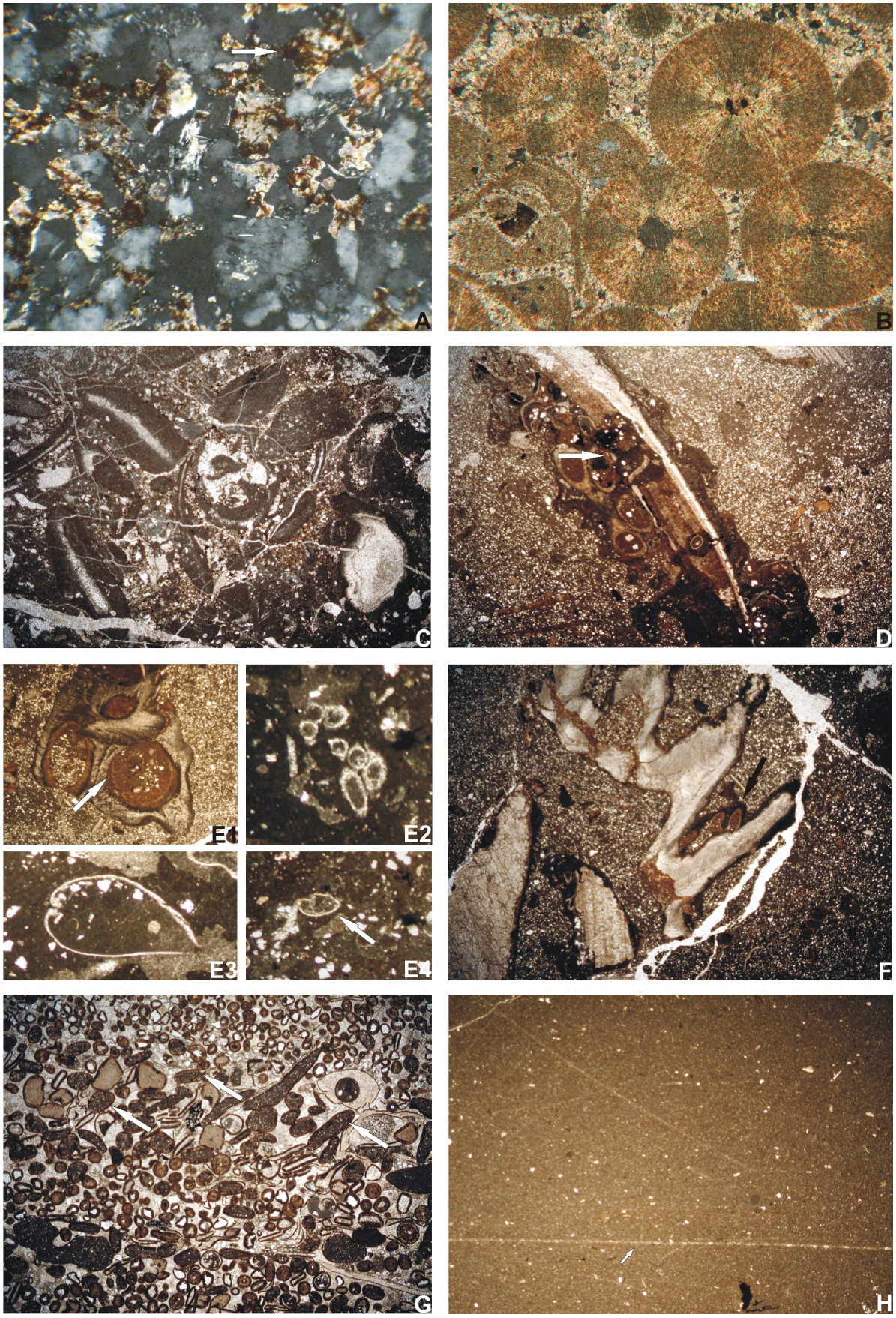

Fig. 5.2.4

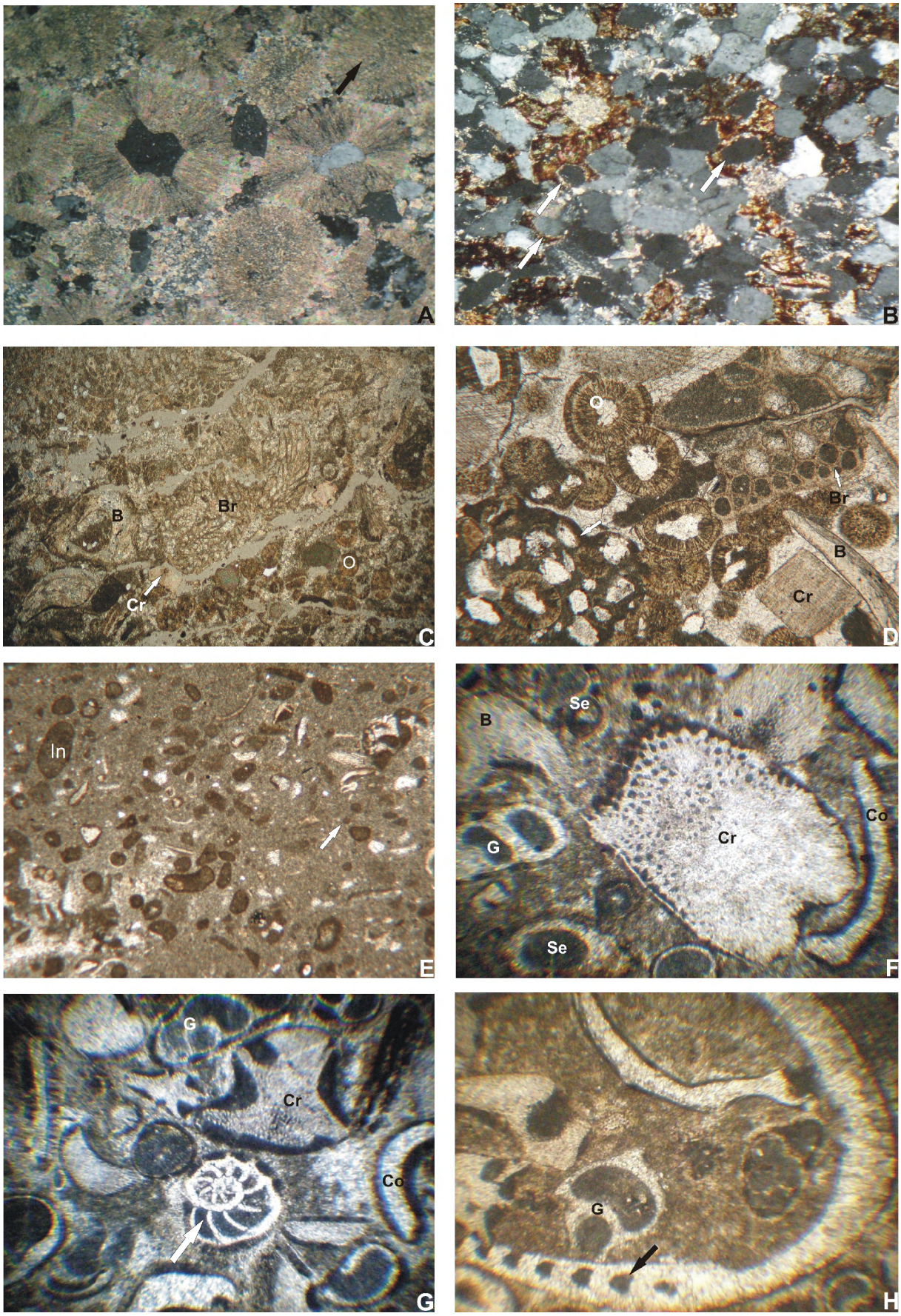

Fig. 5.2.5

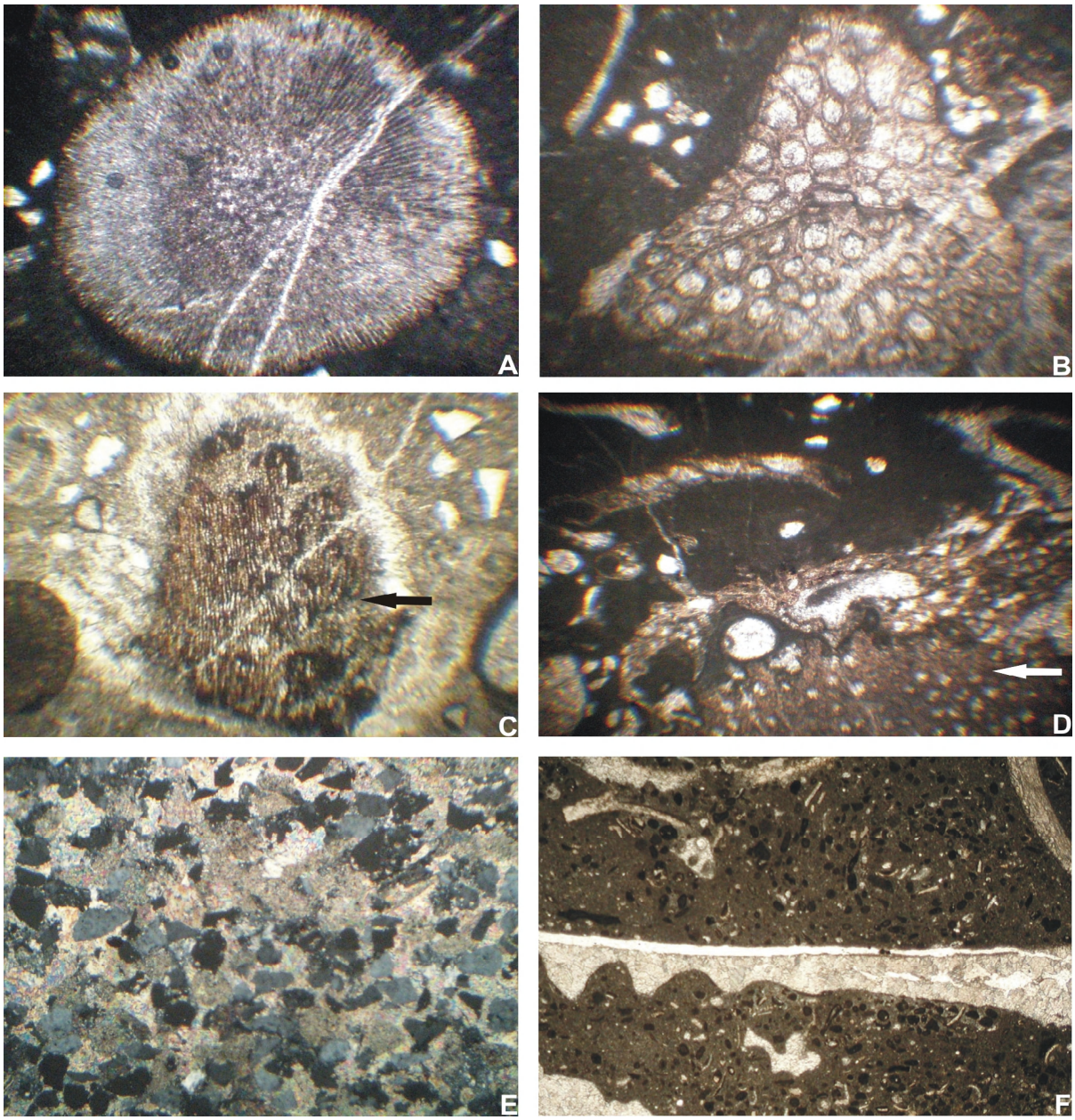

Fig. 5.2.6

5.3. Kamar-e-Mehdi section (co-ordinates: 33° 03′ 47′′ N/56° 25′ 23.2 E)

The section (Fig. 5.3.1) is located in the southeastern part of the Robat-e-Khan 1:100,000 geological map. It has been measured close to Qoleh Nar peak, across the escarpment formed by the rocks of the Magu Group. The section exposes the Kamar-e-Mehdi Formation.

This formation, which has a thickness of 1281 m (Fig. 5.3.1), overlies with erosional contact the Baghamshah Formation. At base, the succession is characterized by calcareous sandstones containing intercalations of silty marl and some thin shell beds. The basal mixed

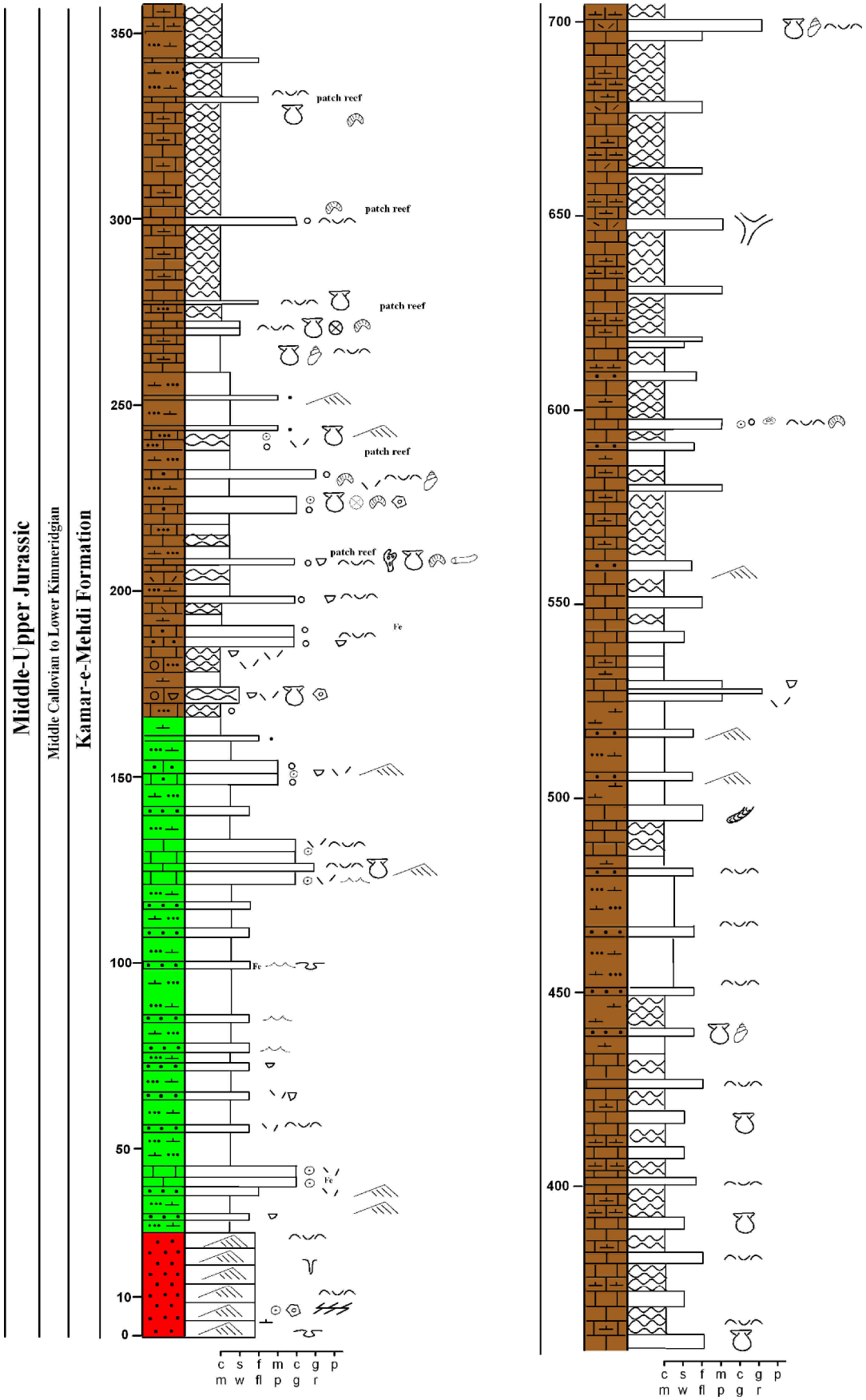

Fig. 5.3.1. Kamar-e-Mehdi Formation in the Kamar-e-Mehdi area. For key of symbols see Fig. 5.8.16.

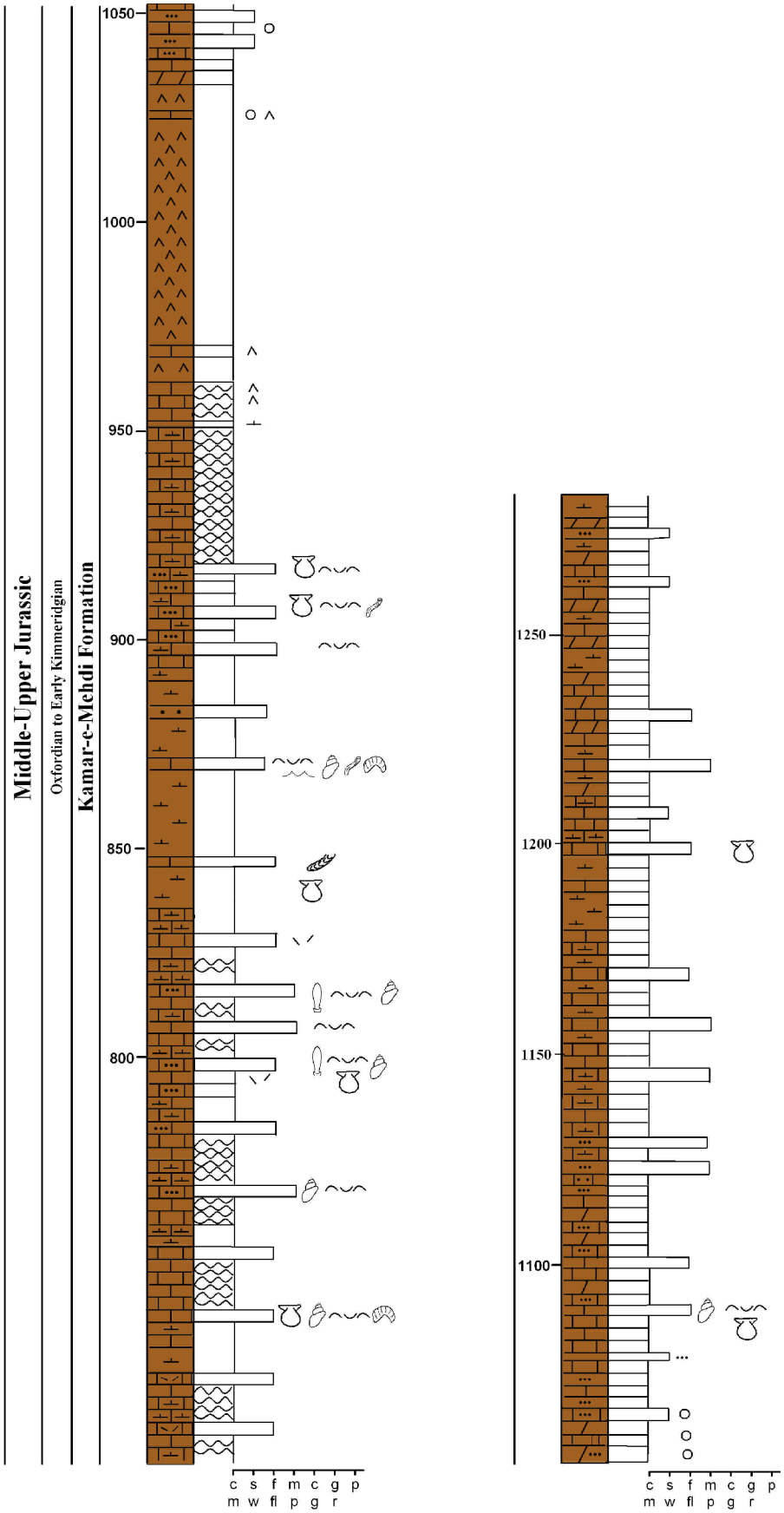
Middle-Upper Jurassic
Oxfordian to Early Kimmeridgian
Kamar-e-Mehdi Formation
1050
1000
950
900
850
800
1250
1200
1150
1100
c s f m c g p
m w fl p g r

Continue

siliciclastic-carbonate rocks are overlain by silty marl, occasionally silty shale with intercalations of grainstone, bio-rudstone (at 125 m), and wackestone (at 170 m). These in turn are overlain by several hundred meters of mostly marl, marly mudstone, mudstone, evaporates (between 962 and 1032 m), and intercalations of wackestone, floatstone, packstone, rudstone and siliciclastic-carbonate rocks. This succession contains abundant pectinids, gastropods, oysters, corals and sponges, the latter three mainly associated with patch reefs. These macrofossils and trace fossils are figured in Chapter 7 and 8, respectively. In this area, the uppermost part of the Kamar-e-Mehdi Formation (Nar Limestone Member) is dolomitic. This part of the formation was therefore measured at Kuh-e-Qoleh Nar.

Fig. 5.3.2. Kamar-e-Mehdi Formation at the Kamar-e-Mehdi section. (A) Basal calcareous sandstone with disconformable contact (arrowed) overlies green silty shale of the Baghamshah Formation. (B) Basal calcareous sandstone of the Kamar-e-Mehdi Formation with ball-and-pillow structures (arrowed) overlying green silty shale of the Baghamshah Formation. (C-D) Planar cross-stratification (C) and low-angle cross-lamination. Note erosional surface (arrowed) (D) within lower to upper part of the basal calcareous sandstones. (E) Intercalated calcareous sandstones containing oscillation ripples at 100 m. (F) Oo-grainstone with sub-parallel-crested ripples (arrowed) at 122 m. (G-H) Irregular coarsening- and thickening-upward cycles, in which the texture changes from marl, marly carbonate mudstone to carbonate mudstone (mostly) and wackestone, packstone, floatstone, and finally rudstone.

Fig. 5.3.3. Kamar-e-Mehdi Formation at the Kamar-e-Mehdi section. (A) Intercalated wave ripple (arrowed) in lower to middle part of the formation. (B) Note abundant small oysters Nanogyra nana (yellow arrow) and coral (white arrow). The oysters form small the patch reefs, mainly in the lower to middle part of the formation. (C) Small heterodont bivalves (yellow arrow) and small cerithiid gastropods (white arrow). (D) The stick-shaped sclerosponge Neuropora occurring in a patch reef in the lower part of the formation. (E-F) Shells of *Radulopecten tipperi* (E) and oyster (F) at the top of cycles throughout the formation. (G-H) Articulated *Radulopecten tipperi* in life position, middle part of the formation. Diameter of pencil: 0.9, of pen : 1.75 cm.

Fig. 5.3.4 Trace fossils from the Kamar-e-Mehdi Formation of the Kamar-e-Mehdi section. (A) *Thalassinoides*. (B) Paired holes of vertical U-tubes of *Diplocraterion* or *Arenicolites*, lower part of the formation. (C, D) *Chondrites* (arrowed) (C) and *Rhizocorallium irregulare* (arrowed) (D) in the middle to upper part of the formation. Diameter of hammer: 3.1 cm of pen: 1.75 cm.

Fig. 5.3.5 Thin-sections of various types of microfacies from the Kamar-e-Mehdi Formation at the Kamar-e-Mehdi section. (A-D) Basal calcarceous sandstone. Note respectively intraclasts (A: arrowed), shell fragment (B: arrowed), ooid (C: arrowed), crinoid ossicle (D: arrowed). Sample p-1; width of photomicrographs: 3 mm (A), 0.5 (B), 1 mm (C) and 1.5 (D) mm. (E) Calcareous sandstone. Note syntaxial echinoderm overgrowth of calcite cements (E: white arrow), lowermost part of the formation. Sample p-2; width of photomicrograph: 1.5 mm. (F-

G) Sandy intra-oo-grainstone, ooids (O), intraclasts (In), and cortoid grains (Co), lower part of the formation. Sample p-4; p-14; width of photomicrographs: 3 mm (F) and 0.6 (G) mm.

Fig. 5.3.6 Kamar-e-Mehdi section. Thin-sections of various types of microfacies of the lower to middle part of the Kamar-e-Mehdi Formation. (A-B) Sandy bio-oo-grainstone. Note probable brachiopod shell fragment (black arrow), superficial ooids, micritized or partly micritized ooids (Mo), cortoid (Co), aggregate grain (Ag), concentric ooid (black arrow) and probably gastropod as a intraclast (Gin) in a sparry carbonate cement, lower part of the formation (sample p-6; width of photomicrographs: 2.5 mm). (C) Oo-grainstone. Note ooids with a thick radially structured cortex and small nucleus and a shell fragment (arrowed), lower part of the formation (sample p-11; width of photomicrograph: 2.5 mm). (D) Sandy bio-pel-grainstone with some intraclasts (In) and cortoids (Co), lower part of the formation (sample p-15; width of photomicrograph: 2.5 mm). (E) Silty bio-wackestone. Note some shell fragments (arrowed), crinoid debris (Cr), and also peloids (P), middle part of the formation (sample p-16; width of photomicrograph: 2.5 mm). (F) Intra-bio-grainstone with some ?peloids. Note scattered crinoid debris (Cr), shell fragments, and also shell moulds and thin micrite rims on the margins of shells, which partly have undergone recrystallisation (neomorphism: white arrows), middle part of the formation (sample p-19; width of photomicrograph: 2.5 mm). (G) Bio-oo-packstone. The ooids either have a concentrically or radially structured cortex and small nucleus (arrowed). Seen are also crinoid debris (Cr), aggregate grains (Ag), cortoids (Co); middle part of the Kamar-e-Mehdi Formation (sample p-21; width of photomicrograph: 5 mm). (H) Bio-floatstone. Note casts of skeletal grains replaced by neomorphic sparry calcite (white arrow), middle part of the formation (sample p-22; width of photomicrographs: 10 mm).

Fig. 5.3.7 Kamar-e-Mehdi section. Thin-sections of various types of microfacies from middle to upper part of the Kamar-e-Mehdi Formation. (A) Sandy oo-pel-wackestone/floatstone. Note long oyster fragment with a foliated microstructure (white arrow), foraminifer (F), crinoid debris (Cr) and a few ooids (O) and peloids (P) (sample p-25; width of photomicrographs: 2.5 mm). (B) Faintly laminated bindstone (sample p-37; width of photomicrograph: 2.5 mm). (C) Silty cortoid-intra-rudstone. Note intraclasts (In) and cortoids (Co) (sample p-39; width of photomicrograph: 10 mm). (D) Sandy bio-wackestone/floatstone. Note long oyster fragment (white arrow), crinoid (Cr), ecinoid spine (Es), and shell fragments (black arrow) (sample p-43; width of photomicrograph: 2.5 mm). (E) Mudstone with gypsum needles (arrowed), upper part of the formation (sample p-46; width of photomicrograph: 2.5 mm). (F) Mudstone with gypsum pseudomorphs and ostracod shells (arrowed), upper part of the formation (sample p-47; width of photomicrograph: 2.5 mm). (G) Bio-wackestone with small shell fragments (arrowed) (sample p-49; width of photomicrographs: 2.5 mm). (H) Silty dolomitic mudstone. Note subhedral- to well-formed dolomite rhombs (black arrow), idiotopic porphyrotopic texture, and relict of crinoid clast (Cr) (sample p-48; width of photomicrograph: 1.5 mm).

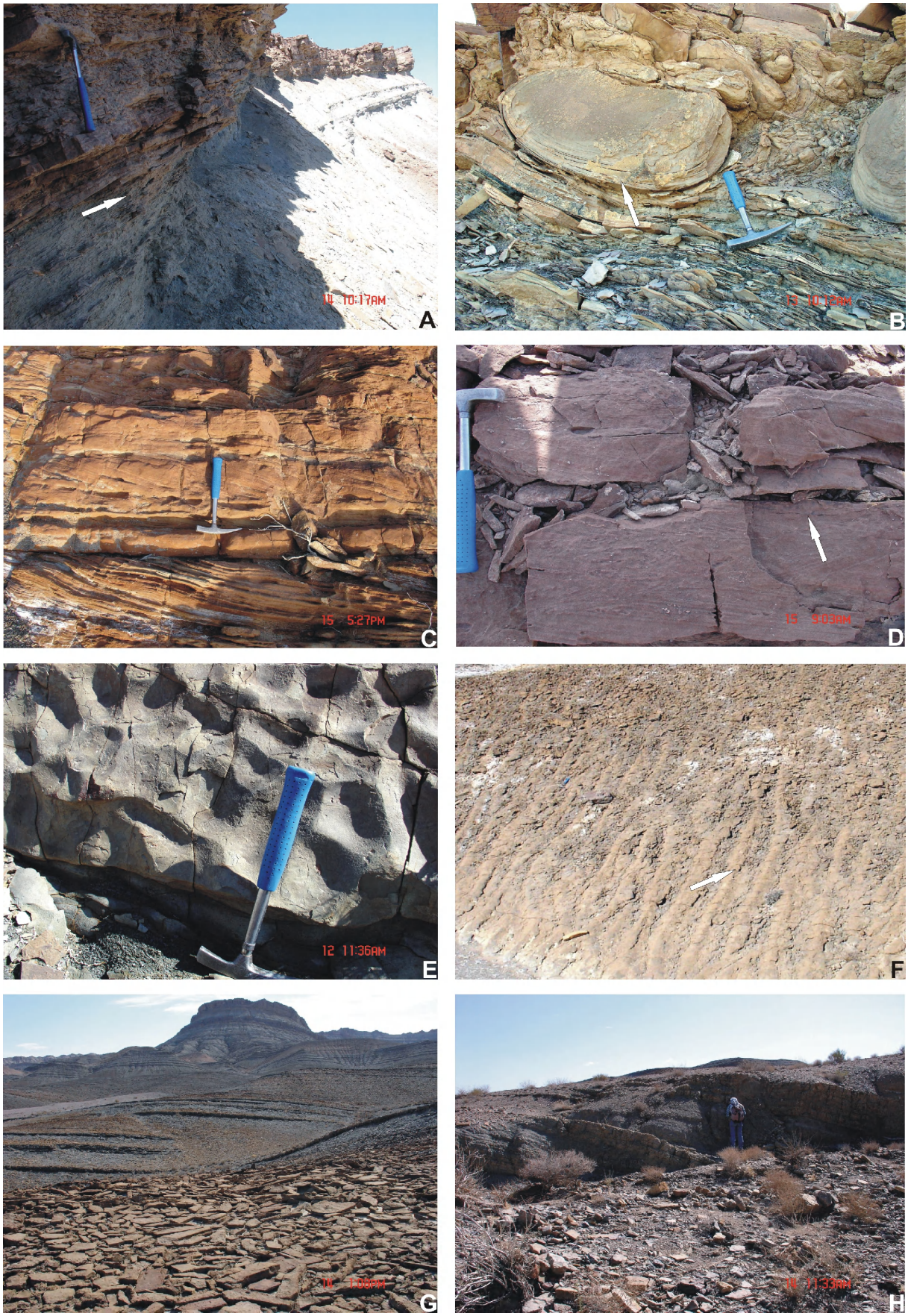

Fig. 5.3.2.

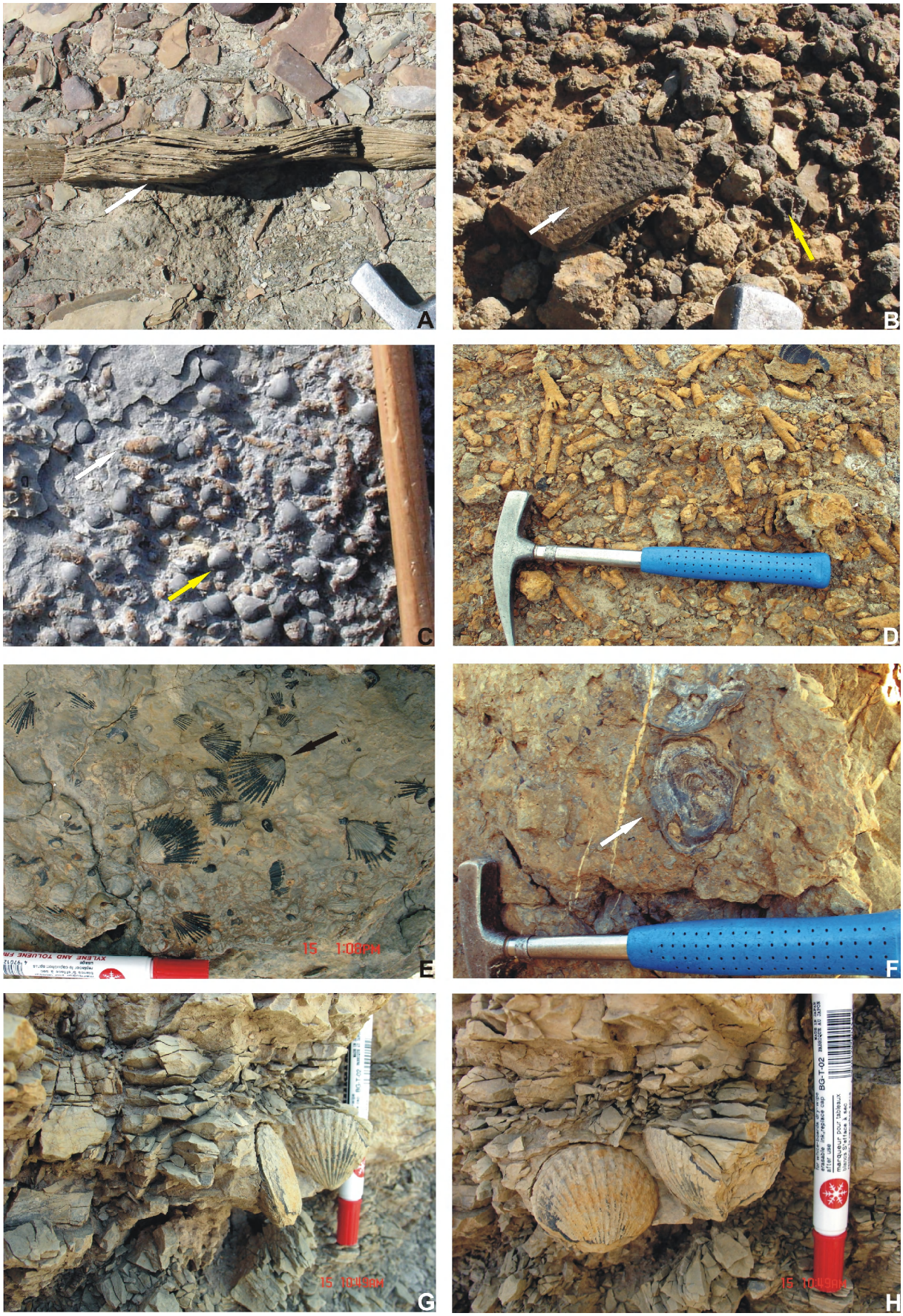

Fig. 5.3.3.

Fig. 5.3.4.

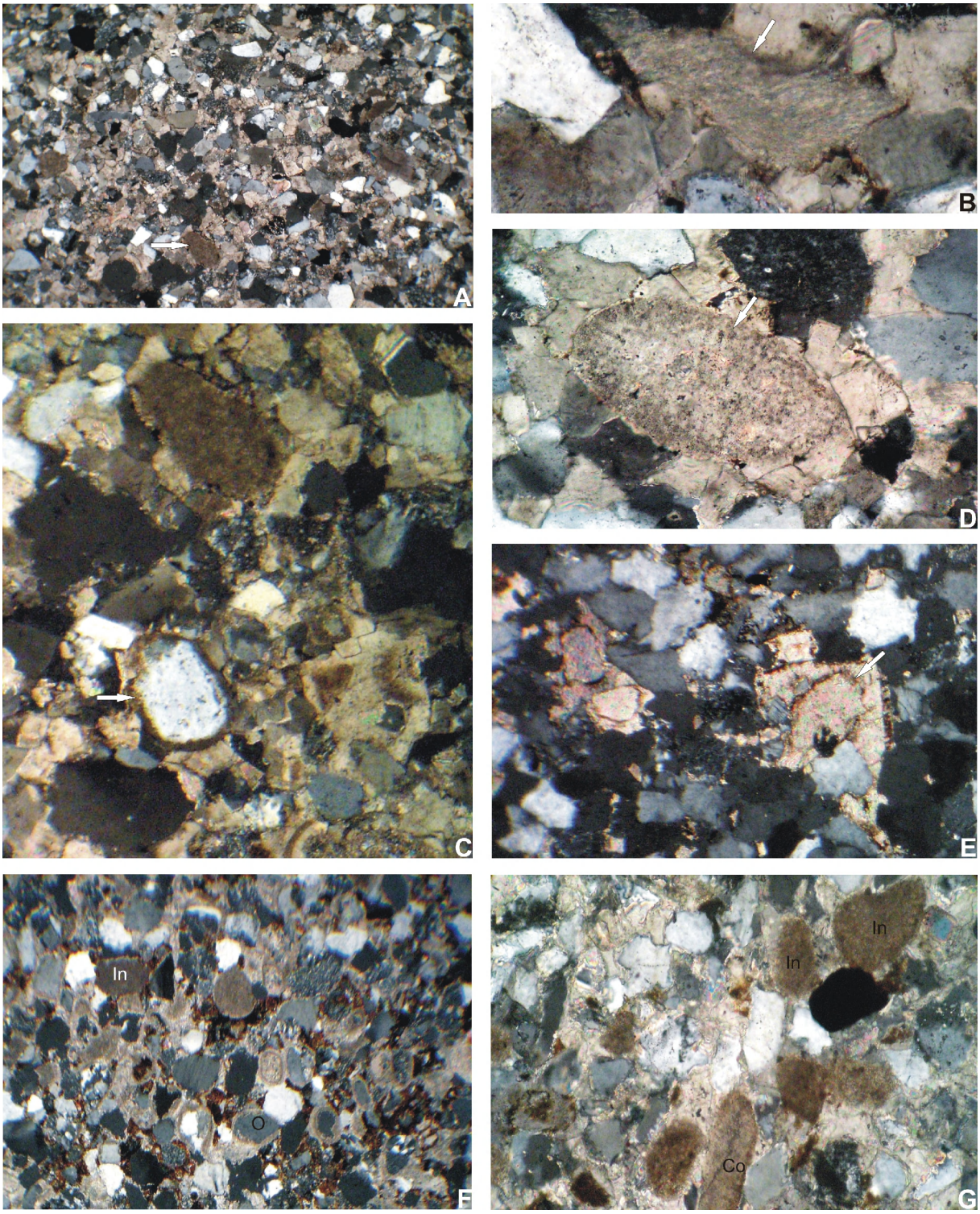

Fig. 5.3.5.

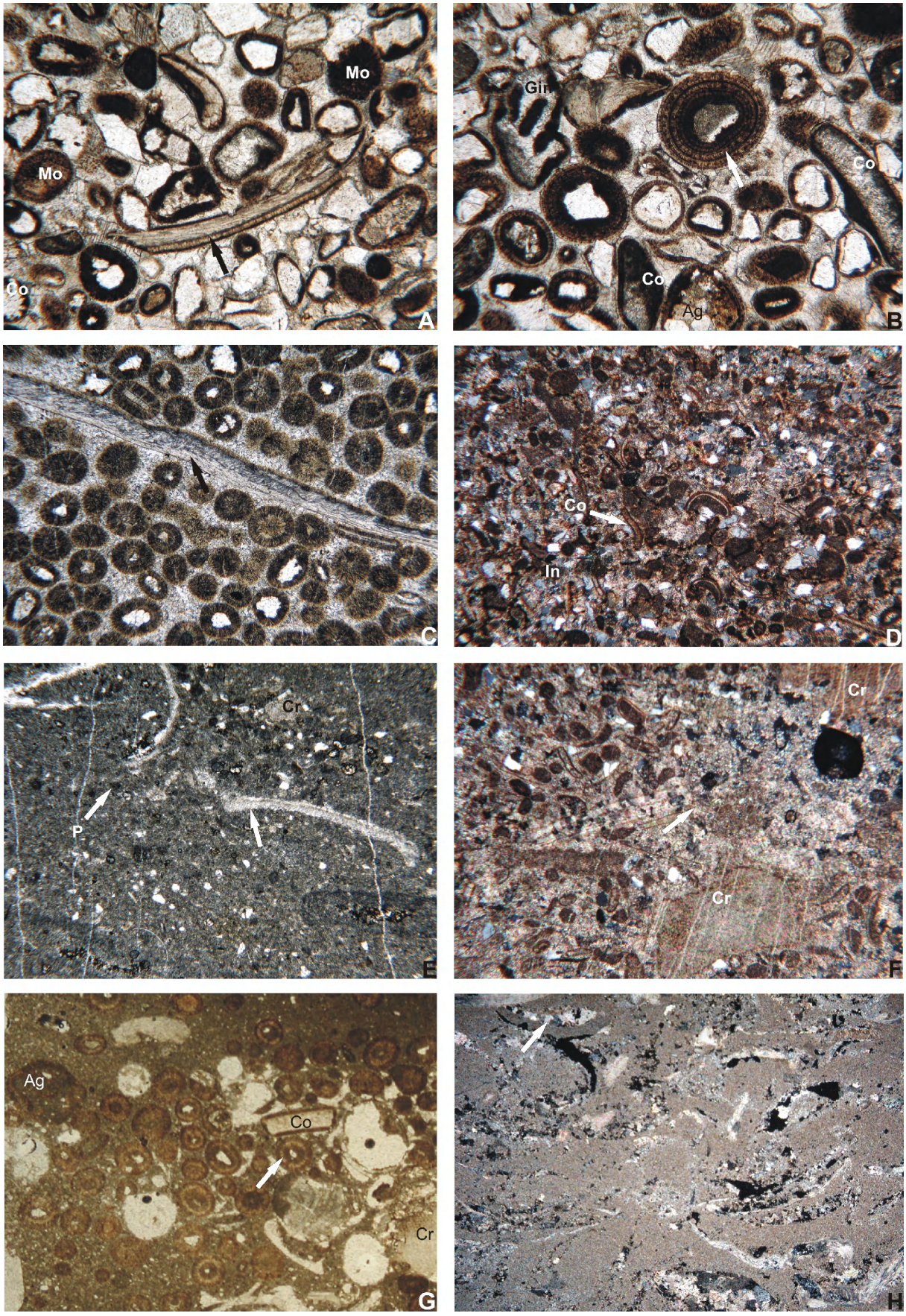

Fig. 5.3.6.

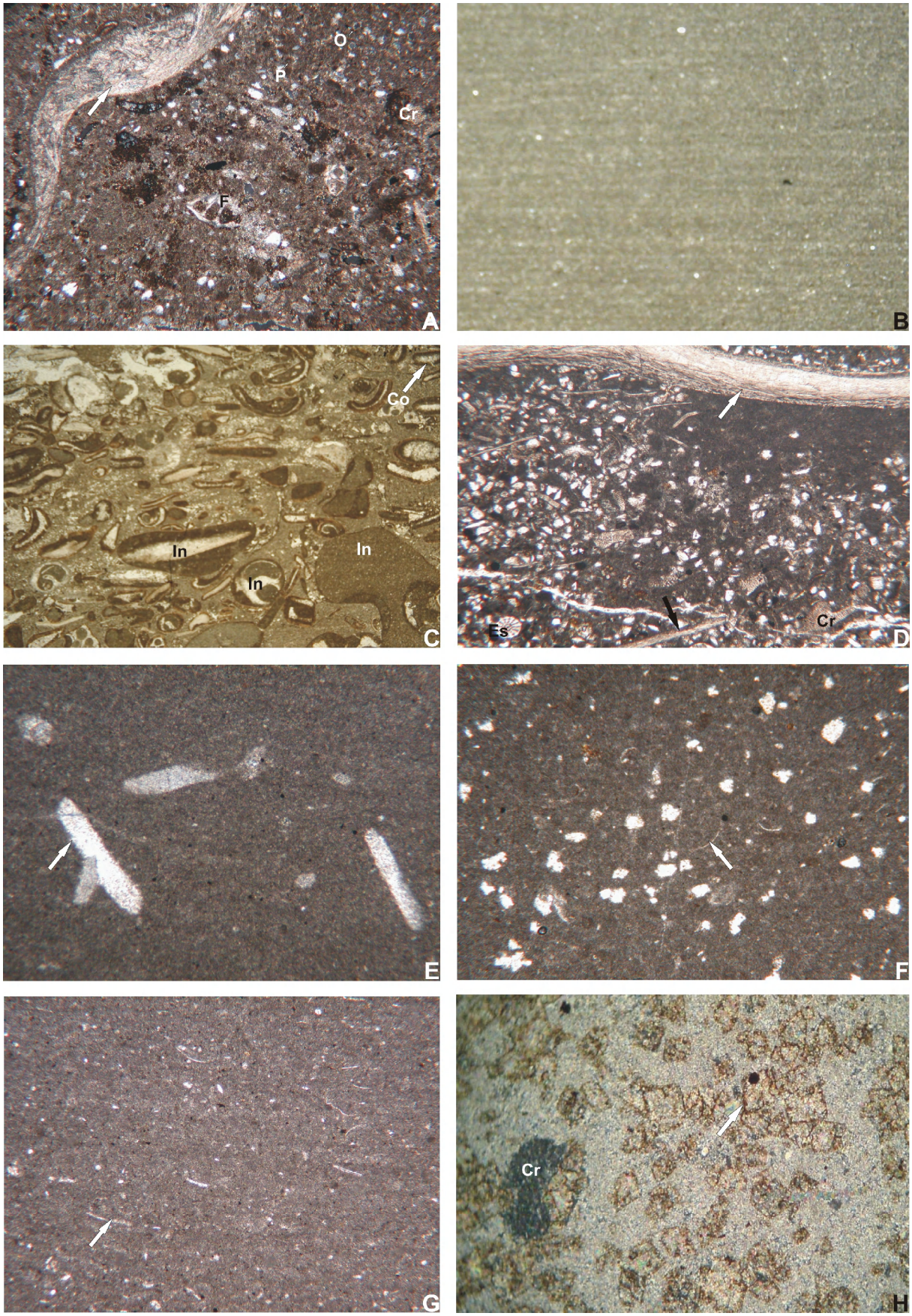

Fig. 5.3.7.

5.4. Qoleh Nar section (co-ordinates: 33° 00′ 49.6′′ N/56° 27′ 11.1 E)

The upper boundary of the Kamar-e-Mehdi Formation (Nar Limestone Member) and the Magu Gypsum Formation of the Garedu Subgroup were measured at Kuh-e-Qoleh Nar, close to the type locality of the Kamar-e-Mehdi Formation (Fig. 5.4.1). The Nar Limestone Member is 75 m thick and is dominated by bindstones, mudstones, and mudstones with gypsum pseudomorphs at the base, and mudstones containing intercalations of rare gypsum pseudomorphs, and gypsiferous marl to silty marl in the middle. Higher up, the member consists of mudstone with a few ostracod shells and intercalations of wacke- to packstone, and mudstones with abundant gypsum pseudomorphs at top. The Nar Limestone Member is overlain disconformably by the Magu Gypsum Formation (at 74 m). The latter consists of red to white gypsiferous silty marl and contains intercalations of packstone (at 87 m), and a calcareous breccia. Higher up, the succession is characterized by alternations of gypsiferous silty marl and gypsum beds with mudstones. Occasionally, the succession turns into dolostone or dolomitic mudstone (at 145 m) and gypsum beds. These facies are followed by siltstone to silty clay. The succession continues with alternations of pack- to grainstone and calcareous sandstone. Higher up (between 255 and 279 m), the latter turns into grainstone. These are followed with conformable contact by green gypsiferous marl (between 280 and 390 m), a few meter-thick alternations of dolomitic mudstone and gypsum, and sandy grainstone (at 403 m). Higher up, thick-bedded to massive gypsum beds (between 410 and 488 m), rudstone, alternations of green gypsiferous marl with thick-bedded gypsum beds (between 489 and 530 m) and red to green gypsiferous marl to silty marl (between 530 and 578 m). In the Qoleh Nar area, the Magu Gypsum Formation is followed with unconformable contact by sandstone of the Lower Cretaceous. Higher up, the basal sandstones turn into grainstone beds containing the foraminifers of *Torremiroella* sp. of Barremian age and *Vercorsella* sp. of the Late Hauterivian.

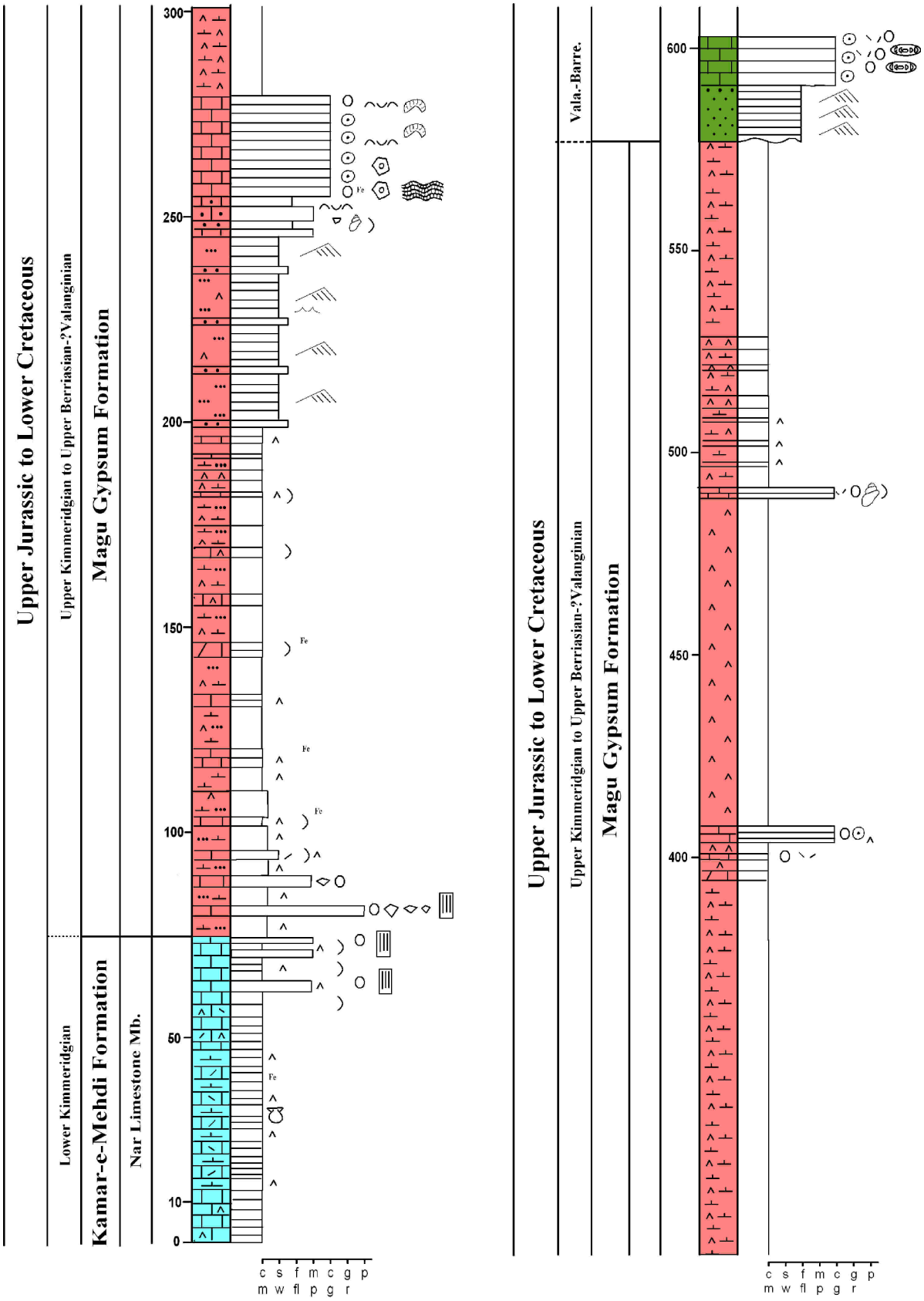

Fig. 5.4.1. Upper part of the Kamar-e-Mehdi Formation (Nar Limestone Member), Magu Gypsum Formation, and the Lower Cretaceous strata (L. Cret.) at Qoleh Nar area. Vala: Valanginian; Barre: Barremian. For key of symbols see Fig. 5.8.16.

Fig. 5.4.2 Features of the Qoleh Nar section. (A) Uppermost part of the Kamar-e-Mehdi Formation (Nar Limestone Member). (B) Disconformable contact (dashed line) between the Nar Limestone Member and the Magu Gypsum Formation. (C) Thin-bedded gypsum beds within gypsiferous silty marls of the lower part of the Magu Gypsum Formation. (D) Herringbone cross-laminated calcareous sandstone (white arrows) and small erosional surfaces (black arrow), middle part of the Magu Gypsum Formation. (E) Aspect of the Nar Limestone Member, Magu Gypsum Formation and Lower Cretaceous. GSM: Gypsiferous silty marl with intercalations of breccia conglomerate, gypsum, mudstone and wacke- to packstone; OGS: calcareous sandstones, packstones and grainstones; GM: Gypsiferous marls with a few intercalated dolomitic mudstone, gypsum, and oo-grainstone beds at top; G: Thick-bedded to massive gypsum beds with a few meters-thick rudstone at top; MSM: Gypsiferous marl to silty marl. (F-G) Cross-laminated sandstone bed (F) and asymmetrical to symmetrical wave ripples. From base to top the symmetrical wave ripples increase. Lowermost part of the Lower Cretaceous (G).

Fig. 5.4.3 Thin-sections of various types of microfacies of the Nar Limestone Member and lower part of the Magu Gypsum Formation. (A) Mudstone with rare gypsum pseudomorphs, lower part of the Nar Limestone Member (sample p-55; width of photomicrograph: 2.5 mm). (B) Very faintly laminated bindstone, lower part of the Nar Limestone Member (sample p-56; width of photomicrograph: 2.5 mm). (C) Mudstone with a few ostracod shells (white arrow), middle to upper part of the Nar Limestone Member (sample p-61; width of photomicrograph: 2.5 mm). (D-E) Photomicrographs of pel-wacke- to packstone containing longitudinal (D) and cross-section (E) of a crustacean coprolite (white arrows); upper part of the Nar Limestone Member (sample p-63; width of photomicrographs: 2.5 mm). (F) Mudstone with abundant gypsum pseudomorphs, uppermost part of the Nar Limestone Member (sample p-64; width of photomicrograph: 2.5 mm). (G) Intra-packstone with gypsum pseudomorphs, lower part of the Magu Gypsum Formation (sample p-66; width of photomicrograph: 2.5 mm). (H) Calcareous breccia. Note that the components are mostly derived from the Nar Limestone, lower part of the Magu Gypsum Formation (sample p-67; width of photomicrograph: 10 mm).

Fig. 5.4.4 Thin-sections of various types of microfacies of the Nar Limestone Member and lower part of the Magu Gypsum Formation. (A) Silty mudstone with rare ostracod shells (white arrow) and signs of meiofaunal bioturbation, lower to middle part of the Magu Gypsum Formation (sample p-72; width of photomicrograph: 2.5 mm). (B) Gypsiferous mudstone with abundant gypsum pseudomorphs and some ostracod shells (white arrow), lower to middle part of the Magu Gypsum Formation (sample p-68; width of photomicrograph: 2.5 mm). (C-D) Sandy bio-intra-pack- to grainstone. Note bryozoans (Br), intraclasts (In), shell fragment (arrowed), and crinoid (Cr) in a microsparry cement, middle part of the Magu Gypsum Formation (sample p-79; width of photomicrographs: 10 mm (C) and 2.5 mm (D)). (E-F) Bio-oo-grainstone under polarized light. Note spherical and some ellipsoidal ooids with mainly thick radial cortex (arrowed) and a crinoid (Cr) in a syntaxial carbonate cement, middle part of the Magu Gypsum Formation (sample p-76; width of photomicrographs: 3 mm (E) and 0.8 mm (F)). (G) Sandy oo-grainstone with thin cortex and large nucleus, middle to upper part of the Magu Gypsum Formation (sample p-180; width of photomicrograph: 10 mm). (H-J) Intra-cortoid-rudstone. Note cortoids (Co), aggregate grains (Ag), benthic foraminifers (Fo), intraclasts (In) and gastropod (G), upper part of the Magu Gypsum Formation (sample p-181; width of photomicrographs: 5 mm (H), 2.5 mm (I) and 5 mm (J)).

Fig. 5.4.5 Thin-sections of microfacies of the Lower Cretaceous. (A) Photomicrograph from a basal fine- to medium-grained feldspathic sandstone of the Lower Cretaceous. (B-C) Photomicrographs from a grainstone bed with foraminifers of *Torremiroella* sp. (B) and *Vercorsella* sp. (C).

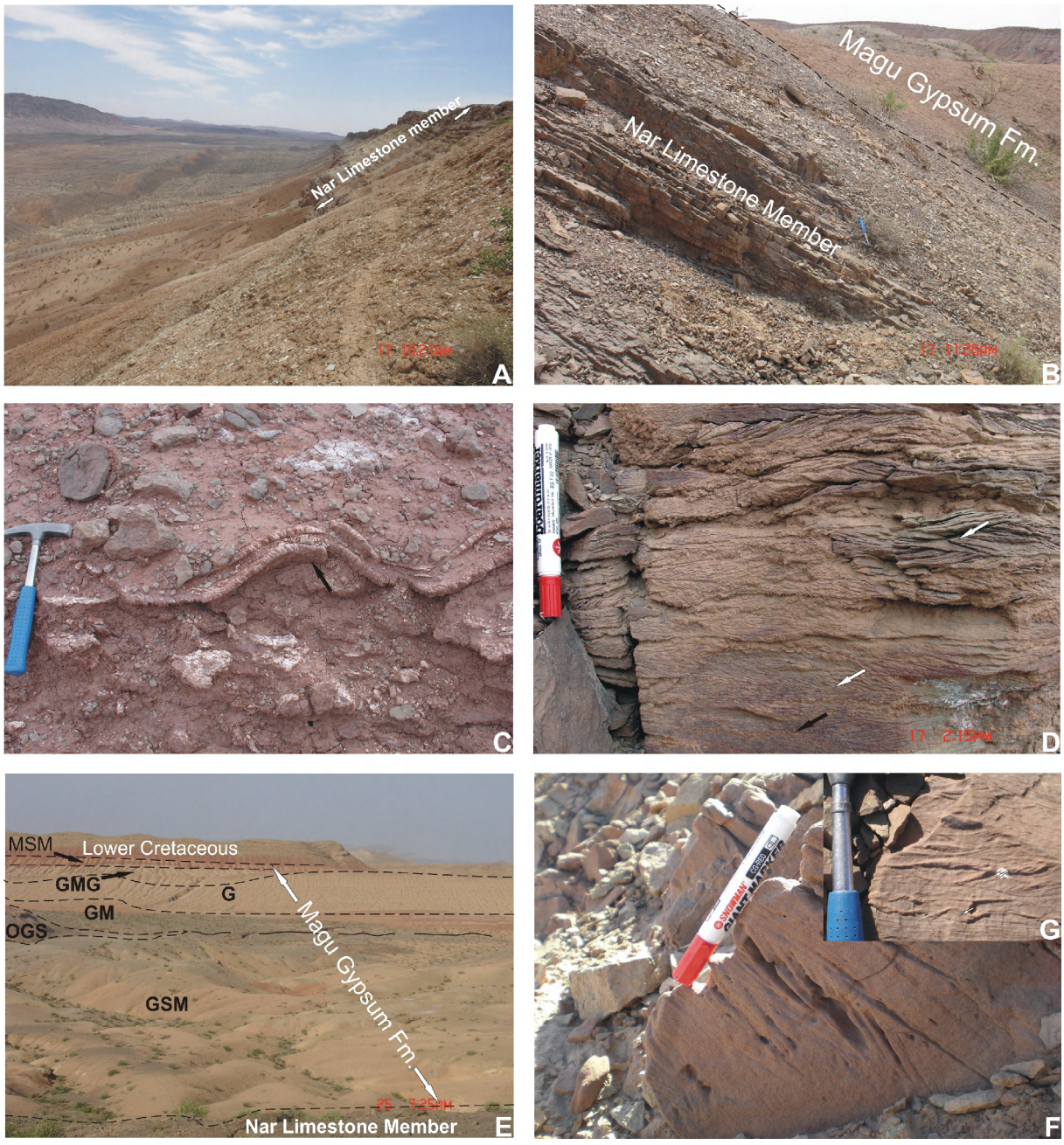
Nar Limestone member
A
Magu Gypsum Fm.
Nar Limestone Member
B
C
D
MSM
Lower Cretaceous
GMG
G
GM
OGS
GSM
Magu Gypsum Fm.
Nar Limestone Member
E
G
F

Fig. 5.4.2

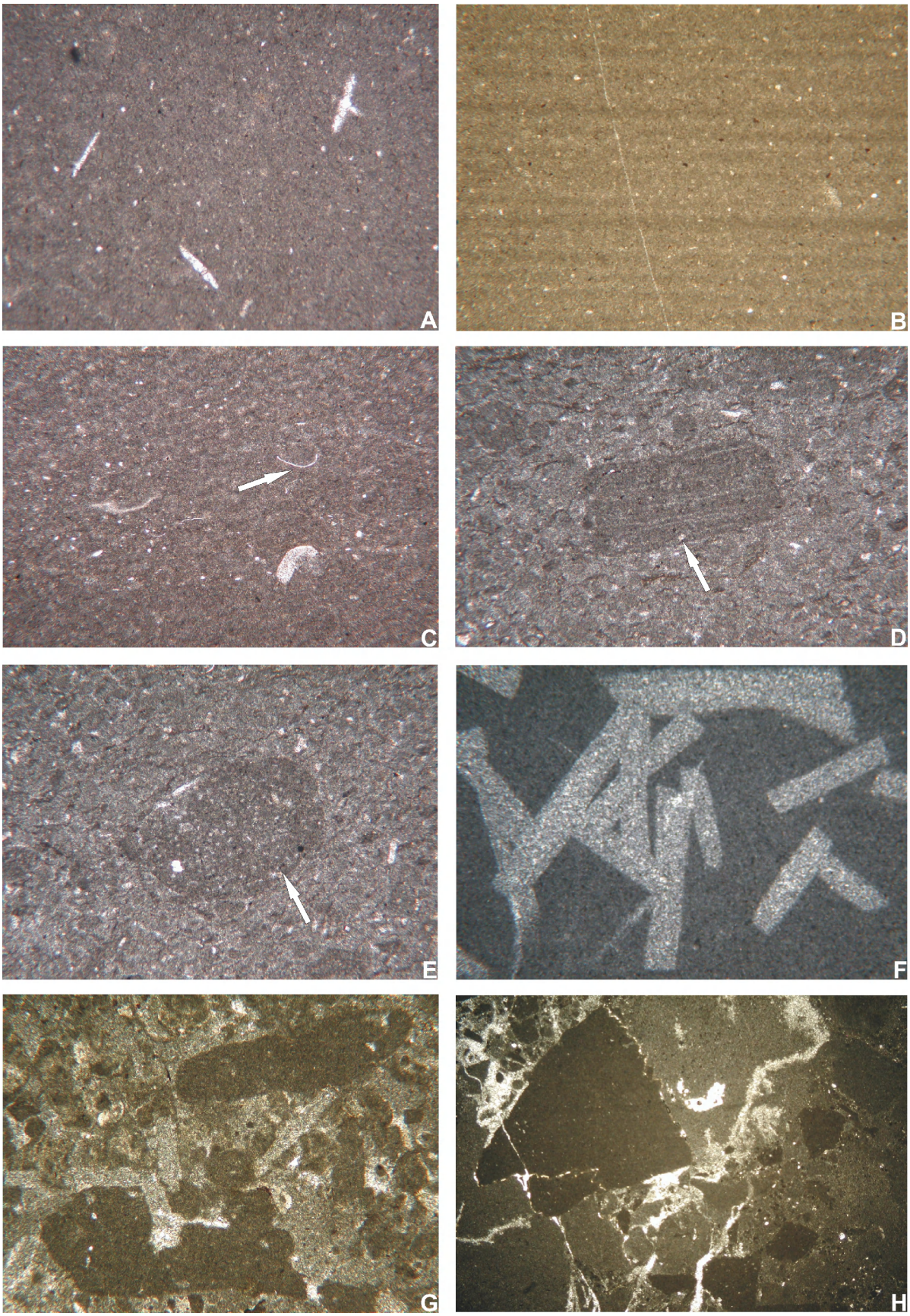

Fig. 5.4.3

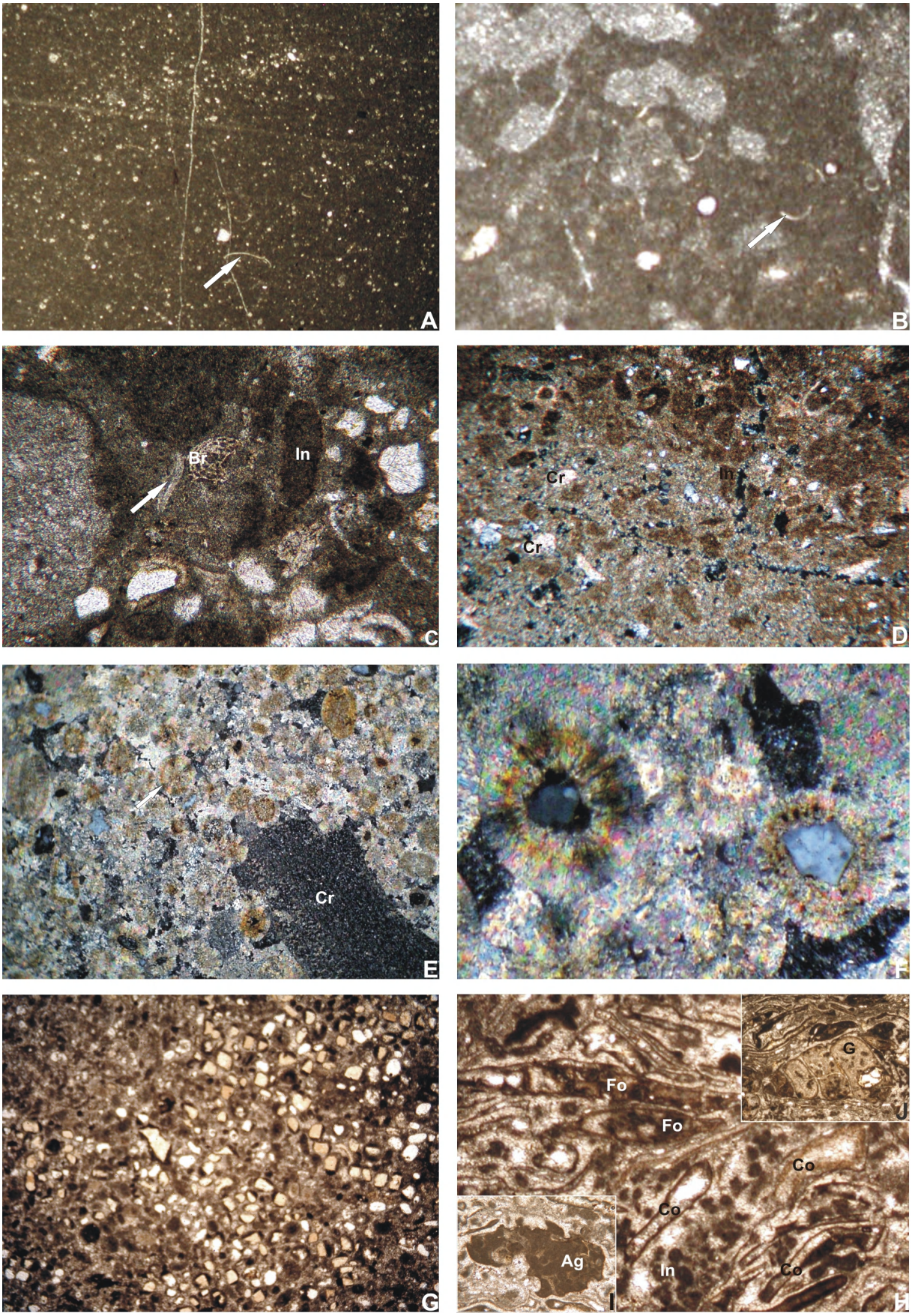

Fig. 5.4.4

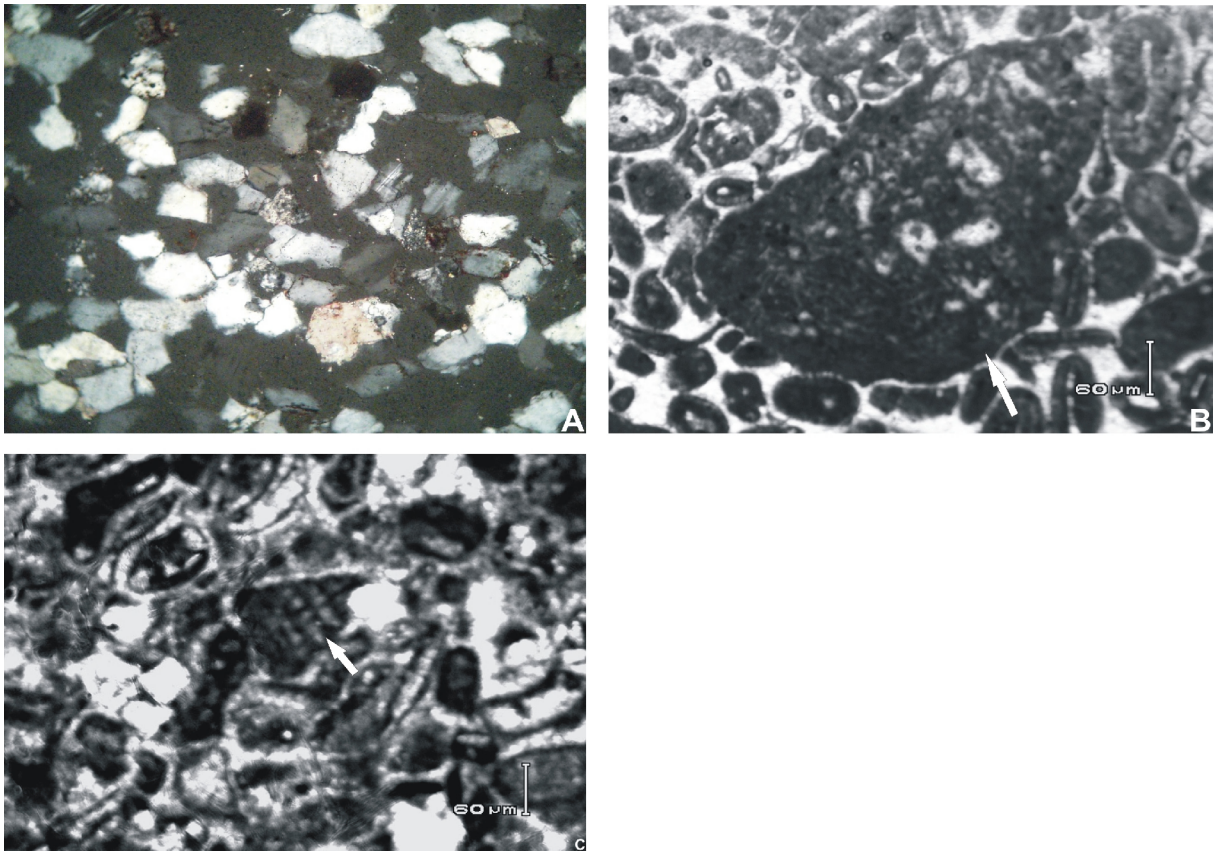

Fig. 5.4.5

5.5. Abdoughi section (co-ordinates: 32° 57′ 23.6′′ N/56° 41′ 48.9 E)

In the Abdoughi section the top 83 m of the Baghamshah Formation and the basal part of the Kamar-e-Mehdi Formation were measured (Fig. 5.5.1). The former consists of calcareous sandstone with intercalated silt to silty clay, which overlie, with sharp base, silty marl with intercalations of sandstone beds. Their age is Middle Jurassic based on the foraminifer *Lenticulina subalata*. The uppermost part of the Baghamshah Formation is overlain, with unconformable contact, by a thick, medium- to coarse-grained calcareous sandstone of the Kamar-e-Mehdi Formation (at 83 m). Higher up, this facies laterally grades into conglomerate and calcareous sandstone (between 119 and 125 m). The succession is followed by alternations of fine- to coarse-grained calcareous sandstone (between 126 and 143 m), in which very thin interlayers of gypsum beds occur. Higher up, alternations of gypsiferous silty clay to silty marl with intercalated sandstones occur. The latter turn into the characteristic siliciclastic-carbonate rocks of the Kamar-e-Mehdi Formation.

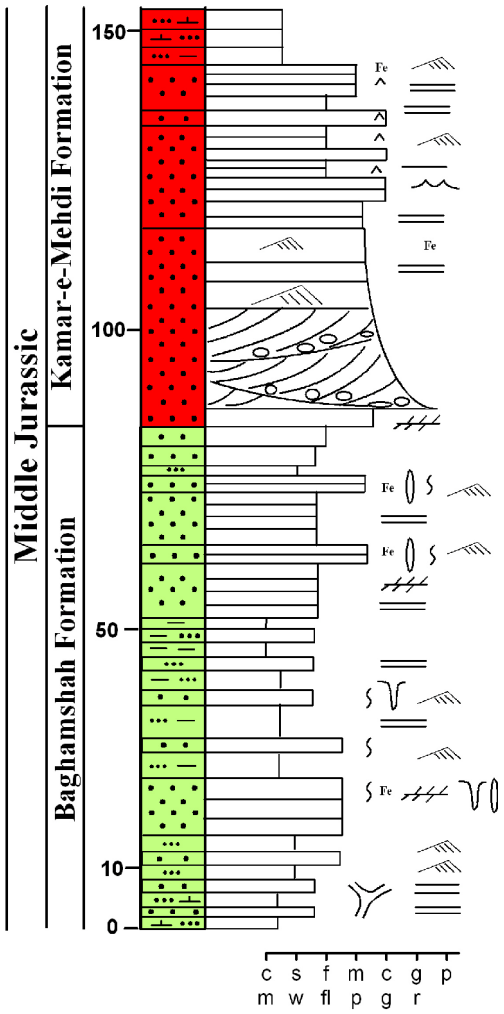

Fig. 5.5.1. Top part of the Baghamshah Formation and base of the Kamar-e-Mehdi Formation at Abdoughi. Note the unconformable contact between the two formations. For key of symbols see Fig. 5.8.16.

Fig. 5.5.2 Sedimentary and ichnological features of the Abdoughi section. (A) Small-scale coarsening-upward cycles of silt and silty clay at base into calcareous sandstone at top; uppermost part of the Baghamshah Formation. (B). Calcareous sandstone with wedge-shaped cross-bedding (arrowed) at 16 m of the measured section; uppermost part of the Baghamshah Formation. (C) Planar cross-stratified calcareous sandstone at 22 m; uppermost part of the. Baghamshah Formation. (D) Paired openings of *Diplocraterion* or *Arenicolites* (arrowed) on bedding plane, at 22 m; uppermost part of the Baghamshah Formation. (E) Calcareous sandstone with *Skolithos* (arrowed) at 75 m; uppermost part of the Baghamshah Formation. (F) Sandstone with trace fossil *Thalassinoides* (arrowed) at 2 m; uppermost part of the Baghamshah Formation. (G) Planar cross-laminated calcareous sandstone of the basal Kamar-e-Mehdi Formation. (H) Trough cross-bedded conglomerate at the base of the Kamar-e-Mehdi Formation.

Fig. 5.5.3 Features of the Abdoughi section. (A-B) Horizontal- to wave ripple-laminated calcareous sandstone (A) containing very thin interlayers of gypsum (B; arrowed); lower part of the Kamar-e-Mehdi Formation. (C) Alternations of gypsiferous silty clay to silty marl and red to brown, strongly weathered cross-stratified calcareous or feldspathic sandstone; lower part of the Kamar-e-Mehdi Formation. (D) Unconformable contact (dashed line) between the uppermost part of the Baghamshah Formation and the Kamar-e-Mehdi Formation (D), (D1) The foraminifer "*Lenticulina subalata*" from the upper part of the Baghamshah Formation (length 75 μm).

Fig. 5.5.4 Abdoughi section. Thin-sections of various types of microfacies. (A) Lithic sandstone. Note some carbonate grain (Ce); uppermost part of the Baghamshash Formation (sample p-160; width of photomicrograph: 1.3 mm). (B) Basal feldspathic sandstone of the Kamar-e-Mehdi Formation. Note a few siliciclastic (Lm), carbonate (Ce) and chert fragments (Ch) (sample p-171; width of photomicrograph: 1.5 mm). (C) Conglomerate, lowermost part of the Kamar-e-Mehdi Formation (sample p-169; width of photomicrograph: 3 mm). (D) Subarkose. Note some carbonate (Ce), chert (Ch) and siliciclastic fragments (Lm); lower part of the Kamar-e-Mehdi Formation (sample p-172; width of photomicrograph: 2.5 mm). (E) Feldspathic sandstone. Note carbonate grain (Ce), siliciclastic grain (Se), chert (ch) and the feldspar microcline (arrowed); lower part of the Kamar-e-Mehdi Formation at 130 m (sample p-174; width of photomicrograph: 1.5 mm). (F) Feldspathic sandstone. Note a few cherts (Ch) and siliciclastic fragments (Lm), lower part of the Kamar-e-Mehdi Formation at 148 m (sample p-173; width of photomicrograph: 1.5 mm).

Fig. 5.5.2.

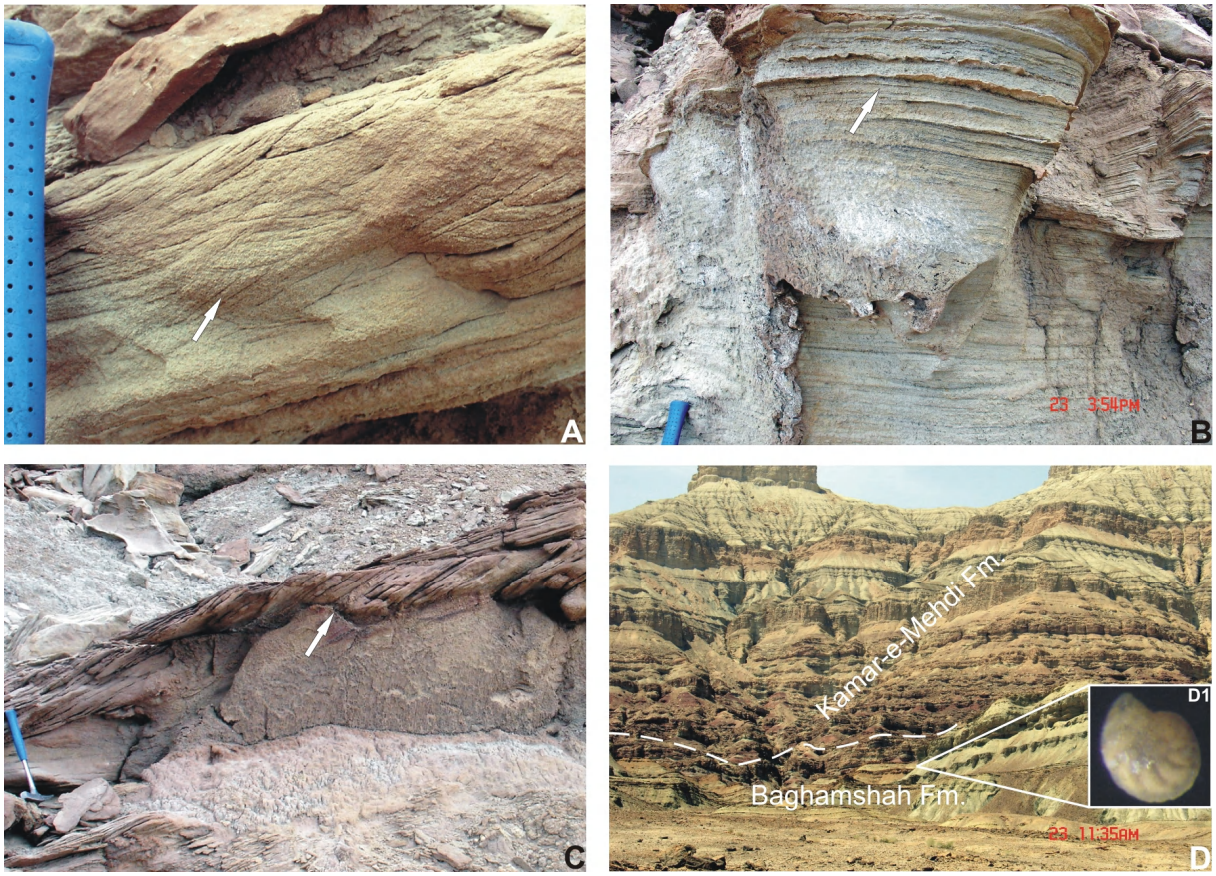

Fig. 5.5.3.

5.6. Ravar section (co-ordinates: 31° 09′ 20.3′′ N/56° 46′ 31.4 E)

In the Ravar area (Fig. 5.6.1), the top 14 m of the Hojedk Formation are characterized by alternations of silty shale to siltstone, quartz sandstone, calcareous sandstone with intercalations of bioturbated sandstones, and shell beds. The Hojedk Formation is overlain with unconformable contact by a 50 cm thick basal conglomerate of the Parvadeh Formation. The latter is followed by 35 m thick alternations of calcareous sandstone and marl with intercalated sandy wackestones. This facies is followed by irregular alternations of calcareous sandstone and grainstone with intercalations of rudstones. In the uppermost part of the Parvadeh Formation, grainstone and rudstone with oysters occur, which are conformably overlain by the Baghamshah Formation (at around 122 m). The latter starts with several coarsening- and thickening-upward cycles of silty clay at base and sandstone beds at top with intercalations of bioturbated intervals (between 122 and 254). Higher up calcareous sandstone occurs, containing rare intercalations of silty marl.

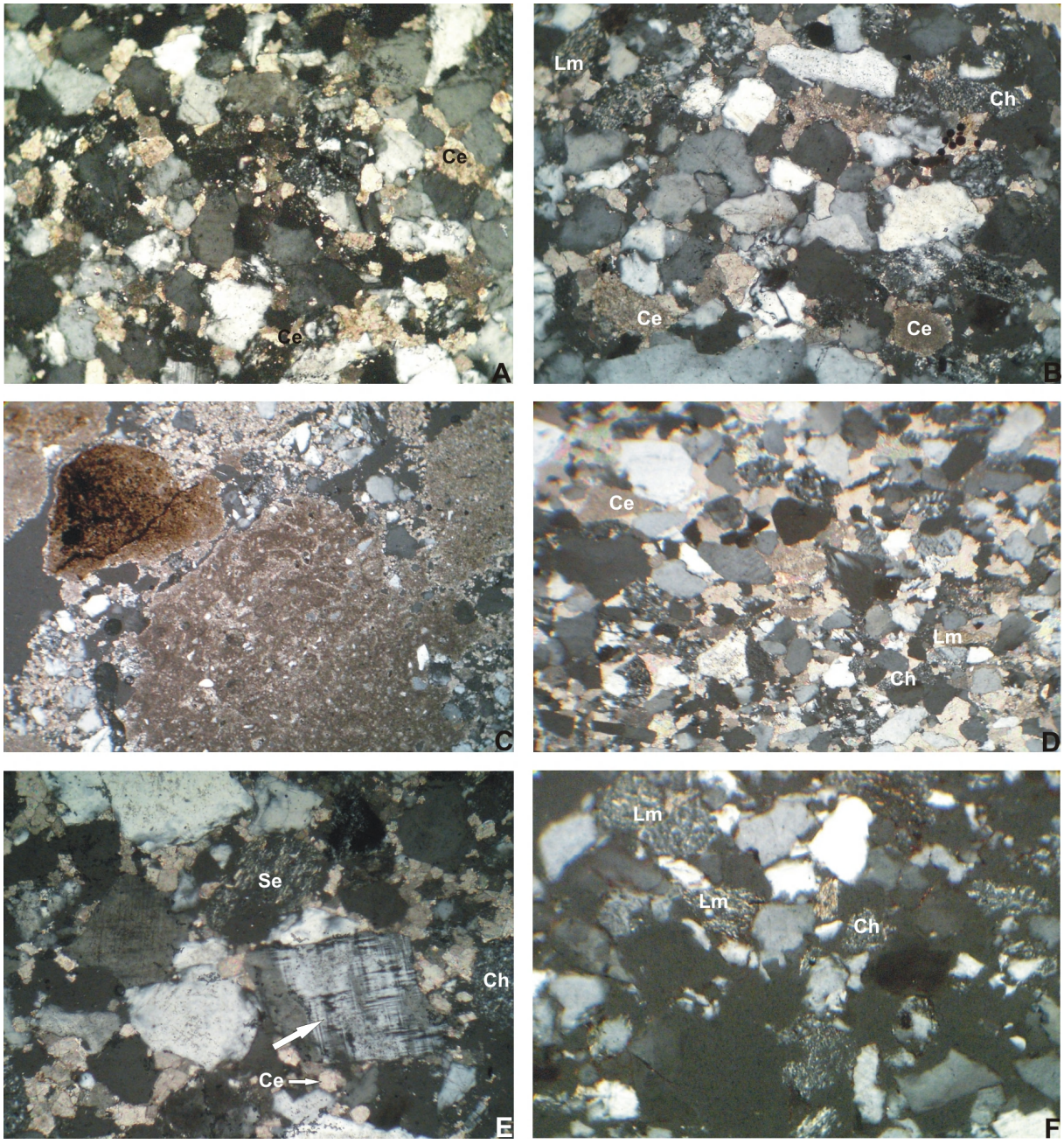

Fig. 5.5.4.

This facies turns into sandstone (at 275 m) and gypsiferous silty clay containing intercalations of sandstone and occasionally rudstone (Fig. 5.6.1). The boundary of the Baghamshah Formation with the basal sandstone of the Kamar-e-Mehdi Formation is unconformable. The sandstones are followed by several 10 m of gypsiferous marl to silty clay (sometimes thick-bedded gypsum beds) with intercalations of sandstones, rudstones, and grainstones (between 383 and 511 m). The succession is followed by a 162 m thick package of nodular, thin- to thick-bedded, wacke- to floatstones at base, mudstones containing intercalations of marl and wacke- to floatstone, silty mudstone, packstone, gypsiferous mudstone, wackestone, dolomitic

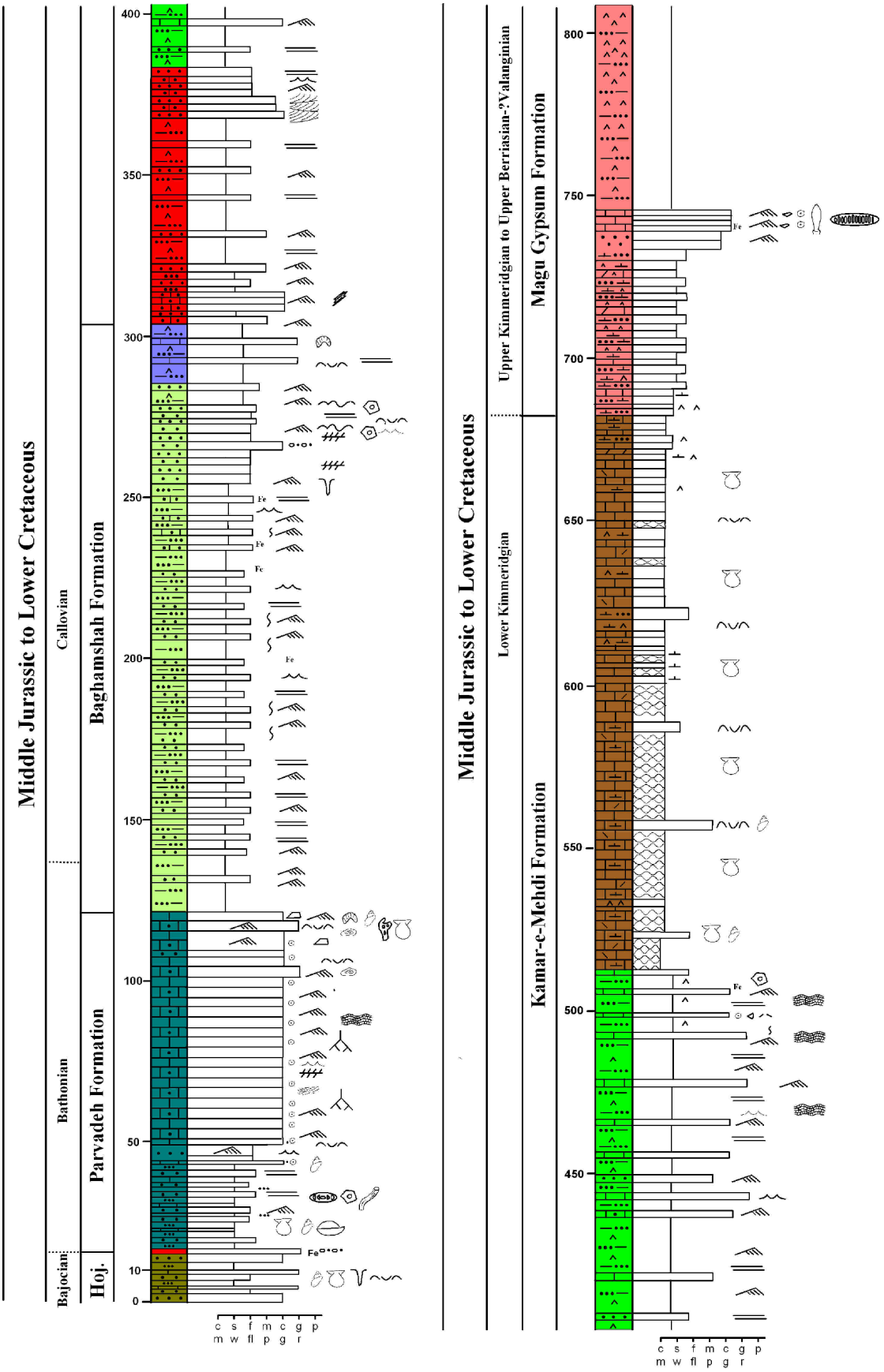

Fig. 5.6.1. Section of the Hojedk (Hoj), Baghamshah, Kamar-e-Mehdi, and Magu Gypsum formations in the Ravar area. For key of symbols see Fig. 5.8.16.

Mudstone, and gypsum beds. At 683 m, the Kamar-e-Mehdi Formation is followed by the Magu Gypsum Formation. The latter consists of alternations of silty marl to silty clay, mudstone to dolomitic mudstone containing intercalations of gypsum beds at base, red to brown sandstone, grainstone with dasycladacean green algae ("*Clypeina jurassica*" of Upper Kimmeridgian to Upper Berriasian age). Alternations of gypsiferous silty clay and thick-bedded gypsum beds occur in the uppermost part of the Magu Gypsum Formation, which forms the core of a syncline (Fig. 5.6.6B). In the Ravar area, the Jurassic rocks are overlain by Lower Cretaceous rocks (Aptian-Albian) with angular unconformity.

Fig. 5.6.2 Ravar section. (A) Alternations of silty shale to siltstone and calcareous sandstone of the Hojedk Formation. Note shell beds with bivalves (A1, A2) and high- spired nerineid gastropod (A3, A4). (B) Low-angle bi-directional cross-laminated calcareous sandstone; uppermost part of the Hojedk Formation. (C-D) *Arenicolites* (arrowed) in calcareous sandstone (C) and paired openings of *Arenicolites* (arrowed) on bedding plane (D); uppermost part of the Hojedk Formation. (E-F, F1) Basal conglomerate of the Parvadeh Formation (Cgl: E). Note also gastropods (G) as component pointing to a marine setting. (G) Field aspect of siliciclastic-carbonate rocks of lower part of the Parvadeh Formation. (H) Bi-directional cross-laminated calcareous sandstone; lower part of the Parvadeh Formation (at 44 m).

Fig. 5.6.3 Ravar section. (A) The trace fossil *Chondrite*s on lower surface; lower to middle part of the Parvadeh Formation. (B-C) Small- (B)- and large scale (C) planar cross-stratified calcareous sandstone to grainstone beds; middle to upper part of the Parvadeh Formation. (D) Weathered oncoid limestones (arrowed), upper part of the Parvadeh Formation. (E) Thin-bedded shell beds with abundant oyster fragments on bedding plane; uppermost part of the Parvadeh Formation. (F) Conformable contact (man marker) between the Parvadeh Formation (left) and the Baghamshah Formation (right) (at around 122 m). (G-H) Large-scale uni- (G) and bi-directional (H) cross-stratified calcareous sandstone beds. Note the mud- or sandstone clasts on the erosional surface (arrowed); Upper part of the Baghamshah Formation (between 254 and 265 m).

Fig. 5.6.4 Ravar section. Features of the Baghamshah Formation. (A-B) Trough cross-bedding (A), bi-directional bundled wave ripples, which towards top turn into current ripples (climbing ripples: arrowed) (B). (C) Bedding-plane view of weathered sub-parallel ripples (black arrow); upper part of the formation. (D-E) Erosional structure such as scour filled with pebbles (D), and concretions (E: arrowed) at the base of large-scale planar-cross stratified calcareous sandstone (see also Fig. 5.6.3G); upper part of the formation. (F-G) Horizontal lamination (F), and oscillation ripples on bedding plane (G); upper part of the formation. (H-H1) Coarsening-upward cycles of gypsiferous silty clay to silty marl with intercalations of thick laminated to thin-bedded sandstone and thin-bedded oyster-rudstones (H1) at base grading into cross-stratified sandstone beds at top; upper part of the Baghamshah Formation.

Fig. 5.6.5 Ravar section. (A-B) Climbing (A) and bi-directional cross-laminated wave ripples (B) in sandstone; lowermost part of the Kamar-e-Mehdi Formation. (C) Wood pieces in sandstone; lower part of the Kamar-e-

Mehdi. Formation. (D) Gypsiferous marl to silty clay (sometimes thick-bedded gypsum beds) with intercalations of limestones such as bio-rudstone and oo-grainstone; lower to middle part of the Kamar-e-Mehdi Formation. (E) Oo-grainstone with tectonic fractures on bedding plane; lower to middle part of the Kamar-e-Mehdi Formation. (F) Basal intra-bio-wacke- to floatstone (at hammer) of the Kamar-e-Mehdi Formation which overlies gypsum bed of the uppermost part of mixed siliciclastic-carbonate rocks of the formation. (G) Thin shell bed at top of a coarsening-upward cycle; Kamar-e-Mehdi Formation. (H) Basal cross-stratified calcareous sandstones to oo-grainstones of the Magu Gypsum Formation.

Fig. 5.6.6 Ravar section. (A) Thick-bedded oolitic limestone; middle part of the Magu Gypsum Formation. (B) Alternations of gypsiferous silty clay and thick-bedded gypsum, uppermost part of the Magu Gypsum Formation, forming core of a syncline.

Fig. 5.6.7 Ravar section. Thin-sections of various types of microfacies. (A) Quartz sandstone. Note few chert (Ch) and fine-grained siliciclastic rock fragments (Se); uppermost part of the Hojedk Formation (sample m-43; width of photomicrograph: 1 mm). (B) Calcareous sandstone. Note a few rounded siliciclastic rock fragments (Se); uppermost part of the Hojedk Formation (sample m-45; width of photomicrograph: 0.5 mm). (C-D) Basal conglomerate of the Parvadeh Formation (C), note shell mould (probably bivalve) filled with neomorphic spar (B) and superficial ooids (D: arrowed), sample m-45 (A); width of photomicrograph: 3 mm (C), 0.5 mm (D). (E) Sandy bio-wackestones. Note the foraminifer "*Lenticulina*" (Fo) and crinoid ossicle (Cr); lower part of the Parvadeh Formation (sample m-47; width of photomicrographs: 0.5 mm (D), 0.5 mm (E)). (F) Micaceous feldspathic sandstone. Note some detrital muscovite grains (Mus); lower part of the Parvadeh Formation (samples m-48, K-137; width of photomicrograph: 1 mm). (G) Sandy bio-oo-grainstone with a few cortoid grains (Co) and bryozoan debris (Br); middle part of the Parvadeh Formation (sample k-140; width of photomicrograph: 5 mm). (H) Well sorted oo-grainstone. Note superficial ooids (sample k-141; width of photomicrograph: 1.5 mm).

Fig. 5.6.8 Ravar section. Thin-sections of various types of microfacies. (A) Onco-rudstone. Note bryozoans (Br), crinoid (Cr), calcareous sponge (Sp) and shell fragment (B) as nuclei of the oncoids; upper part of the Parvadeh Formation (sample k-145; width of photomicrograph: 10 mm). (B) Sandy onco-bio-rudstone. Note large bored shell fragment encrusted by bryozoans (black arrow) and serpulids (white arrow); upper part of the Parvadeh Formation (sample k-148; width of photomicrograph: 10 mm). (C) Feldspathic sandstone with interlocking grains; Lower part of the Baghamshah Formation (sample k-152; width of photomicrograph: 1.5 mm). (D) Ferruginous feldspathic sandstone; lowermost part of the Kamar-e-Mehdi Formation (sample k-157; width of photomicrograph: 0.5 mm). (E) Calcareous sandstone. Note some intraclasts (In); Lower part of the Kamar-e-Mehdi Formation (sample k-159; width of photomicrograph: 2.7 mm). (F) Oyster-rudstone; upper part of the Baghamshah Formation (sample m-40; width of photomicrograph: 3 mm). (G) Lithic feldspathic sandstone. Note a carbonate rock fragment (Ce); upper part of the Baghamshah Formation (in gypsiferous silty clay to marl) (sample m-35; width of photomicrograph: 0.5 mm).

Fig. 5.6.9 Ravar section. Thin-sections of various types of microfacies. (A, A1, B) Calcareous sandstone. Note shell (B) and crinoid (Cr: arrow) fragments in a syntaxial cement; upper part of the Baghamshah Formation (sample m-34; width of photomicrographs: 0.5 mm). (C) Oo-grainstone. Note cortex with radial structures and bryozoan fragments (Br); lower part of the Kamar-e-Mehdi Formation (sample m-39; width of photomicrograph: 0.7 mm). (D) Bio-wacke- to floatstone; lower part of the Kamar-e-Mehdi Formation. Note shell fragments (B), crinoid (Cr), and bryozoan fragments (Br) (sample k-56; width of photomicrograph: 1 mm). (E) Bio- wacke- to floatstone; lower to middle part of the Kamar-e-Mehdi Formation (sample k-176; width of photomicrograph: 5 mm). (F) Silty mudstone; Kamar-e-Mehdi Formation (sample k-179; width of photomicrograph: 10 mm). (G) Intra-packstone within coarsening-upward cycle of the Kamar-e-Mehdi Formation (sample k-180; width of photomicrograph: 5 mm). (H) Mudstone with gypsum pseudomorphs; middle part of the Kamar-e-Mehdi Formation (sample k-184; width of photomicrograph: 5 mm).

Fig. 5.6.10 Ravar section. Thin-sections of various types of microfacies. (A) Bio-wackestone, upper part of the Kamar-e-Mehdi Formation (sample k-188; width of photomicrograph: 2 mm). (B) Calcareous feldspathic sandstone of middle part of the Magu Gypsum Formation (sample k-172; width of photomicrograph: 0.5 mm). (C) Intra-cortoid-grainstone. Note dasycladacean green algae Clypeina jurassica ? (black arrow), fragment of dasycladacean (Da), cortoid grain (Co) and intraclast (In); middle part of the Magu Gypsum Formation (sample k-52; width of photomicrograph: 1.5 mm). (D) Bio-grainstone. Note echinoid plate (Ep), echinoid spine (Es), and intraclast (In); middle part of the Magu Gypsum Formation (sample k-173; width of photomicrograph: 2.5 mm).

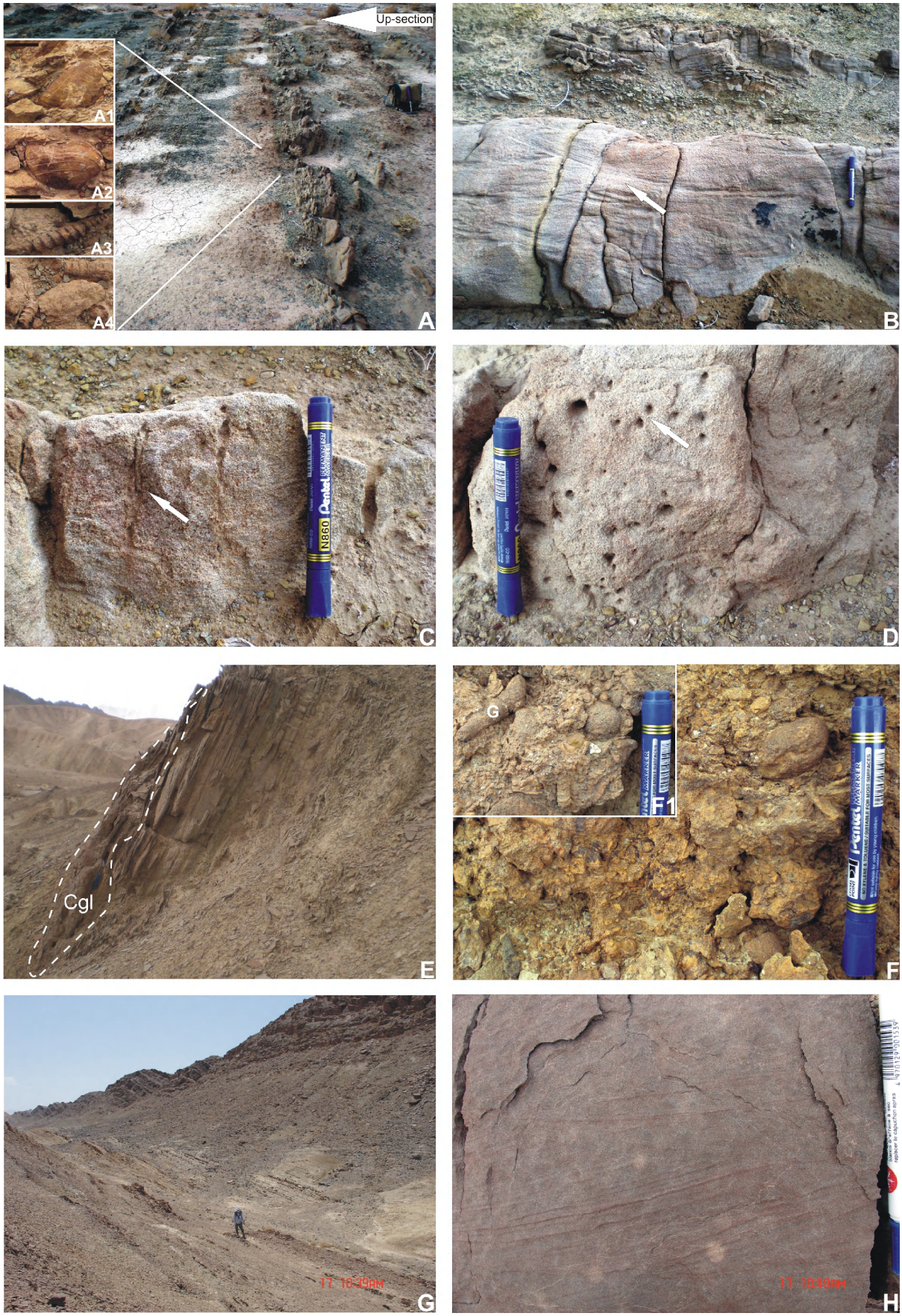

Fig. 5.6.2

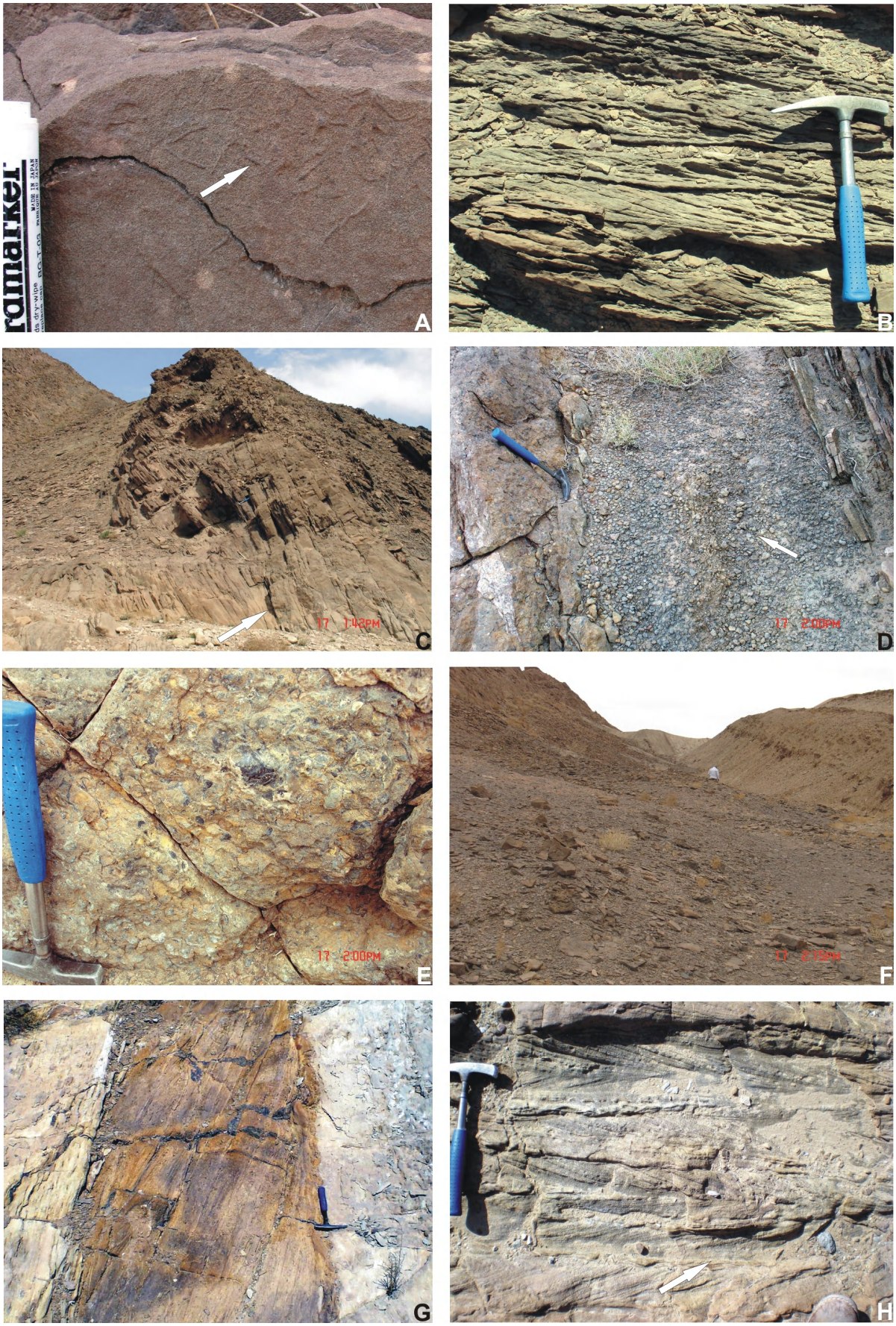

Fig. 5.6.3

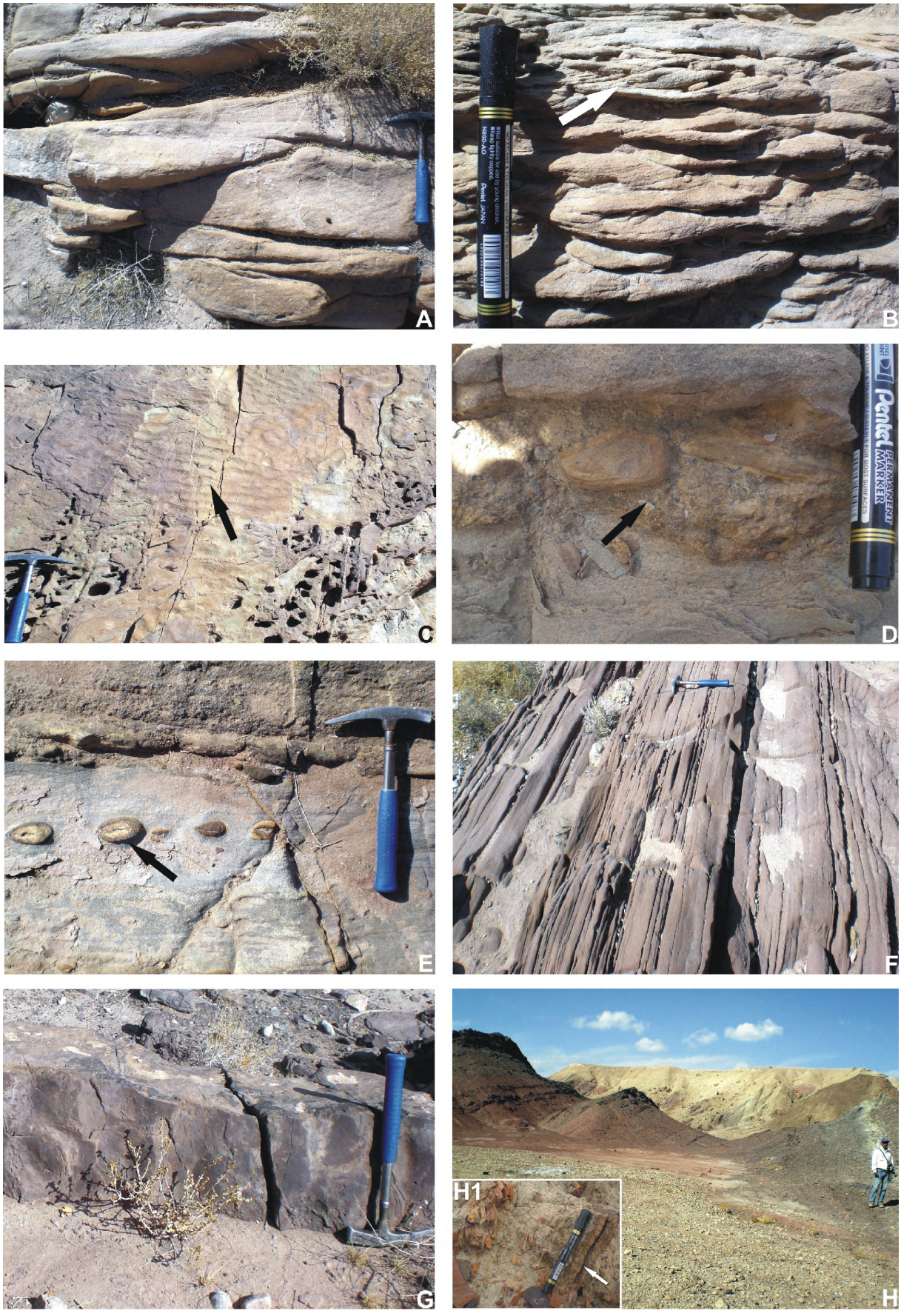

Fig. 5.6.4

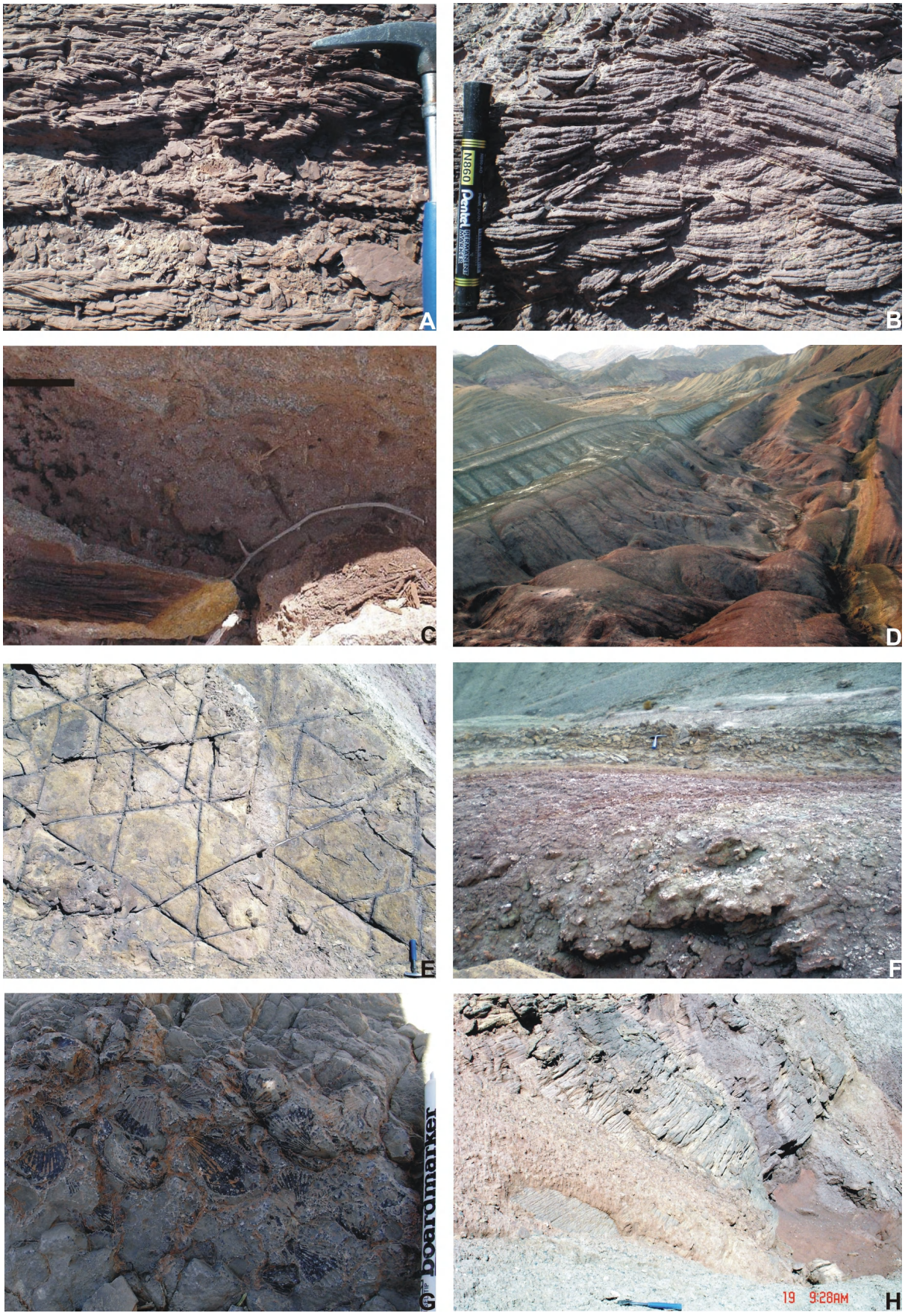

Fig. 5.6.5

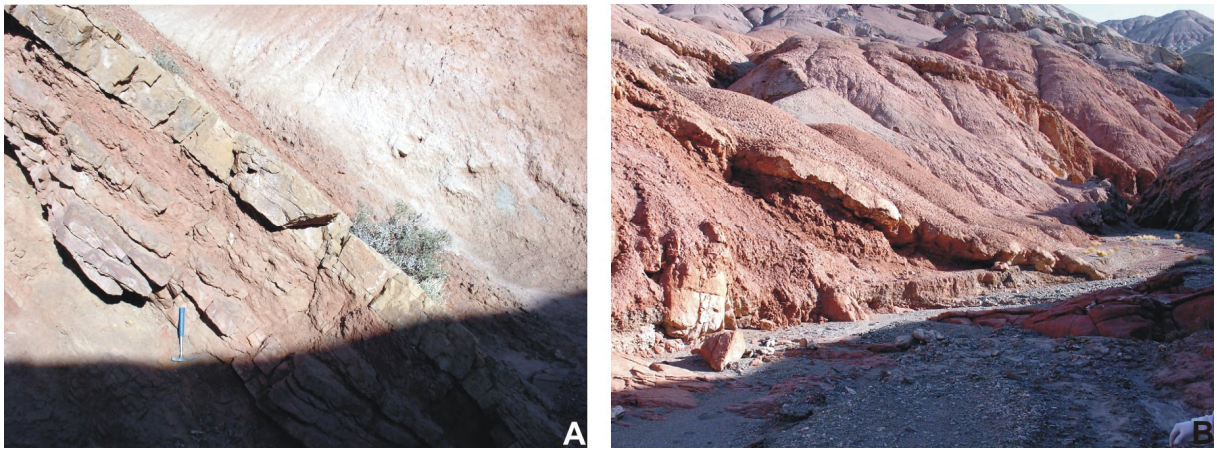

Fig. 5.6.6

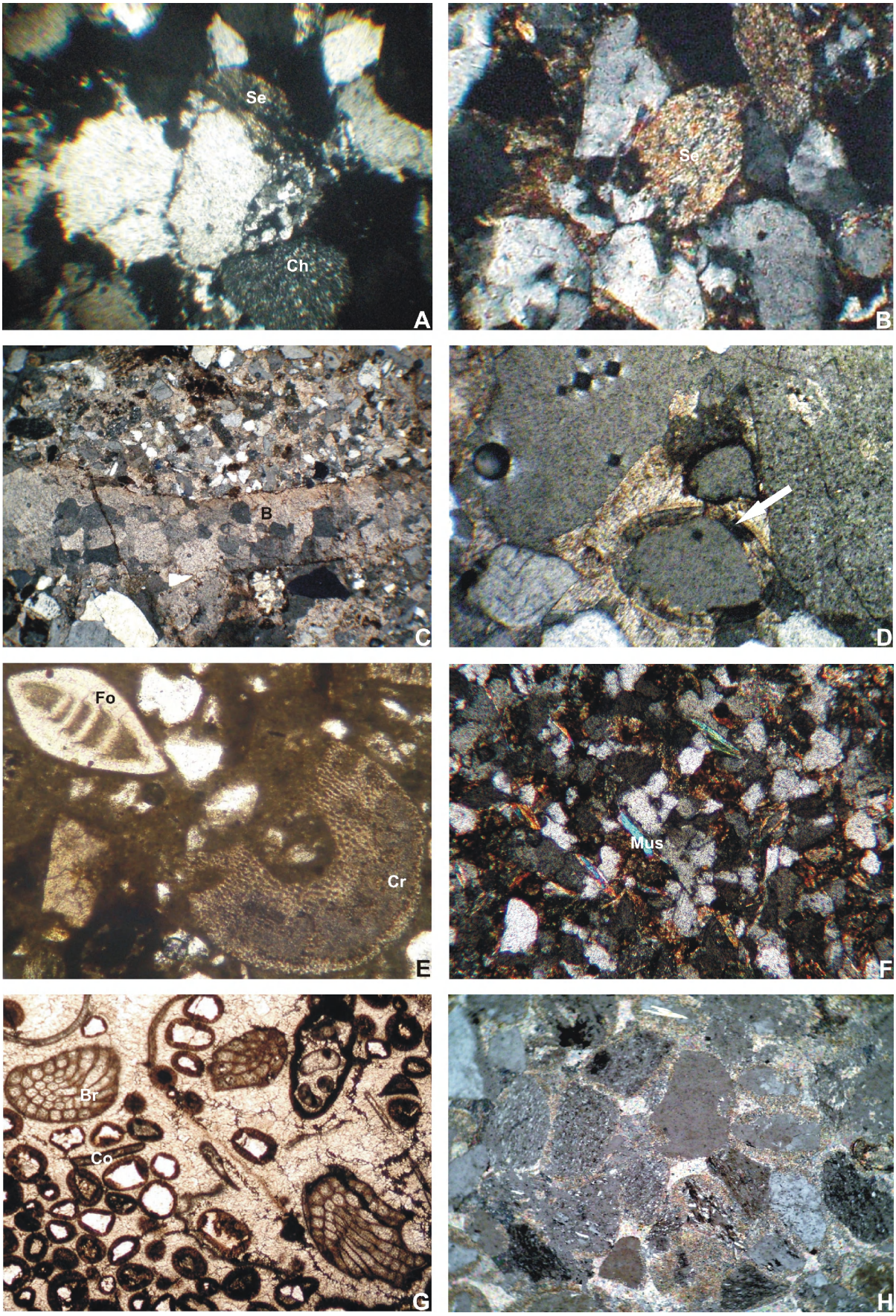

Fig. 5.6.7

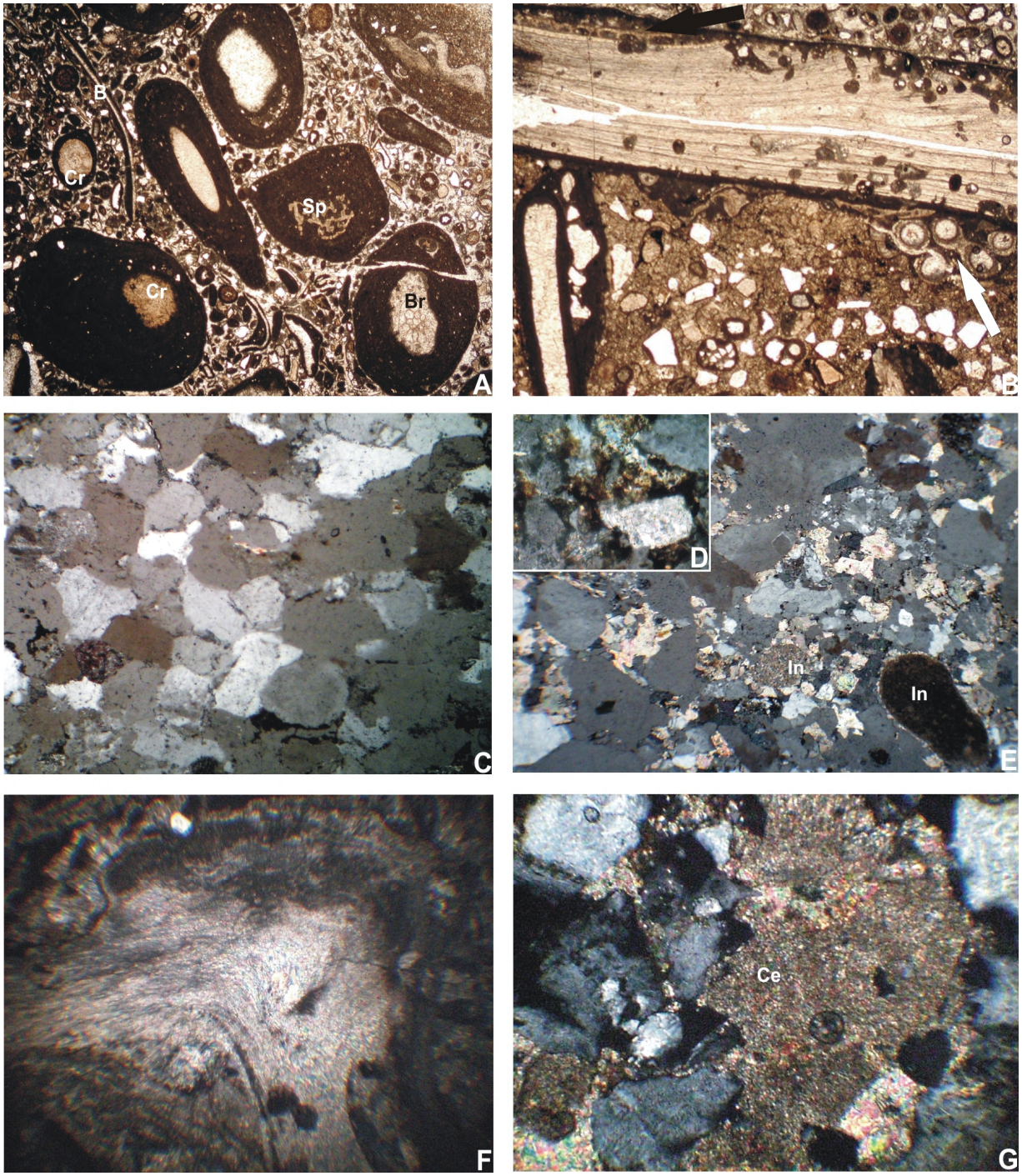

Fig. 5.6.8

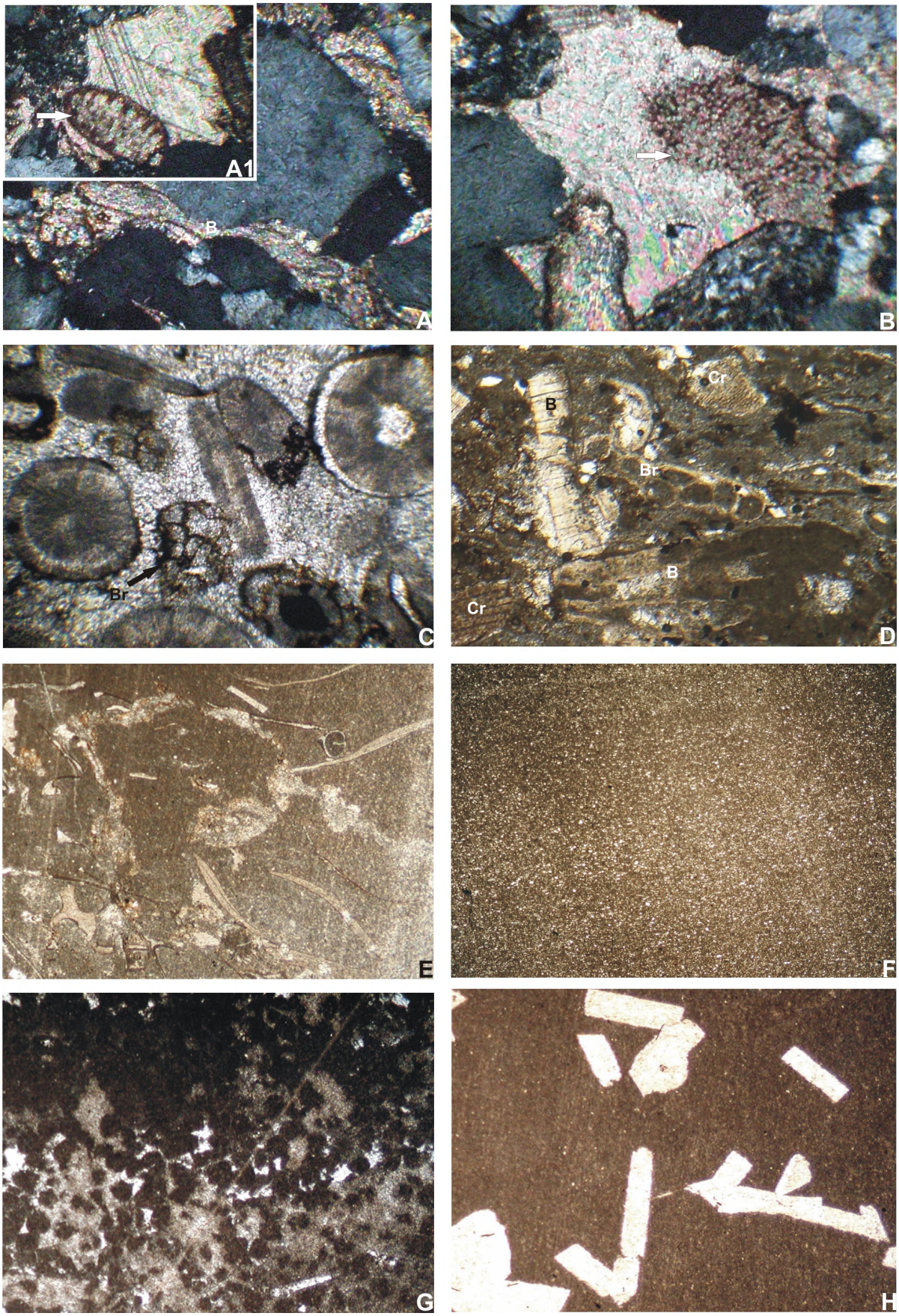

Fig. 5.6.9

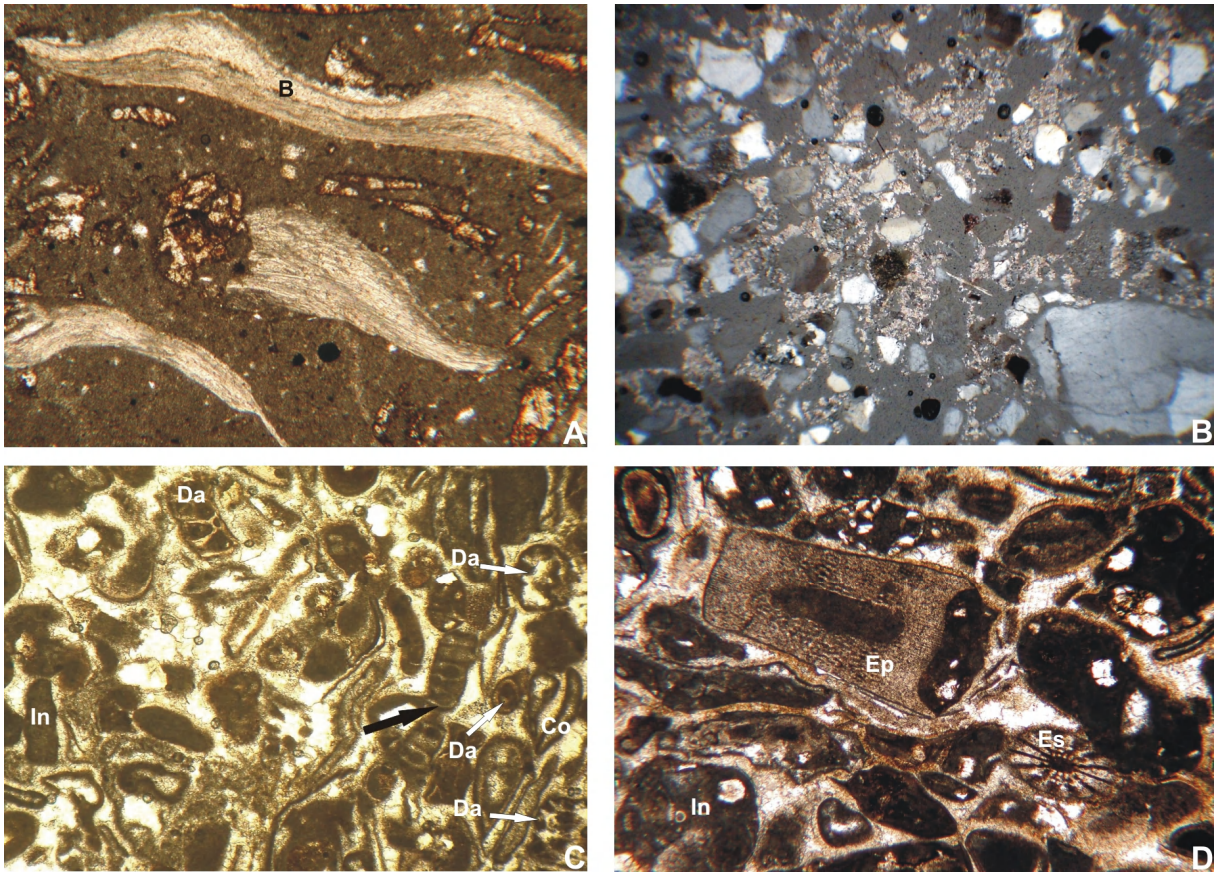

Fig. 5.6.10

5.7. Bidou section (co-ordinates: 31° 49′ 12.2 ′′ N/56° 57′ 51.7′′E)

In the Bidou section (Fig. 5.7.1), the Hojedk Formation is unconformably overlain by the Bidou Formation. The base of the Bidou Formation consists of 27 m of conglomerate with lenticular intercalations of coarse-grained to pebbly sandstones. This facies is followed by a 72 m thick sandstone unit containing, intercalations of conglomerate and conglomeratic sandstones. Higher up, (at 77 m) calcareous sandstone grades into finer siliciclastic rocks (between 100 to 167 m) with alternations of silty clay to gypsiferous silty marl and sandstone (at 120 m), and several meters of calcareous sandstone, the latter passing into grainstone (at 175 m). Higher up, silty marl and nodular mudstone occur, which turn up-section into 15 m of brown gypsiferous silty clay with intercalations of sandstone. At 200 m, the succession is conformably overlain by 11 m of sandy limestone. These limestones turn into grainstones and packstones. Higher up (between 216 to 250 m) coarsening- and thickening-upward cycles starting with gypsiferous marl to silty clay at base and calcareous sandstones at the top follow, which turn into the Pectinid Limestone. The latter consists of packstone, and gypsum (between 252 and 257 m). Still higher up (between 259 and 289 m), marly mudstone and marl occur, followed by grainstone. This facies passes up-section into alternations of wackestone, dolomitic mudstone, and marl (between 316 to 375 m) with intercalations of calcareous sandstone and wacke- to floatstone and packstone (at 359 m). The succession is overlain by 379 m of gypsiferous siliciclastic-carbonate rocks. They consist of decameter-scale alternations of sandstones, gypsiferous silty clay and sandstone at base. This facies turns up-section into conglomeratic sandstone (at 425 m). Further up, the succession changes into sandy calcareous sandstone and continues with silty to sandy mudstone containing intercalations of calcareous sandstone (between 469 and 500 m), alternations of silty clay, silty mudstone, wackestones, calcareous sandstone (up to 606 m), and still higher grainstone. The latter is followed by several metres of gypsiferous silty clay (between 613 and 631 m) and alternations of silty clay, gypsiferous marl, sandstone, mudstone, and gypsum at top (up to 669 m). Up-section, the succession ends with 97 m of silty clay (towards the core of the Upper Siliciclastic Member).

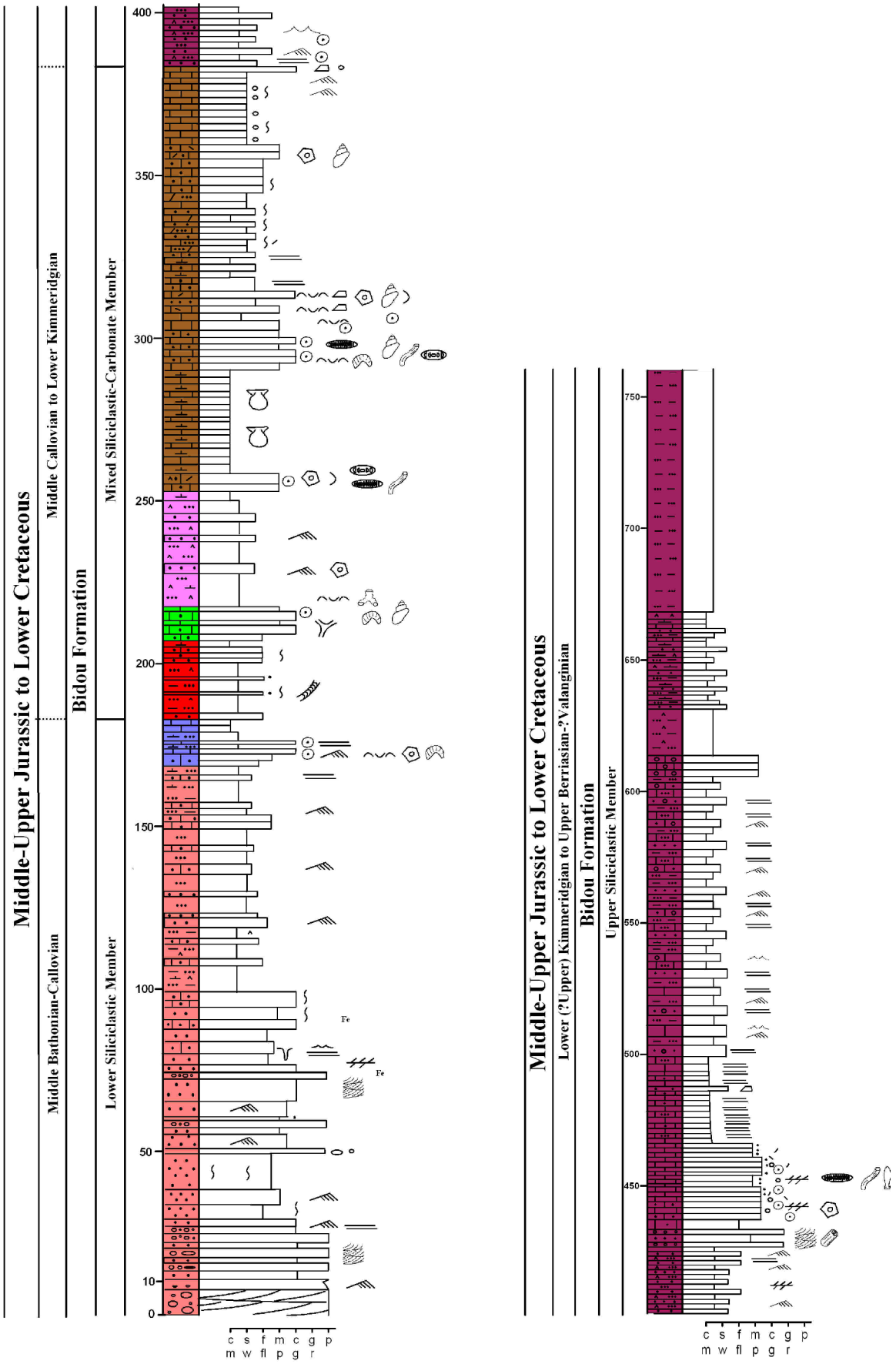

Fig. 5.7.1. Section of the Bidou Formation at Bidou. For key of symbols see Fig. 5.8.16.

Fig. 5.7.2 Bidou Formation at the Bidou section. (A) The basal conglomerate of the Lower Siliciclastic Member of the Bidou Formation (left) overlying with unconformable contact (dashed line) the Hojedk Formation. (B) Crudely bedded basal conglomerate composed of fining-upward cycles. (C) Conglomerate containing lenticular coarse-grained sandstone beds (C.st). Note scattered vertical clasts (Vc), pebbly sandstone (Bi), and the matrix of the conglomerate (black arrow). (D) Poorly bedded conglomerate with signs of tractive transport and clast imbrication in parts (dashed lines) black arrow showing flow direction. (E) Alternations of conglomerate and sandstone. Note crude stratification due to subparallel clast alignment and signs of bimodal (Bi) clast size. (F) Weathered planar cross-stratified calcareous sandstone beds at 76 m. (G) Paired holes of vertical U-tubes of *Diplocraterion* or *Arenicolites* at 77 m (length of bar: 17 mm).

Fig. 5.7.3 Bidou Formation of the Bidou section. (A-B) Silty clay to gypsiferous silty marl (left) and cross-stratified sandstone on right (A) containing climbing ripple lamination (B); lower part of the Lower Siliciclastic Member at 122 m. (C) Disarticulated shell of *Radulopecten tipperi* on bedding plane (length of bar: 17 mm) from oo-grainstone; upper part of the Lower Siliciclastic Member at 174 m. (D) Nodular mudstone at 181 m. (E) Climbing ripple lamination (arrowed) and planar, parallel lamination; lower part of the Mixed Siliciclastic-Carbonate Member. (F) Field aspect of the Mixed Siliciclastic-Carbonate Member (Pectinid Limestone: L). (G) Disconformable contact (dashed line) between the Pectinid Limestone of the Mixed Siliciclastic-Carbonate Member and the Upper Siliciclastic Member. Gsc: Coarsening- and thickening-upward cycle starting with alternations of sandstones and gypsiferous silty clay at base and ending with horizontal to cross-laminated sandstone at top; Cgl: microconglomerate to conglomeratic sandstone at 425 m; Og: oo-grainstone and calcareous sandstone; M: laminated mudstone with intercalated sandstone between 469 and 500 m; Smw: Alternations of silty clay, silty mudstone, silty pel-bio-wackestone and calcareous sandstone with intercalated pel-grainstone beween 500 and 634 m; Gss: alternations of silty clay, gypsiferous marl, sandstone and gypsum at top (between 634 and 669 m); Sc: greyish-brown silty clay (97 m thick towards core of syncline). (H) Planar cross-laminated gypsiferous sandstone of the lower part (Gsc) of the Upper Siliciclastic Member.

Fig. 5.7.4 Bidou Formation of the Bidou section. (A-B) Low-angle bidirectional cross-laminated sandstone, lower part of the Upper Siliciclastic Member (A), and conglomerate (B) containing wood fragments (arrowed) at 425 m. (C-D) Planar cross-laminated sandstone (C), and current ripples on bedding plane (D); lowermost part of the Upper Siliciclastic Member. (E) *Taenidium* with meniscus-shaped back-fill; Mixed Siliciclastic-Carbonate Member at 180 m, length of bar: 12 mm. (F) *Thalassinoides* (arrowed) with horizontal box-like networks, Mixed Siliciclastic-Carbonate Member at 218 m, diameter of pen 17.5 mm. (G) Horizontal burrow system of *Ophiomorpha* (arrowed); Mixed Siliciclastic-Carbonate Member at 218 m (length of the bar: 17.5 mm).

Fig.5.7.5 Thin-sections of various types of microfacies from the Bidou Formation of the Bidou section. Lm: Shale or slate debris; Ch: Chert (>3 sub-grains <0.030 mm); Qp2-3: polycrystalline quartz with 2-3 sub-grains; Qp >3c: polycrystalline quartz with >3 sub-grains (>0.062 mm); Qp >3f: polycrystalline quartz with >3 sub-grains (0.030-0.062 mm); F: feldspar; O: ooid; Mo: micritized or partly micritized ooids; Ce: extrabasinal carbonate fragment; Se: extrabasinal siliciclastic fragment; Cm: carbonate cement; Cm1: ferroan carbonate cement; Cm2: Fe-oxide cement. (A) Sublitharenite; lowermost part of the Lower Siliciclastic Member (sample

m-87; width of photomicrograph: 4 mm). (B) Feldspathic arenite. Note a siliciclastic fragment (Se) with preferredly oriented sub-grains at 36 m (sample m-92; width of photomicrograph: 3 mm). (C) Feldspathic arenite, Lower Siliciclastic Member at 77 m (sample k-93; width of photomicrographs: 1 mm). (D) Feldspathic arenite, at 114 m (sample M-28; width of photomicrograph: 1 mm). (E) Feldspathic arenite, upper part of the Lower Siliciclastic Member at 170 m. Sample m-29; width of photomicrograph: 1 mm. (F) Feldspathic arenite, lower part of the Mixed Siliciclastic-Carbonate Member at 189 m (sample k-97; width of photomicrograph: 1 mm). (G) Sandy crystalline carbonate at 207 m. Sample k-99; width of photomicrograph: 0.5 mm. (H) Oo-grainstone, at 175 m (sample k-98; width of photomicrograph: 2.5 mm).

^

Fig. 5.7.6 Thin-sections of various types of microfacies from the Bidou Formation of the Bidou section; O: ooid; Mo: micritized or partly micritized ooid; Co: cortoid; Cr: crinoid; Os: ostracod; Da: dasycladacean; Se: serpulid; B: shell fragment. (A) Bio-oo-grainstone; uppermost part of the Lower Siliciclastic Member at 175 m. Sample k-98; width of photomicrograph: 2.5 mm. (B) Feldspathic arenite; Mixed Siliciclastic-Carbonate Member at 227 m. Sample m-94; width of photomicrograph: 1 mm. (C) Oo-bio-packstone; lowermost part of the Pectinid Limestone of the Mixed Siliciclastic-Carbonate Member at 253 m. Sample m-90; width of photomicrographs: 0.5 mm. (D-G) Bio-packstone; lower part of the Pectinid Limestone at 254 m. Sample m-93; width of photomicrograph: 2 mm (D), 1 mm (E), 2 mm (F) and 1.5 mm (G). (H) Oo-grainstone; lower part of the Pectinid Limestone. Note ?dasycladacean green algae (arrowed). Sample m-92; width of photomicrograph: 1 mm.

Fig. 5.7.7. Thin-sections of various types of microfacies from the Mixed Siliciclastic-Carbonate and the brownish-red gypsiferous Upper Siliciclastic Member of the Bidou section; O: ooid; Mo: micritized or partly micritized ooids; Co: cortoid; Cr: crinoid; Ec: ?echinoderm; Os: ostracod; Oy: oyster; G: gastropod; B: shell fragment; In: intraclast; P: peloid; Fo: foraminifer; A: algae; Qp2-3: polycrystalline quartz with 2-3 sub-grains; Qp>3c: Polycrystalline quartz with >3 sub-grains (> 0.062 mm); Qmn: non-undulatory quartz grain; Qmu: undulatory quartz grain; F: feldspar: Cm: carbonate cement; Cm1: Fe-oxide carbonate cement. (A-C) Sandy cortoid-oo-grainstone. Note thin, white finely prismatic isopachous cement around ooids (B). Fo: *Trocholina*? sp., Mixed Siliciclastic-Carbonate Member at 299 and 314 m. Sample k-105, k-108; width of photomicrograph: 2.5 mm. (D-E) Sandy bio-packstone; Mixed Siliciclastic-Carbonate Member at 359 m. Sample k-110; width of photomicrograph: 2.5 mm (D) and 1 (E) mm. (F) Intra-Pel-grainstone; Pectinid Limestone of the Mixed Siliciclastic-Carbonate Member at 384 m (sample k-119; width of photomicrograph: 2.5 mm). (G) Calcareous sandstone, lowermost part of the Upper Siliciclastic Member (sample k-122; width of photomicrograph: 1 mm). (H) Conglomeratic sandstone (subarkose); Upper Siliciclastic Member at 425 m (sample k-124; width of photomicrograph: 2.5 mm).

Fig. 5.7.8. Thin-sections of various types of microfacies from the Upper Siliciclastic Member at the Bidou section; O: ooid; Mo: micritized or partly micritized ooids; Es: echinoid spine; Cr: crinoid; Se: serpulid; Da: dasycladacean green algae; In: intraclast; Cm: carbonate cement; G: gypsum. (A) Calcareous sandstone at 436 m (sample k-125; width of photomicrograph: 1 mm). (B-C) Calcareous sandstone at 452 m (sample k-126; width of photomicrograph: 2.5 mm). (D) Calcareous sandstone at 485 m (sample k-127; width of photomicrograph: 1

mm). (E) Silty pel-grainstone at 621 m (sample k-130; width of photomicrograph: 10 mm). (F) Gypsiferous mudstone at 664 m (sample k-133; width of photomicrograph: 10 mm).

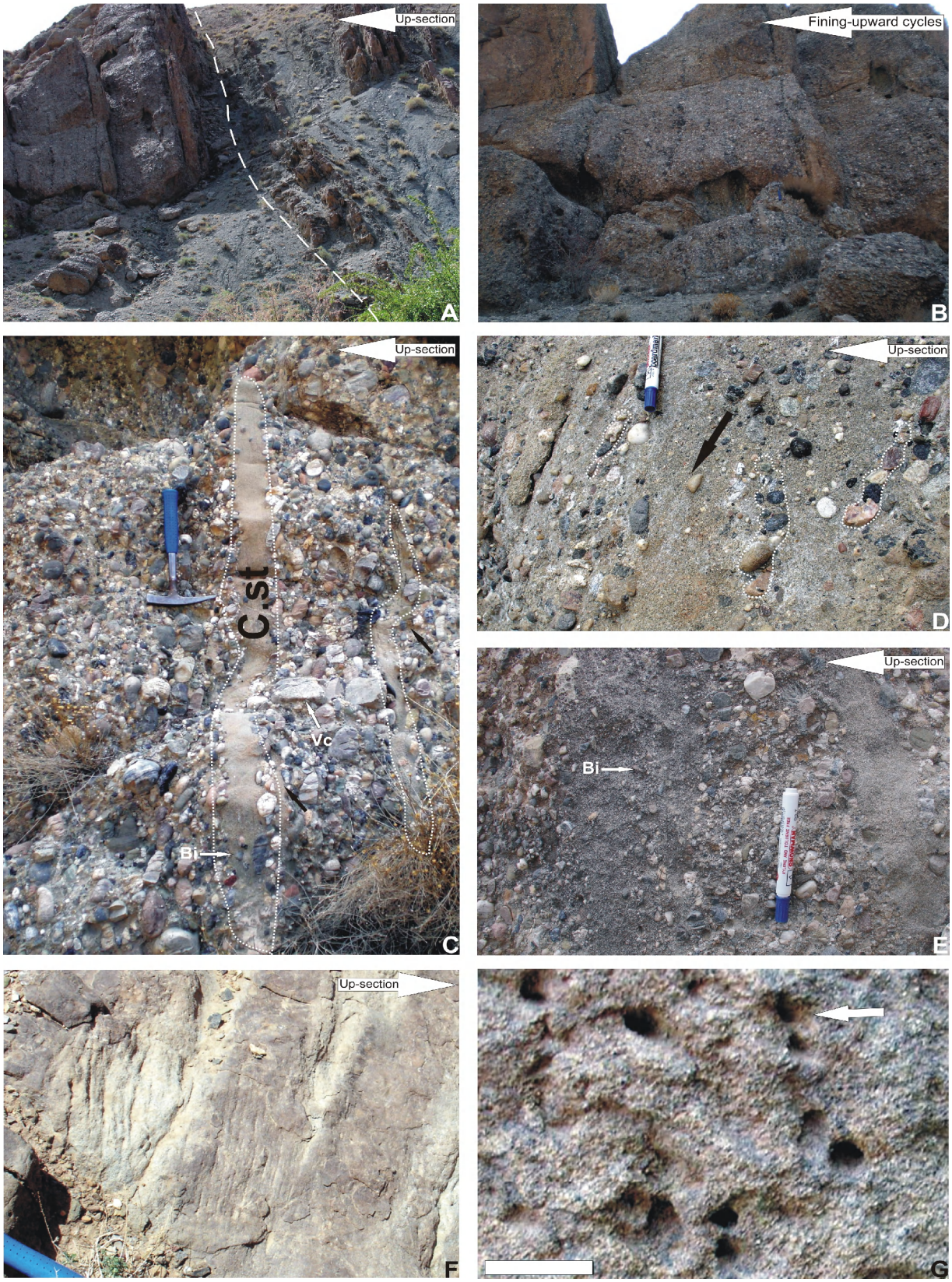

Fig. 5.7.2.

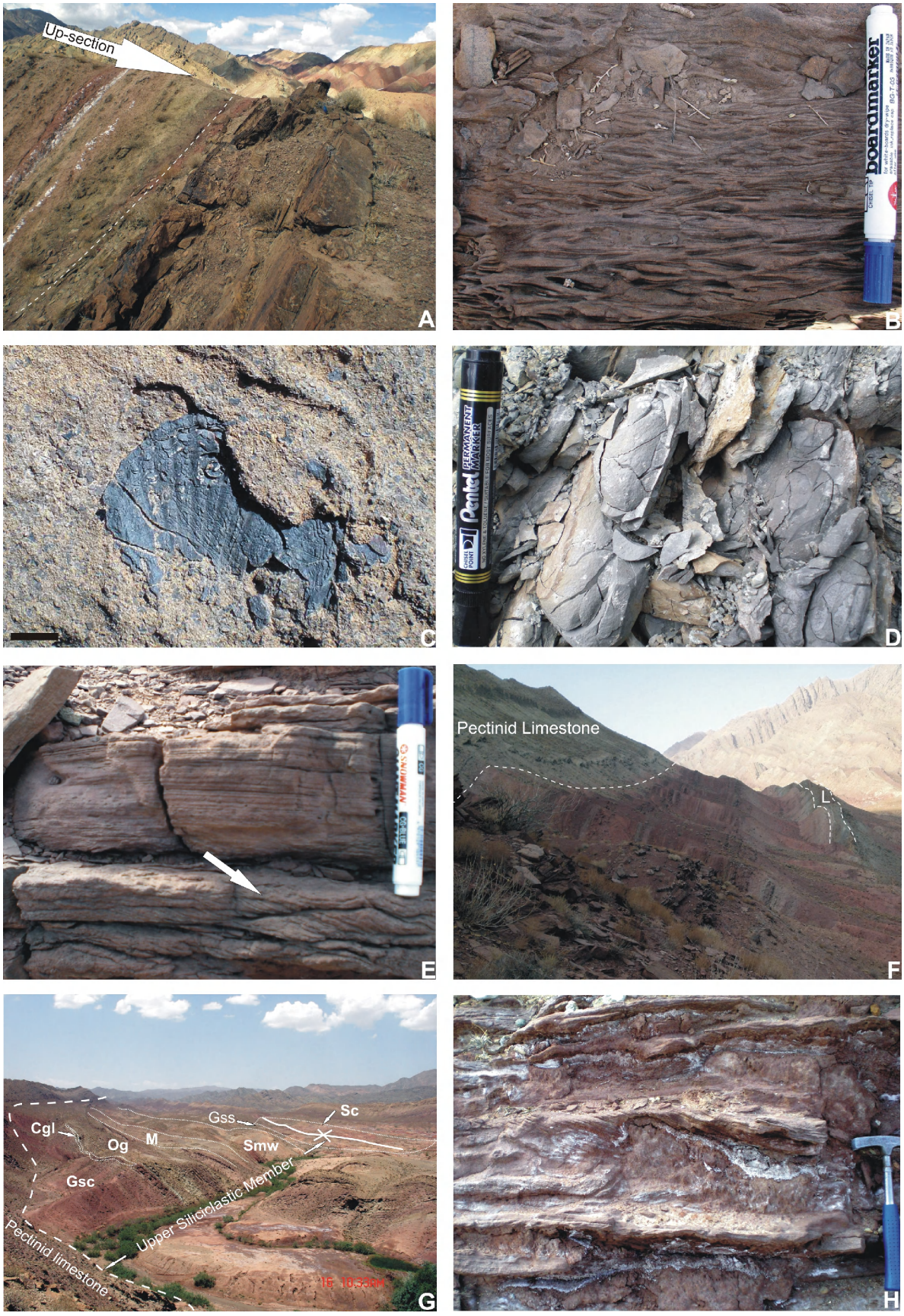
Up-section
A
boardmarker
B
C
Pentel
PERMANENT MARKER
D
E
Pectinid Limestone
L
F
Cgl
Og
M
Gss
Sc
Smw
Gsc
Upper Siliciclastic Member
Pectinid limestone
G
H

Fig. 5.7.3.

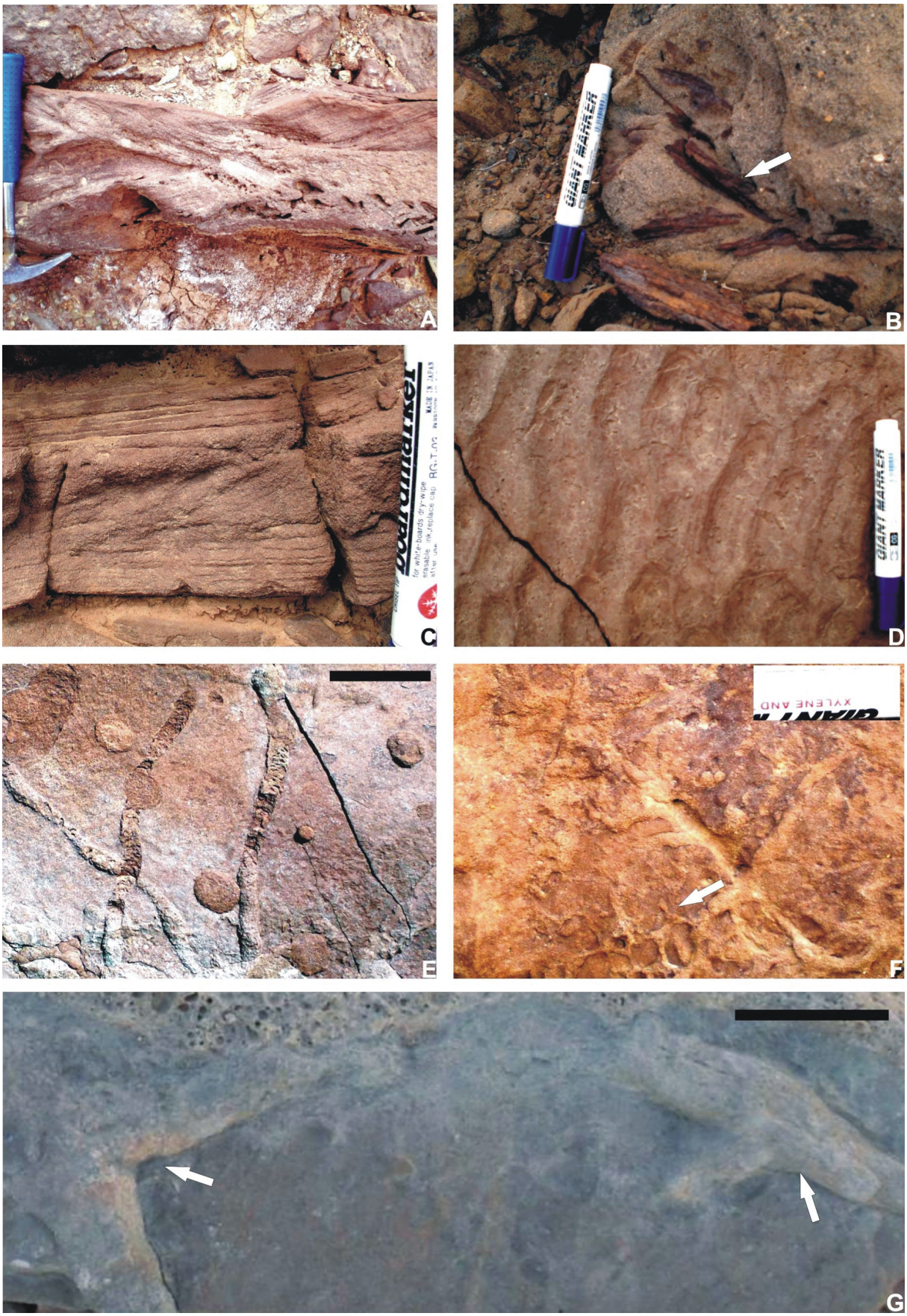

Fig. 5.7.4.

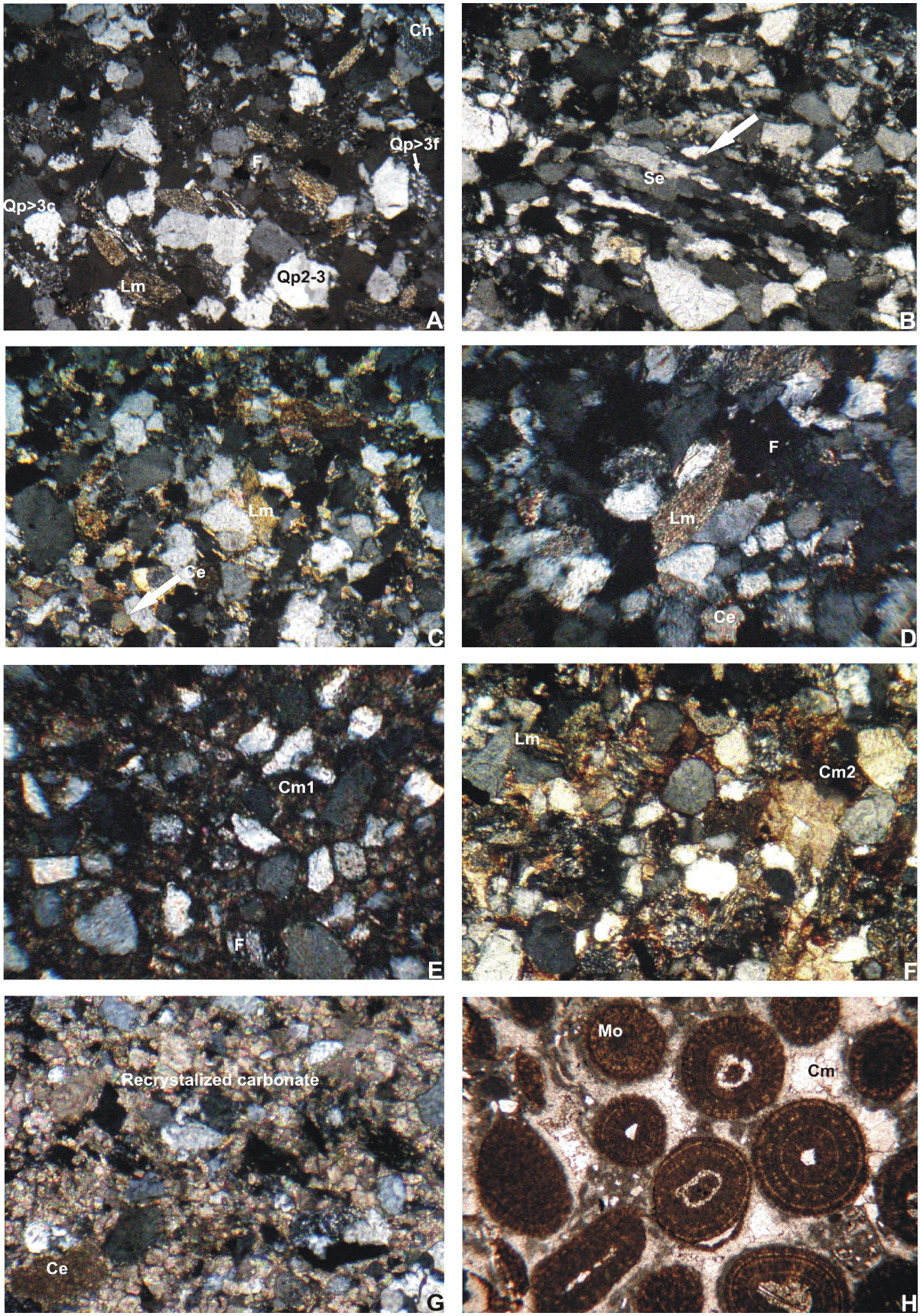
Ch
Qp>3f
F
Qp>3c
Lm
Qp2-3
A
Se
B
Lm
Ce
C
F
Lm
Ce
D
Cm1
F
E
Lm
Cm2
F
Recrystalized carbonate
Ce
G
Mo
Cm
H

Fig. 5.7.5.

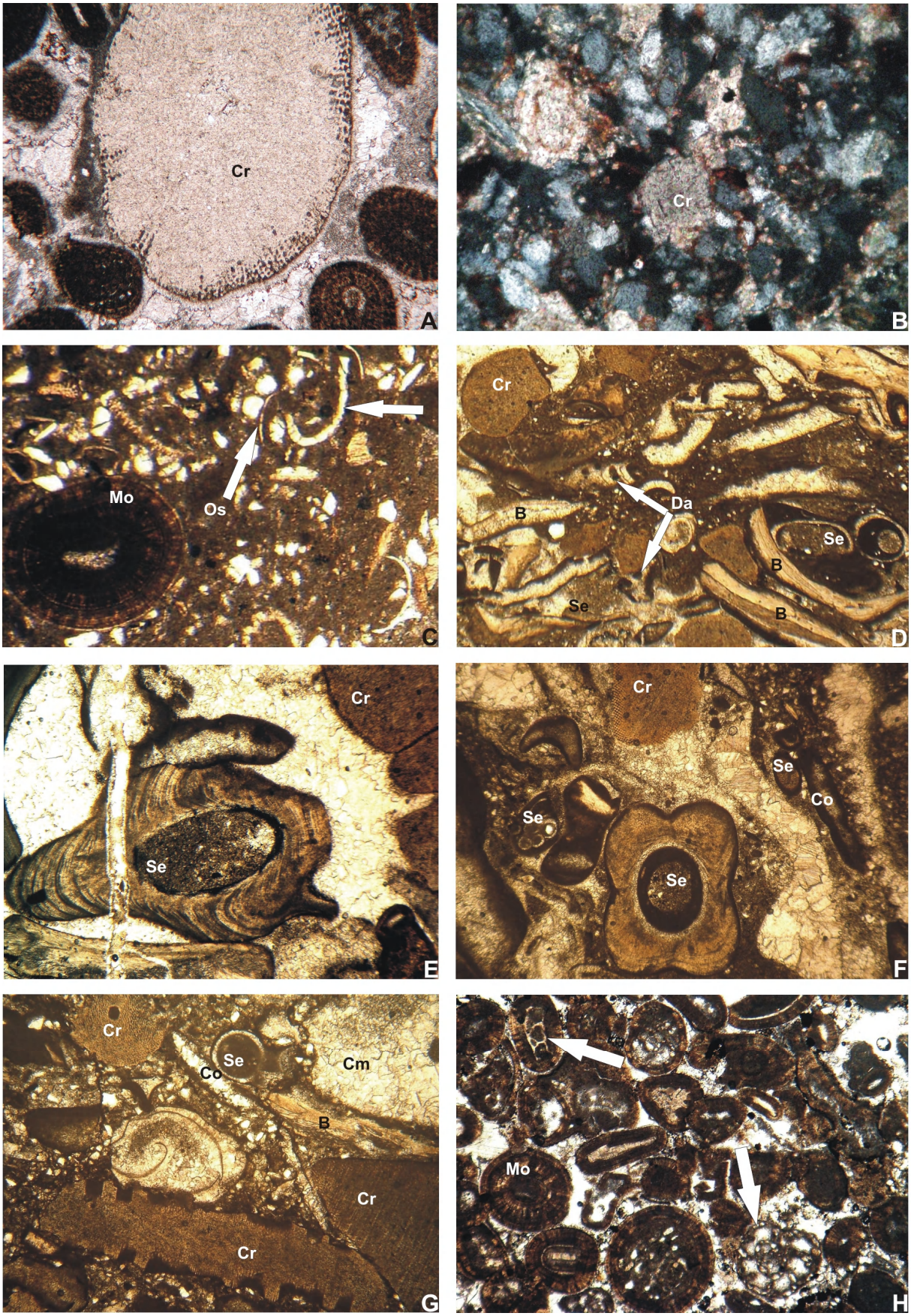
Cr
A
Cr
B
Mo
Os
C
Cr
Da
B
Se
B
Se
B
D
Cr
Se
E
Cr
Se
Co
Se
Se
F
Cr
Se
Co
Cm
B
Cr
Cr
G
Mo
H

Fig. 5.7.6.

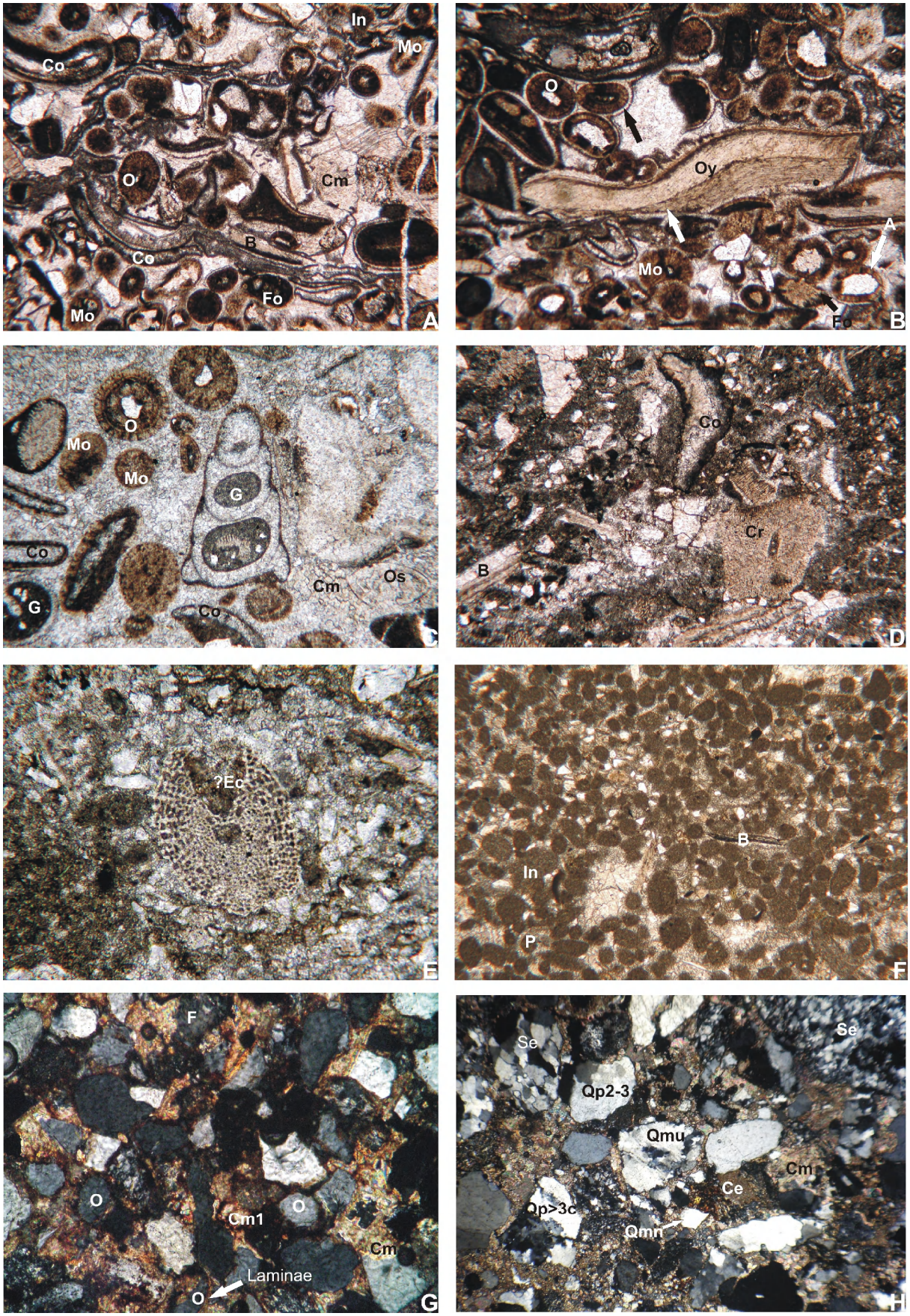
In
Mo
Co
O
Cm
B
Co
Fo
Mo
A
O
Oy
A
Mo
Fo
B
O
Mo
Mo
G
Co
G
Cm
Os
Co
C
Co
Cr
B
D
?Ec
E
B
In
P
F
F
O
Cm1
O
Cm
Laminae
O
G
Se
Se
Qp2-3
Qmu
Cm
Ce
Qp>3c
Qmn
H

Fig. 5.7.7.

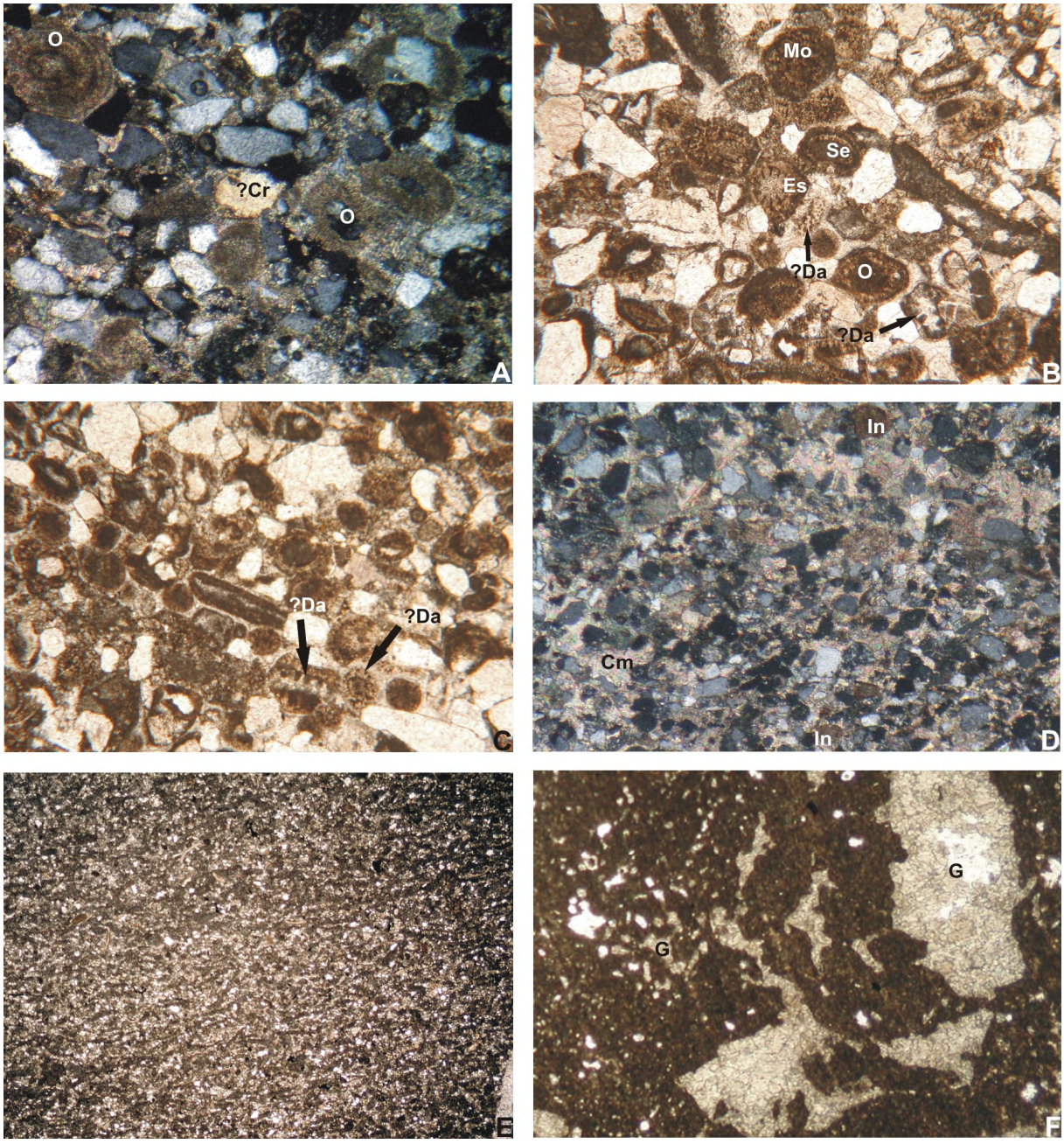

Fig. 5.7.8.

5.8. Bolboulieh (co-ordinates: 30° 07′ 24.4′′ N/57° 22′ 22.2″ E) and Mohamadshah (co-ordinates: 30° 25′ 23.7′′ N/57° 18′ 09.3″ E)

In the Bolboulieh area, the uppermost 34 m of the Hojedk Formation (Fig. 5.8.1) are characterized by irregularly coarsening-upward cycles developing from silty shale/siltstone to sandstones. The top part of these sandstones turns into intercalations of conglomeratic/pebbly sandstone, quartz-sandstone, silty limestone and oncolitic rudstone. In the Bolboulieh and Mohamadshah area, the Hojedk Formation is unconformably overlain by the Lower Siliciclastic Member of the Bidou Formation, the latter starting with a 0.5 to 3.5 m thick

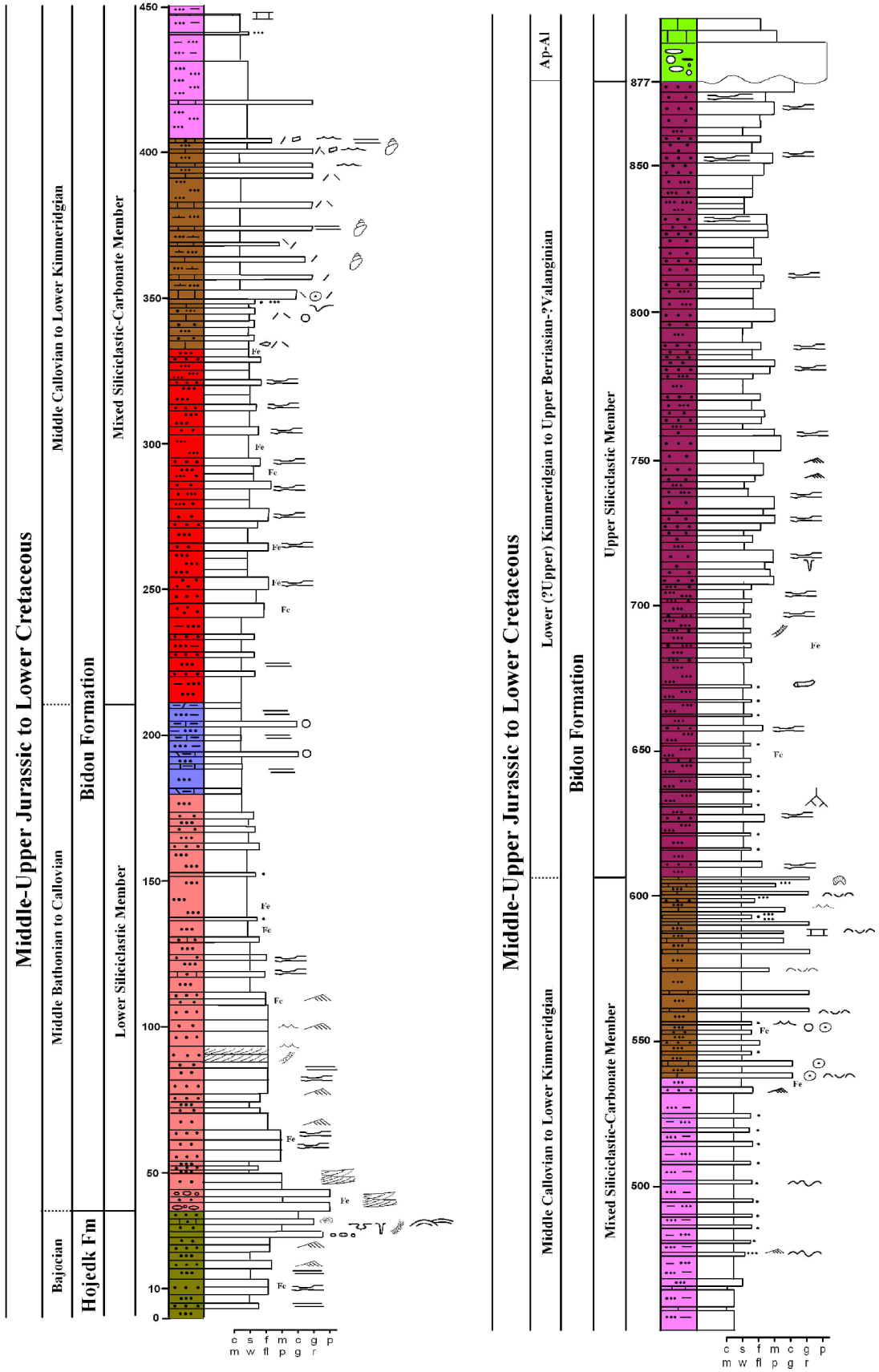

Fig. 5.8.1. Bolboulieh section of the Hojedk Formation, the Lower Siliciclastic, Mixed Siliciclastic-Carbonate, and Upper Siliciclastic members of the Bidou Formation, and the unconformable contact with early Cretaceous strata. Al: Albian; Ap: Aptian.

conglomerate, which laterally may turn into coarse-grained to pebbly sandstone beds. This facies is followed by a 69 m thick (Bolboulieh section) and 61.5 m thick (Mohamadshah section) unit of medium- to coarse-grained sandstone, which up-section turns into fining-upward cycles with sandstones. Higher up, at 64.5 m (Mohammadshah) and at 112 m (Bolboulieh), the facies turns into alternations of sandstones and siltstone. In the Bolboulieh section this facies is followed (at 180 m) by alternations of siltstone/argillaceous shale and non-fossiliferous mudstone or pel-grainstone and in the Mohamadshah section (at 87.5 m) by silty to marly shale containing intercalations of dolomitic mudstone, grainstone and rudstone. Higher up at Bolboulieh (between 211 and 331 m) and Mohammadshah (between 125 and 186 m) the facies changes into siliciclastic rocks at the base of the Mixed Siliciclastic-Carbonate Member. The latter is characterized by alternating siltstone and silty clay with sandstones. In the Bolboulieh area (between 331 and 609 m) this facies is followed by alternations of silty shale, silty clay containing intercalated sandstone and limestones (between 430 and 531 m), alternations of silty marl with sandstones to limestones. The latter consists of dolomitic grainstone (at about 335 m), grainstone (at 350 m), rudstone and floatstone (at 408 m). Higher up (between 559 and 609 m) calcareous sandstone with rudstone intercalations occur. In the Mohamadshah section, the facies is characterized by alternations of siltstone, silty clay (between 268 and 324 m) and sandstone and bioturbated sandstone containing intercalations of rudstone, wackestone, and floatstone (between 189 and 268 m) and intercalations of rudstone (at 450 m). In the Mohamadshah section (between 324 to 425 m), the facies is followed by silty mudstone containing intercalations of siltstone, sandstone, grainstones, rudstone, marly shale and calcareous sandstone containing intercalated grainstones. The succession is overlain by the Upper Siliciclastic Member, 270 m thick in the Bolboulieh section and 52 m thick (top faulted) in the Mohamadshah section. This facies is characterized by alternations of purple to brown silty shale/siltstone and lenticular sandstone which is overlain with unconformable contact by Early Cretaceous (Albian-Aptian) rocks.

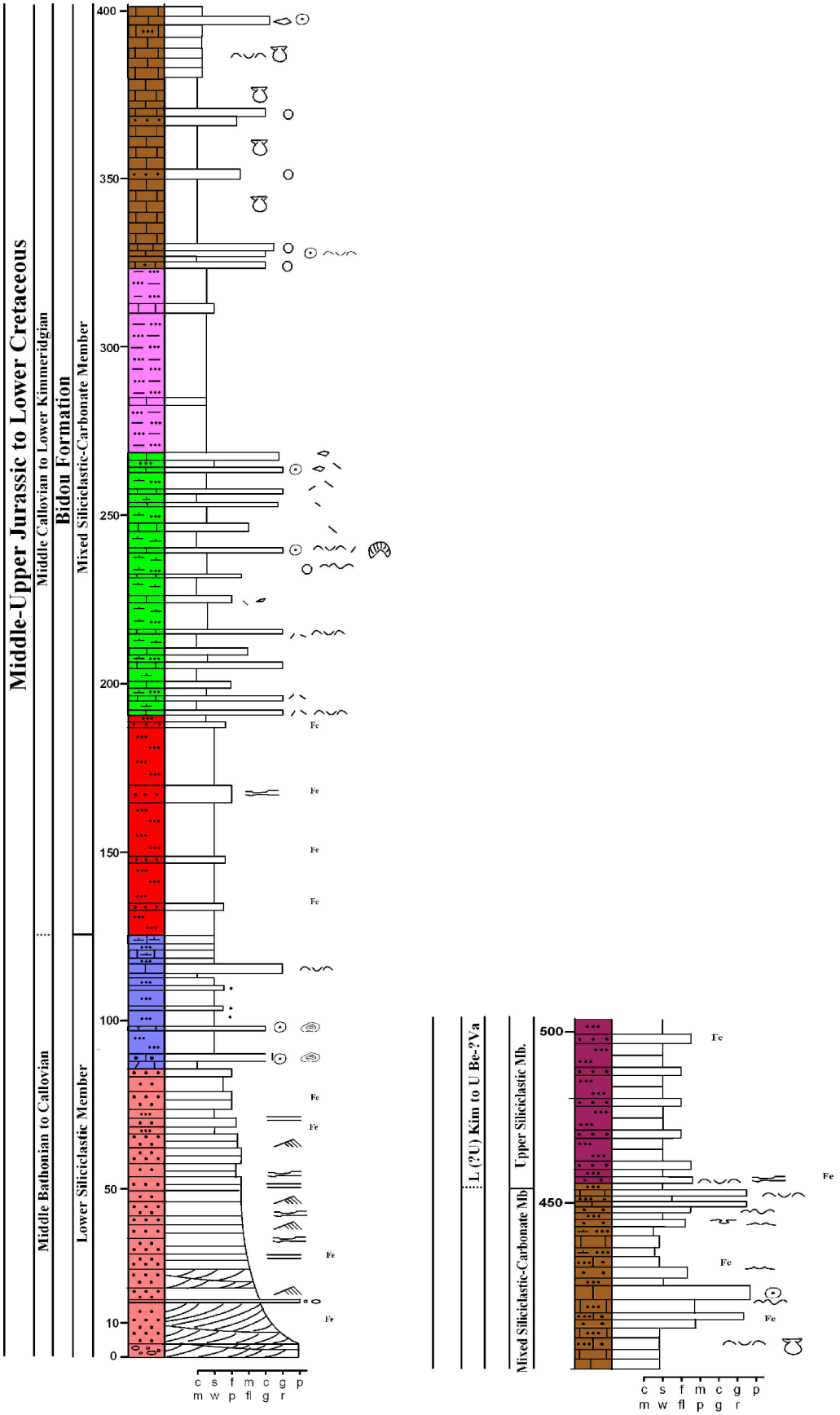

Fig.5.8.2. Section of the Bidou Formation at Mohamadshah. L: Lower; U: Upper; Kim: Kimmeridgian; Be: Berriasian; Va: Valanginian; Mb: Member.

Fig. 5.8.3. Uppermost part of the Hojedk Formation, Bolboulieh section. (A) Coarsening-/shallowing-upward succession from silty shale/siltstone to thin- to thick-bedded sandstones. (B) Lenticular thick-bedded quartz-sandstone marked by dashed line. (C) Horizontal to low-angle cross-laminated quartz sandstone. (D) Sandstone with sharp base (arrowed) overlying siltstone/silty shale. (E) Load casts (arrowed) on lower surface of sandstone. (F) Hummocky cross-stratified sandstone. (G) Wave-rippled silty limestone. (H) Oncolitic limestone with shell fragments. Arrow pointing to oncoid.

Fig. 5.8.4. Bolboulieh section; lowermost (A-C), lower and lower to middle (E-F) part of the Lower Siliciclastic Member. (A) Intercalated Conglomerate (arrowed) in the basal sandstones. (B) Silty-sandy matrix-supported, poorly sorted, oligomict conglomerate. (C) Large-scale trough cross-bedding (arrowed) in sandstones. (D) Flute casts. Arrow showing current direction; Mohamadshah section. (E-F) Fining-upward succesions from sandstones to silty shale/siltstone. (G-H) Field aspect of unconformable contact (stippled line) between the Hojedk and Bidou formations (Lower Siliciclastic Member: LSM). Seen also is the conformable contact (stippled line) between the Lower Siliciclastic and the Mixed Siliciclastic-Carbonate members (M.S.C.M), and the conformable contact between the latter member and the Upper Siliciclastic Member (U.S.M) of the Bidou Formation. Cgl: Intercalated conglomerate; S,si: mainly sandstone and subordinate siltstone/silty shale; Si,s: mainly siltstone/silty shale and subordinate sandstone; L: limestone of upper part of the Lower Siliciclastic Member; Cret: Aptian-Albian Cretaceous rocks overlying the Bidou Formation with unconformable contact.

Fig. 5.8.5. Mohamadshah and Bolboulieh sections; Bidou Formation. (A) Conformable contact (high relief stippled line) between the Lower Siliciclastic (L.S.M) and the Mixed Siliciclastic members (M.S.C.M); L: Intercalated limestone of upper part of the L.S.M; Mohamadshah section. (B, B1, B2) Conformable contact (stippled line) between the Mixed Siliciclastic-Carbonate- and the Upper Siliciclastic members (U.S.M). Note the elongated lenticular sandstone (Lent.S) at the base of the Upper Siliciclastic Member (B), alternations of thin-bedded sandstones, limestones and silty shale (B1), and alternations of purple silty shale and sandstone (B2) at the base of the Upper Siliciclastic Member; Mohamadshah section. (C) Conformable contact (arrowed) between silty shales containing intercalated mudstone and pel-grainstone (L) and red to brown siliciclastic rocks at top of the Lower Siliciclastic Member; Bolboulieh section. (D) Conformable contact (arrowed) between Siliciclastic and Carbonate units of the Mixed Siliciclastic-Carbonate Member; Bolboulieh section. (E) Discontinuous lenticular sandstones (white arrow), upper part of the lower Siliciclastic member; Bolboulieh section. (F) Scour and fill structures (at hammer) at the base of the lenticular sandstone, Bolboulieh section. (G) Sharp-based sandstone; Bolboulieh section. (H) Load cast at the base of sandstone; Bolboulieh section.

Fig. 5.8.6. (A-C) Alternations of calcareous sandstones and limestones with silty shale/marl (A), bioturbated sandstone (B), load casts or ball and pillow structures (C); upper part of the Mixed Siliciclastic-Carbonate Member; Mohamadshah section. (D-G) Graded-bedding (D; arrowed), bioclastic lag (E; arrowed), intraclasts floating in limestone (F; arrowed), and (G) alternations of calcareous sandstone and limestone with silty shale/marl; middle part of the Mixed Siliciclastic-Carbonate Member; Bolboulieh section. (H) Brown laminated

silty clay and mudstone with intercalated thin-bedded sandstones and mudstones, middle part of the Mixed Siliciclastic-Carbonate Member; Bolboulieh section.

Fig. 5.8.7. (A) Oscillation-rippled sandstone within brown laminated silty clay and mudstone; middle part of the Mixed Siliciclastic-Carbonate Member; Bolboulieh section. (B) Conformable contact (arrowed) between grey to green silty clay to silty marl containing intercalations of thin- to thick-bedded limestone at top of the Mixed Siliciclastic-Carbonate Member and the base of the Upper Siliciclastic Member. (C) Lenticular thick-bedded sandstone in lower part of the Upper Siliciclastic Member; Bolboulieh section. (D) Gutter cast on lower surface of sandstone, top of the Mixed Siliciclastic-Carbonate Member; Bolboulieh section. (E) Shells within laminated thin- to medium bedded sandstone, top of the Mixed Siliciclastic-Carbonate Member; Mohamadshah section. (F) Alternations of sandstone and silty shale/siltstone of the upper siliciclastic member; Bolboulieh section.

Fig. 5.8.8. (A-B) *Gyrochorte* isp.; scale: 10 mm (A), paired tubes of *Diplocraterion* or *Arenicolites*; scale: 12 mm (B), lowermost part of the Lower Siliciclastic Member; Bolboulieh section. (C) *Chondrites* isp., lower part of the Upper Siliciclastic Member; Bolboulieh section. Scale: 10 mm. (D) *Rhizocorallium irregulare,* middle part of the Mixed Siliciclastic-Carbonate Member; Bolboulieh section; scale: 17 mm. (E-F) *Taenidium* isp. (E) and *Planolites* isp. (F); lower part of the Upper Siliciclastic Member; Bolboulieh section; scale: 17 mm.

Fig. 5.8.9. Thin-sections of various types of microfacies from the Lower Siliciclastic Member at the Bolboulieh and Mohamadshah sections. Lm: Shale or slate debris; Ch: Chert (>3 sub-grains <0.030 mm); Qp2-3: polycrystalline quartz with 2-3 sub-grains; Qp>3c: polycrystalline quartz with >3 sub-grains (>0.062 mm); Ce: extraclasts; Se: siliciclastic clasts; Cm1: ferroan carbonate cement; Cf: ?calcite replacement on feldspar. (A) Basal conglomerate of the Bidu Formation. Note rounded siltstone or very fine-sand grains; Bolboulieh section (sample M-15; width of photomicrograph: 10 mm). (B) Quartzarenite; Bolboulieh section (sample M-9; width of photomicrograph: 2 mm). (C) Sublitharenite; Note grain suturing (arrowed); Bolboulieh section (sample M-13; width of photomicrograph: 2.5 mm). (D-H) Litharenite; Mohamadshah section (sample M-51; width of photomicrographs: 2.5 mm (D), 1.mm (E-H)).

Fig. 5.8.10. Thin-sections of various types of microfacies from the Bidou Formation at the Bolboulieh and Mohamadshah sections. Lm: Shale or slate debris; Ch: Chert (>3 sub-grains <0.030 mm); Qp>3c: polycrystalline quartz with >3 sub-grains > 0.062 mm; F: feldspar; Fser: sericite replacement on feldspar; Fcl: chlorite replacement of feldspar; Ce: extraclasts. (A-B) Sublitharenite, Lower Siliciclastic Member, Mohamadshah section (sample M-18; width of photomicrograph: 1 mm). (C-D) Sublitharenite. Note grain suturing (arrowed), Lower Siliciclastic Member, Mohamadshah section (sample M-54; width of photomicrograph: 1 mm). (E-F) Lithic arkose (E), Feldspathic greywacke (F); upper part of the Lower Siliciclastic Member, Bolboulieh section (samples M-16, 18b; width of photomicrographs: 1mm (E) and 2.5 mm (F)). (G-H) Lithic arkose; lower part of the upper siliciclastic member, Bolboulieh section (sample M-10; width of photomicrographs: 2.5 mm (G), 1 mm (H)).

Fig. 5.8.11. Thin-sections of various types of microfacies from the Bidou Formation of the Bolboulieh and Mohamadshah sections. (A, B1) dolostone; upper part of the Lower Siliciclastic Member; Mohamadshah section. Note intercrystalline pores (arrowed) between anhedral- and some euhedral dolomitic crystals which are impregnated with iron-oxide (A), pel-grainstone (B1), middle part of the Lower siliciclastic Member, Bolboulieh section (samples K-57, m-15; width of photomicrograph: 0.5 mm (A) and 1 mm (B1)). (B-D) Vesicular mudstone of the middle part of the Mixed Siliciclastic-Carbonate Member. Note thin laminae of micrite (B: white arrow), patches of probably algal and cyanobacterial peloids (C-D: black arrow). Note also intraparticle pores, which are filled with mostly secondary opaque minerals during chemical weathering; Bolboulieh section (sample K-31a, b; width of photomicrographs: 10 mm (B), 2.5 mm (C) and 1 mm (D)). (E-F) Laminated silty bindstone (E). Note needles which are probably sponge spicules (F); upper part of the Mixed Siliciclastic-Carbonate Member; Mohamadshah section (sample K-80; width of photomicrographs: 10 mm (E) and 1 mm (F)). (G-H) Bio-oo-grainstone containing concentric- to radial structural ooids (O) and micritized bioclastic ooids (arrowed) (G), oyster rudstone (H) with shell of an *Actinostreon* (arrowed); upper part of the Lower Siliciclastic Member; Mohamadshah section (sample m-25, 26; width of photomicrograph: 3 mm (G) and 4 mm (H)).

Fig. 5.8.12. Thin-sections of various types of microfacies from the lower part of the Mixed Siliciclastic-Carbonate Member of the Bidou Formation, Bolboulieh section. (A-B) Dolomitized bio-pel-grainstone. Note peloids (white arrows), bioclasts (black arrows), which are partly or completely recrystallized. Intraparticle pores in bioclasts (B: white arrows) suffered aggrading neomorphism, indicated by the coarsening of calcite crystals (sample K-24; width of photomicrographs: 7 mm). (C-E) Oo-grainstone. Note ooids (O) ranging from well-sorted, spherical to ellipsoidal (C). Note also syntaxial echinoderm overgrowth of calcite cements (D: white arrow) and the concentric laminae lost by micritization (arrowed). Occasionally, crinoid fragments form nucleus of an ooid (E: black arrow) (sample K-25; width of photomicrograph: 3 mm (C), 1 mm (D), and 2 mm (E)). (F-G) Silty bio-rudstone. Note that the bioclasts have been replaced by sparry calcite (black arrow) (sample M-26a; width of photomicrographs: 10 mm (F) and 2.5 (G)). (H) Bio-rudstone. Note abundant bivalve bioclasts (B), the moulds replaced by sparite, and gastropods (G), which can be seen nearly in longitudinal section (sample K-29; width of photomicrograph: 10 mm).

Fig. 5.8.13. Thin-sections of various types of microfacies from the lower (A) and upper part (B-D) of the Mixed Siliciclastic-Carbonate Member of the Bidou Formation, Bolboulieh section, and the lower (G-H) and upper part (E-F) of the Mixed Siliciclastic-Carbonate Member of the Bidou Formation, Mohamadshah section. (A) Bio(gastropod)-floatstone. Note abundant shell fragments of gastropods both in longitudinal (Ls) and oblique (Os) sections. The shell has been replaced by sparite, internal cavities (white arrow) filled with micrite (sample K-30; width of photomicrograph: 10 mm). (B) Calcareous sandstone. Note non-skeletal carbonate grains such as pellets and simple ooids (arrows) (sample K-37; width of photomicrograph: 2.5 mm). (C-D) Bio(bivalve)-rudstone. Note abundant densely packed fragments of bivalves (B) surrounded by a microspar cement, and discontinuous finely-laminated sub-horizontal fine-grained micrite within the grain-supported background sediment (sample K-38; width of photomicrographs: 2.5 (C) and 10 mm (D)). (E-F) Silty bio-rudstone. Note the roughly rectangular areas outlined with dark micrite envelopes which are recrystalized molluscan fragments,

probably bivalves. The thin, dark-brown micrite rims on the margins of the shells are formed by endolithic algae, the margins having suffered destruction by micro-borings (E: white arrow). The skeletal grains occur within a silty to sandy microsparry ferroan calcite (E) or granular mosaic cement (F). Note sharp contact between very fine- to fine-grained calcareous sandstone (black arrow) and bio-rudstone and subrounded crinoid framents (Cr) (samples K-78 and K-81; width of photomicrographs: 2.5 mm). (G-H) Cortoid-bio-rudstone. Note rounded skeletal coated grains (white arrows). Note also foliated shell fragments of bivalves (B), oysters (Oys), and gastropods (G) (sample K-61; width of photomicrographs: 10 mm).

Fig. 5.8.14 (A-C) Intra-bio-packstone/grainstone, lower part of the Mixed Siliciclastic-Carbonate Member of the Bidou Formation; Mohamadshah section. Note both shell moulds and their micrite rims, partly having experienced neomorphic recrystallisation (white arrows). Recrystallisation also occurs in the very fine-grained carbonate matrix (black arrows). Two intraclasts contain gastropods (G) (sample K-62, width of photomicrographs: 2.5 mm).

Fig. 5.8.15 Thin-sections of various types of microfacies from the upper part of the Mixed Siliciclastic-Carbonate Member of the Bidou Formation, Mohamadshah section. (A) Silty bioturbated mudstone. Note a sandwiched horizontal thinly laminated mudstone layer. The sediment is bioturbated demonstrated by the irregular distribution of silt grains. Seen also a few ostracods (Os) (sample K-68; width of photomicrographs: 2 mm). (B) Bioturbated siltstone/very fine-grained sandstone. Note dark spots (white arrow) indicative of intense bioturbation (sample K-26b; width of photomicrographs: 2 mm). (C-D) Silty cortoid-bio-rudstone. Note poorly sorted rounded bioclasts or cortoid grains (white arrow), which are covered by a thin micrite envelope. The nuclei of cortoids are mainly composed of crinoid (Cr), shell, and gastropod (G) fragments. Note also micritic grains of pellets commonly without internal structures, and microbial grains (Mc) (sample K-25b; width of photomicrographs: 3.5 mm (C) and 1 mm (D)). (E) Calcareous sandstone. Note non-skeletal grains, which are similar to pellets (sample K-71, width of photomicrograph is 2 mm). (F) Silty to sandy intra-oo-grainstone. Note spherical and/or ellipsoidal ooids (O) with thin radial cortex containing a large nucleus, composed of carbonate fragments, skeletal grains, or quartz grains. See also some subrounded to rounded intraclasts (In) and a few rounded coated grains (Co: white arrow) and foraminifer? (Fo) within a microspar cement (sample K-72;width of photomicrographs: 2.5 mm).

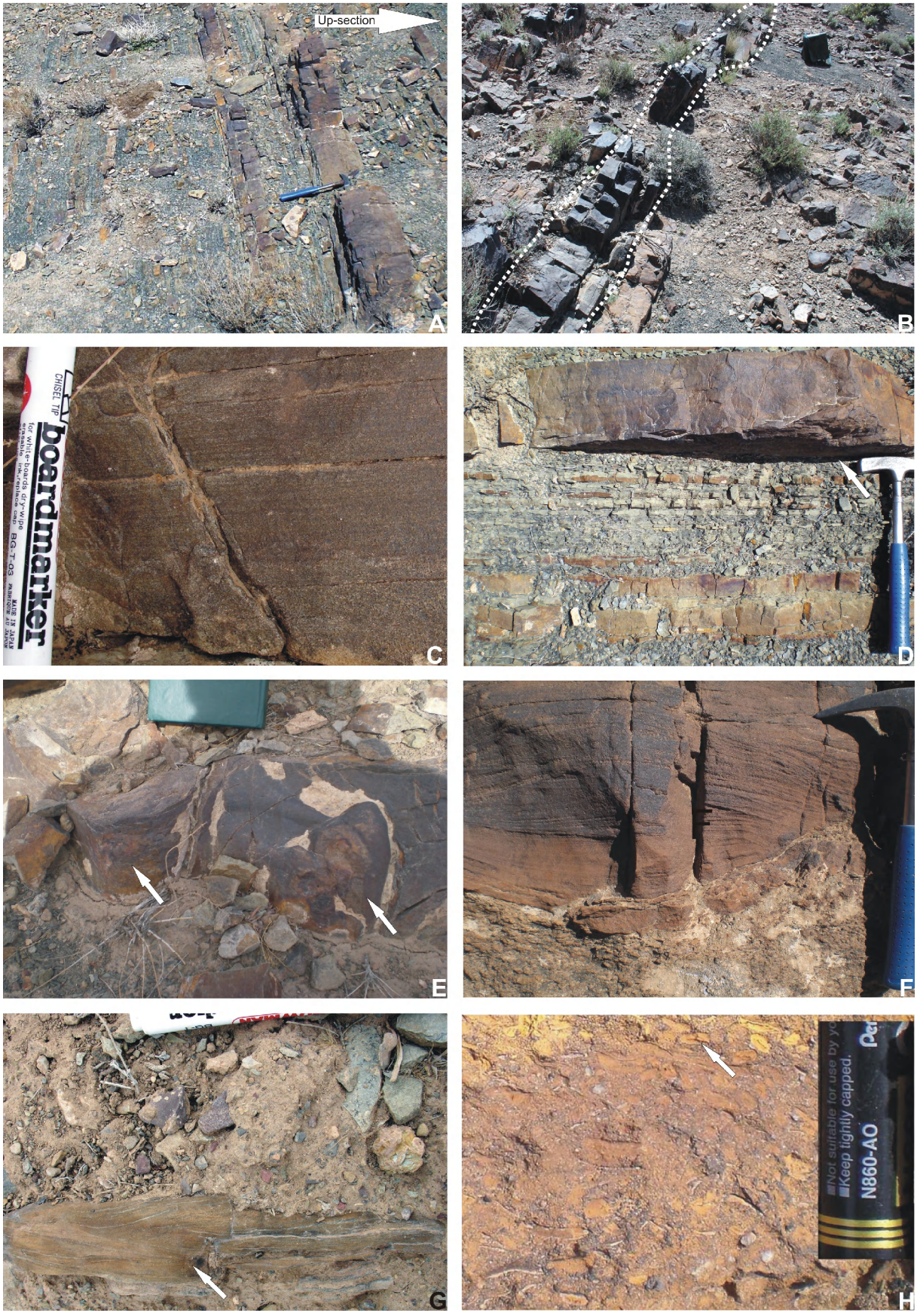

Fig. 5.8.3

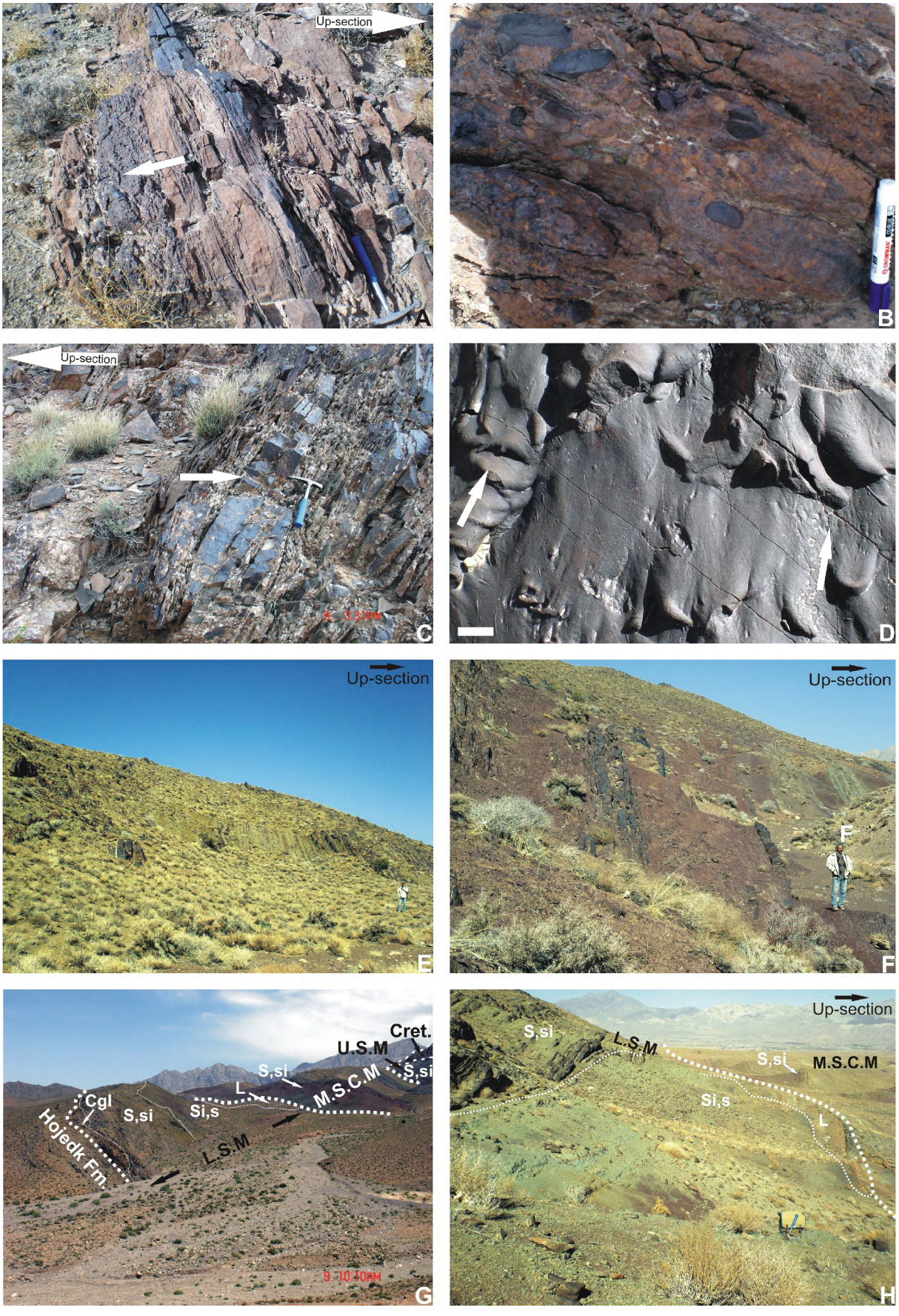
Up-section
A
B
Up-section
C
D
Up-section
E
Up-section
F
F
Cret.
U.S.M
S,si
S,si
L
M.S.C.M
Cgl
S,si
Si,s
Hojedk Fm.
L.S.M
G
Up-section
S,si
L.S.M
S,si
M.S.C.M
Si,s
L
H

Fig. 5.8.4

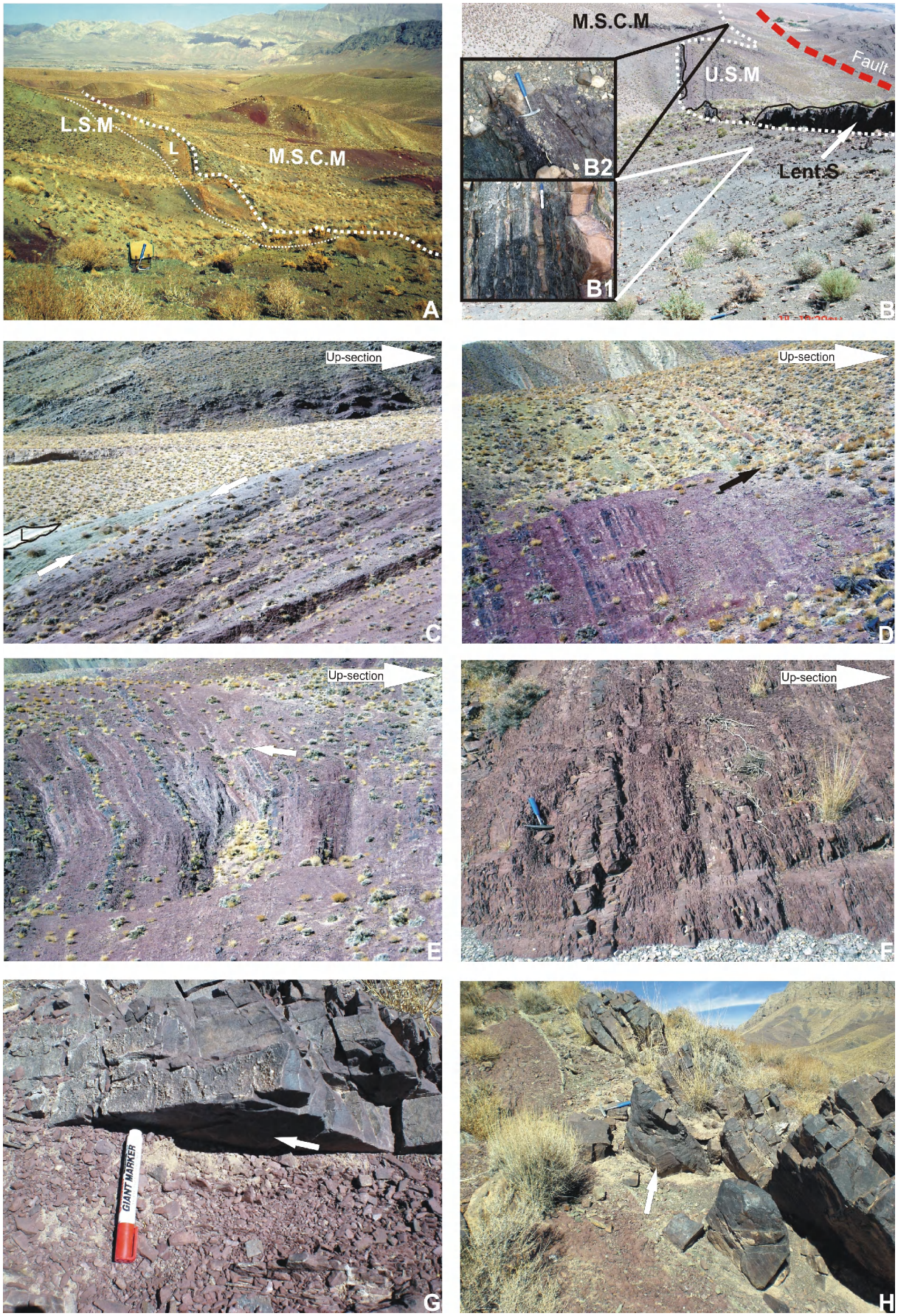
L.S.M
L
M.S.C.M
A
M.S.C.M
U.S.M
Fault
B2
Lent.S
B1
B
Up-section
C
Up-section
D
Up-section
E
Up-section
F
GIANT MARKER
G
H

Fig. 5.8.5

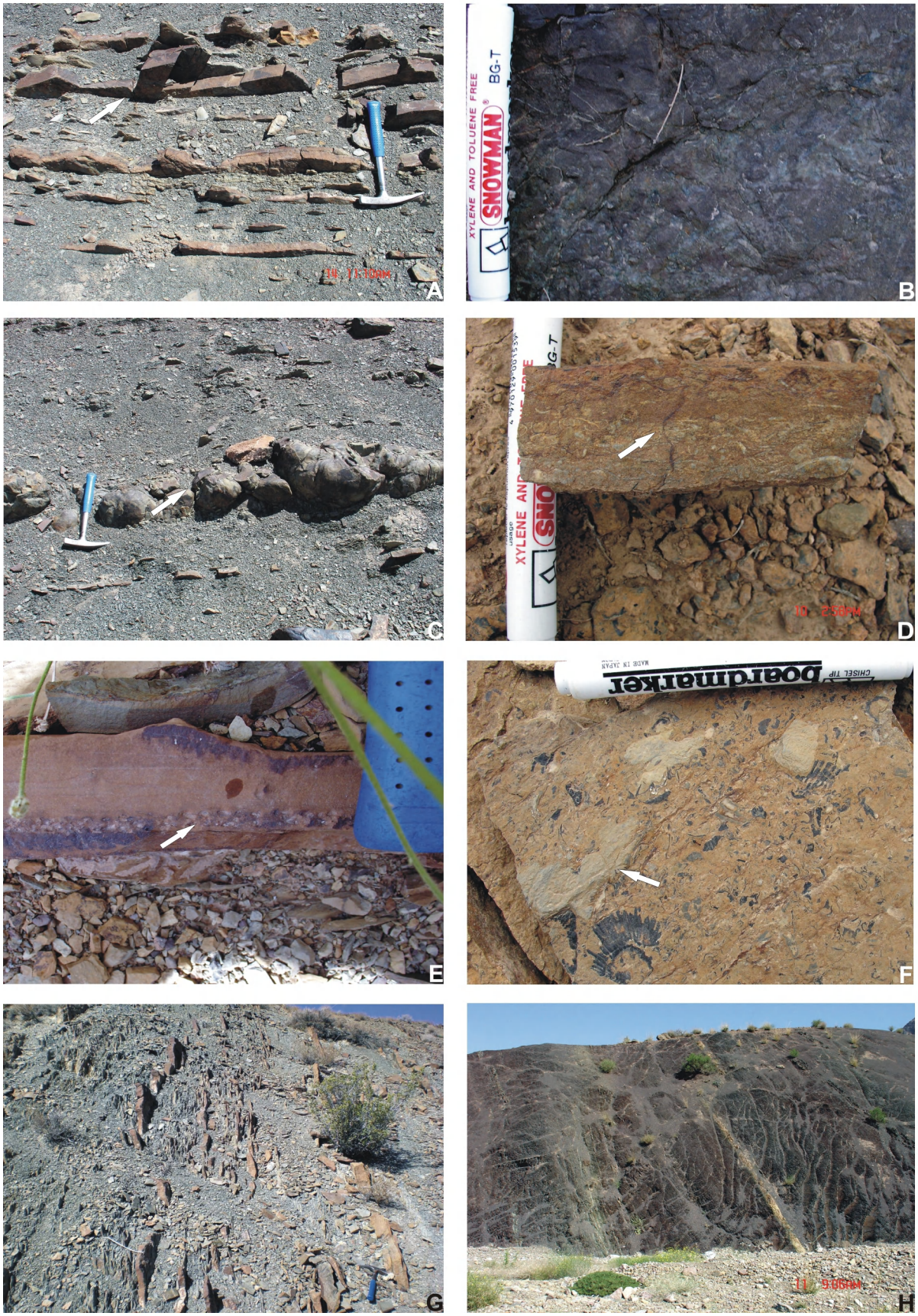

Fig. 5.8.6

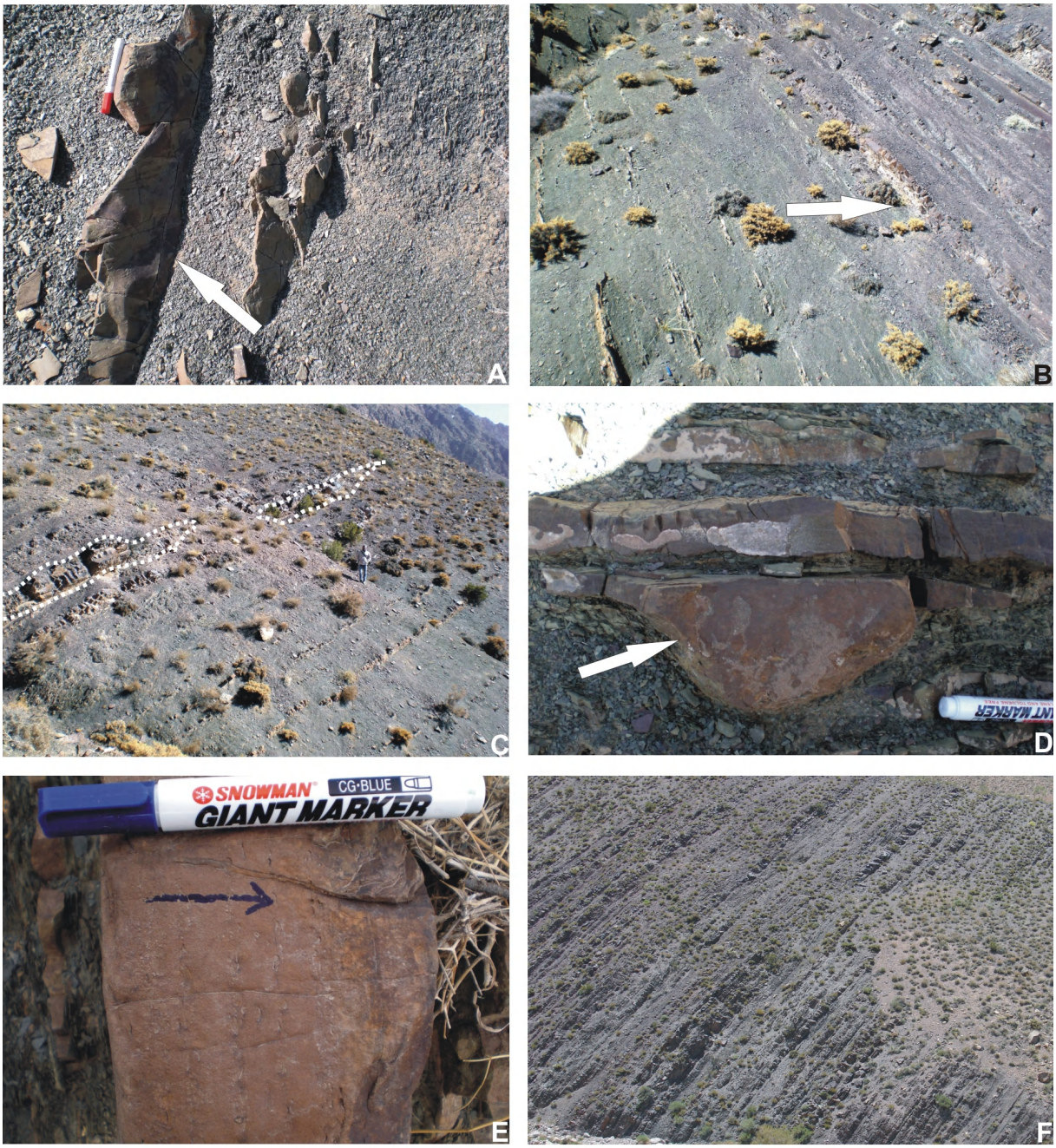

Fig. 5.8.7

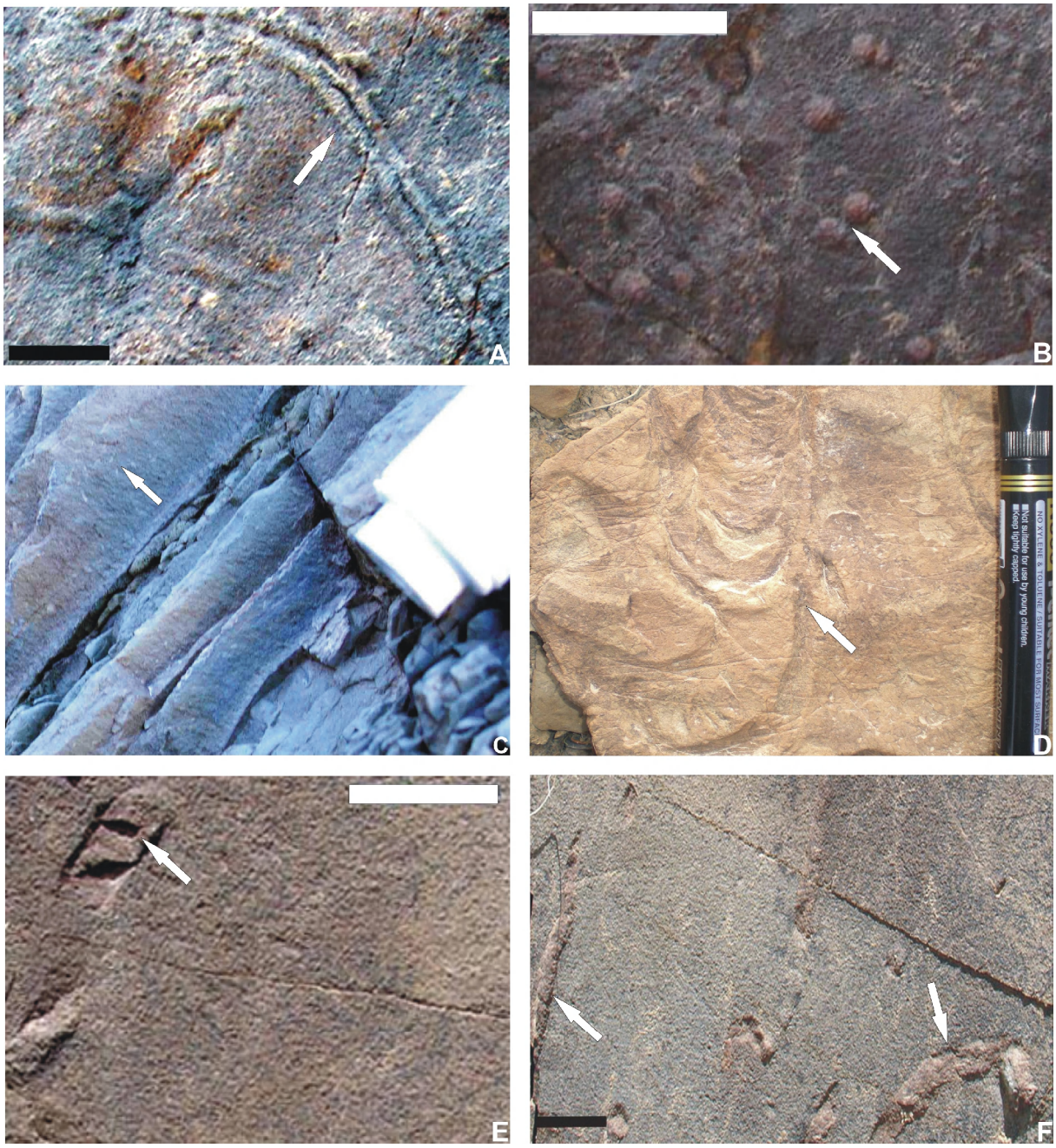

Fig. 5.8.8

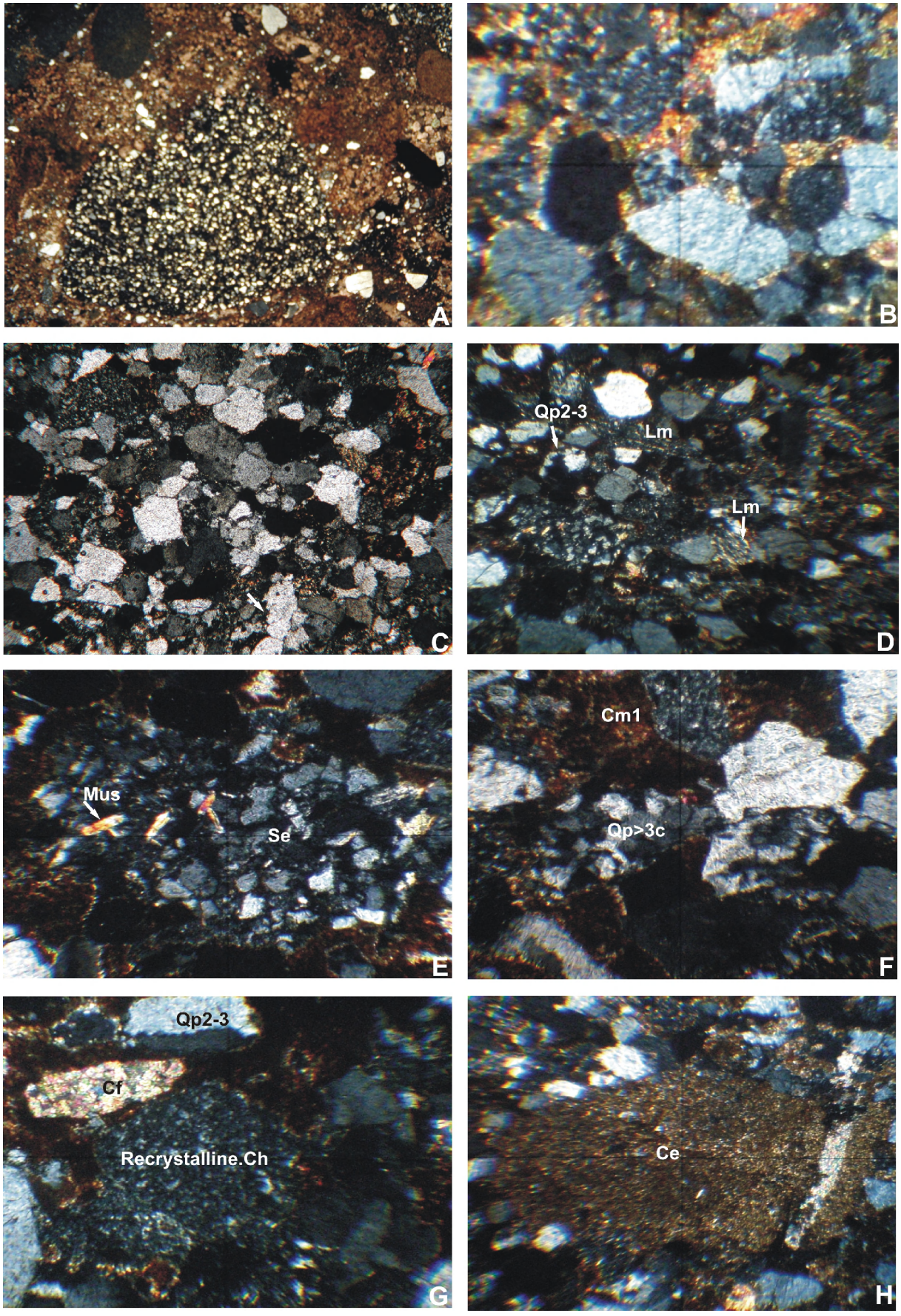
A
B
C
Qp2-3
Lm
Lm
D
Mus
Se
E
Cm1
Qp>3c
F
Qp2-3
Cf
Recrystalline.Ch
G
Ce
H

Fig. 5.8.9

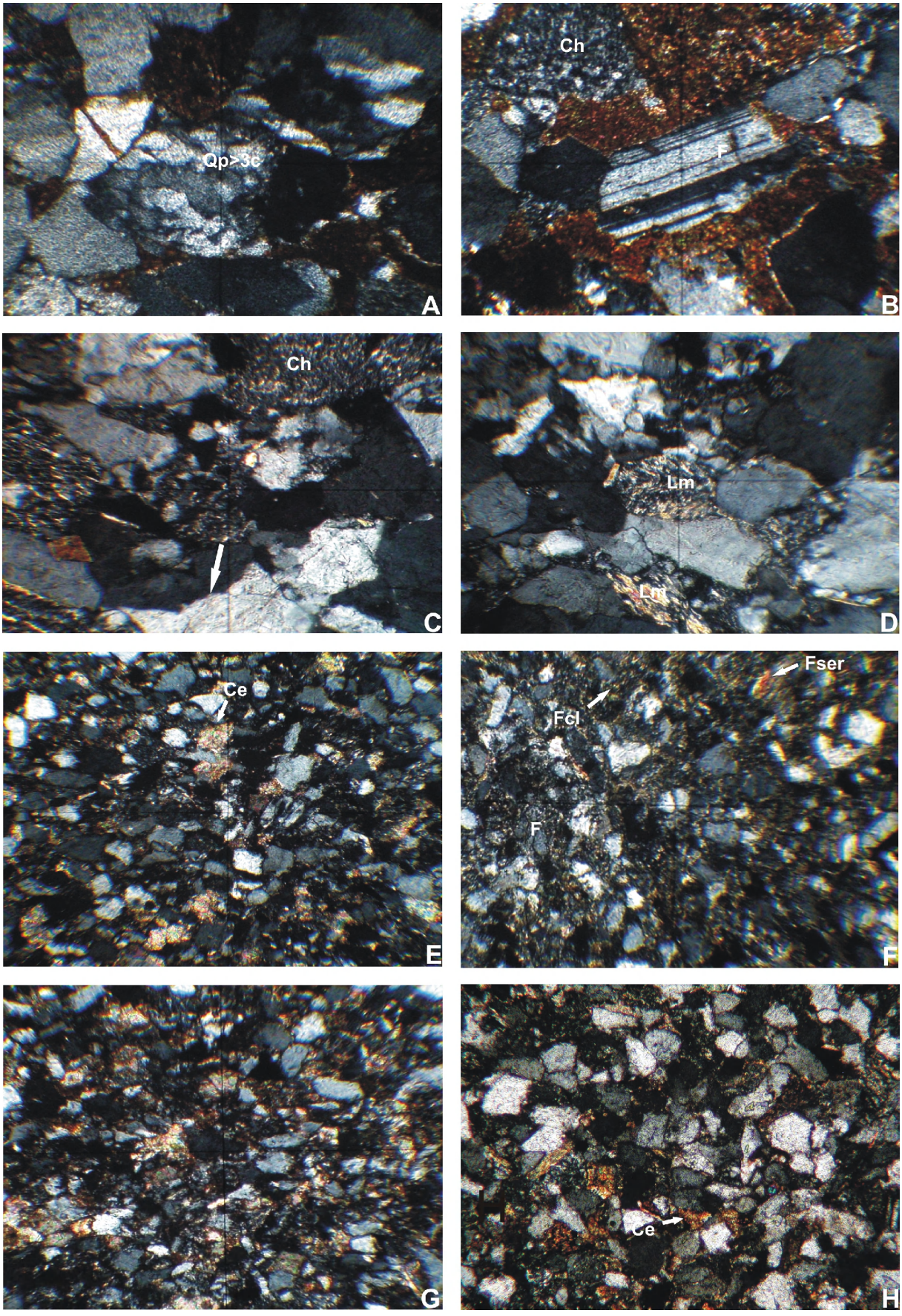

Fig. 5.8.10

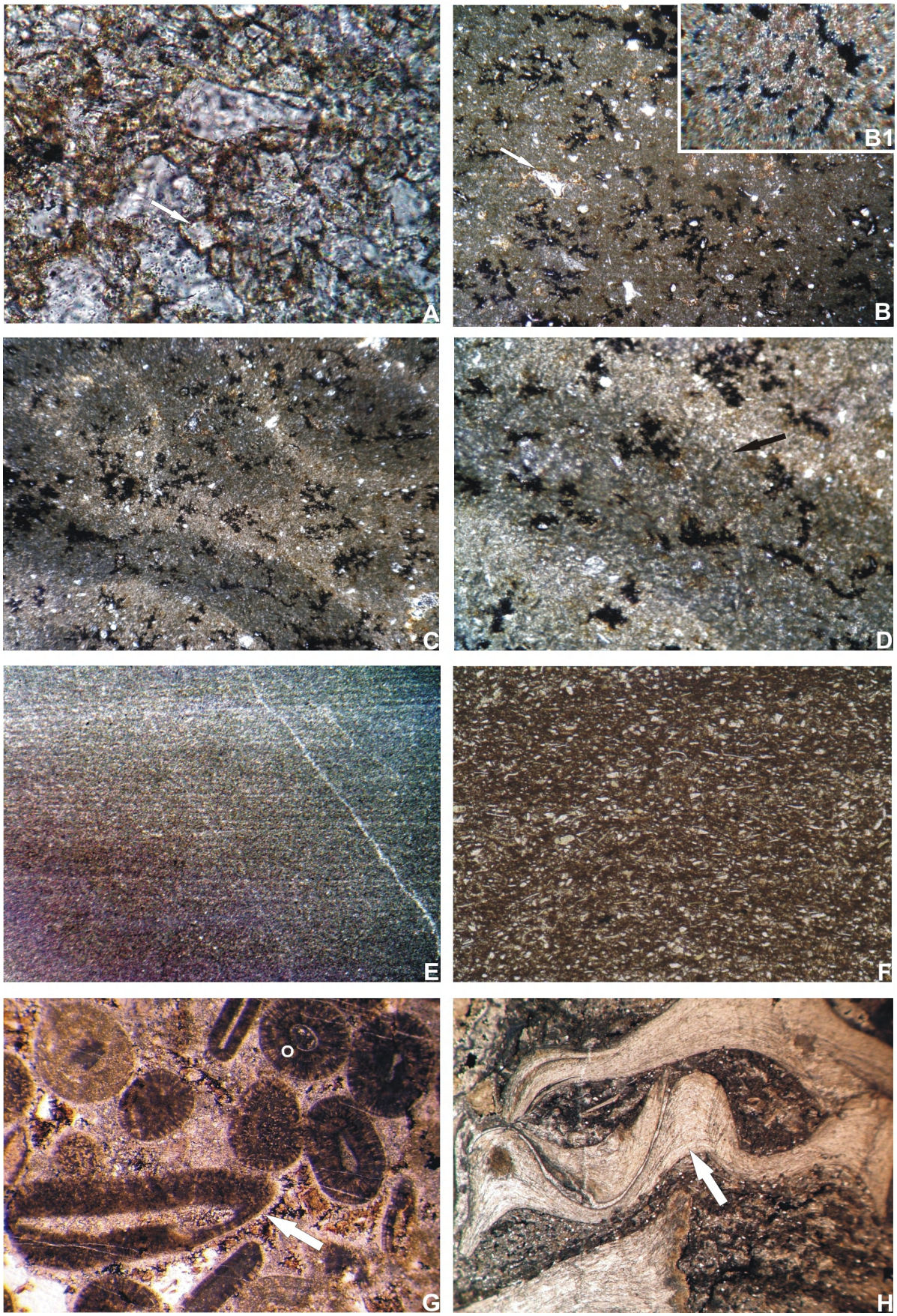

Fig. 5.8.11

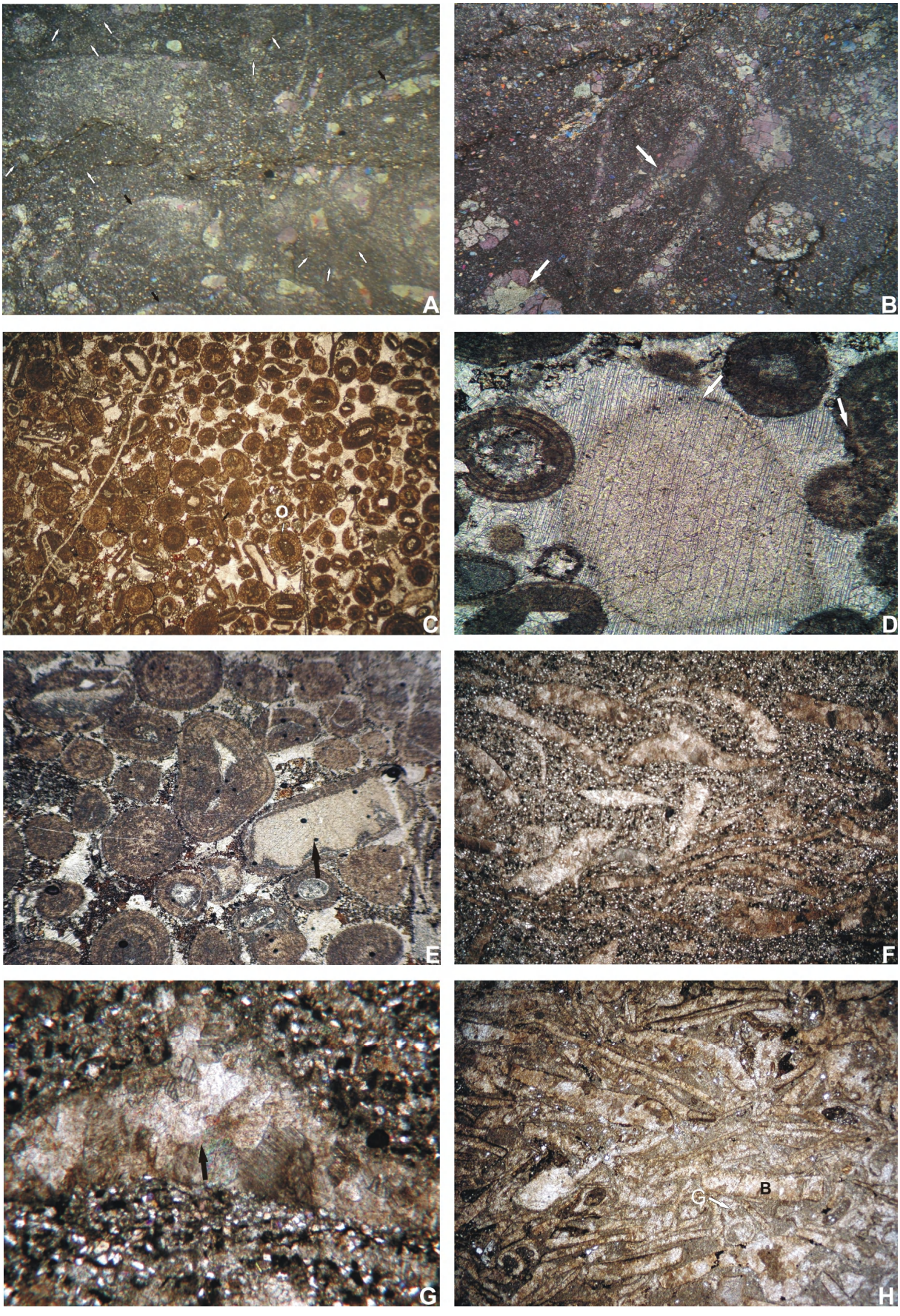

Fig. 5.8.12

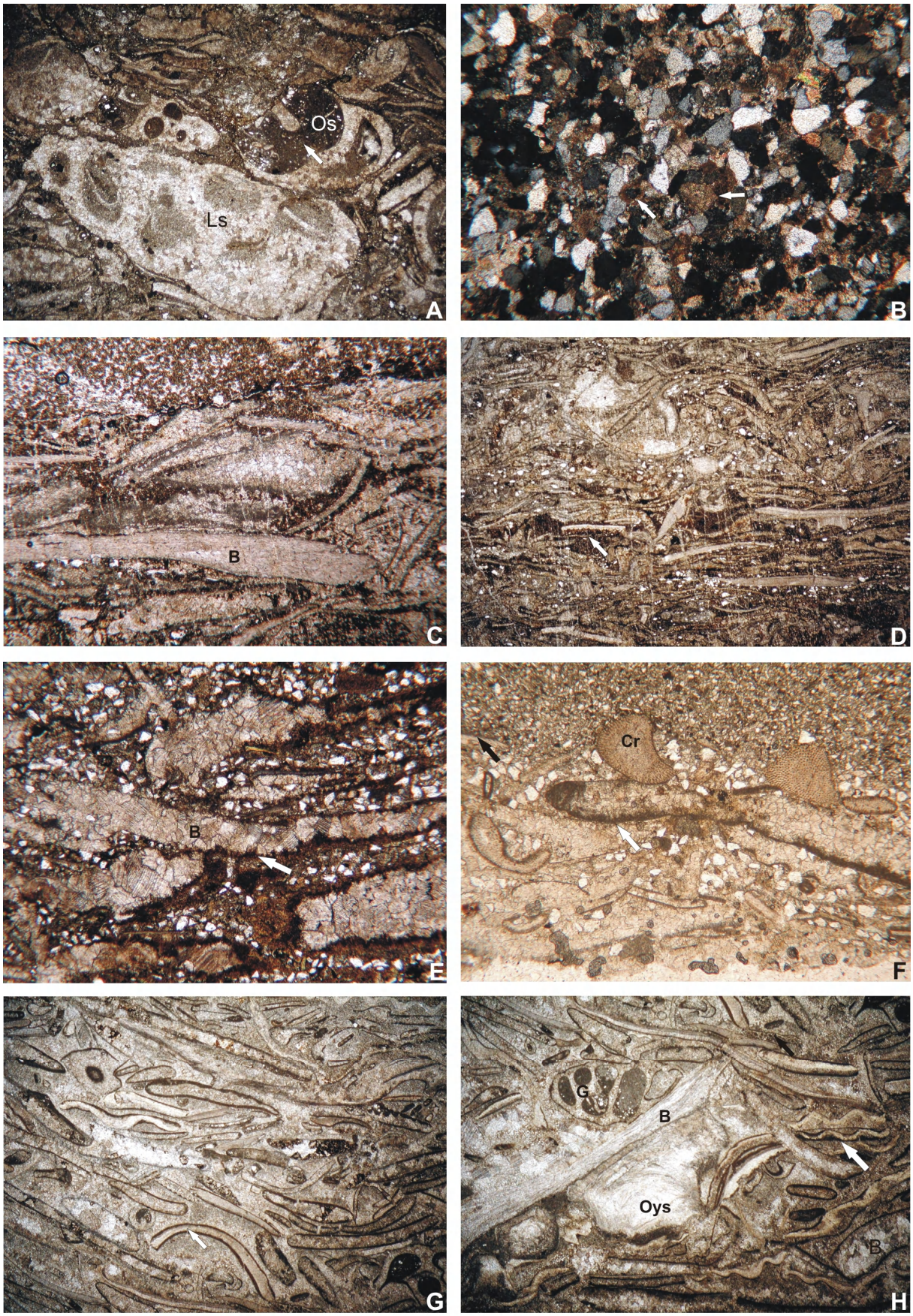

Fig. 5.8.13

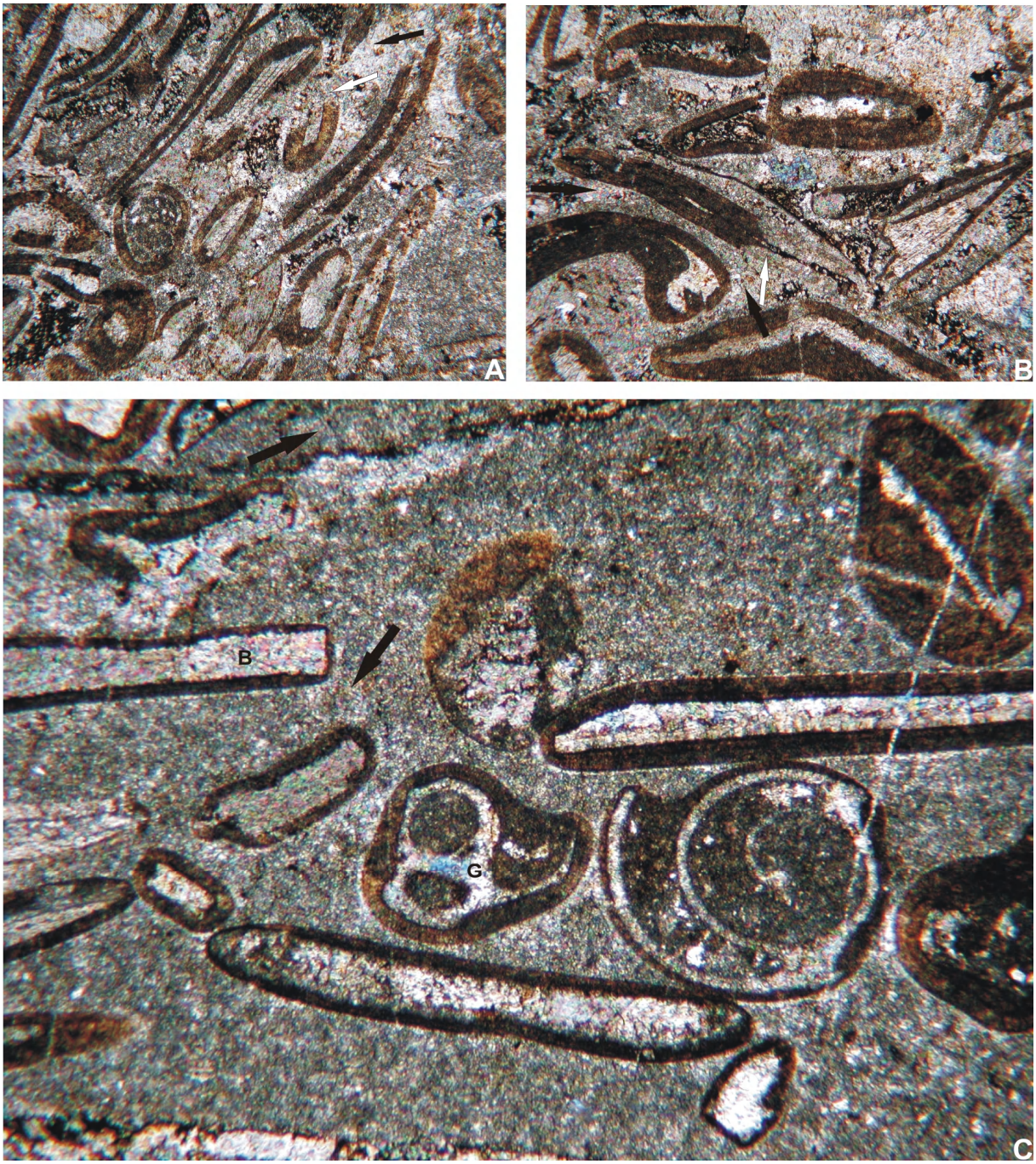

Fig. 5.8.14

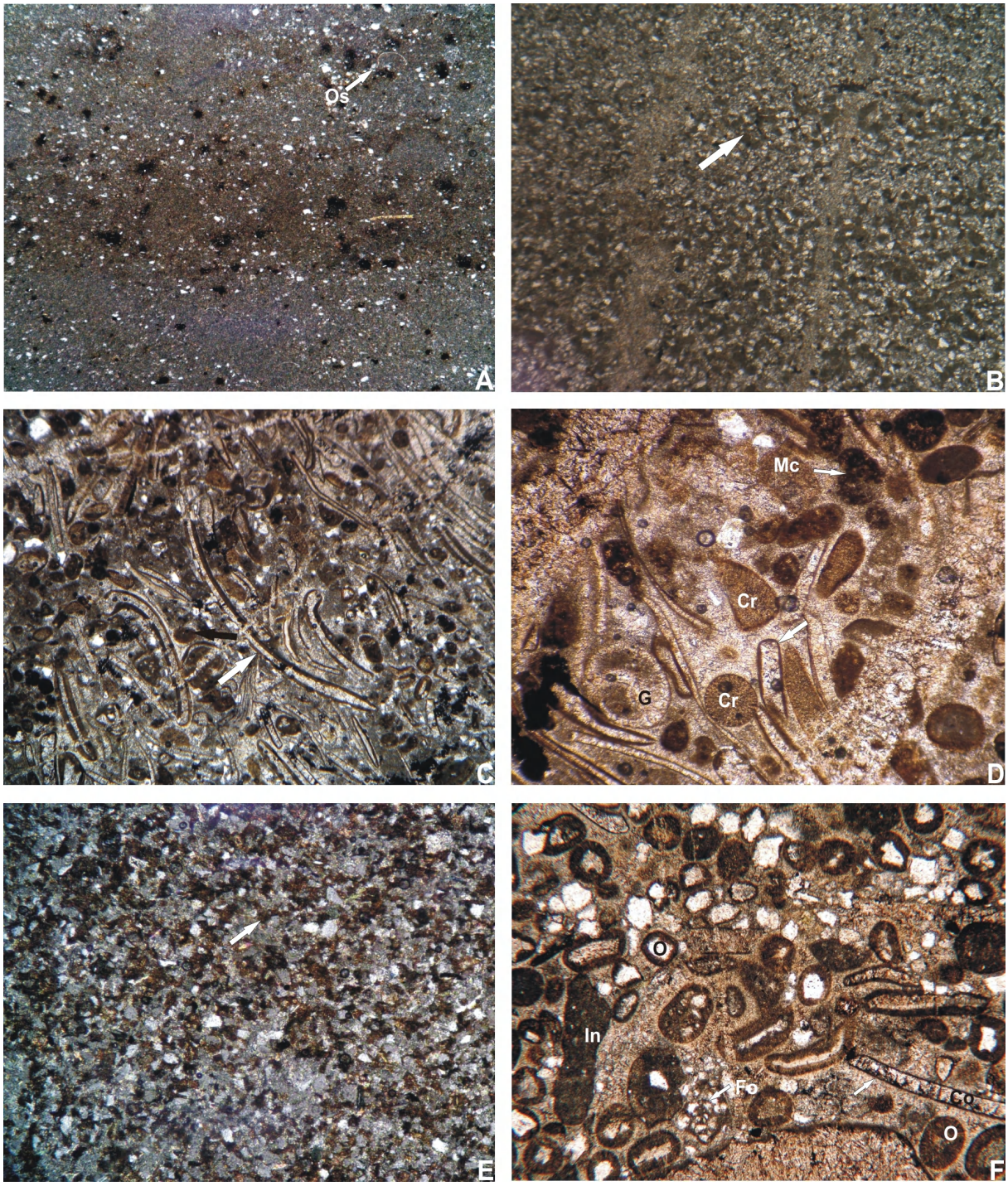

Fig. 5.8.15

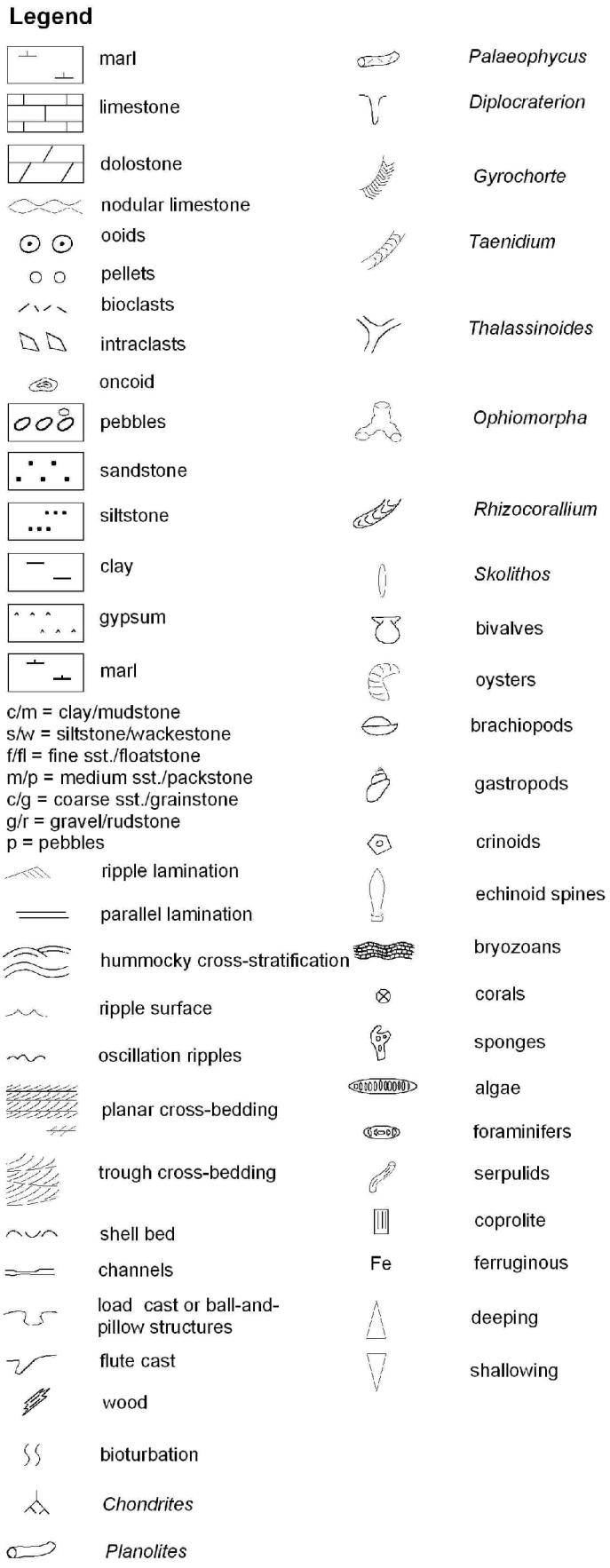

Fig. 5.8.16. Legend

6 Lithostratigraphy

Based on AGHANABATI (1977, 1998), the Upper Triassic-Jurassic succession can be subdivided into a numbers of formations, which can be combined into two groups separated by unconformities related to tectonic events. The Shemshak Group (Norian-Bajocian) is intercalated between the Early and the Mid-Cimmerian tectonic event (see also FÜRSICH et al. 2009; WILMSEN et al. 2009) and the Magu Group (Bajocian-Upper Jurassic) is sandwiched between the Mid and the Late Cimmerian tectonic event. In the new lithostatigraphic scheme of WILMSEN et al. (2003, 2009), the Magu Group on the northern Tabas Block is subdivided into three subgroups, i.e. the Baghamshah, Esfandiar and Garedu subgroups. In the southern Tabas Block the equivalent term is Bidou Group (AGHANABATI 2004; WILMSEN et al. 2009). In the present study, the name Bidou Formation has been used in the Bidou, Mohamadshah and Bolboulieh sections (Kerman-Zarand area). The formation is subdivided into three members, i.e. the Lower Siliciclastic Member (equivalent to the Parvadeh and Baghamshah formations), the Mixed Siliciclastic-Carbonate Member and the Upper Siliciclastic Member (equivalent to the Kamar-e-Mehdi and Magu Gypsum formations).

6.1 Hojedk Formation

In the Ravar and Bolboulieh sections, several meters of the uppermost part of the Hojedk Formation have been measured in order to identify the lower boundary of the Bidou Formation.

6.1.1. *Type locality*: According to STÖCKLIN & SETUDEHNIA (1991), no type section has been designated. The Hojedk Formation is named after the village and coal-mine of Hojedk, north of Kerman. The hills north and west of Hojedk are the type area. The name has been approved by the Stratigraphic Committee in 1964 (Geol. Survey Iran, Geol. Dept. file No. 3, unpublished). Lithologically, it consists of alternations of feldspathic to quartz-sandstones with green, brownish-grey shales containing several coal lenses (especially coal horizon D) as well as thin carbonates with macrofossils such as bivalves and plants.

6.1.2.*Hojedk Formation in the Bolboulieh area* The uppermost 34 m of the Hojedk Formation (Fig. 5.8.1) are characterized by irregularly coarsening-/shallowing-upward cycles (Fig. 5.8.3A) developing from olive-green to dark-grey, thin- to thick-laminated silty shales/siltstones to grey, brown or milky lenticular, horizontal- to unidirectionally low-angle cross-laminated, fine- to medium-grained, thin- to thick-bedded feldspathic to quartz sandstones (Fig. 5.8.3B-C). The sandstones commonly exhibit a sharp base (Fig. 5.8.3D) and

occasionally load casts (Fig. 5.8.3E). The top part of these sandstones turns into brown sandstones containing 30 cm thick lenticular intercalations of conglomeratic/pebbly sandstone, hummocky cross-stratified sandstone (Fig. 5.8.3F), quartz-sandstone (Fig. 5.8.9B), wave-rippled silty limestone (Fig. 5.8.3G) and thick-bedded oncolitic rudstone with abundant shell fragments (Fig. 5.8.3H). Recognizable trace fossils are *Diplocraterion* or *Arenicolites* and *Gyrochorte* (Fig. 5.8.8A-B). In the Bolboulieh and Mohamadshah sections (Figs. 5.8.1-2), the Hojedk Formation is unconformably overlain by the Bidou Formation.

6.1.3. *The Hojedk Formation in the Ravar area*: In the Ravar area (Fig. 5.6.1), the top 14 m of the Hojedk Formation is characterized by alternations of olive to green, or dark-grey silty shale to siltstone, light-brown trough-cross-laminated, thin- to thick-bedded quartz sandstone, and calcareous sandstone (Figs. 5.6.2A-B, 5.6.7A-B) with intercalations of bioturbated sandstones containing the trace fossils *Diplocraterion*/*Arenicolites* (Fig. 5.6.2C-D), and shell beds. The latter contain bivalves, and high-spired nerineid gastropods (Fig. 5.6.2A1, 2). The Hojedk Formation is overlain by a 50 cm thick basal conglomerate of the Parvadeh Formation (Fig. 5.6.2E-F, F1, 7C).

6.1.4. *Remarks*: In Central Iran, the Hojedk Formation consists predominantly of soft sandstones and argillaceous shales. In contrast to the more quartzitic sandstones of the Shemshak Formation, the formation contains also some sandy and oncolitic limestone beds with marine fauna. Its thickness ranges from 500 to 1000 m (SEYED-EMAMI et al. 2001). In the northern Tabas Block, the Hojedk Formation overlies the marine Badamu Formation and the upper boundary is characterized by a major unconformity. On the Lut Block, the Hojedk Formation is generally marine and can be dated using ammonites (e.g., SEYED-EMAMI et al. 2004b). Towards the west, its character changes to marginal marine and fluvial, including coal swamps (WILMSEN et al. 2009).

6.1.5. *Age*: The age of the Hojedk Formation is mainly based on its stratigraphic position above the Badamu Formation and below the Parvadeh Formation. According to AGHANABATI (2004) the Hojedk Formation ranges from the Upper Bajocian to the Lower Bathonian (SEYED-EMAMI et al. 2001), whereas AGHANABATI & REZAEE (2009) assumed the formation to range from the Middle Bajocian to the Middle Bathonian.

6.2. Parvadeh Formation

From the north-western to the southern Tabas Block (from Echellon to Ravar areas), this formation is several tens of meters thick, but toward the Kerman-Zarand area, it laterally

grades into the Lower Siliciclastic Member of the Bidou Formation. In the present study, the Parvadeh Formation have been measured in the Ravar section.

6.2.1. ***Type locality*** The Parvadeh Formation is named after Parvadeh Village, south of Tabas, but type locality is in northwest of Tabas, east of Kuh-e-Echellon (AGHANABATI 2004). At the type localithy, the Parvadeh Formation is 46 m thick and is characterized by 7 m of conglomerate at base which is followed by 39 m of dark-grey thick-bedded microbial limestone and rarely oncolitic limestone. The formation overlies the Hojedk Formation with unconformable contact and has a conformable contact with the Baghamshah Formation.

6.2.2. ***Parvadeh Formation in the Ravar area*****:** The basal conglomerate of the 109 m thick Parvadeh Formation (Fig. 5.6.1) overlies the Hojedk Formation with unconformable contact. It is followed by 35 m of alternations of greenish-grey to light-brown horizontal to low-angle cross-laminated calcareous sandstones and marls (Fig. 5.6.2G) with intercalated sandy bio-wackestones (Fig. 5.6.7E) containing the bivalves *Trigonia* and *Inoperna*, and high-spired gastropods such as nerineids. This facies is followed by irregular alternations of brown to grey, trough cross-laminated (at 44 m; Figs. 5.6.2H, 5.6.7F), small- to large-scale planar cross-stratified (Fig. 5.6.3B, C), thin- to thick-bedded calcareous sandstone (Fig. 5.6.7H) and sandy bio-oo-grainstone (Fig. 5.6.7G) with intercalations of onco-rudstones (Figs. 5.6.3D, 5.6.8A), sandy onco-bio-rudstones (Fig. 5.6.8B), and the trace fossil *Chondrite*s (Fig. 5.6.3A). In the uppermost part of the Parvadeh Formation, the succession is followed by intra- and bio-grainstone and bio- /onco-rudstone with oyster debris (Fig. 5.6.3E). The Parvadeh Formation is conformably overlain by the Baghamshah Formation (Fig. 5.6.3F).

6.2.3. Remarks: According to AGHANABATI (1977), the Parvadeh Formation is restricted to the northern part of the Tabas Block. It contains several tens of meters of dark-grey, thick-bedded oncolitic, microbial, occasionally oolitic limestones with a decimeter- to meter-thick basal conglomerate containing quartzite, milky quartz, and sandstone pebbles. The widespread unconformity and conglomerate layer at the base of the Parvadeh Formation indicate a phase of non-sedimentation, uplift and erosion, followed by renewed deposition (WILMSEN et al. 2009). Depending on the relief, the basal sediment represents deposits of braided streams or transgressive lags.

6.2.4. Age: The base of the Parvadeh Formation at Ravar is assigned to be Bathonian according to the presence of the ammonites *Procerites*, *Oxycerites*, *Cadomites*, and perisphinctids (SAYFOURI 2007). The formation is Bathonian in age in the Nayband area (AGHANABATI 1998), and according to the ammonites *Procerites* cf. *schloenbachi*, *Phaulozigzag*, and *Siemiradzkia pseudorjasanensis*, it has a Late Bajocian-Middle Bathonian

age south of the Tabas area. On the Lut Block, the formation is assigned to the upper Middle Jurassic based on the presence of bivalves such as *Radulopecten tipperi*, ?*Ceratomya concentrica* and *Plagiostoma* and on gastropods (AGHANABATI 1998). According to SEYED-EMAMI et al. (1991) the age of the formation on the Tabas Block ranges from the Late Bajocian (northwest of Kuh-e-Naybandan) to the Middle Bathonian (Kuh-e-Echellon). AGHANABATI & REZAEE (2009) suggested a Middle-Late Bathonian age.

6.3 Baghamshah Formation

In the Doshakh (Fig. 5.2.1) and Abdoughi areas (Fig. 5.5.1), the top of the Baghamshah Formation has been measured in order to identify the lower boundary of the Kamar-e-Mehdi Formation. The whole thickness of the formation has been measured in the Ravar area to compare it stratigraphically with the Bidou Formation in the Kerman area.

6.3.1. *Type locality*: Lasht-e-Baghamshah, in the central Shotori Mountain, ENE of Tabas (STÖCKLIN et al. 1965).

The formation is composed mainly of shale, light-green marly shale with some sandstone and limestone intercalation. The thickness reaches up to 496 m.

6.3.2. ***Upper part of the Baghamshah Formation in the Doshakh area*:** The uppermost part of the Baghamshah Formation constitutes the base of the studied section (Fig. 5.2.1) and consists of 109 m of coarsening-upward cycles of greenish-grey, light-brown silty marl, silt and very fine-grained feldspathic sandstone beds with horizontal lamination to very low-angle cross-stratification (Fig. 5.2.2A). There are several intercalations of carbonates, such as oo-grainstone (Fig. 5.2.4B; at 23, 29 and 37 m), intra-oo-grainstone (Fig. 5.2.4G; at around 86 m), onco-floatstone/packstone (between 25 and 39 m; Fig. 5.2.4C), bio-wackestone (Fig. 5.2.4E2-E4; at 50 m), and of bioturbated silty bio-floatstone (Fig. 5.2.4D, E1; at 69 m). The latter contain fragments of perisphinctid ammonites, the bivalves *Grammatodon* (*G.*), *Arcomytilus*, *Pleuromya*, *Chlamys* (*C.*), *Radulopecten tipperi*, and *Actinostreon gregareum*, and rhynchonellid brachiopods. Sedimentaty structures of sandstones include erosional bases (Fig. 5.2.2B), hummocky-cross-stratification (at 10 m; Fig. 5.2.2E) and oscillation (at 16 m; Fig. 5.2.2F) and sub-parallel-crested ripples (at 18 m; Fig. 5.2.2G). The trace fossils *Planolites* (at 84 m; Fig. 5.2.2H), *Thalassinoides* and *Neonereites* (Fig. 5.2.3A) are also found. The upper boundary of the Baghamshah Formation with the Kamar-e-Mehdi formation is an erosional surface.

6.3.3. *Upper part of the Baghamshah Formation in the Abdoughi area*: The succession consists of greenish-brown, very thickly laminated to thick-bedded, fine- to medium-grained

calcareous sandstone with intercalated red to greyish-green silt to silty clay (Figs. 5.5.1, 2A) and sedimentary structures such as horizontal to medium-angle cross-stratification, some wedge-shaped cross-bedding (at 16 m, Fig. 5.5.2B), planar cross-bedding (at 22 m, Fig. 5.5.2C), and some biogenic sedimentary structures such as vertical trace fossils (*Diplocraterion* or *Arenicolites* (Fig. 5.5.2D) and *Skolithos* (Fig. 5.5.2E)). These facies overlie with sharp base dark-green to greenish-grey silty marl with intercalations of sharp-based, horizontal, wavy laminated sandstone beds with *Thalassinoides* (at 2 m, Fig. 5.5.2F). Their age is Middle Jurassic based on the foraminifer *Lenticulina subalata* (KALANTARI 1969) (Fig. 5.5.3D1). The uppermost part of the Baghamshah Formation is overlain with unconformable contact by a thick siliciclastic facies of the basal Kamar-e-Mehdi Formation (at 83 m).

6.3.5. *Description of the Baghamshah Formationin in the Ravar area*: The formation is 163 m thick and overlies the Parvadeh Formation conformably (at around 122 m; Fig. F.6.3F). The formation starts with several coarsening- and thickening-upward cycles of greenish-grey to brown silty clay at base and greenish-brown, horizontal to cross-stratified sandstone beds at top (e.g., Fig. 5.6.8C) with intercalations of bioturbated intervals (between 122 and 254 m). Higher up, brownish-green medium- to coarse-grained calcareous sandstone (Fig. 5.6.9A-A1, B) occurs, containing shell and crinoid fragments with rare intercalations of silty marl. Sedimentary structures consist of uni- and bi-directional cross-stratification (between 254 and 267 m; Fig. 5.6.3G-H,) with scours (at 262 m; Fig. 5.6.4D), concretions (Fig. 5.6.4E), and sub-parallel to oscillation ripples (at 268 m; Fig. 5.6.4C). Higher up (at 275 m), this facies turns into brown horizontal-laminated sandstone (Fig. 5.6.4F) with oscillation ripples (Fig. 5.6.4G). At 277 m, coarsening- and thickening-upward cycles start with several 10 m thick of greenish-brown to grey gypsiferous silty clays (Fig. 5.6.4H) containing intercalations of thickly laminated to thin-bedded sandstone (Fig. 5.6.8G) and occasionally brown, thin-bedded oyster-rudstone (Fig. 5.6.4H1, 5.6.8F). The Baghamshah Formation is followed unconformably by the basal thick-bedded, cross-stratified sandstone (Fig. 5.6.8D, E) of the Kamar-e-Mehdi Formation.

6.3.5. *Remarks*: According to STÖCKLIN et al. (1965), the Parvadeh Formation in the Tabas and the Shotori areas is followed gradationally by pale-green silty to marly shales with intercalations of sandstones and rare intercalations of oolitic to oncolitic limestones. Based on WILMSEN et al. (2003, 2009), the Baghamshah Formation is fairly marly and fine-grained in the western part of the Tabas Block, whereas towards the east, the silt and sand content increases. At the boundary with the Lut Block, it is represented by intercalations of silts and fine-grained, often sharp-based sandstone beds. According to AGHANABATI (1998), the

thickness of the Baghamshah Formation varies across the Shotori Range, for instance from 400 m in Ghaleh Chal, to 600 m at Kuh-e-Biragh and 376 m at Shadouk. In the Kalmard area, it reaches 585 m, in the Parvadeh area up to 1000 m and north of Kerman more than 800 m. KLUYVER et al. (1983) assumes the Baghamshah Basin to have been rather deep in the Shotori Range, but much shallower in the Tabas area.

6.3.6. ***Age*****:** The Baghamshah Formation has been assigned a ?middle Late Bathonian to early Middle Callovian age based on ammonites (SEYED-EMAMI et al. 1997, 1998, 2002, 2005). According to AGHANABATI & REZAEE (2009) the Baghamshah Formation in east-central Iran ranges from Upper Bathonian to the Upper Callovian.

6-4 Gypsum-Pecten Limestone (Kamar-e-Mehdi Formation)

Different parts of the Kamar-e-Mehdi Formation have been measured in the Echellon, Doshakh, Kamar-e-Mehdi, Abdoughli, and Ravar areas. The formation is equivalent to the Gypsum-Pecten Limestone of HUCKRIEDE et al. (1962).

6.4.1. ***Type locality*****:** The Kamar-e-Mehdi Formation has been introduced by WILMSEN et al. (2003) with the type locality in the Kamar-e-Mehdi area close to Qoleh Nar peak SW of Tabas. According to HUCKRIEDE et al. (1962), this Upper Jurassic unit consists of thin-bedded limestones, marl and gypsum with abundant pectinid bivalves. It is widely distributed from north of Kerman to north of Kalmard area.

6.4.2. ***Lower part of the Kamar-e-Mehdi Formation in the Doshakh area*****:** The base of the Kamar-e-Mehdi Formation (Fig. 5.2.1) is formed by a 8.1 m thick brown, very fine- to fine-grained calcareous sandstone (at 108 m; Figs. 5.2.3E, 5.2.5B). Sedimentary structures mainly consist of large-scale planar cross-stratification (Fig. 5.2.3E), which usually resembles that found at top of the Baghamshah Formation. The facies overlies a greenish-grey to brown sandy oo-grainstone (Fig. 5.2.5A) in thickness in 4.5 m. The latter probably forms the top of the Baghamshah Formation and overlies green silty marl (at 103.5 m). Small bivalves of uniform size occur on bedding planes (Fig. 5.2.3D), and horizontal trace fossils such as *Palaeophycus* (Fig. 5.2.3B) occur in the lower parts of the basal calcareous sandstone as do vertical trace fossils such as *Diplocraterion* or *Arenicolites* (Fig. 5.2.3C). The mixed siliciclastic-carbonate rocks at the base of the Kamar-e-Mehdi Formation are followed by grey to light-brown bio-oo-grainstone (between 112 and 128 m; Fig. 5.2.5D) beds with intercalations of bio-oo-packstone (Fig. 5.2.5C) and, intra-cortoid-bio-wacke- to -floatstone (Figs. 5.2.5F-H, 5.2.6A-D). This facies is mainly thickly laminated to medium-cross-bedded, with some distinct planar cross-stratification, oscillation ripples (Fig. 5.2.3F), and with some

bioturbated intervals. The second mixed siliciclastic-carbonate cycle starts at 132 m with alternations of silty marl and very fine-grained calcareous feldspathic sandstone (Fig. 5.2.6E). At the base of the sandstones some ball-and-pillow structures are seen, and on the weathered surfaces small wavy-crested to oscillation ripples occur. At 154 m this facies is overlain by brown, well bedded silty to sandy bio-floatstone with some shell fragments (Fig. 5.2.6F). Up-section, the rocks are mostly marl, pure mudstones, silty mudstones with irregular coarsening- and thickening-upward cycles, in which intercalations of intra-pel-wackestone (Fig. 5.2.5E) and sandy bio-floatstone occur (at 231 m). The latter contain corals such as *Pseudocoenia slovenica*, which are encrusted with *Serpula* (*Darsoserpula*), and bivalves such as *Camptonectes* (*C.*), *Radulopecten tipperi*, *Plagiostoma*, *Actinostreon gregareum, Nanogyra nana* as well as numerous fragments of oysters, gastropods, cidaroid spines, and calcisponges near the top of the measured section.

6.4.3. ***Uppermost part of the Kamar-e-Mehdi Formation in the Echellon area*****:** The top part of the Kamar-e-Mehdi Formation has been measured in order to identify the lower boundary of the Magu Gypsum Formation. The succession is characterized by 22 m of yellow to cream-coloured, well-bedded mud-, wackestones, and marl with intercalations of bio-pel-grainstones (Fig. 5.1.4C), bio-rudstones (Fig. 5.1.4D) and thin-bedded shell layers with *Radulopecten tipperi*, *Ceratomya concentrica*, small heterodont bivalves, *Nanogyra nana*, and *Liostrea*. The succession continues with a green gypsiferous marl containing thin-bedded layers of mudstone with gypsum needles (Fig. 5.1.4A), mudstone containing rare shell fragments (Fig. 5.1.4B) and very thin-bedded shell beds. The Nar Limestone Member (at 63 m; Fig. 5.1.2A) with gradual contact follows from hereon.

6.4.4. ***Kamar-e-Mehdi Formation in the Kamar-e-Mehdi area*****:** This formation, which has a thickness of 1281 m, overlies the Baghamshah Formation with erosional contact (Fig. 5.3.2A). At the base, the succession is characterized by brown, very fine- to fine-grained calcareous sandstones (Fig. 5.3.5A-D), 27.60 m in thickness, which contain thin intercalations of green silty marl similar to that occurring in the upper part of the Baghamshah Formation, some shell beds and vertical U-shaped trace fossils (Fig. 5.3.4B). Primary sedimentary structures such as planar cross-stratification (Figs. 5.3.2C), low-angle herringbone cross-lamination (Fig. 5.3.2D) and ball-and-pillow structures (Fig. 5.3.2B) are observed in the brown calcareous sandstones. The basal mixed siliciclastic-carbonate rocks are overlain by greenish-grey to white silty marl, sometimes silty shale with intercalations of light-brown, very thin- to medium-bedded sandy intra-oo-grainstones (Fig. 5.3.5F-G). The latter exhibit oscillation ripples (Fig. 5.3.2E), ball-and-pillow structures (at 100 m), cross-stratified, thin- to

thick-bedded sandy bio-oo-grainstones (Fig. 5.3.6A-B), brown thin- to thick-bedded oo-grainstones with sub-parallel-crested ripples (at 122 m; Figs 5.3.2F, 5.3.6C), bio-rudstones (at 125 m) with *Radulopecten tipperi* and *Camptonectes* (*Camptochlamys*), and up-section (at 150 m), sandy bio-intra-grainstone (Fig. 5.3.6D) and silty bio-wackestone (Fig. 5.3.6E; at 170 m). They are overlain by several hundred meters of carbonates, evaporates, and intercalations of siliciclastic rocks, such as carbonate mudstone, marly mudstone, marl, sandstone, silty marl, gypsum (at 962 to 1032 m), dolostone and siltstone beds. The soft rocks are white, yellowish, greenish to light-brown, well bedded, with a nodular texture, and contain abundant bivalves, in particular pectinids. The limestones are mostly developed as carbonate mudstone (e.g., Fig. 5.3.7B, E, F) and dolomitic mudstone (Fig. 5.3.7H) and are arranged in irregular coarsening- and thickening-upward cycles, in which the microfacies changes to bio-wackestone (e.g., Fig. 5.3.7G), sandy oo-pel-/ and bio-wackestone/floatstone (e.g., Fig. 5.3.7A, D), bio-floatstone (e.g., Fig. 5.3.6H), bio-oo-packstone (e.g., Fig. 5.3.6G), and finally silty cortoid-intra-rudstone (e.g., Fig. 5.3.7C). Numerous articulated or disarticulated bivalves (e.g., pectinids; Fig. 5.3.3E), or shell fragments of oysters (Fig. 5.3.3F), gastropods, and other macrofossils are observed at top of the cycles (Fig. 5.3.2G-H). For instance, *Radulopecten tipperi* was found in several cycles at 175, 214, 244, 362, 740, 1080, 1200 m, in which a few articulated *Radulopecten tipperi* apparently were buried while still alive (Fig. 5.3.3G-H). *Nanogyra nana* mainly formed small patch reefs (Fig. 5.3.3B) at around 214, 595, 740, and 875 m. Other fossils include *Pholadomya* (*Bucardiomya*), *Inoperna*, *Homomya*, *Pteria*, *Camptonectes* (*C.*), *Placunopsis*, *Protocardia* (*P.*), *Ceratomya concentrica*, *Pinna*, *Nuculana*, *Corbulomima*, *Gervillella*, small heterodonts, nerineid, ampullinid and small cerithiid gastropods (e.g., Fig. 5.3.3C), *Serpula* (*Cycloserpula*), corals (Fig. 5.3.3B, B1), and the sclerosponge *Neuropora* (Fig. 5.3.3D). The latter three taxa are associated with the patch reefs. These macrofossils are figured in Chapter 7. The trace fossils *Thalassinoides* (Fig. 5.3.4A) and *Rhizocorallium irregulare* (Fig. 5.3.4D) were found in calcareous sandstones mainly in lower to middle parts of the Kamar-e-Mehdi Formation and *Chondrites* in silty carbonate mudstone in the upper part of the formation (Fig. 5.3.4C). The trace fossils of the Kamar-e-Mehdi section have been described in detail in Chapter 8. In this area, the uppermost part of the Kamar-e-Mehdi Formation (Nar Limestone Member) is dolomitic. This part of the formation was therefore measured at Kuh-e-Qoleh Nar.

6.4.5. ***Lower part of the Kamar-e-Mehdi Formation in the Abdoughi area*** The Kamar-e-Mehdi Formation overlies the top of the Baghamshah Formation with unconformable contact. The base is characterized by greenish-grey, medium- to coarse-grained calcareous sandstone

with low- to medium-angle planar cross-lamination (Figs. 5.5.2G, 5.5.4B). Higher up, this facies laterally grades into a large-scale trough cross-bedded, greenish-grey conglomerate with maximum pebble diameters of 15 cm (Figs. 5.5.2H, 5.5.4C) and horizontal to low-angle cross-laminated calcareous sandstone (between 119 and 125 m, Fig. 5.5.4D). The succession is followed by alternations of greenish-grey to reddish-brown horizontal to low-angle cross-laminated and wave ripple-laminated (Fig. 5.5.3A), fine- to coarse-grained calcareous sandstone (between 125 and 143 m, Fig. 5.5.4E), in which very thin interlayers of gypsum beds (Fig. 5.5.3B) occur. Higher up, alternations of reddish-grey gypsiferous silty clay to silty marl with red to brown strongly weathered cross-stratified calcareous or lithic sandstone intercalations are found (Figs. 5.5.3C, 5.5.4F). This succession turns into the characteristic siliciclastic-carbonate rocks of the Kamar-e-Mehdi Formation (Fig. 5.5.3D).

6.4.6. *Kamar-e-Mehdi Formation in the Ravar area*: The basal thick-bedded cross-stratified sandstone (Fig. 5.6.8D, E) of the Kamar-e-Mehdi Formation overlies with unconformable contact the Baghamshah Formation. The sandstones contain sedimentary structures such as climbing ripples (between 305 and 383 m; Fig. 5.6.5A) and bidirectional cross-lamination (Fig. 5.6.5B) with some wood fragments (Fig. 5.6.5C). In addition, trough cross-bedding (at around 369 m; Fig. 5.6.4A) and wave ripples (at 375 m, Fig. 5.6.4B) occur. Higher up, these cycles turn into several 10 m of reddish-brown, grey to green gypsiferous marl to silty clay (occasionally thick-bedded gypsum beds) with intercalations of limestones and fine-grained sandstone (between 383 and 511 m; Fig. 5.6.5D) such as pale to reddish-brown thin- to thick-bedded bio-rudstones and oo-grainstones (Figs. 5.6.5E, 5.6.9C). The succession is followed by 162 m of nodular, thin- to thick-bedded, intra-bio-wacke- to floatstones at base (Figs. 5.6.5F, 5.6.9D), mudstones containing intercalations of marl and bio-wacke- to floatstone (Fig. 5.6.9E), silty mudstone (Fig. 5.6.9F), intra-packstone (Fig. 5.6.9G), gypsiferous mudstone (Fig. 5.6.9H), bio-wackestone (Fig. 5.6.10A), dolomitic mudstone, and gypsum beds in coarsening- and thickening-upward cycles. Macrofossils include *Radulopecten tipperi*, *Myophoplas multicostata*, *Ceratomya concentrica*, *Pholadomya* (*Ph.*) sp., *Protocardia* (*P.*) sp., and small heterodont bivalves. Higher up (at 683 m) the Kamar-e-Mehdi Formation, which is 378 m thick, is followed by the Magu Gypsum Formation with erosional contact.

6.5. Nar Limestone Member of the Kamar-e-Mehdi Formation

This unit has been measured in the Echellon and Qoleh Nar areas.

6.5.1. *Type locality*: Kamar-e-Mehdi area (AGHANABATI 1977). The Nar Limestone Member can be subdivided into three parts: The lower limestones consist of thick- to very thick-bedded fine-grained limestone to recrystallized limestone with ostracod debris. The middle part consists of a alternations of light-green marl and well-bedded marly limestone, and the upper part of limestones which are similar to the lower limestones and contain microfossils such as *Thaumatoporella parvovesiculifera*, *Fourenia* solaevensis, Alveosepta jaccardi? and Valvulinella jurassica.

6.5.2. *Nar Limestone Member in the Echellon area*: The member is 69 m thick and overlies gypsiferous green to white marls gradually. It is characterized by violet to grey laminated bindstones to very thick-bedded mudstones (Fig. 5.1.4E-F). Bioclasts include ostracods and probably rare foraminifers. The middle part is characterized by alternations of greenish-grey, coarsely laminated to thin-bedded mudstone (Fig. 5.1.2A) containing rare shell fragments (e.g., *Radulopecten tipperi*) and green gypsiferous marl. In the upper part, grey, very faintly laminated to thick-bedded mudstone occurs (Fig. 5.1.4G). The Nar Limestone Member has an erosional contact with the Magu Gypsum Formation (at 133 m; Fig. 5.1.2B).

6.5.3. *Nar Limestone Member in the Qoleh Nar area*: The Nar Limestone Member is 75 m thick (Fig. 5.4.2A), and is dominated by faintly laminated bindstones (Fig. 5.4.3B), medium- to thick-bedded mudstones, and mudstones with gypsum pseudomorphs at the base (Fig. 5.4.3A). Thin- to medium-bedded mudstones containing intercalations of gypsiferous marl to silty marl, mudstones with rare gypsum pseudomorphs, and occasionally internal and external moulds of *Radulopecten tipperi* occur in the middle unit (between 13 and 48 m). Higher up, the member consists of medium- to very thick-bedded mudstone with a few ostracod shells (Fig. 5.4.3C) and intercalations of pel-wacke- to packstone (at around 63 and 73 m; Fig. 5.4.3D-E), and mudstones with abundant gypsum pseudomorphs at top (Fig. 5.4.3F). The Nar Limestone Member is followed with erosional contact by the Magu Gypsum Formation (at 74 m; Fig. 5.4.2B).

6.5.4. *Remarks*: The Kamar-e-Mehdi Formation has been described by AGHANABATI (1977, 1978) and Wilmsen et al. (2009). The upper part of the formation is formed by the Nar Limestone Member (WILMSEN et al. 2003, 2009), earlier on regarded by AGHANABATI (1977) as a separate formation.

6.5.5. *Age*: In the northern Tabas Block, the base of the Kamar-e-Mehdi Formation is Early-Middle Callovian in age according to the presence of ammonites (SEYED-EMAMI et al. 1997, 2002) or Middle Callovian (WILMSEN et al. 2009). The upper part of the Kamar-e-Mehdi Formation (Nar Limestone Member) is Early Kimmeridgian in age according to the presence

of a numbers of agglutinated foraminifers. AGHANABATI & REZAEE (2009) assumed the age of the Kamar-e-Mehdi Formation to range from the Early Oxfordian to the Late Tithonian.

6.6 Magu Gypsum Formation

The formation has been measured in the Echellon, Qoleh Nar and Ravar areas.

6.6.1. *Type locality*: Kuh-e-Qoleh Nar in the Tabas area (AGHANABATI 1977). The formation is 582 m thick, consisting of gypsum with intercalations of limestone at base followed by alternations of gypsum and gypsiferous sandy marls, fine-grained limestones, marl, gypsum, and fossiliferous limestones containing the microfossils *Agathamina* sp., *Sigmoilina* sp., *Ammobaculina* sp., *Cladocoropsis* sp., *Thaumatoporella parvovesiculifera*, and *Chara* sp., indicating a Late Tithonian age (AGHANABATI 1998). Higher up, gypsum, marl, and fossiliferous limestones occur containing the microfossils *Carjerika* sp., *Cylindroporella* sp., miliolides, and algae of Late Jurassic-Early Cretaceous age. The top of the formation is marl.

6.6.2. *Magu Gypsum Formation in the Qoleh Nar area*: This succession, with a thickness of 495 m, overlies the Nar Limestone Member with erosional contact (at 74 m; Fig. 5.4.2B). It consists of red to white gypsiferous silty marl and gypsum and contains intercalations of intra-packstone (at 87 m; Fig. 5.4.3G), and a calcareous breccia (at 81 m; Fig. 5.4.3H) with carbonate cement. The components are mostly derived from the Nar Limestone and are strongly weathered and fractured. Higher up (between 88 and 198 m), the succession is characterized by alternations of white to red gypsiferous silty marl and gypsum beds of variable thickness, with mudstone intercalations (Fig. 5.4.4A) containing rare ostracod shells and gypsiferous mudstone intercalations (Fig. 5.4.4B). Occasionally, the succession turns into red to grey thick-bedded dolostone or dolomitic mudstone (at 145 m) and thin- to thick-bedded gypsum beds (at around 188 m; Fig. 5.4.2C). These facies are followed by reddish-brown to greenish-grey siltstone to silty clay, which occur between 199 and 246 m. The succession continues with alternations of sandy bio-intra-pack- to grainstone (between 247 and 254 m; Fig. 5.4.4C-D) and herringbone cross-laminated calcareous sandstone (Fig. 5.4.2D) with some intraclasts and peloids. Higher up (between 255 and 279 m), the latter turn into bio-oo-grainstone beds (Fig. 5.4.4E-F) with the macrofossils *Nanogyra nana* and *Actinostreon qregareum*. Petrographically, the grainstones contain a few bioclasts (e.g., of crinoid origin). The grainstones are followed with conformable contact by red to greyish-green gypsiferous marl (between 280 and 390 m), a few meter-thick alternations of dolomitic mudstone and thick-bedded gypsum, and sandy oo-grainstone (at 403 m; Fig. 5.4.4G). Higher up, white to green, thick-bedded to massive gypsum beds (between 410 and 488 m), thick-

bedded intra-cortoid-rudstone, 2-3 m thick (Fig. 5.4.4H) containing miliolid foraminifers, gastropods, ostracods and shell fragments, alternations of green gypsiferous marl with white to green, thin to very thick-bedded gypsum beds (between 489 and 530 m), and red to green gypsiferous marl to silty marl (between 530 and 578 m). In the Qoleh Nar area, the Magu Gypsum Formation is followed with unconformable contact by cross-laminated sandstone (Figs. 5.4.2F-G, 5.4.5A) of the Lower Cretaceous (Fig. 5.4.2E). Higher up, these basal sandstones turn into grainstone beds containing the foraminifers *Torremiroella* sp. of Barremian age (Fig. 5.4.5B) and *Vercorsella* sp. of Upper Hauterivian (Fig. 5.4.5C).

6.6.3. ***Magu Gypsum Formation in the Echellon area*****:** The formation, 388 m thick overlies the Nar Limestone Member and consists of red to white gypsiferous silty clay at the base, with thin- to thick-bedded, strongly weathered and fractured mudstone beds which are very similar to the Nar Limestone Member (Fig. 5.1.2C, E). The thickness of the mudstone layers increases up-section. Between the mudstones some wackestones with agglutinating foraminifera, ostracods and shell fragments are intercalated (Fig. 5.1.4H). Higher up, the succession is characterized by alternations of gypsiferous silty clay with thin- to thick-bedded mudstone (Fig. 5.1.2C) containing intercalations of thin- to thick-bedded gypsum beds (Fig. 5.1.2D) which turn into medium- to thick-bedded mudstone to dolomitic mudstone (at 215 m; Fig. 5.1.2F, 5B) with some intercalated red to white gypsiferous silty clays. The latter turn into a lenticular, coarsening-upward, crudely bedded and poorly sorted calcareous conglomerate (Figs. 5.1.2E-G, 3A-C). This conglomerate is followed by red silty clay to silty marl with some intercalated calcareous conglomerate beds (Fig. 5.1.3D), herringbone cross-bedded fine- to medium-grained calcareous sandstone beds (Figs. 5.1.3E-F, 5C) containing *Ophiomorpha* isp. (Fig. 5.1.3G) and *Skolithos* isp. (Fig. 5.1.3H), and sandy bio-oo- and sandy oo-grainstone containing ostracod, and coralline algae (Fig. 5.1.5D-F; between 283 to 304 m). Higher up, these facies turn, with conformable contact, into thick, monotonous, red gypsiferous silty marl (Fig. 5.1.2E; between 305 and 369 m), with intercalated grey to white dolostone beds (between 370 and 388 m), and alternations of red gypsiferous silty marl and dark-red to greenish-white 3-5 m thick gypsum beds (Fig. 5.1.2E; between 397 and 435 m). Up-section, the thickness of massive gypsum beds increases. Lithostratigraphically the Magu Gypsum Formation of the Echelon section resembles that of the Kuh-e-Qoleh Nar type locality.

6.6.4. ***Magu Gypsum Formation (=Ravar Formation) in the Ravar area*****:** In the Ravar area, the Ravar series or Ravar Formation exhibits the same lithology as the Magu Gypsum Formation in the Tabas area, Therefore there is no need for a separate name, and the Magu

Gypsum Formation is used in the following. At 683 m of the Ravar section the formation overlies the Kamar-e-Mehdi Formation with erosional contact. The latter consists of alternations of mainly brown to red, greenish-grey gypsiferous silty marl to silty clay with mudstone and dolomitic mudstone containing intercalations of gypsum beds at base. Red to brown cross-stratified sandstone (Figs. 5.6.5H, 5.6.10B), intra-cortoid- and bio-grainstone (Figs. 5.6.6A, 5.6.10C-D) with dasycladacean green algae (*Clypeina jurassica*?) of Late Kimmeridgian to Late Berriasian age, and some echinoids in the middle (between 737 and 745 m) are followed by alternations of gypsiferous silty clay and thick-bedded gypsum beds in the uppermost part of the formation. The latter forms the core of a syncline (Fig. 5.6.6B). In the Ravar area, the Jurassic rocks are overlain by Lower Cretaceous rocks (Aptian-Albian) with angular unconformity.

6.6.5. *Remarks*: According to STÖCKLIN (1961), AGHANABATI (1998) and SEYED-EMAMI (1999) the siliciclastic-evaporitic rocks of the Magu Gypsum and Garedu Red Bed formations indicate widespread regression and represent an evaporitic-lagoonal setting in east central Iran.

6.6.6. *Age*: Based on RUTTNER et al. (1968) and SEYED-EMAMI et al. (2005), the Magu Gypsum Formation is Late Kimmeridgian-Tithonian in age. According to AGHANABATI (1977), the age of the Magu Gypsum Formation is Late Tithonian in the Kuh-e-Qoleh Nar, and Early Cretaceous (Berriasian) at Kalshoor-e-Anaraki. AGHANABATI & REZAEE (2009) stated that in East Central Iran, the Magu Gypsum Formation ranges from the Late Tithonian to the Early Berriasian. However, in the present study, the Magu Gypsum Formation of the Ravar area is assigned a Late Kimmeridgian to Late Berriasian age according to the dasycladacean green alga *Clypeina jurassica*? (Fig. 5.6.10C). In the Qoleh Nar area the Magu Gypsum Formation is followed with unconformable contact by Lower Cretaceous sediments. The latter are Late Hauterivian to Barremian in age based on the presence of the foraminifers *Torremiroella* sp. and *Vercorsella* sp. (Fig. 5.4.5B, C). Therefore, in the study area, the age of the Magu Gypsum Formation is considered between Late Kimmeridgian to Late Berriasian-?Valanginian.

6.7 Bidou Formation

In the Zarand-Kerman area (Bidou, Mohamadshah and Bolboulieh sections), the Bidou Formation can be subdivided into three members, i.e. Lower Siliciclastic Member, Mixed Siliciclastic-Carbonate Member, and Upper Siliciclastic Member.

6.7.1. Type locality: HUBER & STÖCKLIN (1954) introduced the Bidou Series for the rock succession exposed north of Kerman near to the village Bidou close to the Hojedk coal mine. According to them the succession consists of a basal conglomerate, followed by green to red marl and sandstone in the middle part and by limestone at the top. The latter has been subdivided into two parts, the lower part consists of three, very thick to massive limestone units, which are separated by intercalations of gypsiferous sandy marl and marly limestone, whereas the upper part consists of red marl and sandstone.

6.7.2. *Bidou Formation in the Bidou area*

6.7.2.1. *Lower Siliciclastic Member*: The Lower Siliciclastic Member is 182 m thick and rests on the Hojedk Formation with an unconformity (Figs. 5.7.1, 5.7.2A). The base of the Bidou Formation consists of a 27 m thick brown to greenish-grey, large-scale trough cross-bedded, conglomerate composed mainly of subrounded to rounded pebbles. Within the conglomerate, there are lenticular intercalations of greenish-brown, thin- to thick-bedded coarse-grained to pebbly sandstones (Fig. 5-7-2C-E). This facies is followed by a 72 m thick, greenish-grey to brown, parallel-laminated to cross-stratified sandstone unit (5.7.5A-B) containing intercalations of thick-bedded conglomerates and conglomeratic sandstones. Higher up, a thick-bedded calcareous sandstone (at 77 m; Figs. 5.7.2F, 5.7.5C) with *Diplocraterion* or *Arenicolites* (Fig. 5.7.2G) grades into finer siliciclastic rocks (between 100 to 167 m) with alternations of pale-green, brown, silty clay to gypsiferous silty marl (Fig. 5.7.3A) and parallel-laminated, cross-stratified, fine- to medium-grained sandstone (Fig. 5.7.5D) with climbing ripple-lamination (at 120 m; Fig. 5.7.3B), and several meters of greyish-brown, parallel-laminated to cross-stratified calcareous sandstone (Fig. 5.7.5E). The latter passes into greenish-grey, thin- to medium-bedded bio-oo-grainstones (at 175 m; Figs. 5.7.5H, 5.7.6A) with fragments of *Radulopecten tipperi* (Fig. 5.7.3C), oysters, and crinoids. Higher up silty marl and nodular mudstone occur (Fig. 5.7.3D).

6.7.2.2. *Mixed Siliciclastic-Carbonate Member*: This member starts with 15 m of thick, brown gypsiferous silty clay with intercalations of mainly thin-bedded sandstone (Fig. 5.7.5F) containing the trace fossil *Taenidium* (Fig. 5.7.4E). At 200 m, 11 m of thick, light-brown, cross-stratified, thick-bedded sandy limestone occur (Fig. 5.7.5G) containing the trace fossils *Thalassinoides* and *Ophiomorpha* (Fig. 5.7.4F-G). These limestones turns into thick-bedded oo-grainstones and packstones. Higher up (between 216 to 252 m) coarsening- and thickening-upward cycles follow, starting with light-red gypsiferous marl to silty clay at base and horizontal to cross-bedded calcareous sandstones (Fig. 5.7.6B) containing occasionally climbing ripple lamination (Fig. 5.7.3E-F) at top. This succession is followed by pectinid

limestones (at 252 m; equivalent to the Kamar-e-Mehdi Formation) consisting of white to light-grey sandy oo-bio-wackestone (Fig. 5.7.6C), bio-packstone (Fig. 5.7.6D-G), and thin- to medium-bedded gypsum (between 252 and 257 m). Higher up (between 259 and 289 m), thin- to medium-bedded marly mudstone containing fragments of pectinids such as *Radulopecten tipperi* are followed by yellowish-grey, medium- to very thick-bedded sandy cortoid-oo-grainstone (Fig. 5.7.7A-C). This facies passes up-section into alternations of silty wackestone, pel-wackestone, dolomitic mudstone, and marl (between 316 to 375 m, Fig. 5.7.3F) with intercalations of very fine-grained calcareous sandstone and silty bio-wacke- to floatstone (between 315 and 338 m) and sandy bio-packstone (at 359 m, Fig. 5.7.7D-E). The thickness of the member is 200 m.

6.7.2.3. ***Upper Siliciclastic Member*****:** The Mixed Siliciclastic-Carbonate Member is unconformably overlain by the 379 m thick, brownish-red gypsiferous Upper Siliciclastic Member (equivalent to the Magu Gypsum Formation). It consists of decameter-scale alternations of thin- to medium-bedded sandstones (Figs. 5.7.3G (Gsc), 5.7.7G), gypsiferous silty clay, and horizontal to cross-laminated thick-bedded sandstone at base (Figs. 5.7.3H, 5.7.4A). This facies turns up-section into grey to light-brown conglomeratic sandstone containing wood fragments (at 425 m; Figs. 5.7.4B, 5.7.7H). Up-section, the succession changes into calcareous sandstone (Fig. 5.7.8A-B), and continues with silty to sandy horizontal-laminated mudstone containing intercalations of very fine-grained calcareous sandstone (between 469 and 500 m; Fig. 5.7.8C), alternations of silty clay, silty mudstone, silty pel-bio-wackestones, horizontal to very-low angle cross-laminated calcareous sandstone (up to 606 m), and still higher up of pel-grainstone (Fig. 5.7.8E). The latter turns into several metres of gypsiferous silty clay (between 613 and 631 m) and alternations of silty clay, gypsiferous marl, very fine-grained sandstone, mudstone (Fig. 5.7.8F), and thick-bedded gypsum at top (up to 669 m). Up-section, the succession is followed by 97 m of greyish-brown silty clay (towards the core of Ravar syncline).

6.7.4. Bolboulieh and Mohamadshah areas

6.7.4.1. ***Lower Siliciclastic Member*****:** In the Bolboulieh and Mohamadshah sections (Figs. 5.8.1-2), the uppermost part of the Hojedk Formation is unconformably overlain by the Lower Siliciclastic Member of the Bidou Formation. The latter starts with 0.5 to 3.5 m thick brown to greenish-grey, large-scale trough cross-bedded, silty to sandy, matrix-supported, poorly sorted conglomerate (Figs. 5.8.4A-B, 9A) with sandstone, limestone, rounded claystone and dolostone pebbles. Such a conglomerate layer is commonly developed between the Bajocian Hojedk Formation and the overlying Bidu Formation (see also Fürsich et al. 2009), which

laterally turns into coarse-grained to pebbly sandstone beds. This facies is followed by a 69 m thick (Bolboulieh section) and 66.5 m thick (Mohamadshah section) package of red to brown lenticular to trough cross-bedded, thick- to very thick-bedded medium- to coarse-grained sandstone (Figs. 5.8.4C, 5.8.9C-H, 5.8.10A-B), which towards top turns into fining-upward cycles with low-angle planar- or cross-stratified sandstones, occasionally containing flute cast on lower surfaces (Fig. 5.8.4D-E). Trace fossils are rare but *Taenidium* occurs within wave-rippled, low-angle cross-laminated sandstones at the top. Higher up, at 64.5 m (Mohamadshah) and at 112 m (Bolboulieh) of the sections, these facies turn into alternations of reddish-brown to greenish-grey discontinuous, lenticular, ripple-bedded, thin- to thick-bedded sandstones and poorly laminated siltstone. The latter increases up-section (Fig. 5.8.4F, H). The sandstone beds occasionally display very low-angle cross-bedding. In the Bolboulieh section (at 180 m), this facies is followed by alternations of dark-grey laminated siltstone/argillaceous shale and yellowish thin-laminated non-fossiliferous mudstone and pel-grainstone (Figs. 5.8.4G, L, 5.8.11B1). In the Mohamadshah section (at 87.5 m) this facies is characterized by dark-grey silty to marly shale containing intercalations of yellowish thinly laminated, dolomitic mudstone, bio-oo-grainstone (Figs. 5.8.4H, 5.8.5A, L, 5.8.11G) and thick-bedded, silty bio-rudstone containing Chlamys (C.) and large oysters (Figs. 5.8.4H, L, 5.8.11H). Higher up at Bolboulieh (between 211 and 331 m) and Mohammadshah (between 125 and 186 m) the facies changes into red to brown fine-grained siliciclastic rocks at the base of the Mixed Siliciclastic-Carbonate Member.

6.7.4.2. *Mixed Siliciclastic-Carbonate Member*: This succession starts with several decameters of alternating red, brown and more rarely greenish-grey laminated siltstone and silty clay with lenticular (Fig. 5.8.5C-E), thin- to very thick-bedded, sometimes ripple-bedded, and horizontal laminated to very low-angle cross-stratified sandstones. The sandstones exhibit scour and fill structures (Fig 5.8.5F), a sharp base (Fig. 5.8.5G), and some load casts (Fig. 5.8.5H). In this facies, recognisable trace fossils or plant fragments are very rare.

In the Bolboulieh area (between 331 and 609 m) this facies is followed by alternations of green to grey poorly laminated silty shale, brown, laminated silty clay containing intercalations of fine-grained sandstones and thin-bedded limestones with oscillation ripples on bedding plane (between 430 and 531; Figs. 5.8.6H, 5.8.7A, 5.8.11B-D), alternations of silty marl with light-brown to greenish-grey thin- to thick-bedded, symmetrical wave to oscillation ripple-bedded, occasionally bioturbated, very fine- to fine-grained sandstones (Fig. 5.8.6A) and limestones (Fig. 5.8.6G). The latter consist of horizontal-laminated to thick-

bedded, dolomitized bio-pel-grainstone (about 335 m; Fig. 5.8.12A-B), grey lenticular, thick-bedded to massive oo-grainstone (at 350 m; Fig. 5.8.12C-E), yellowish-grey to light-brown thinly laminated to medium-bedded silty bio-rudstone (Fig. 5.8.12F-G), bio-rudstone (Fig. 5.8.12H), and bio(gastropod)-floatstone (at 408 m; Fig. 5.8.13A) with the trace fossil *Rhizocorallium irregulare*. Higher up (between 559 and 609 m) very thin- to thick-bedded calcareous sandstone (Fig. 5.8.13B) containing bivalve-rudstones (Fig. 5.8.13C-D) with small heterodont bivalves and pectinid and oyster fragments occur.

In the Mohamadshah section, the facies is characterized by alternations of green to grey poorly laminated siltstone, brown laminated silty clay (between 268 and 324 m) and light-brown to greenish-grey thin- to thick-bedded sandstone and bioturbated sandstone (Fig. 5.8.6B) containing intercalations of limestones such as thin- to medium-bedded, horizontal to ripple-bedded cortoid-bio-rudstone (Fig. 5.8.13G-H), intra-bio-packstone/grainstone (Fig. 5.8.14A-C) with *Rhizocorallium irregulare* (between 189 and 268 m) and intercalations of silty bio-rudstone (e.g., at 450 m; Fig. 5.8.13E-F). The calcareous sandstones with intercalated thin-bedded limestones exhibit a sharp base (Fig. 5.8.6A), some load casts or ball and pillow structures (Fig. 5.8.6C), bioclastic lags (Fig. 5.8.6E) at or near their bases and also graded bedding (Fig. 5.8.6D). In the limestones (mainly rudstones) also some intraclasts (at 270 m Moh.) and 400 m (Bol.; Fig. 5.8.6F) occur. The size of intraclasts varies from several mm to cm, and the composition of grains is similar to neighbouring lithologies. Macrofossils consisting of *Actinostreon gregareum* and *Nanogyra nana* are seen on bedding planes. In the Mohamadshah section (between 324 to 425 m), this facies is followed by thickly laminated to thick-bedded, very low-angle cross-laminated, occasionally nodular silty mudstone and silty bioturbated mudstone (Fig. 5.8.15A) It contains intercalations of thin-bedded, bioturbated siltstone/very fine-grained sandstone (Fig. 5.8.15B), silty cortoid-bio-rudstone (Fig. 5.8.15C-D), grey marly shale in the lower parts, hummocky ripple-stratified calcareous sandstone with some load casts (Fig. 5.8.15E), and thin- to medium-bedded, cross-laminated silty to sandy intra-oo-grainstones (Fig. 5.8.15F). Macrofossils consist of *Radulopecten tipperi*, *Chlamys* (*C.*), *Pteria*, *Placunopsis*, *Nicaniella*, *Protocardi*a (*Protocardia*), small heterodont bivalves, *Nanogyra nana*, and *Actinostreon gregareum*.

6.7.4.3. *Upper Siliciclastic Member*: This succession is about 270 m thick in the Bolboulieh and 52 m thick (top of the member is faulted) in the Mohamadshah section. It overlies, with gradual base, the Mixed Siliciclastic-Carbonate Member (Fig. 5.8.7B-C). This facies is characterized by alternations of purple to brown silty shale/siltstone and lenticular sandstone (Fig. 5.8.7B, C, F) containing some horizontal, uni- or bi-directional very low-angle cross-

laminated, ripple-bedded, thin- to very thick-bedded sandstones (Fig. 5.8.10G-H). These facies also contain *Chondrites* (Fig. 5.8.8C), *Planolites*, *Taenidium* (Fig. 5.8.8E-F) and some shell fragments (probably bivalves) on bedding planes. The member is overlain with unconformable contact by Early Cretaceous (Albian-Aptian) rocks.

6.7.5. *Remarks and Age*: HUBER & STÖCKLIN (1954) assumed an early to middle Cretaceous age for the Pectinid Limestone of the Kamar-e-Mehdi area and the "Mixed Siliciclastic-Carbonate Member" (in the present study) of the Bidou Formation. In contrast, HUCKRIEDE et al. (1962) suggested an Oxfordian to Kimmeridgian age and stated that the Hojedk Formation of the Ravar-Kerman Basin is discontinuously overlain by the Bidou Formation. SEYED-EMAMI (1999) suggested that the "Bidou Series" is composed of the Bidou Formation (Bathonian-Callovian), Pectinid Limestone Formation (upper Callovian-Kimmeridgian), and Ravar Formation (Kimmeridgian and probably Tithonian). In the Kerman area, the Asad-Abad Formation has been introduced for the Upper Jurassic siliciclastic rocks (AGHANABATI 1998), which has been subdivided into three parts ranging in age from Callovian-Oxfordian to Kimmeridgian. South-east of Kerman, the middle part of the Asad-Abad Formation indicates an Oxfordian to ?Kimmeridgian age (POLYANSKII 1984) and its upper part probably Kimmeridgian. According to AGHANABATI & REZAEE (2009) the Bidou Formation also has an age between the Middle Bathonian and Berriasian. In the present study, lithostratigraphically the Bidou Formation is an equivalent of the Magu Group (Fig. 6.8.1). However the Lower Siliciclastic Member is considered Middle Bathonian-Callovian (equivalent to the Parvadeh and the Baghamshah formations), the Mixed Siliciclastic-Carbonate Member is assigned a Middle Callovian-Early Kimmeridgian age (equivalent to the Kamar-e-Mehdi Formation) (see also SEYED-EMAMI et al. 1997, 2002 and WILMSEN et al. 2009) and the Upper Siliciclastic Member is thought to be equivalent of the Magu Gypsum Formation ranging from the Late Kimmeridgian to the Late Berriasian-?Valanginian in age.

6.8. Lithostratigraphic correlation

The lithostratigraphic units of the Magu Group of the north- western Tabas Block can be correlated with the members of the Bidou Formation in the southern Tabas Block (Figs. 4.1, 6.8.1). In the present study, the basal conglomerate of the Parvadeh Formation of the Magu Group, which extends from the Tabas to the Ravar area, and of the Bidou Formation from Zarand to the Kerman area, is considered to represent as a sequence boundary (SB) and also a key bed (datum). This sequence boundary is an erosional unconformity related to the Bajocian Mid-Cimmerian tectonic movements (FÜRSICH et al. 2009). In the Ravar area, the Parvadeh

Formation is followed by the Baghamshah, Kamar-e-Mehdi, and Magu Gypsum formations which can be analogue with these in the western and northern Tabas Block. For correlating the Magu Group with the Bidou Formation in the Zarand-Kerman area, facies association, composition of the siliciclastic and carbonate rocks, lateral changes, geometry, sedimentary structures (Chapters 5, 9-11), macro- and trace fossil contents (Chapter 7-8) of each formations or members have been investigated. According to the above mentioned investigations, the Baghamshah Formation in the Tabas area extends laterally toward Ravar area, but the formation in Zarand-Kerman area turns into the middle to upper part of the Lower Siliciclastic Member of the Bidou Formation. The Echellon Limestone Mb of the Echellon area (WILMSEN et al. 2003) occurring in the lower part of the Kamar-e-Mehdi Formation, can be traced to Doshakh and to some extent to the Kamar-e-Mehdi area. The Kamar-e-Mehdi Formation which is superbly exposed in the northern and western Tabas Block can be traced for a great distance, being widespread also in the Ravar- Zarand area, and still more toward south of Kerman (Bolboulieh section). However, in the southern Tabas Block, it changes into the Mixed Siliciclastic-Carbonate Member of the Bidou Formation. Finally, the Magu Gypsum Formation in the Tabas area, laterally grades into the Upper Siliciclastic Member of the Bidou Formation. In the Tabas area, the Nar conglomerate of the lower part of the Magu Gypsum formation, merely occurs in the Echellon area. It is very likely, in the northern Tabas Block, the Esfandiar Limestone Plateform have had a higher elevation than itself in the western Tabas Block. This condition has facilitated the erosion of the Esfandiar Limestone Platform producing the components of the Nar conglomerate during tectonic activities in the Central-East Iranian Microcontinent, the so-called Late-Cimmerian Movements, this conglomerate intensely decreases toward the western Tabas Block but can be compared with these (less than 1.5 m) of the Magu Gypsum Formation in Ravar area and also with the oligomict micro-conglomerate to pebbly sandstone in the lower part of the Upper Siliciclastic Member in the Bidou area. Eventually, the Magu Gypsum Formation and Upper Siliciclastic Member of the Bidou Formation are overlain with unconformable contact by the Lower Cretaceous.

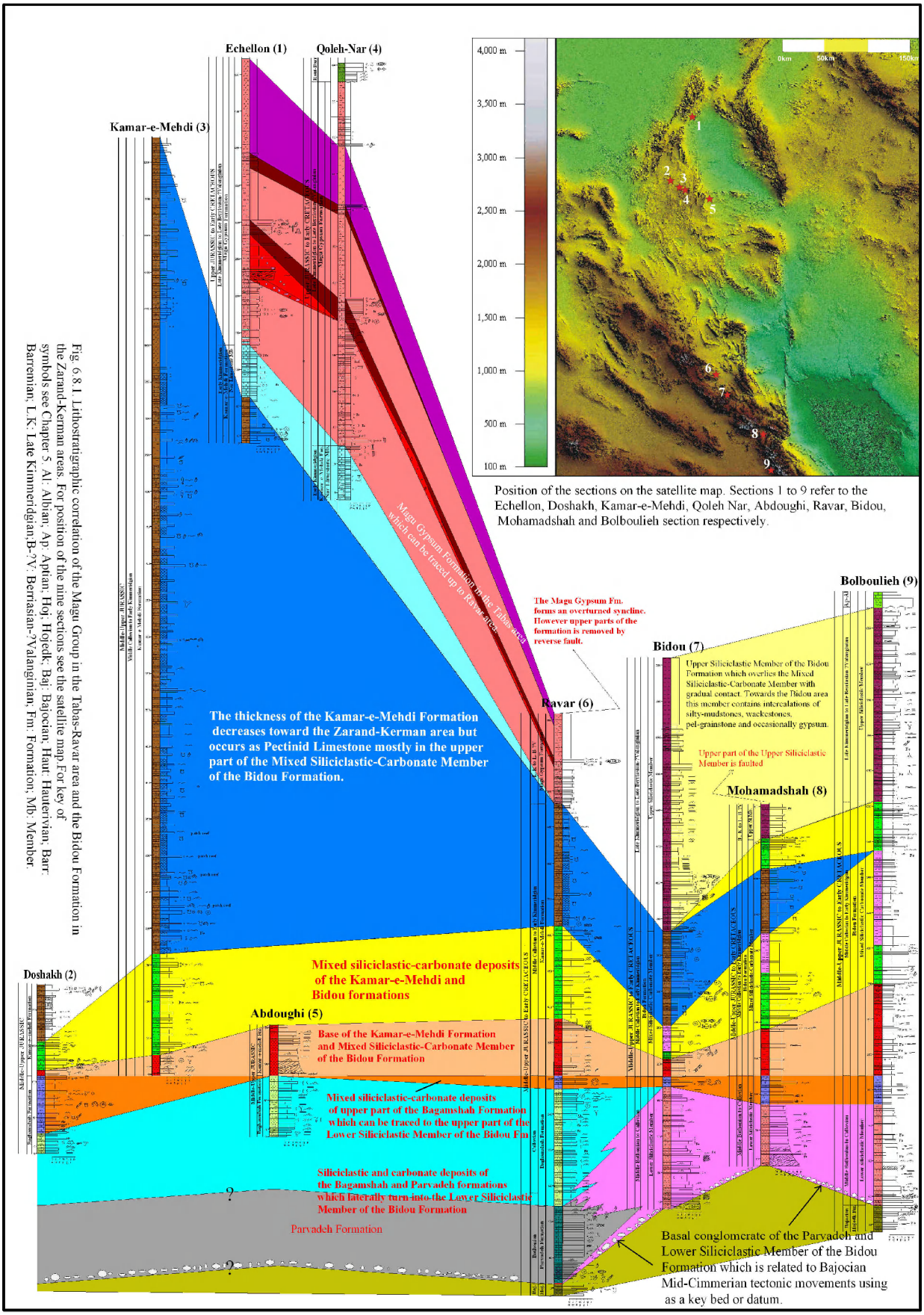

Fig. 6.8.1. Lithostratigraphic correlation of the Magu Group in the Tabas-Ravar area and the Bidou Formation in the Zarand-Kerman areas. For position of the nine sections see the satellite map.For key of symbols see Chapter 5. Al: Albian; Ap: Aptian; Hoj: Hojedk; Baj: Bajocian; Haut: Hauterivian; Barr: Barremian; L.K: Late Kimmeridgian;B-V: Berriasian-?Valanginian; Fm: Formation; Mb: Member.

7 Macrobenthic fauna

The benthic faunas of the Middle-Upper Jurassic strata consist predominantly of bivalves (e.g., *Radulopecten tipperi* and *Nanogyra nana*), followed by gastropods, ammonites (e.g., perisphinctids), corals (e.g., *Pseudocoenia slovenica*), sponges (e.g., *Neuropora*), and brachiopods (Pls. 1-3, Table 7.1). The Kamar-e-Mehdi Formation (Middle Callovian-Early Kimmeridgian) is more fossiliferous than the other formations.

7.1 Parvadeh Formation

The lower part of the Parvadeh Formatiom contains the bivalves *Trigonia* and *Inoperna* and some high-spired gastropods. This part is generally low diverse. The faunas occur in alternations of greenish-grey to light-brown horizontal to low-angle cross-laminated calcareous sandstone and marl with intercalated sandy bio-wackestones.

According to FÜRSICH & WERNER (1991), *Trigonia* sp. is a shallow-infaunal suspension-feeder and lived on a soft substrate (FÜRSICH & WERNER 1986, HOLZAPFEL 1998). *Inoperna* is endobyssate and common in a moderately soft substrate. The high-spired gastropods (e.g., nerineids) were encountered in very shallow marine, fine- to medium-grained sandstone in the uppermost part of the Hojedk Formation and lowermost part of the Parvadeh Formation. They lived in a high energy environment. From the above discussion, the Parvadeh Formation has been deposited in a very shallow-marine environment with high water energy.

7.2 Baghamshah Formation

In the Doshakh area, the upper 109 m of the siliciclastic-carbonate rocks of the Baghamshah Formation contain fragments of perisphinctid ammonites, the bivalves *Grammatodon* (*G.*) sp., *Arcomytilus*, *Pleuromya* sp., *Chlamys* (*C.*) sp., *Radulopecten tipperi*, and *Actinostreon gregareum*, and rhynchonellid brachiopods.

Semi-infaunal suspension-feeders such as *Grammatodon* sp. more often occur in carbonate than in siliciclastic substrates (FÜRSICH 1982). Epifaunal, byssate suspension-feeders such as *Chlamys* (*C.*) sp., *Radulopecten tipperi* and the cemented oyster *Actinostreon gregareum* show a pronounced preference for fine sand and carbonate-rich substrates with admixtures of quartz or bio- and intra-clasts and lived on substrates indicative of intermediate energy conditions and firmer substrates. In contrast, *Pleuromya* lived as a deep burrower in soft argillaceous silty to sandy silty substrates below the fair weather wave-base (FÜRSICH et al. 2004). The epibyssate suspension-feeder *Arcomytilus* dominates in micrites but is also common in sandy silt and silty, or sandy bioclastic limestones (FÜRSICH & WERNER 1986).

The suspension-feedering rhynchonellid brachiopods could live both on hard and firm substrates (FÜRSICH & WERNEr 1991). The presence of stenohaline groups such as ammonites and brachiopods indicate a fully marine environment.

7.3. Kamar-e-Mehdi Formation

The Kamar-e-Mehdi Formation in the Doshakh, Kamar-e-Mehdi, Echellon and Ravar areas consists mostly of marl, pure mudstones, silty mudstone, silty clay, silty marl, and fine-grained calcareous sandstone. The upper 100 m are mainly gypsiferous mudstone, dolomitic mudstone, and gypsum. The formation is highly fossiliferous whereby bivalves dominate (e.g., small heterodonts and the oysters *Nanogyra nana* and *Actinostreon gregareum*), followed by gastropods (e.g., nerineids, ampullinids, and small cerithiids), corals (e.g., *Pseudocoenia slovenica* and *P. limbata*), sclerosponges (*Neuropora*) and calcisponges, echinoids, the serpulids *Serpula* (*Cycloserpula*) sp. and *Serpula* (*Darsoserpula*) sp., and brachiopods. Among them (Table 7.1; Pls. 1-3), *Radulopecten tipperi* is particularly common throughout the formation. Its distribution can be traced for a great distance, occurring also in the Mixed Siliciclastic-Carbonate Member of the Bidou Formation of the Zarand-Kerman area. According to WILMSEN et al. (2009) the benthic macrofauna of the Kamar-e-Mehdi Formation is moderately diverse (about 50 taxa). The upper part of the high-frequency cycles contain disarticulated bivalves, gastropods and occasionally brachiopods, while the lower part contains articulated specimens, but mostly not in life position. The oyster *Nanogyra nana*, corals, and sponges are mainly observed in small patch reefs. The presence of stenohaline group such as brachiopods and corals indicates euhaline conditions (normal marine environment). According to BOUCOT et al. (1958), the degree of disarticulation is a reliable means of determining the relative amount of taphonomic reworking. Thus, the dominance of disarticulated bivalves in this association indicates that reworking took place. Consequently, the faunal associations rarely occur in situ, but commonly have been reworked under a moderately high energy regime (i.e., they are parautochthonous). Low sedimentation rates can be inferred from the predominance of epifaunal cemented oysters and encrusters such as the serpulids *Serpula* (*Cycloserpula*) sp. and *Serpula* (*Darsoserpula*) sp.

7.4. Bidou Formation

In the Bidou, Mohamadshah and Bolboulieh areas, especially in the Mixed Siliciclastic-Carbonate Member of the Mohamadshah area, the bivalves *Radulopecten tipperi*, *Chlamys* (C.) sp., *Pteria* sp., *Placunopsis* sp., *Nicaniella* sp., *Protocardi*a (*Protocardia*) sp., small

heterodonts, and *Nanogyra nana, Actinostreon gregareum* occur within mainly nodular silty carbonate mudstone, marly shale, and bioturbated carbonate mudstone with intercalations of very fine-grained sandstone. The presence of stenohaline groups such as corals, sponges, brachiopods, crinoids and echinoderms point to a fully marine environment of normal salinity within the Kamar-e-Mehdi Formation. According to WILMSEN et al. (2009), the presence of coral patch reefs indicates the euphotic zone and thus a water depth of only tens of meters. Some of the fossils are encrusted by algae, serpulids, and bryozoans which are evidence of a long residence time of skeletal elements on the sea floor, a relatively low rate of sedimentation and also a moderate to low water energy (see FÜRSICH & WERNER 1991). In terms of ecological guilds, the bivalves of the Kamar-e-Mehdi Formation include

- epifaunal byssate suspension-feeders (EbF) such as *Radulopecten tipperi*, *Pteria* sp., *Camptonectes* (*C.*) sp., *Plagiostoma* sp., and *Eopecten* sp. According to FÜRSICH & WERNER (1986) these taxa show a pronounced preference for fine-grained sandy and carbonate-rich substrates with admixtures of quartz or bio- and intraclasts. Apparently such substrates were relatively firm, thus enabling the establishment of epifaunal communities. Most epifaunal associations indicate intermediate energy conditions. Cemented epifaunal organisms such as corals, oysters, and serpulids are also abundant on these substrates. According to FÜRSICH et al. (2004), some epifaunal forms colonised small benthic islands (e.g., dead shells lying on the sea floor).
- shallow infaunal suspension-feeders (IfF) such as *Ceratomya concentrica*, *Protocardia* (*P.*) sp., *Anisocardia,* and *Nicaniella* sp., many of them being common in most facies types (FÜRSICH & WERNER 1986).
- deep infaunal suspension-feeders (ItF) in the present study are represented by *Pholadomya* (*Bucardiomya*) *lirata* (J. DE C. SOWERBY, *Homomya* sp., and *Myophoplas multicostata*. They occur in nearly all siliciclastic facies types and in carbonates with admixtures of quartz sand and silt.
- epifaunal, cemented suspension-feeders; *Placunopsis* sp. (FÜRSICH 1982), and oysters such as *Liostrea* sp., *Nanogyra nana* and *Actinostreon gregareum* lived cemented to substrates. According to FÜRSICH et al. (2004), such hard substrates are dominated by cemented and byssate taxa, less commonly by endolithic bivalves. They occur either where low rates of sedimentation produced shell pavements that served as secondary hard substrates or where due to omission and erosion, synsedimentarily formed concretions became exhumed and formed a cobble substrate colonised by oysters (e.g., the *Actinostreon erucum-Nanogyra nana* association), brachiopods, serpulids, and byssate, boring and other encrusting bivalves.

- semi-infaunal suspension-feeding bivalves such as *Modiolus* (*M.*) sp., *Pinna* sp., and *Gervillella* sp.
- infaunal suspension-feeders such as *Corbulomima* sp. which lived in soft, preferentially argillaceous silty substrates. In addition, soft substrates were populated mainly by nuculid bivalves and a range of small infaunal suspension-feedering bivalves such as *Nicaniella* (FÜRSICH et al. 2004). Occasionally, currents and waves produced pavements of abundant, well-sorted Nicaniella. Corals such as *Pseudocoenia slovenica* and *P. limbata*, which were occasionally encrusted with *Serpula* (*Darsoserpula*) mainly formed small patch reefs on hard substrates with low sedimentation rates. Epifaunal, mobile gastropods such as ampullinids and small cerithiids are mainly common in medium-grained sand and occur in low numbers in most other of sediments (FÜRSICH & WERNER 1986).

Table 7.1 Stratigraphic distribution of macrofossils in the studied sections. Ra: Ravar, Bo: Bolboulieh, Do: Doshakh, Ab: Abdoughi, Ec: Echellon, Ka: Kamar-e-Mehdi, Qo: Qoleh Nar, Bi: Bidou, M: Mohamadshah; M1: Lower Siliciclastic Member, M2: Mixed Siliciclastic-Carbonate Member, M3: Upper-Siliciclastic Member. The numbers refer to the number of individuals. I: infaunal; SI: semi-infaunal; E: epifaunal; N: nekton; t: deep-infaunal; f: shallow-infaunal; z: cemented; b: byssate; m: mobile; F: suspension-feeder; H: herbivore; mC: microcarnivorous; D: detritus-feeder.

Taxa	**life habit/ feeding mode**	**Hojedk Fm**		**Parvadeh Fm**	**Baghamshah Fm**			**Kamar-e-Mehdi Fm**					**Nar Limestone Mb**		**Bidou Formation**									**Magu Gypsum Fm**		
															M1			M2			M3			Ec	Qo	Ra
		Ra	Bo	Ra	Do	Ab	Ra	Ec	Do	Ka	Ab	Ra	Ec	Qo	Bi	M	Bo	Bi	M	Bo	Bi	M	Bo			
Bivalves																										
Radulopecten tipperi	EbF				1			2	1	14		1	1	2					1							
Arcomytilus	SIF				1					1																
Modiolus (*M.*) sp.	SIF									1																
Pteria sp.	EbF									1									1							
Gervillella sp.	SIF									1																
Pinna sp.	SIF									1																
Camptonectes (*Camptochlamys*) sp.	EbF								1	4																
Chlamys (*C.*) sp.	EbF				1														1							
Placunopsis sp.	EzF									1									1							
Trigonia sp.	IfF			1																						
Nicaniella sp.	IfF									1									1							
*Protocardi*a (*Protocardia*) sp.	IfF							3		4		2							2							
Anisocardia sp.	IfF							1		1																
Pholadomya (B.) lirata	ItF									3																
Homomya sp.	ItF									4																
Ceratomya concentrica	IfF							2		3		1														
Myopholas multicostata	ItF											1														
Pleuromya sp.	ItF				1																					
Plagiostoma sp.	EbF								1																	
Inoperna sp.	SIF			1						1																

Taxa	life habit/ feeding mode	Hojedk Fm		Parvadeh Fm	Baghamshah Fm			Kamar-e-Mehdi Fm					Nar Limestone Mb		Bidou Formation										Magu Gypsum Fm		
		Ra	Bo	Ra	Do	Ab	Ra	Ec	Do	Ka	Ab	Ra	Ec	Qo	M1			M2			M3			Ec	Qo	Ra
															Bi	M	Bo	Bi	M	Bo	Bi	M	Bo			
Platymyoidea sp.	ItF											1														
Grammatodon (G.) sp.	SIF				1																					
Small heterodont bivalve indet.	IfF							1		1		1							2							
Oysters																										
Nanogyra nana	EzF							1		5									2						1	
Liostrea sp.	EzF			1				3																		
Actinostreon gregareum	EzF								1	3									1						1	
ammonites																										
perisphinctid ammonites	N				1																					
Gastropods																										
Ampullinid	ImH									4																
Nerineid	EmD	1		1						1																
Small cerithiid	EmH?									4																
Zygopleurid	EmH																									
Brachiopods																										
Rhynchonellid	EsF				1																					
Corals																										
Pseudocoenia slovenica	zmC								1																	
Pseudocoenia limbata	zmC										1															
Serpulids																										
Dorsoserpula sp.	EzF								1																	
Cycloserpula	EzF									3																
Sponges																										
Calcisponges	EzF								1																	

Taxa	life habit/ feeding mode	Hojedk Fm		Parvadeh Fm	Baghamshah Fm			Kamar-e-Mehdi Fm					Nar Limestone Mb		Bidou Formation										Magu Gypsum Fm		
		Ra	Bo	Ra	Do	Ab	Ra	Ec	Do	Ka	Ab	Ra	Ec	Qo	M1			M2			M3			Ec	Qo	Ra
															Bi	M	Bo	Bi	M	Bo	Bi	M	Bo			
Neuropora sp.	EzF									1																
Echinoderms																										
Cidaroids (spines)	EmD								1	1																

Explanation of plates

PLATE 1

Fig. 1. *Arcomytilus* sp., Kamar-e-Mehdi Formation, Kamar-e-Mehdi section, x2. Side view of left valve.

Fig. 2. *Modiolus* (*M.*) sp., composite mould of articulated specimen, Kamar-e-Mehdi Formation, Kamar-e-Mehdi section. A: Dorsal view, x2, B: side view of left valve, x2.

Fig. 3. *Pteria* sp. Concentration of internal moulds with fragments of *Radulopecten* sp., Mixed Siliciclastic-Carbonate Member, Bidou Formation, Mohamadshah section. Scale= 10 mm.

Fig. 4. *Gervillella* sp. Incomplete composite mould forming, together with small heterodont bivalves, a shell pavement, Kamar-e-Mehdi Formation, Kamar-e-Mehdi section. Scale= 10 mm.

Figs. 5-6. *Radulopecten tipperi* Cox, 1969. From the Kamar-e-Mehdi Formation, Kamar-e-Mehdi section. 5A: View right valve, x1, 5B: view of left valve, x1, 5C: dorsal view, x1. 6A: Side view of strongly abraded left valve, 6B: dorsal view, x1.

PLATE 2

Fig. 1. *Camptonctes* (*Camptochlamys*) sp., external mould from the Kamar-e-Mehdi Formation, Kamar-e-Mehdi section, x1.

Fig. 2. *Placunopsis* sp. A. The small composite moulds form, together with other heterodont bivalves, a shell pavement. B. *Nicaniella* sp. Mixed Siliciclastic-Carbonate Member of the Bidou Formation, Mohamadshah section. Scale= 10 mm.

Fig. 3. *Trigonia* sp. Articulated composite mould from the Parvadeh Formation, Ravar section. Side view of left valve, x0.5.

Fig. 4. *Protocardi*a (*Protocardia*) sp., composite moulds from the Kamar-e-Mehdi Formation, Kamar-e-Mehdi section. Scale = 10 mm.

Figs. 5-6. *Pholadomya* (*Bucardiomya*) *lirata* (J. DE C. SOWERBY, 1823). **5**. Articulated composite mould from the Kamar-e-Mehdi Formation, Echellon section. Side view of left valve, x1. 6A. Side view of left valve, x2, B: posterior view, x2 from the same formation.

Fig. 7. *Homomya* sp. Articulated composite mould from the Kamar-e-Mehdi Formation, Kamar-e-Mehdi section. Side view of right valve, x1.

Fig. 8. *Ceratomya concentrica* (J. DE C. SOWERBY, 1822). Articulated internal mould from the Kamar-e-Mehdi Formation, Kamar-e-Mehdi section. A: View of left valve, x1, B: anterior view, x1.

PLATE 3

Fig. 1. *Ceratomya concentrica* (J. DE C. SOWERBY, 1822). Articulated internal moulds from the Kamar-e-Mehdi Formation, Ravar section. Scale= 10 mm.

Fig. 2. *Myopholas multicostata* (AGASSIZ, 1842). Incomplete composite moulds from the Kamar-e-Mehdi Formation, Ravar section. A: Side view of ?left valve, x2, B: side view of ? left valve, x2.

Fig. 3. *Platymyoidea* sp. Articulated composite mould from the Kamar-e-Mehdi Formation, Ravar section. View of right valve, x0.5.

Fig. 4. *Actinostreon gregareum* (J. SOWERBY, 1815). Kamar-e-Mehdi Formation, Kamar-e-Mehdi section. Side view of left valve, x1.

Figs. 5-6. *Actinostreon* sp. Incomplete specimens from the Kamar-e-Mehdi Formation, Kamar-e-Mehdi section**. 5**A: External view of left valve, 5B: internal view of left valve. 6A: Side view of left valve, encrusted by *Nanogyra nana* (J. SOWERBY, 1822), 6B: internal view of left valve. Scale= 10 mm.

Fig. 7. Zygopleurid gastropod. Composite mould from the Kamar-e-Mehdi Formation, Kamar-e- Mehdi section. Apertural view, x2.

Fig. 8. Gastropod indet. Poorly preserved internal mould from the Kamar-e-Mehdi Formation, Kamar-e-Mehdi section**.** Abapertural view, x1.

Fig. 9. Ampullinid gastropod. Internal mould from the Kamar-e-Mehdi Formation, Kamar- e-Mehdi section. A: Abapertural view, x2, B: apical view, x2.

Fig. 10. Rhynchonellid brachiopod. From the Baghamshah Formation, Doshakh section. View of brachial valve, x2.

Figs. 11-12. *Pseudocoenia slovenica* TURNSEK, 1972. Specimens encrusted with *Serpula* (*Dorsoserpula*) sp., Kamar-e-Mehdi Formation, Doshakh section, x1.

Fig. 13. *Pseudocoenia limbata* (GOLDFUSS, 1829), Kamar-e-Mehdi Formation, Ravar section. Upper surface view x1.

PLATE 1

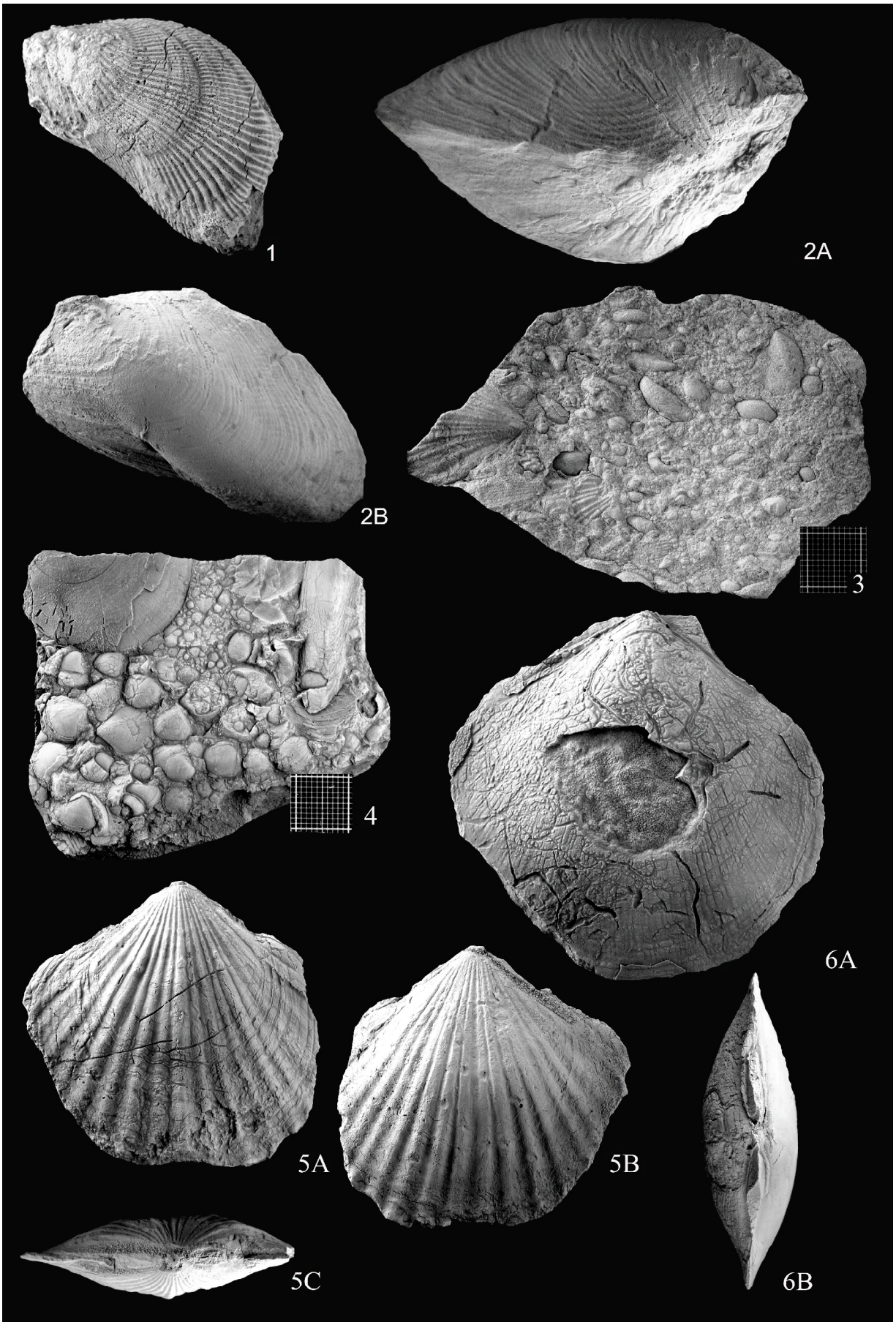

PLATE 2

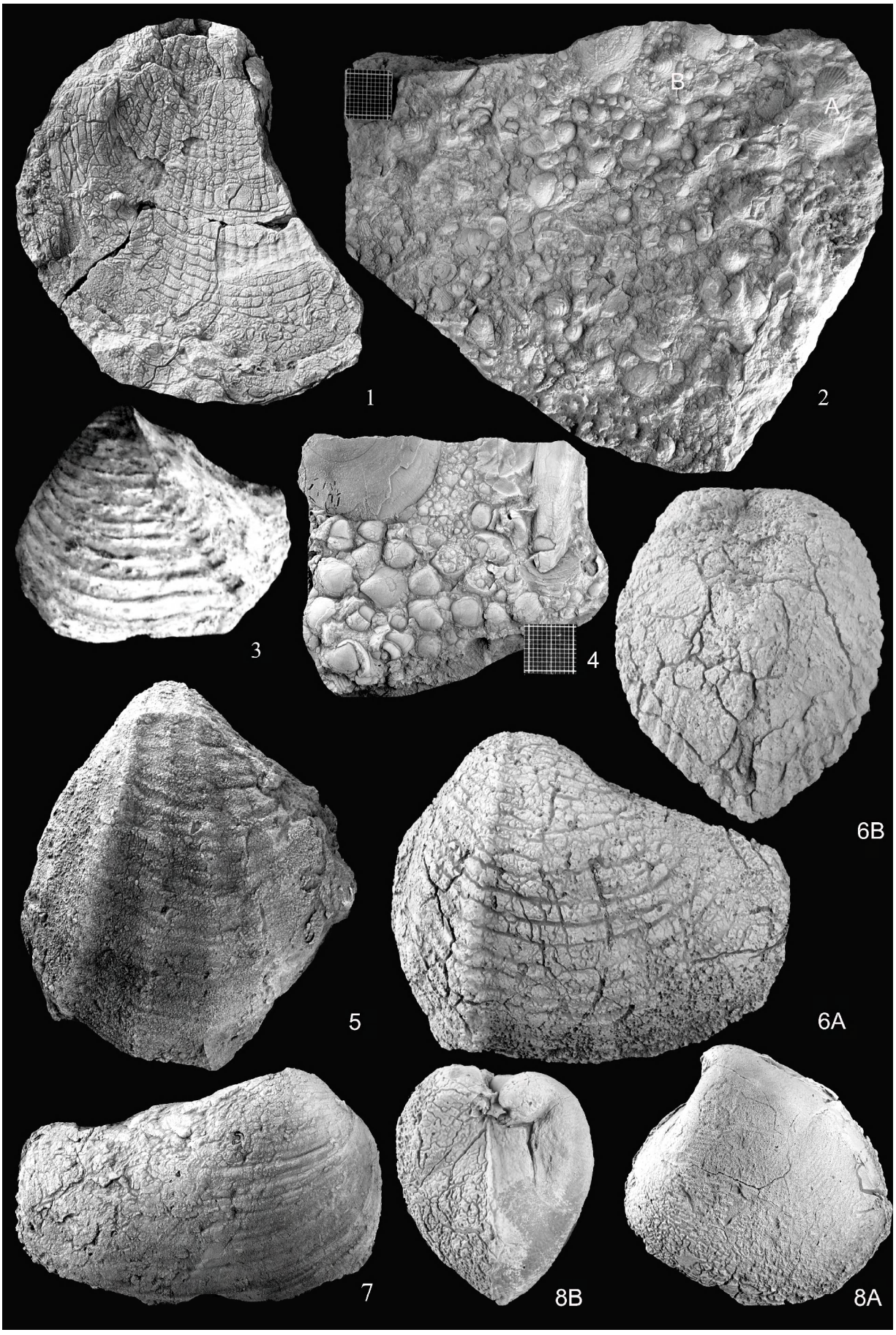

PLATE 3

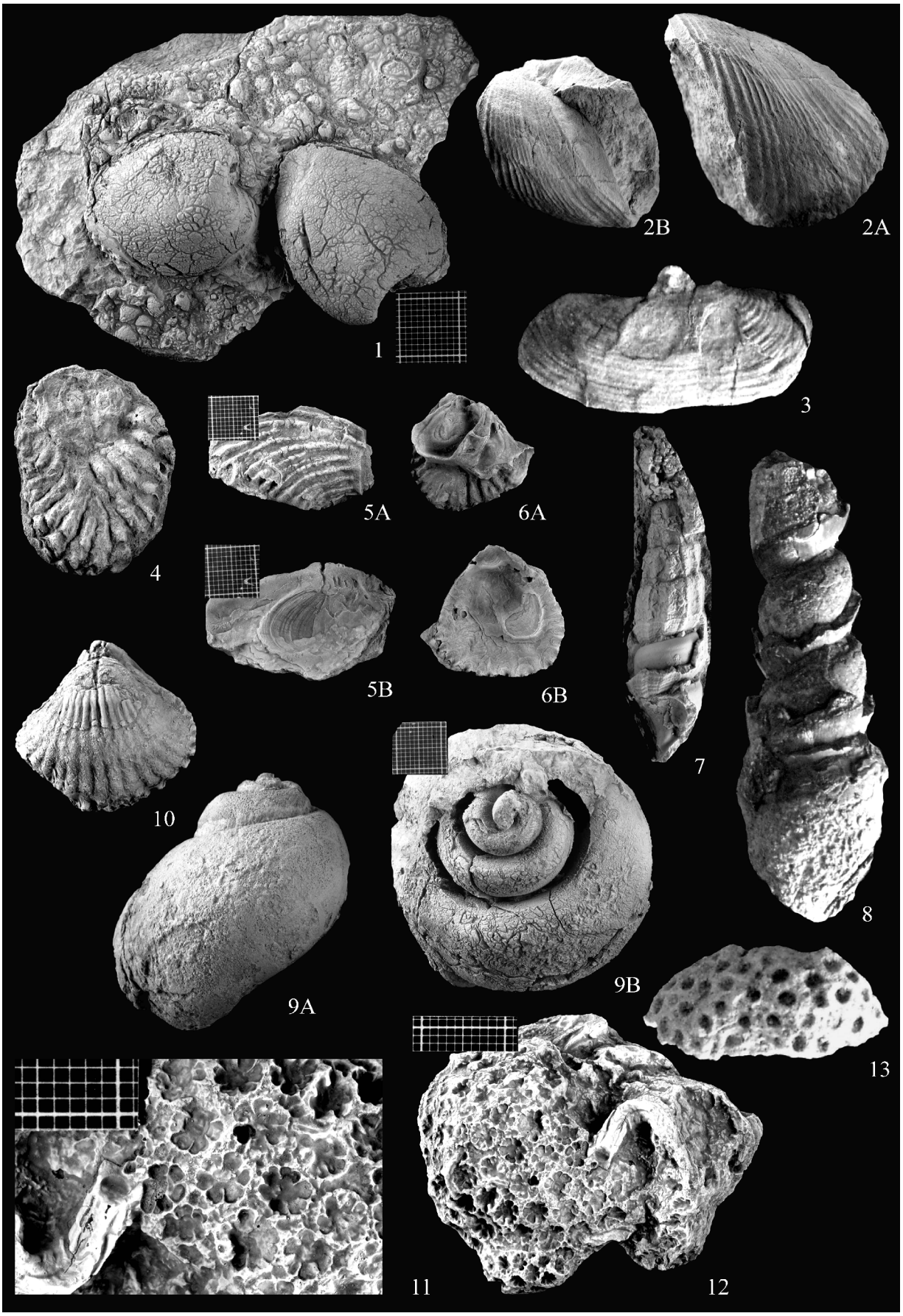

8 Ichnotaxonomy

Trace fossils, although not uleiquitors, are common elements of the sedimentary succession. They belong to the Skolithos and Cruziana ichnofacies of SEILACHER (1967). Their distribution corresponds well with sedimentary structures. Whereas elements of the Skolithos ichnofacies denote high-energy environments, ichnotaxa of the Cruziana ichnofacies indicate open marine to lagoonal, generally somewhat quieter environments. In the following, the various ichnotaxa encountered in the course of the study are briefly described and interpreted.

Ichnogenus *Palaeophycus* HALL, 1847
Palaeophycus isp.
Pl. 4, Fig. 1

Description: Simple cylindrical burrows, 6 to 9 mm in diameter. Burrows commonly intersecting each other, surface of walls smooth or rarely with faint or distinct lining.

Remarks: *Palaeophycus* HALL, 1847 is a cylindrical or sub-cylindrical burrow, horizontal to oriented more or less obliquely to bedding. The burrows are commonly unbranched, but may branch occasionally. The surface is smooth or, rarely, exhibit faint longitudinal striae. The burrows can be followed for up to 20 cm.. Based on MACEACHERN et al. (2007), *Palaeophycus* occurs in both continental ichnofacies such as the Scoyenia, Glossifungites and Mermia ichnofacies and marine softground ichnofacies such as the Skolithos and Cruziana ichnofacies (see also BROMLEY, 1996).

Occurrence: Base of the Kamar-e-Mehdi Formation in the Doshakh area.

Ichnogenus *Skolithos* HALDEMANN, 1840
Skolithos isp.
Pl. 4, Fig. 2

Description: *S*imple, straight tubes or pipes perpendicular to bedding, with a cylindrical to sub-cylindrical cross-section. The diameter is 5 to 8 mm and length observed 5 to 19 cm.

Remarks: *Skolithos* is characterized by unbranched, vertical to steeply inclined, cylindrical to sub-cylindrical, usually unlined burrows with distinct or indistinct wall which may be smooth to rough, or annulated. The fill is massive, the burrow diameter may vary slightly along its length (FILLION & PICKERILL, 1990). *Skolithos* is common in the Skolithos ichnofacies which is regarded as typical of high energy, very shallow-water environments, but it is also typical of other shifting sand environments, such as the tops of storm sand sheets and the tops of turbidity flows (BENTON & HARPER, 1997). According to MACEACHERN et al. (2007), the *Skolithos* ichnofacies usually grades landward into supratidal or terrestrial zones and seaward to subtidal environments of reduced water energy. According to CRIMES et al. (1981), *Skolithos* may appear in deeper water deposits wherever energy levels, food supply, and hydrographic and substrate characteristics are suitable.

Occurrence: Hojedk, Baghamshah, Kamar-e-Mehdi and Magu Gypsum formations of the Echellon, Doshakh, Abdoughi and Bolboulieh areas.

Ichnogenus *Diplocraterion* TORELL, 1870
?*Diplocraterion* isp.
Pl. 4, Fig. 3

Description: The specimens consist merely of paired openings of tubes, which belong to vertical U-shaped burrows, either *Diplocraterion* or *Arenicolites.* Some of the shafts are funnel-shaped. Diameter of tubes 6 mm, distance between openings 10 mm.

Remarks: *Diplocraterion* is a vertical U-shaped burrow with spreite, always perpendicular to bedding plane (FÜRSICH, 1974). *Arenicolites* differs from *Diplocraterion* in the absence of a spreite. It is considered as a dwelling burrow. Although *Arenicolites* is typically a shallow-marine trace fossil, it has also been reported from non-marine and deep-water deposits (FILLION & PICKERILL, 1990). Based on FÜRSICH (1975) both *Diplocraterion* and *Arenicolites* indicate a high energy, usually very shallow environment (see also HÄNTZSCHEL, 1962) and according to MACEACHERN et al. (2007), belong to the *Skolithos* ichnofacies.

Occurrence: Hojedk, Baghamshah, Kamar-e-Mehdi and Bidu formations of the Bolboulieh, Ravar, Doshakh, Kamar-e-Mehdi, and Bidou areas.

Ichnogenus *Ophiomorpha* LUNDGREN, 1891
Ophiomorpha isp.
Pl. 4, Figs. 4-5

Description: Horizontal, cylindrical and branching burrows (diameter between 5-9 mm). Outer surface of burrow lining characteristically mammillate due to the presence of small pellets.

Remarks: *Ophiomorpha* is characterized by three-dimensional burrow systems, consisting of horizontal and vertical cylindrical tunnels (diameter 0.5-3 cm) with dichotomous branching, branches generally forming acute angles. Local swellings close to or at points of branching are commonly developed. The tunnels are internally smooth, but the outer surface of the burrow lining is characteristically mammillate due to the presence of spherical to ovoid pellets, which are several mm, rarely more, in diameter. The tunnels may also be only partly lined by pellets; longitudinal ridges occur on the outer surface of some burrow fillings. Occasionally, the burrows penetrate the sediment to a depth of more than 1 m (HÄNTZSCHEL, 1975). According to MACEACHERN et al. (2007) and BENTON & HARPER (1997) *Ophiomorpha* is generally regarded as indicator of marine environments and belongs to the *Skolithos* ichnofacies. It is generally accepted (e.g., SCHLIRF 2003; UCHMAN 1991, 1995) that *Ophiomorpha* is an indicator of high energy conditions in a shallow-water environments, but also occurs in deep-see settings in connection with turbidites. However, it is also present in fan-fringe facies (UCHMAN 1999). The earliest shallow-marine *Ophiomorpha* were reported from middle Pennsylvanian strata in Utah and the earliest deep-marine *Ophiomorpha* was described from Upper Jurassic flysch deposits (WETZEL et al., 2007).

Occurrence: Baghamshah, Bidou, and Magu Gypsum formations of the Doshakh, Bidou and Echellon areas.

Ichnogenus *Thalassinoides* EHRENBERG, 1944
Thalassinoides isp.
Pl. 5, Fig. 1

Description: Branching cylindrical burrows with either horizontal on box-like networks. Diameter of burrows 6 to 9 mm. Burrows enlarged at branching points. Unlike *Ophiomorpha*, *Thalassinoides* has smooth walls.

Remarks: *Thalassinoides* is composed of cylindrical tubes that branch and form a two- to three-dimensional system with Y- and T-shaped tunnel junctions. Horizontal networks are connected with the surface by more or less vertical shafts. Fill structures result from active filling or collapse of the burrow walls (WETZEL 1983; for detailed description see FÜRSICH 1973a). *Thalassinoides* is characteristic of shelf environments and indicates moderate to low water energy (FÜRSICH, 1975; HÄNTZSCHEL, 1962). Based on MACEACHERN et al. (2007) they mostly belong to the *Cruziana* ichnofacies which is most characteristic of permanently subtidal, poorly sorted and unconsolidated substrates in shallow marine settings. *Thalassinoides* typically ranges from moderate energy levels below the fair-weather wave base but above storm wave base, to lower energy levels in deeper, quieter waters. According to FREY et al. (1984), also *Thalassinoides* is most typical of shallow-marine environments. FARROW (1966) described *Thalassinoides* differing between littoral environments with exceptionally dense, wide burrows and sub-littoral environments with low density, narrow burrows in Bajocian limestones near Blea Wyke, Yorkshire.

Occurrence: Baghamshah, Kamar-e-Mehdi and Bidu formations of the Doshakh, Abdoughi, Kamar-e-Mehdi, and Bidou areas.

Ichnogenus *Gyrochorte* HEER, 1865
Gyrochorte isp.
Pl. 5, Fig. 2

Description: Double row, 4-6 mm wide and 12 cm long, preserved as low, straight to moderately curved positive epireliefs with chevron-like sculpture.

Remarks: Horizontal trace generally up to 5 mm wide (rarely 10 mm), preserved as positive epirelief as plaited ridges with biserially arranged, obliquely aligned pads of sediment. In hyporelief preserved as smooth biserial grooves separated by a median ridge. Course strongly winding and direction changing sharply. The traces may intersect themselves or other traces. Ridges and the corresponding grooves generally separated by vertical distance of 1 cm or less. usually preserved in siliciclastic sediments and commonly associated with ripple surfaces. Produced by worm-shaped animal moving obliquely through the sediment (HEINBERG 1973) Based on MACEACHERN et al. (2007) GYROCHORTE belongs to the Cruziana ichnofacies (see also BROMLEY, 1996).

Occurrence: Uppermost part of the Hojedk Formation of the Bolboulieh area.

Ichnogenus *Taenidium* HEER, 1877
Taenidium isp.
Pl. 5, Fig. 3

Description: Mainly horizontal, sinuous, cylindrical burrows with distinct back-fill of alternating meniscus-shaped packets. Width and length of burrows may vary; in the specimen figured on Pl. 5, Fig. 3 the diameter of the burrow is 7 mm.

Remarks: *Taenidium* is a cylindrical burrow with distinct meniscate backfills and commonly branched. Some *Taenidium* (e.g., *T. fischeri* HEER, 1877) form a rootlike system of burrows radiating downward. However, *Taenidium* is now regarded as a feeding burrow which was filled periodically in a backward direction. According to HÄNTZSCHEL (1975), the burrow occurs in a wide range of environments but FÜRSICH (1998) stated the ichnogenus is a common element of many shelf succession.

Occurrence: Bidu Formation of the Bolboulieh and Bidou areas.

Ichnogenus *Rhizocorallium* ZENKER, 1836
Rhizocorallium irregulare MAYER, 1954
Pl. 5, Fig. 4

Description: Gentle curved, horizontal U-shaped burrows with spreite. Limbs of U-tube more or less parallel, several cm long and nearly 3 cm wide. Diameter of tubes 8 to 12 mm.

Remarks: The spreite in *Rhizocorallium* is always protrusive, but the burrow outline may vary considerably. Straight, short burrows are found as well as long, sinuous, planispiral or trochospiral ones. Furthermore, the burrows may branch. Commonly, several varieties can be found on one and the same bedding plane. Orientation may be parallel or oblique to bedding. Especially in short burrows, the limbs of *Rhizocorallium* are sometimes vertically retrusive. *Rhizocorallium* can be divided into three ichnospecies: *Rh. jenense* represents more or less straight, short, oblique spreiten-burrows and can be interpreted as domichnia of a suspension-feeder; *Rh. irregulare* represents long, sinuous, branching and planispiral forms, and *Rh. uliarense* trochospiral spreiten-burrows. The latter two are interpreted as fodinichnia (FÜRSICH, 1974). *Rhizocorallium* occurs mostly in shallow marine deposits. Its total range, however is from the deep-sea (e.g., UCHMAN, 1992) to marginal marine or very shallow water (e.g., FARROW, 1966), or even non-marine deposits (FÜRSICH & MAYR, 1981). *Rhizocorallium* occurs also in the Glossifungites ichnofacies which is characteristic of firm but unlithified substrates, such as dewatered muds. In this case, the burrow walls usually exhibit scratch marks.

Occurrence: Kamar-e-Mehdi and Bidu formations of the Kamar-e-Mehdi, Bolboulieh and Mohamadshah areas.

Ichnogenus *Chondrites* von STERNBERG, 1833
Chondrites isp.
Pl. 5, Fig. 5

Description: Dichotomously branching, vertically to horizontally oriented cylindrical burrows. The three-dimensional character of *Chondrites* can be visualized by imagining an upside-down tree, with a main burrow ("trunk") and increasingly complex branches extending

downward into the sediment. The tunnels branch in regular or irregular patterns, the angle of branching is variable, the diameter of tunnels around 1 to 1.5 mm.

Remarks: *Chondrites* can be described as a three-dimensional tube system ramifying at angles of 30° to 60°.The burrows consist of a vertical shaft close to the sea floor (proximal part) and a ramifying down-wards distal lower part. In the distal part the tubes are decreasingly inclined to the horizontal plane (WETZEL 1981). According to WETZEL & UCHMAN (1998), see also HÄNTZSCHEL, 1975), *Chondrites* consists of a regularly branching tunnel system containing a small number of mastershafts open to the surface, which ramify at depth to form a dendritic structure. According to MACEACHERN et al. (2007), *Chondrites* occurs in the Cruziana, Glossifungites, Zoophycos and, less commonly, in the Nereites ichnofacies. BENTON & HARPER (1997) regarded *Chondrites* more typically of near-shore to off-shore shelf environments.

Occurrence: Kamar-e-Mehdi, Parvadeh and Bidu formations of the Kamar-e-Mehdi, Ravar, and Bolboulieh areas.

Ichnogenus *Planolites* NICHOLSON, 1873
Planolites isp.
Pl. 5, Fig. 6

Description: Simple meandering burrow oriented horizontal or oblique to bedding. It differs from *Palaeophycus* by its lack of a burrow lining. Width of the burrows ranges from 7 to 9 mm. Burrows are unbranched and irregularly developed.

Remarks: *Planolites* is an unbranched, cylindrical to sub-cylindrical burrow (diameter up to 15 mm), straight to gently curved, more or less horizontal or oblique to bedding, penetrating the sediment in irregular course and direction. Burrows may cross one another (HÄNTZSCHEL 1975). *Planolites* is interpreted as a feeding burrow made by a worm-like animal. *Planolites* differs from *Palaeophycus* primarily by having unlined walls and a burrow fill differing in texture from that of the adjacent rock. Fills may differ also in fabric, composition, and colour (PEMBERTON & FREY, 1982). *Planolites* and *Palaeophycus* are also differentiated by the wall structure, which is found only in the latter one. *Planolites* is usually restricted to stuffed burrows and consequently interpreted as produced by deposit-feeders (FÜRSICH, 1974).

Occurrence: Baghamshah, Kamar-e-Mehdi, and Bidu formations in the Doshakh and Bolboulieh areas.

Explanation of plates

Plate 4

Fig. 1. *Palaeophycus* isp. (arrowed) from the lower part of the Kamar-e-Mehdi Formation; Doshakh section. Scale= 10 mm.

Fig. 2. *Skolithos* isp., from the middle part of the Magu Gypsum Formation; Echellon section. Scale= 10 mm.

Fig. 3. Vertical U-shaped burrow (*Diplocraterion* or *Arenicolites*) from the lower part of the Kamar-e-Mehdi Formation; Kamar-e-Mehdi section. Scale= 17 mm.

Fig. 4-5. *Ophiomorpha* isp. from the middle part of the Magu Gypsum Formation of the Echellon section (4) and Mixed Siliciclastic-Carbonate Member (5) of the Bidou Formation, Bidou section. Scale= 17 mm.

Plate 5

Fig. 1. *Thalassinoides* isp. from the lower part of the Mixed Siliciclastic-Carbonate Member of the Bidou Formation; Bidou section. Scale= 10 mm.

Fig. 2. *Gyrochorte* isp. from the uppermost part of the Hojedk Formation; Bolboulieh section. Scale= 10 mm.

Fig. 3. *Taenidium* isp. from the lower part of the Upper Siliciclastic Member of the Bidou Formation; Bolboulieh section. Scale= 17 mm.

Fig. 4. *Rhizocorallium irregulare* from the middle part of the Kamar-e-Mehdi Formation; Kamar-e-Mehdi section. Scale= 10 mm.

Fig. 5. *Chondrites* isp. from the lower part of the Upper Siliciclastic Member of the Bidou Formation; Bolboulieh section. Scale= 17 mm.

Fig. 6. *Planolites* isp. from the lower part of the Upper Siliciclastic Member of the Bidou Formation; Bolboulieh section. Scale= 17 mm.

PLATE 4

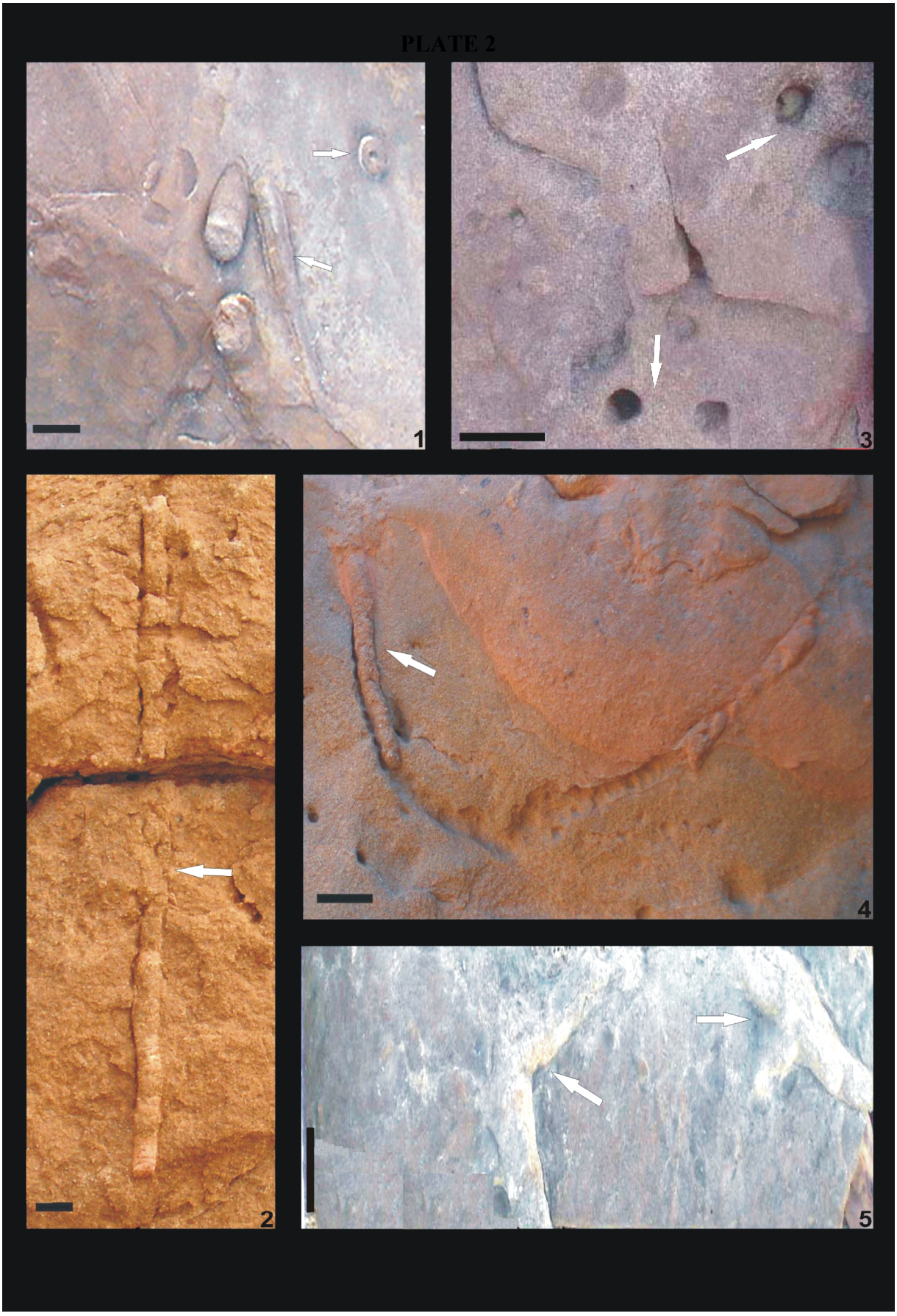

PLATE 5

Table 8.1 Distribution of ichnotaxa in the studied sections. Ra: Ravar, Bo: Bolboulieh, Do: Doshakh, Ab: Abdoughi, Ec: Echellon, Ka: Kamar-e-Mehdi, Qo: Qoleh Nar, Bi: Bidou, M: Mohamadshah and Bo: Bolboulieh areas, M1: Lower Siliciclastic Member, M2: Mixed Siliciclastic-Carbonate Member, M3: Upper Siliciclastic Member. b: Base of the formation or member; l: lower part of the formation or member; m: middle part of the formation or member; u: upper part of the formation or member; c: common

Ichnotaxonomy	**Hojedk Fm**		**Parvadeh Fm**	**Baghamshah Fm**			**Kamar-e-Mehdi Fm**					**Nar Limestone Mb**		**Bidou Formation**									**Magu Gypsum Fm**		
	Ra	Bo	Ra	Do	Ab	Ra	Ec	Do	Ka	Ab	Ra	Ec	Qo	M1			M2			M3			Ec	Qo	Ra
														Bi	M	Bo	Bi	M	Bo	Bi	M	Bo			
Palaeophycus isp.								l*																	
Skolithos isp.		u			u					l														m	
?*Diplocraterion* isp.	u	u				m		l	l					l											
Ophiomorpha isp.				u													l							m	
Thalassinoides isp.				u	u			lm									l								
Gyrochorte isp.		u																							
Taenidium isp.																l	l					l			
Rhizocorallium irregulare									l									l	l						
Chondrites isp.			l						u													l			
Planolites isp.				u				l														l			
Bioturbated intervals	u	u		u	u	l	c	c	c	c	c						c		c						

9 Sedimentary petrography

9.1 introduction

In order to trace source rocks, palaeogeography and syntectonic events of the Middle to Upper Jurassic strata, a petrographic analysis has been carried out on sand-sized siliciclastic rocks, clay minerals and heavy minerals. About 250 framework grains per thin-section were counted. Sandstones were classified according to PETTIJOHN et al. (1987). Their provenance was determined based on DICKINSON et al. (1983, 1985, see Table 1, 2), and petrographic composition was quantified with the conventional point-counting method of Gazzi-Dickinson as described by INGERSOLL et al. (1984). Minerals >0.625 mm were counted according to the mineral type. To evaluate the relative importance of plutonic and metamorphic rocks as quartz sources, polycrystalline quartz, non-undulatory and undulatory monocrystalline quartz were plotted in a double-triangular diagram following the technique of BASU et al. (1975) and TORTOSA et al. (1991). For determining the climatic-physiographic control on sediment composition, the diagram of WELTJE et al. (1998) (see Table 2) and the simple QFR (=QmFLt) ternary plot of SUTTNER et al. (1981) were used. The latter was performed for discriminating sources of metamorphic and plutonic rocks under humid or arid climatic conditions. In the present study, unweathered samples of sand-sized siliciclastic rocks were collected across the stratigraphic succession. Recalculated modal data from point counting of the framework grains are listed in Table 2. About 40 samples of sandstones were crashed to a diameter of 125 to 250 μm and weighed in the laboratory (each weighing 2 kg). The weighted samples were mixed with tungsten compounds of a specific gravity of 2.90 gr/cm³ to separate heavy minerals from light minerals. After drying the heavy minerals, the magnetic and non-magnetic fractions were separated by magnet with a certain magnetic load. Finally, thin-sections of the heavy minerals were produced. Qualitative variation in mineral composition of the shaly samples were estimated from X-ray diffraction (XRD, analysed in Geological Survey of Iran). The analysis of clay minerals in shaly and marly successions is also thought to be useful for detecting changes in the source areas in sedimentologically homogeneous materials (ARRIBAS 2003).

9.2. Description of grain types, calculated parameters and counted symbols

According to ZUFFA (1980), detrital grains can be grouped into four categories of non-carbonate extrabasinal (Nce), carbonate extrabasinal (Ce), non-carbonate intrabasinal (Nci), and carbonate intrabasinal (Ci). The studied detrital grains of sandstones are mainly of

extrabasinal origin. These grains contain a wide variety of quartz, feldspar, mica, and chlorite (Table 1). Quartz is the dominant component and is present as monomineral quartz grains or as quartz constituents of coarse polymineralic grains. Monomineralic quartz grains are monocrystalline non-undulose (Qmn), monocrystalline undulose (Qmu), and the polycrystalline varieties Qp2-3 and Qp>3, following the criteria of BASU et al. (1975) and TORTOSA et al. (1991). Four parameters of detrital quartz are potentially useful in identifying the source rocks of the quartz. These parameters consist of the amount of undulatory quartz (flat or U-stage extinction angle >5°), amount of non-undulatory quartz (flat or U-stage extinction angle ≤5°), amount of polycrystalline quartz, and number of crystal units per single polycrystalline grain. The most effective distinction of source rock type is accomplished when all four parameters are used together. In the study area, the Qp>3 is classed into Qp>3c and rare Qp>3f as a function of sub-grain size. Thus, Qp>3c represents polycrystalline grains with more than three sub-grains greater than 0.062 mm in size. The size of sub-grains in the Qp>3f class is between 0.030 mm and 0.062 mm. Based on DICKINSON (1985), the Qp2-3, Qp>3c, Qp>3f and chert varieties are included in the Qt of triangle (QtFL) (see also PETTIJOHN et al. 1987). The values in the QFR diagram of PETTIJOHN et al. (1987), which is similar to the DICKINSON triangle (QtFL), are not expressed graphically but are used in the Table (3) to describe sandstone composition with a nomenclature of regular usage (e.g., arkose, litharenite, quartzarenite). Feldspar grains (F) are subordinate and clay minerals, muscovite, chlorite, sericite or carbonate replacements on feldspar also are included in these groups (Ffi, Fmus, Fcl, and Fser, respectively). Non-carbonate lithic fragments (Lt) are mostly fine-grained (<0.062 mm) such as some slate or silty shale (Lm) and chert (in QmFLt). Chert grains (sub-grains <0.030 mm in size) do not exhibit a clear texture and thus their sedimentary origin can not be identified. Non-carbonate lithic fragments are always present but rare (mostly less than 4% of total grains). Based on SUTTNER et al. (1981), rock fragments are grains with two or more phases or crystals where (1) no single crystal is >90 % of the total volume of the particle and (2), at least two phases or crystals are both >0.063 mm in size (see also INGERSOLL et al. 1984). The extrabasinal carbonate grains (Ce) in the sandstones are mainly fine-grained limestone. CAVAZZA et al. (1993) showed the relevance of this petrographic class when sandstones break up into individual grains to produce recycled detrital components and monocrystalline calcite grains. Extrabasinal carbonate grains are of low abundance in siliciclastic rocks, but locally their abundance increases, for instance in the sandstones of the lower part of the Upper Siliciclastic Member of the Bidou Formation. Non-carbonate and intrabasinal carbonate grains (Nci and Ci, respectively) are common in the carbonate rocks

e.g., in the Kamar-e-Mehdi Formation, and contain non-carbonate grains e.g., gypsum. Carbonate grains include intraclasts (In), mainly peloids, ooids, cortoids, and bioclastic fragments such as bivalves, gastropods, and crinoids. These grains are not derived from a source rock but originated within the basin.

Table 1. Key of counted petrographic symbols for which quantitative data have been obtained.

Siliciclastic grains (extrabasinal) or non-carbonate extrabasinal (Nce)	Quartz	Qmn	Non-undolose monocrystalline quartz
		Qmu	Undulose monocrystalline quartz, undulosity > 5
		Qp2-3	Polycrystalline quartz with 2-3 sub-grains
		Q>3c	Polycrystalline quartz with >3 sub-grains (> 0.062 mm)
		Q>3f	Polycrystalline quartz with >3 sub-grains (0.030-0.062 mm)
	Feldspar	F	Feldspar, single crystals
		Fser	Sericite replacement on feldspar
		Ffi	Clay mineral replacement on feldspar
		Fcl	Chlorite replacement on feldspar
		Fmus	Muscovite replacement on feldspar
		Cl	Chlorite
	Mica	Mus	Muscovite
		Bio	Biotite
		Ch	Chert (>3 subgrains <0.030 mm)
		Lm	Shale-Slate
carbonate extrabasinal (Ce)		Ce	Fine- to coarse-grained carbonate grains
Non-carbonate intrabasinal (Nci)		Rip	Rip-up clasts
		G	Gypsum
			Iron-oxide
carbonate intrabasinal (Ci)		In	Intraclast
		O	Ooid
		P	Peloid
		Co	Cortoid
		Onco	Oncoid
		Ag	Aggregate grain
		Fo	Fossils such as bivalve, gastropods, crinoids
Cm (cement)		Cm1	Carbonate cement
		Cm2	Quartz cements
		Cm3	Clay cement
		Cm5	Ferroan carbonate cement
		Cm4	Fe-oxide cement

Table 2. Calculated parameters for classification and determination of the origin, climatic-physiographic controls and tectonic setting of siliciclastic rocks.

Reference	triangles		Calculated parameter reference
DICKINSON et al. (1983, 1985), QtFL and QmFLt triangles)	Qt		Qmn + Qmu + Qp2-3 + Qp > 3c + Qp > 3f + Ch
	F		F + Ffi + Fser + Fcl + Fmus
	L		Nce+Ce
	Qm		Qmn + Qmu
	F		F + Ffi + Fser + Fcl + Fmus
	Lt		Qp > 3f + Ch + Nce+Ce+ Qp2-3 + Qp>3c
WELTJE et al. (1998)	Q (%)		Quartz percentage (Q/Q+F+R) × 100
	F (%)		Fedspar percentage (F/Q+F+R) × 100
	R (%)		Rock fragment percentage (R/Q+F+R) × 100
			In (Q/F) = Q/F logratio
			In (Q/R) = Q/R logratio
Climate (rainfall)		C	0 for (semi) arid and mediterranean
			1 for sub-humid
			2 for humid
Relief		R	0 for high (mountain)
			1 for moderate (hills)
			2 for low (plains)
Weathering index (Iw=CR)		Iw	0 means unweathered
			1 means slightly weathered
			2 means moderately weathered
			4 means intensely weathered
Four variable plot (Qmn Qmu Qp Qp2-3) of nature of quartz population (BASU et al. 1975 and TORTOSA et al. 1991)	Qmn		Qmn
	Qmu		Qmu
	Qp		Qp > 3c + Qp > 3f
	Qp2-3		`Qp2-3

9.3 Siliciclastic rocks with gravel-sized clasts (conglomerate)

Petrographically, the basal oligomict conglomerate of the Bidou, Parvadeh and monomict conglomerate or breccia (Fig. 5.4.3H) of the Magu Gypsum formations are texturally sandy to clast-supported (Figs. 5.1.3A, 5.6.2F, 5.7.2C), with a wide range of grain sizes. Maximum-size of the clasts is up to 15 cm in Bidou, 8 cm in Ravar and 30 cm in the Echellon area. The larger clasts are generally more rounded than smaller ones The clasts are composed of sandstones (arkose and quartzarenite), siltstones, cherts, some low-grade metamorphic siliciclastic rocks (in the Bolboulieh, Mohamadshah, Bidou and Ravar areas), and mostly carbonate mudstone fragments (in the Echellon

area). In the latter area, the conglomerate (Fig. 5.1.2G) also consists of mainly bivalves e.g., *Radulopecten tipperi* as clasts and recrystallized shell debris (Fig. 5.1.5A). The matrix is a reddish carbonate mudstone with angular to subangular sand-sized quartz grains. In the Zarand-Ravar area, from Bidou towards Ravar, the size of the clasts in the basal conglomerate of the Parvadeh Formation decreases. The latter consists of macrofossils, e.g., articulated bivalves and high-spired gastropods and also of shell moulds, which are usually filled with neomorphic spar (Fig. 5.6.7C). In the Kerman-Ravar area, the components and matrix have been cemented with ferruginous carbonate (Fig. 5.8.9A). The matrix is composed of angular to subangular and a few subrounded to rounded siliciclastic and carbonate grains. Monocrystalline quartz grains show uniform and undulose extinction and polycrystalline quartz grains mostly contain more than three sub-grains. The sub-grain boundaries are mainly sutured, concave-convex and elongated, the latter occasionally showing a preferred direction (sheared quartz).

9.4 Siliciclastic rocks with sand-sized clasts

Petrographically, the studied siliciclastic rocks of the Middle-Upper Jurassic strata consist of several petrofacies e.g., arkose to subarkose with variable percentages of relatively unstable feldspar grains, sublitharenite, few litharenite, quartzarenite (Table 3), and locally pebbly sandstone and calcareous sandstone. Principal components of the sandstones include quartz grains, feldspar grains, and rock fragments. Quartz grains prevail. They are mainly monocrystalline and less commonly polycrystalline. The monocrystalline grains show uniform (Qmn; more than 75%) and undulose extinctions (Qmu; e.g., Fig. 5.3.4E) and the polycrystalline grains include polycrystalline quartz with 2-3 sub-grains (Qp2-3; Fig. 5.8.9D, G), polycrystalline quartz with more than 3 sub-grains (Qp>3c; Fig. 5.3.4F, 5.7.5A), a few Q>3f (Table 1; Fig. 5.7.5A), and microcrystalline quartzose grains such as chert (Fig. 5.6.7A). Feldspar grains are partly replaced by sericite, chlorite (e.g., Fig. 5.8.10F), calcite (e.g., Fig. 5.2.4A, 5.8.9G) and muscovite (Fig. 5.6.7F). Rock fragments consist of shale or rarely slate (Lm) (between 1 to 7 %, e.g., Fig. 5.7.5A, 5.8.10D), chert (2 to 8 %) and extrabasinal carbonate debris (Fig. 5.8.10E). The carbonate grains in sandstones of the Kamar-e-Mehdi and Magu Gypsum formations are often intrabasinal (Table 1; Ci) and are composed of peloids, ooids, intraclasts, and bioclasts (e.g., Fig. 5.3.5A-D; between 10 and 50 %). For determination of roundness of detrital grains in sandstones, the fact that occasionally chemical weathering has affected the roundness of the grains, mostly on the edges of grains, must be taken into account. Chemical rounding usually produces embayments (e.g., Fig. 5.7.5E),

which do not occur on mechanically rounded grains. In the Bolboulieh, Mohamadshah, and Bidou sections the size of the siliciclastic grains in the Lower Siliciclastic Member of the Bidou Formation varies respectively from medium- to very coarse-grained in the lower, and very fine- to fine-grained in the upper part of the fining-upward cycles. Texturally, the sandstones are mostly immature (Figs. 5.8.9D-H, 5.7.5A-B), poorly-sorted (Figs. 5.8.9C, 5.8.10B), and the grains are mainly angular. In the upper part of the Lower Siliciclastic Member, however, the sandstones are very fine- to fine-grained, immature, moderately sorted, and the grains are angular to subangular (Fig. 5.8.10E). The grains at the base of the Mixed Siliciclastic-Carbonate Member are almost immature, poorly sorted, and are altered subrounded to occasionally rounded (Fig. 5.7.5F). In the lower part of the Upper Siliciclastic Member grains are mostly very fine-to fine-grained, immature to mature, poorly sorted, and altered subrounded (Figs. 5.8.10G-H, 5.7.7G). In the Bidou area, the latter member laterally turns in its middle part into immature, poorly sorted, pebbly sandstone, in which siliciclastic and carbonate grains are angular to subrounded containing quartz grains (Qmn, Qmu, Qp2-3, Qp>3c), carbonate grains (Ce), very fine-grained sandstone debris, and occasionally wood fragments (Figs. 5.7.4B, 5.7.7H). Higher up there are lateral changes into mature, well sorted, subangular to subrounded calcareous sandstone, containing intrabasinal carbonate grains (Ci) such as intraclasts, superficial, concentric or radial ooids, echinoid spines, and algal fragments (?dasycladaceans) (Fig. 5.7.8A-C).

In the Ravar area, sandstones in the uppermost part of the Hojedk Formation are mature, very well sorted and the grains are well-rounded (Fig. 5.6.7A-B). In the lower part of the Parvadeh Formation, sandstones are immature to submature, moderately sorted, and the grains are altered subrounded (Fig. 5.6.7F). In contrast, the sandstones in the Baghamshah Formation are mostly mature, very well-sorted and the siliciclastic grains are well rounded (Fig. 5.6.8C). From Ravar to the Tabas area, intrabasinal carbonate grains (Ci) such as intraclasts, superficial ooids, and bioclasts (Fig. 5.6.8E), and angular extrabasinal carbonate grains (Ce; Fig. 5.5.4D) occur in the basal sandstone of the Kamar-e-Mehdi Formation. Texturally, this sandstone is fine- to very fine-grained, submature to mature, moderately to well-sorted, and the grains are mainly subangular to subrounded and occasionally well rounded (Figs. 5.3.5A-D, 5.2.5B). Finally, the basal calcareous sandstones of the Magu Gypsum Formation in the Ravar area are immature, poorly sorted, and the grains are angular to subangular (Fig. 5.6.10B). Siliciclastic grain boundaries usually show signs of compaction, which partly caused cementation between siliciclastic grains. Soft and flexible lithic fragments such as shale or slate have been turned into pseudomatrix by compaction, which led to deformation

and squeezing of the fragments between framework grains as a cement (e.g., Fig. 5.8.10D). Apart from grain re-packing during early compaction, some grains have suffered dissolution leading to penetration of one grain by another (e.g. concave-convex contacts; Fig. 5.8.9C). Where this process is intense, the contact between grains has become sutured (Fig. 5.8.10C). Compaction and lithification decreased primary porosity. However, in calcareous sandstones and sandy limestones secondary porosity, mostly in shell fragments that are usually filled with sparry carbonate, has been observed (Fig. 5.8.13E-F). The matrix consists of predominantly silt, clay, and pseudomatrix. The latter has been produced by breaking down of shale fragments, or carbonate debris (Fig. 5.8.9H). Cement in rocks of the Lower Siliciclastic Member is mainly composed of carbonate (Fig. 5.8.9B), ferroan calcite (Fig. 5.7.5F), and Fe-oxide (Fig. 5.8.9G; mainly hematite). The latter obscures the carbonate cement or clayey matrix and imparts a distinctive red color to the rock, especially in the conglomerates and sandstones of the lowermost part of the Bidou Formation (Fig. 5.8.9F). This hematite also formed specks concentrated on the rims of detrital grains as a result of diagenetic processes at the base of the Kamar-e-Mehdi Formation (Fig. 5.3.5E).

Table 3. Main components (%) of sandstones. Sa: sample, Sec: section, Fm/Mb: Formation/Member, Bi. Bidou, Ra: Ravar, Bo: Bolboulieh, Mo: Mohamadshah, Ab: Abdoughi, Qo: Qoleh Nar, Ka: Kamar-e-Mehdi, Do: Doshakh, Ec: Echellon, Hoj: Hojedk Formation, Lsm: Lower Siliciclastic Member, Msc: Mixed Siliciclastic-Carbonate Member, Usc: Upper Siliciclastic Member, Mgf: Magu Gypsum Formation, Kam: Kamar-e-Mehdi Formation and Bag: Baghamshah Formation. For key of abbreviations see Table 1.

Sa	Name	Sec	Fm/ Mb	Qt	F	L	Qm	Lt	Qmn	Qmu	Qp2-3	Qp
M-32	Arkose	Bi	Hoj	36.74	54.58	8.68	36.74	8.68	67.67	20.17	5.87	6.29
M-43	Subarkose	Ra	Hoj	90.38	5.76	3.86	90.00	4.24	76.59	10.65	0	12.76
M-44	Arkose	Ra	Hoj	44.48	49.29	6.23	43.48	7.23	64.72	19.98	3.05	12.25
M-45	Subarkose	Ra	Hoj	88.75	6.25	5	88.75	5	88.73	5.63	1.40	4.24
M-87	Arkose	Bo	Hoj	61.38	36.99	1.63	61.06	1.95	51.30	31.71	4.85	12.14
M-13	Sublitharenite	Bo	Hoj	80	4.45	15.55	75.55	20	67.64	17.66	5.88	8.82
M-12	Sublitharenite	Bo	Hoj	75	11.12	13.88	72.22	16.66	65.38	15.38	3.86	15.38
K-9	Quartzarenite	Bo	Hoj	95.09	0.99	3.92	87.25	11.76	75.28	13.48	3.24	8
K-87b	Sublitharenite	Bi	Lsm	70.8	6.66	22.60	68.34	25	83.52	3.52	3.52	9.44
K-88	Litharenite	Bi	Lsm	64.28	7.15	28.57	64.28	28.57	92.22	3.33	0	4.45
K-90	Sublitharenite	Bi	Lsm	92	2	6	91.2	6.8	81.30	16.08	0.86	1.76
K-91	Sublitharenite	Bi	Lsm	79.5	7	13.5	76	17	87.42	6.28	1.88	4.40
K-92	Arkose	Bi	Lsm	48.75	36.25	15	42.5	21.25	61.76	23.52	8.82	5.88
K-93	Arkose	Bi	Lsm	69.04	27.61	3.35	69.04	3.35	99.31	0.69	0	0
M-18	Sublitharenite	Mo	Lsm	75	9.10	15.90	70.45	20.45	67.74	12.92	9.67	9.67
M-1a	Sublitharenite	Bo	Lsm	75.60	7.33	17.07	68.29	24.38	64.28	10.73	7.14	17.85
M-23	Subarkose	Mo	Lsm	90.38	7.69	1.93	90.38	1.93	87.23	6.38	2.14	4.25
M-24	Subarkose	Mo	Lsm	90.58	8.84	0.58	90.58	0.58	91.55	2.59	3.89	1.97
M-28	Arkose	Mo	Lsm	41.25	55	3.75	41.25	3.75	90.47	9.53	0	0
M-51	Sublitharenite	Mo	Lsm	86.36	4.54	9.10	72.72	22.74	65.62	21.88	0	12.5
M-8	Arkose	Bo	Msc	36.84	39.48	23.68	34.21	26.31	73.07	15.38	3.86	7.69
M-5	Arkose	Bo	Msc	37.66	44.16	18.18	35.06	20.78	74.07	18.53	3.70	3.70
K-97	Arkose	Bi	Msc	53.75	35	11.25	53.75	11.25	83.72	9.30	0	6.98
K-111	Subarkose	Bi	Msc	74.28	21.42	4.30	74.28	4.30	100	0	0	0
K-106	Arkose	Bi	Msc	52.22	41.11	6.67	52.22	6.67	100	0	0	0
K-100	Arkose	Bi	Msc	33.33	58.33	8.34	33.33	8.34	95	5	0	0
M-10b	Arkose	Bo	Usm	45.31	41.07	13.62	43.31	15.62	82.75	10.37	3.44	3.44
K-117	Arkose	Bi	Usm	33.75	30	36.25	33.75	36.25	81.48	18.52	0	0
K-118	Arkose	Bi	Usm	50	43.75	6.25	47.5	8.75	89.48	10.52	0	0

K-122	Arkose	Bi	Usm	71.42	27.14	1.44	71.42	1.44	84	10	0	6
M-63	Subarkose	Ec	Mgf	77	12	11	77	11	93.50	6.50	0	0
M-64	Arkose	Qo	Mgf	64.16	33.34	2.5	64.16	2.5	94.80	5.20	0	0
P-1	Subarkose	Ka	Kam	71	16	13	67.5	16.5	78.5	18.5	1.48	1.48
P-2	Arkose	Ka	Kam	72.13	26.22	1.65	72.13	72.13	81.81	4.54	0	13.65
P-54	Subarkose	Ka	Kam	85.83	11.67	2.5	85.83	2.5	86.40	5.84	3.88	3.88
P-55	Subarkose	Ka	Kam	67.30	24.05	8.65	67.30	8.65	88.57	2.85	5.73	2.85
P-172	Subarkose	Ab	Kam	64.66	22.68	12.66	61.32	16	84.23	13.58	0	2.19
P-173	Arkose	Ab	Kam	67.59	27.77	4.64	64.81	7.42	80	8.57	4.28	7.15
P-174	Arkose	Ab	Kam	39.28	35.72	25	38.21	26.07	88.78	10.28	0	0.94
K-159	Subarkose	Ra	Kam	72	24	4	71	5	63.38	22.53	8.45	5.64
K-160	Arkose	Ra	Kam	48.33	46.67	5	48.33	5	56.89	34.49	8.62	0
K-161	Arkose	Ra	Kam	40	50	10	10	10	46.87	37.5	6.25	9.38
K-163	Arkose	Ra	Kam	50.58	47.05	2.37	50.58	2.37	65.11	18.60	2.34	13.95
K-152	Arkose	Ra	Bag	60	40	0	60	0	95.83	4.17	0	0
M-32b	Quartzarenite	Ra	Bag	95	0	5	94	6	76	8	4	12
P81	Arkose	Do	Bag	42.36	53.68	3.96	41.06	5.26	90.25	9.75	0	0
M-34	Arkose	ra	Bag	71.73	15.21	13.06	71.73	13.06	90.90	3.03	0	6.07
P-158	Arkose	Ab	Bag	42.85	34.28	22.87	40	25.72	82.14	14.28	0	3.57
P-166	Subarkose	Ab	Bag	71.42	24.28	4.30	68.57	7.15	83.33	8.33	1.56	6.78

9.5 Siliciclastic rocks with silt- and clay-sized grains

Qualitative variation in the mineral composition of the shaly samples from the Hojedk, Bidou, Baghamshah, and Magu Gypsum formations was estimated from X-ray diffraction (XRD, analysed in the Geological Survey of Iran). The analysis revealed quartz, calcite, illite, chlorite, feldspar, mica, hematite, gypsum, halite, and dolomite (Table 4). According to Table (4), illite and chlorite are abundant in most phyllosilicates of the formations, but quartz, calcite and feldspar are commonly present in higher percentages, whereas gypsum and dolomite are less abundant. In the Magu Gypsum Formation, halite is the most abundant mineral, but its abundance varies locally. Clay minerals can be useful environmental indicators (e.g., MCCONCHIE et al. 1979). However, they need to be interpreted with caution because clays found in a given environment may not have formed there, different clays may form in the same environment depending on controls such as source rock type and drainage, and one type of clay mineral can form in a variety of environments when parent rock types and drainage conditions are similar. Hydrolysis is the major process involved in the break-down of primary silicates to clay minerals. Hence, the amount of precipitation, circulation of water among the primary minerals, and temperature are of prime importance. The influence of biota, and organic decomposition products is commonly great. However, the above mentioned factors are those that generally favour the formation of each type of clay but not all need apply to the formation of a particular clay, and the absence of any factor may not preclude the formation of a particular clay. According to ALONSO-AZCARATE et al. (1997), clay mineral assemblages within shaly and marly beds may also be useful for detecting changes in the source areas in sedimentologically homogeneous material. ARRIBAS et al. (2003) also believe

that clay minerals from interbedded shales maintain the source signal related to the corresponding petrofacies.

Table 4. Qualitative variation in mineral composition of shaly and marly samples. Fm/Mb: Formation/Member, LSM: Lower Siliciclastic Member, MSCM: Mixed Siliciclastic-Carbonate Member, USM: Upper Siliciclastic Member, Magu: Magu Gypsum Formation, Bag: Baghamshah Formation. Dol: Dolomite, Hal: Halite, Gyp: Gypsum. Cal: Calcite, Chl: Chlorite. The number of stars correlates with the abundance of the minerals.

Fm/Mb	Section	Sample	Quartz	Cal	Dol	Hal	Feldspar	Mica	Hem	Gyp	Illite	Chl
Hojedk	Bolboulieh	M-16	*****	*			**				***	****
Hojedk	Mohmmadabad	M-17	*****	*			**				****	***
Hojedk	Bidu	M-31	****		*						**	***
Hojedk	Ravar	M-43	******	*****	****		*				***	**
LSM	Bolboulieh	M-2	******	**			*****		*		****	***
LSM	Bolboulieh	M-3	******	**			*****		*		***	****
MSCM	Bolboulieh	M-6	*****	***			*				**	****
USM	Bolboulieh	M-9	*****	**			*				***	****
LSM	Mohamadshah	M-19	*****	*			**				***	****
MSCM	Mohamadshah	M-22	*****	***			*				**	****
USM	Mohamadshah	M-24	*****	****			*				***	**
USM	Mohamadshah	M-29	*****	**			*				****	***
LSM	Bidou	M-34	*****	*			**	****				***
MSCM	Bidou	M-35	*****				**	****	*			***
MSCM	Bidou	M-39	*****	***			**			****	*	
Magu	Ravar	M-54	*******	*****		**** ****	******		*	**	***	****
Bag	Doshakh	M-84	*****	****			***				*	**

9.6 Heavy minerals

In addition to the major constituents, the sandstones of the Hojedk and Bidou formations contain a suite of opaque and transparent heavy minerals consisting of zircon, tourmaline, rutile, monazite, apatite, hornblende, antophyllite, enstatite, biotite, epidote, siderite, chlorite, hematite, magnetite, limonite, and pyrite in different percentages (Tables 5-6; see also Figs. 9.6.1-3). These minerals were analysed under the transmitted and polarized light microscope

Table 5. Calculated counts, percentages, and grain shapes of heavy minerals. Fm/Mb: Formation/Member, Bol: Bolboulieh, Moh: Mohamadshah, LSM: Lower Siliciclastic Member, MSCM: Mixed Siliciclastic-Carbonate Member, USM: Upper Siliciclastic Member.

Sample	**Heavy minerals**	**Section**	**Fm/Mb**	**Number of mineral grains per 7 gr**	**Percentage of grains (%)**	**Grain shape**
M-13	zircon	Bol	Hojedk	88	47.82	Mostly subangular to subrounded
	apatite			3	1.63	Subangular to subrounded
	pyrite			4	2.17	Angular to subangular
	rutile			3	1.64	Subangular
	chlorite			2	1.09	Subrounded
	biotite			2	1.09	Subgular
	monazite			2	1.09	Angular
	siderite			3	1.64	Angular to subangular
	limonite			28	15.21	Angular to subangular

	magnetite			6	3.26	Angular to subangular
	hematite			35	19.02	Angular to subangular
	altered heavy minerals			8	4.34	
M-44b	clorite	Ravar	Hojedk	124	20.63	Mostly angular to subangular
	biotite			370	61.56	Mostly angular to subangular
	zircon			12	2	Angular to subrounded
	epidote			57	9.50	Mostly angular to subangular
	hematite			26	4.33	Very angular to angular
	magnetite			6	0.99	Mostly angular to subangular
	limonite			4	0.66	Mostly angular to subangular
	altered heavy minerals			2	0.33	

Table 6. Calculated counts, percentages, and grain shapes of heavy minerals in members of the Bidou Formation. Bol: Bolboulieh, Moh: Mohamadshah, LSM: Lower Siliciclastic Member, MSCM: Mixed Siliciclastic-Carbonate Member, USM: Upper Siliciclastic Member.

Sample	**Heavy Minerals**	**Section**	**Member**	**Number of mineral grains per 7 gr**	**Percentage of grains (%)**	**Grain shape**
M-87b	enstatite	Bol	LSM	11	1.82	Very angular to angular
	pyrite			36	5.96	Very angular to subangular
	zircon			24	3.97	angular
	antophyllite			3	0.49	Very angular
	apatite			1	0.16	Very angular
	biotite			4	0.66	Very angular to angular
	magnetite			38	6.29	Mostly angular to subangular
	hematite			284	44.25	Mostly angular to subangular
	limonite			115	19/03	Mostly angular to subangular
	altered heavy minerals			17	2.81	
M-18	zircon	Moh	LSM	18	18.75	Subangular to subrounded, a few rounded
	chlorite			10	10.41	Angular to subangular
	monazite			4	4.16	Angular
	hornblende			2	2.09	Angular
	siderite			2	2.09	Angular
	apatite			2	2.09	Subrounded
	magnetite			9	9.38	Mainly subangular to subrounded
	hematite			39	40.62	Mostly angular to subangular
	altered heavy minerals			10	10.41	
M-5	zircon	Bol.	MSCM	8	8.43	Angular to subrounded
	chlorite			6	6.31	Subangular
	siderite			14	14.74	Angular to subangular
	monazite			2	2.11	Angular
	magnetite			11	11.57	Angular
	hematite			45	47.36	Angular to subangular
	altered heavy minerals			9	9.48	
M-8	zircon	Bol.	MSCM	6	6.75	Subrounded to rounded
	rutile			1	1.13	Subrounded
	apatite			2	2.24	Angular to rounded
	monazite			1	1.13	Angular
	tourmaline			5	5.61	Angular
	biotite			1	1.13	Angular
	chlorite			2	2.24	Subangular
	magnetite			9	10.11	Subangular

	hematite			59	66.29	Subangular to subrounded
	altered heavy minerals			3	3.37	
M-21	zircon	Moh.	USM	4	5.63	Angular
	rutile			1	1.40	Subrounded
	apatite			3	4.22	Angular to rounded
	hornblende			1	1.40	Angular
	chlorite			12	16.90	Angular to subangular
	monazite			2	2.81	Angular
	tourmaline			2	2.81	Angular
	siderite			5	7.04	Angular to subangular
	magnetite			2	2.81	Subangular to subrounded
	hematite			36	49.35	Subangular to subrounded
	altered heavy minerals			4	5.63	
M-30	zircon	Moh.	USM	4	9.10	Rounded
	apatite			5	11.36	Rounded
	hornblende			4	9.10	Angular to subangular
	monazite			6	13.63	Angular
	chlorite			4	9.10	Angular to subangular
	magnetite			2	4.54	Angular
	hematite			17	38.63	Angular to subangular, some subrounded
	altered heavy minerals			2	4.54	

Heavy mineral figures

Fig. 9.6.1 (A) Detrital grains of chlorite, zircone (arrowed) under transmitted light; Hojedk Formation of the Ravar section (sample M-44b, width of photomicrograph 250 μm). (B) Detrital grain of siderite under polarized light; Hojedk Formation of the Bolboulieh section (sample M-13, width of photomicrograph 250 μm). (C-D) Detrital grain of monazite under transmitted light (C) and under polarized light (D); Lower Siliciclastic Member of the Mohamadshah section. Sample M-18, width of photomicrographs 250 μm. (E-F) Detrital grains of apatite under polarized light (E) and under transmitted light (F); Upper Siliciclastic Member of the Mohamadshah section. Sample M-30, width of photomicrographs 500 μm.

Fig. 9.6.2 (A-B) Detrital grains of hornblende under polarized light (A) and under transmitted light (B); Lower Siliciclastic Member of the Mohamadshah section. Sample M-18, width of photomicrographs 250 μm. (C-D) Detrital grain of tourmaline under polarized light (C) and under transmitted light (D); Mixed Siliciclastic-Carbonate Member of the Bolboulieh section. Sample M-8, width of photomicrographs 250 μm. (E) Detrital grains of magnetite (black arrow) and hematite (white arrow) under transmitted light; Lower Siliciclastic Member of the Bolboulieh section. Sample M-87b, width of photomicrograph 1 mm. (F) Detrital grains of limonite under transmitted-light; Hojedk Formation of the Bolboulieh section. Sample M-13, width of photomicrograph 400 μm. (G) Detrital grain of pyrite under transmitted light; Hojedk Formation of the Bolboulieh section. Sample M-13, width of photomicrograph 400 μm. (H) Detrital grain of chlorite under transmitted-light; Mixed Siliciclastic-Carbonate Member of the Bolboulieh section. Sample M-5, width of photomicrograph 200 μm.

Figs. 9.6.3 (A) Detrital grain of chlorite under polarized light; Mixed Siliciclastic-Carbonate Member of the Bolboulieh section. Sample M-5, width of photomicrograph 200 μm. (B, D) Detrital grains of pyroxene (enstatite) under transmitted light (B) and polarized light (D); Lower Siliciclastic Member of the Bolboulieh section. Sample M-87b, width of photomicrographs 250 μm. (C, E) Detrital grain of biotite under transmitted light (C) and polarized light (E); Lower Siliciclastic Member of the Bolboulieh section. Sample M-87b width of photomicrographs 250 μm. (F) Detrital grains of zircon and rutile under transmitted light; Hojedk Formation of the Bolboulieh section. Sample M-13, width of photomicrograph 300 μm.

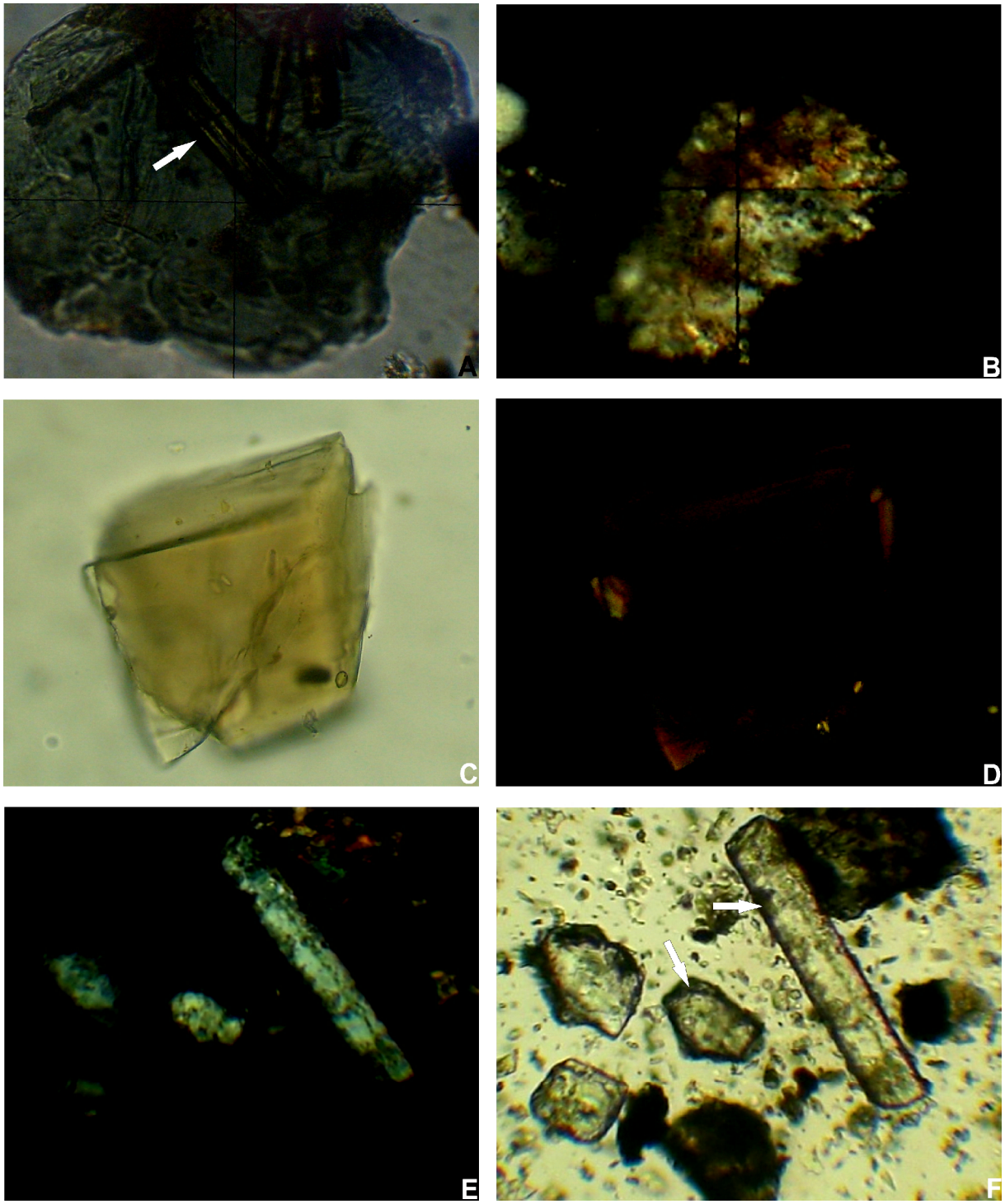

Fig. 9.6.1

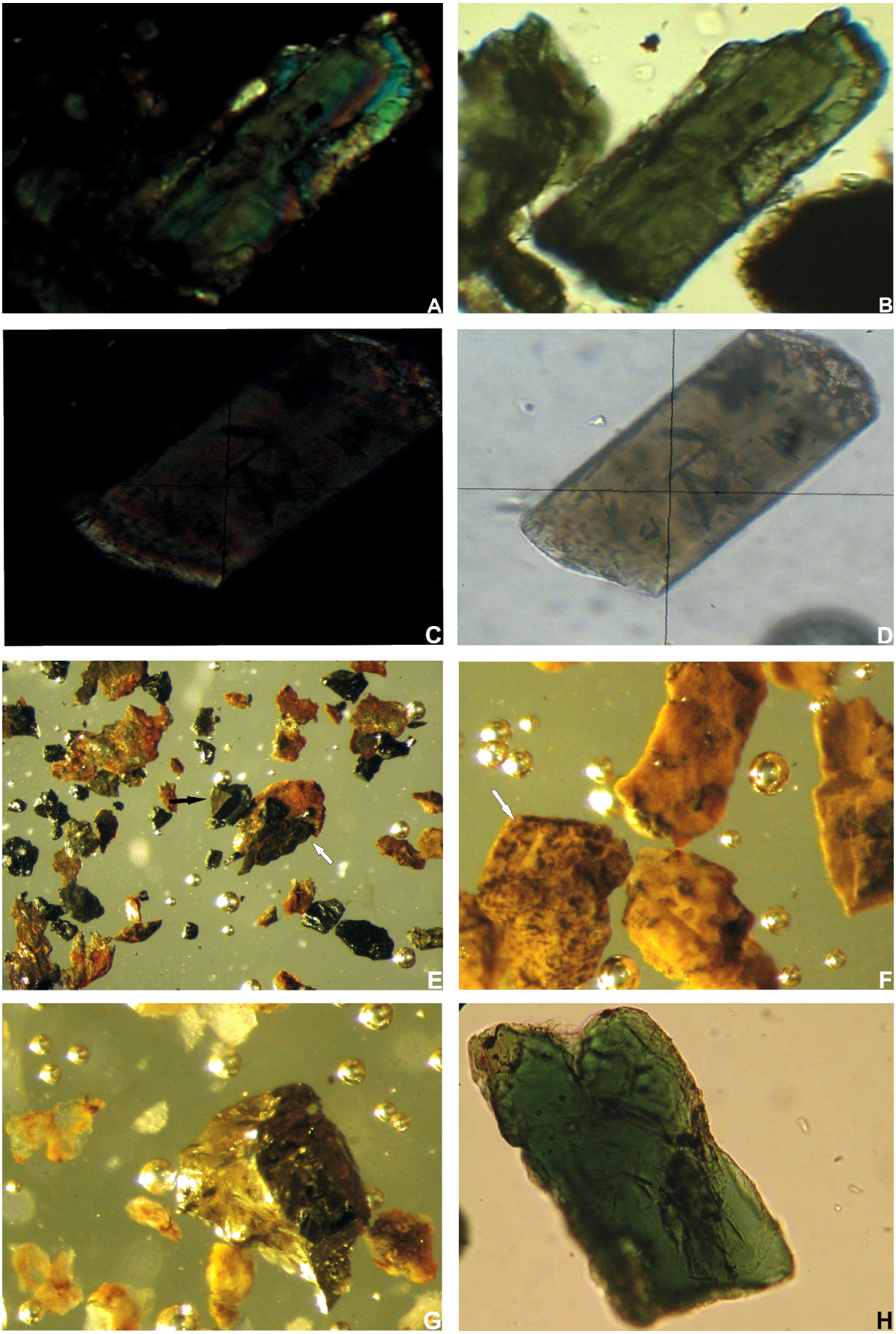

Fig. 9.6.2

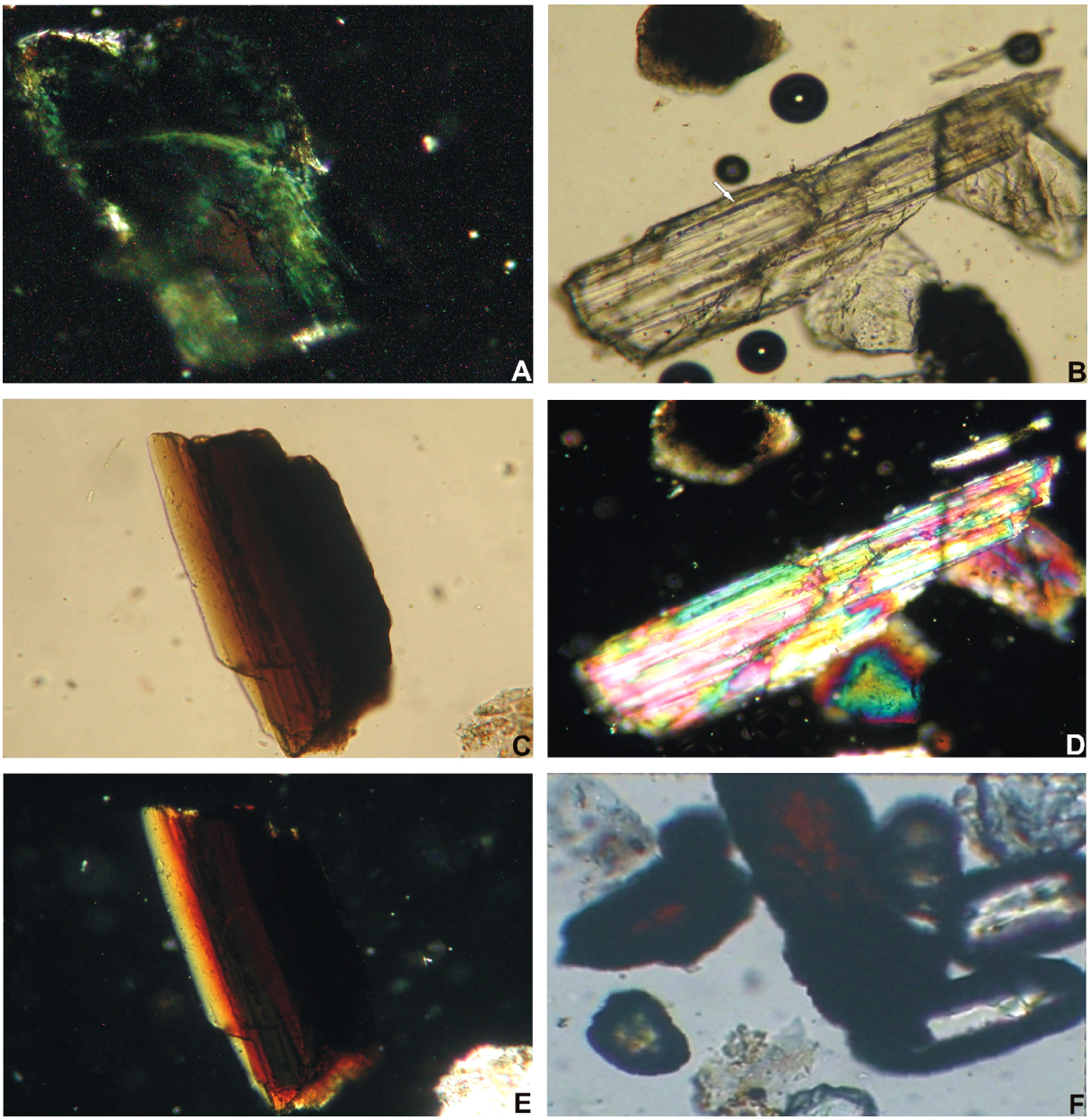

Figs. 9.6.3

10 Facies and sedimentary environments

The analysis of facies associations of Middle to Upper Jurassic strata is based on the study of thin-sections, which has been supplemented by observations in the field, and is based on e.g., WILSON (1975), FLÜGEL (2004), STOW (2005), KHOSRO-TEHRANI (2007), FÜRSICH (1975), FÜRSICH et al. (2003, 2005, 2009), WILMSEN et al. (2009) and others.

10.1 Braided stream deposits (fluvial channel fill deposits)

10.1.1. *Characteristic features*

These facies comprise <1 to 27 m thick, mostly fining-upward packages of conglomerate with an erosional base, large-scale trough cross-bedding, and some indistinct stratification. They are sandy to clast-supported, poorly sorted, oligomict (in the Bidou and Parvadeh areas), and monomict in the Echellon area (Figs. 5.7.2A-D, 5.1.3A, D). The larger clasts are generally more subrounded to rounded than smaller ones. Maximum size of the clasts is up to 15 cm in Bidou, 8 cm in Ravar and 30 cm in the Echellon area. Within the conglomerate most of the clasts are scattered randomly, but some show imbrication, scattered vertical clasts (Vc), and signs of tractive transport. Bed thickness varies from 20 cm to 3.5 m, and fossils are generally absent, except rare plant fragments. The conglomerates laterally turn into lenticular to bedded large-scale trough cross-stratified, poorly sorted, immature, coarse-grained feldspathic to litharenite sandstones (Figs. 5.7.2C-E, 5.8.4C) with subrounded to rounded pebbles ranging from 0.2 to 2 m in diameter, which are often, randomly scattered. The contact between conglomerates and sandstones is sharp to gradational.

10.1.2 *Interpretation*

The fining-upward, large-scale trough cross-bedded, sandy to clast-supported conglomerates with lenticular intercalations of poorly sorted, coarse-grained to pebbly sandstones are indicative of fluvial channel deposits of a high flow regime, which have been produced by braided river systems (e.g., EINSELE 1992). In the Bolboulieh and Mohamadshah areas, these conglomerates rarely display characteristic fabrics but in the Bidou and Echellon areas imbrication of clasts have been observed.

10.1.3 Occurrence

Lower part of the Lower Siliciclastic Member of the Bidou Formation in the Bolboulieh, Mohamadshah, and Bidou areas, and lower part of the Magu Gypsum Formation in the Echellon area.

10.2 Low sinuosity river deposits

10.2.1 *Characteristic features*

These facies are characterized by low-angle laminated to cross-stratified, mainly poorly-sorted, immature, often feldspathic to litharenite sandstone units (e.g., 5.7.5A-B, see also Chapter 9 for details) containing intercalations of lenticular, thick-bedded conglomerates and conglomeratic sandstones. Towards top, these facies fine-upward into low-angle planar- or cross-stratified sandstones, occasionally with flute cast on lower surfaces (Fig. 5.8.4D). Trace fossils are rare but *Taenidium* occurs within low-angle cross-laminated sandstones at the top.

10.2.2 *Interpretation*

As most of the sandstones are lenticular (mainly with a convex base and flat top), and exhibit asymmetric ripple marks, they very likely represent channel deposits of low sinuosity rivers (e.g., COLLINSON 1996). Faintly bioturbated sandstones (Fig. 5.7.2F-G) containing the trace fossils *Diplocraterion* or *Arenicolites* are related to relative sea-level changes and have been deposited during a phase of slow sea-level rise or subsidence within a generally regressive unit (lowstand systems tract: LST) in the lower parts of the Bidou Formation (e.g., COE 2003).

10.2.3 Occurrence

Lower part of the Lower Siliciclastic Member of the Bidou Formation in the Bolboulieh, Mohamadshah, and Bidou areas.

10.3 Overbank and flood plain deposits

10.3.1 *Characteristic features*

The facies is characterized by several decameters of alternating red, brown and greenish-grey laminated siltstone and silty clay with lenticular (Figs., 5.8.5C-E), thin- to very thick-bedded, occasionally ripple-bedded and horizontal laminated to very low-angle cross-stratified sandstones. The sandstone units may fine-upwards or coarsening-upwards and show climbing ripple lamination, and chaotic bedding (Bidou area, Fig. 5.7.3A-B). The sandstones exhibit scour and fill structures (Fig 5.8.5F), a sharp base (Fig. 5.8.5G), and some load casts (Fig. 5.8.5H). In this facies, recognisable trace fossils or plant fragments are very rare.

10.3.2 *Interpretation*

Deposition of the oxidized red to brown, greenish grey, non-fossiliferous siltstone, mudstone/argillaceous silt units took place in interchannel areas such as overbank/flood plain environments. The elongated lenticular sandstones correspond to flood events, where bed-load capacity was sufficient to transport sand material into the flood basin areas (FIELDING

1984). The coarsening-/thickening-upward successions are interpreted to represent infilling of the interchannel areas by fine-grained crevasse splay sediments (e.g., WALKER & CANT 1984; FARRELL 1987; MIALL 1985; COLLINSON 1996; AMIREH 1997). The concentration of shale intraclasts (rip-up clasts) in some beds with a channel morphology implies erosion of underlying strata. The sharp, flat bases of sandstones are indicative of high flow velocities (HUNTER & CLIFTON 1982). Climbing ripple lamination is common in fluvial sediments. They are particularly abundant in areas of overbank flow and flood plains (MCKEE 1966a) and natural levees. COLEMAN & GAGLIANO (1965) found climbing-ripple lamination in the Mississippi River delta. In these cases the laminations are restricted to subaqueous levees of the delta front and to subaerial levees. Fining-upwards units represent laterally extensive channel sandstones deposited by laterally migrating, sinuous rivers.

10.3.3 Occurrence

Lower part of the Mixed Siliciclastic-Carbonate Member of the Bidou Formation in the Bolboulieh, Mohamadshah, and Bidou areas.

10.4 Levee deposits

10.4.1 *Characteristic features*

These sediments consist of a few meters of non-fossiliferous brown to grayish-green lenticular, very fine- to fine-grained sandstones with intercalations of silty shale to siltstone.

10.4.2 *Interpretation*

The lenticular sandstones with intercalations of siltstone most likely to represent subaerial/subaqueous levee sediments. These facies gradationally overlie the channel-fill deposits and have been deposited during peak flood (e.g., FARRELL 1987).

10.4.3 Occurrence

Middle to upper part of the Lower Siliciclastic Member of the Bidou Formation in the Bolboulieh, Mohamadshah, and Bidou areas.

10.5 Lower to upper delta front deposits

10.5.1 *Characteristic features*

These facies are characterized by alternations of purple to brownish-red silty shale/siltstone with lenticular, thin- to thick-bedded very fine-grained lithic arkose and feldspathic greywacke (Fig. 5.8.7B, C, F). Some sandstones display horizontal, uni- or bi-directional, very low-angle cross-lamination, containing *Chondrites* (Fig. 5.8.8C), *Planolites*, *Taenidium* (Fig. 5.8.8E-F) and some shell fragments (probably bivalves) on bedding planes. Occasionally

thin-bedded sandstones exhibit a sharp-base and occasionally gutter cast on lower surfaces. Up-section, this facies turns into lenticular thick- to very thick-bedded, immature, fine- to medium-grained often feldspathic sandstones within coarsening-shallowing upwards units. In the Bidou area (Fig. 5.7.3G (Gsc)), intercalated thin- to medium-bedded sandstones (Figs. 5.7.3H) occasionally contain superficial ooids (5.7.7G). In the latter area, at top of the thickening-shallowing upward-cycles (Gsc) immature micro-conglomerate to conglomeratic sandstones containing wood fragments are intercalated (Figs. 5.7.4B, 5.7.7H).

10.5.2 *Interpretation*

The sharp base of the mainly thin-bedded sandstones is indicative of high flow velocities and the silty shale to siltstones indicate a low to moderate energy regime (e.g., FÜRSICH et al. 2003). The trace fossils *Diplocraterion*/*Arenicolites* are interpreted to represent a very shallow marine environment and high-energy conditions (FÜRSICH 1975). Lenticular feldspathic sandstones and conglomeratic sandstones containing abundant wood fragments at the top of the coarsening-/shallowing-upward cycles indicate relative sea level fall. Very likely these sandy sediments are related to upper delta front deposits, which gradationally overlie silty shale/siltstone to very fine-grained sandstones of the lower delta front, the latter also containing gutter casts which often occurs in shallow marine to offshore setting.

10.5.3 Occurrence

Lower to upper part of the Upper Siliciclastic Member in the Bolboulieh and Mohamadshah areas, and lower part of the latter member in the Bidou area.

10.6 Bay/shallow lagoonal? siliciclastic deposits

10.6.1 *Characteristic features*

These facies are dominated by fine-grained siliciclastic rocks such as dark-grey laminated silt, clay, calcareous shales, siliciclastic mudstones and carbonaceous silty clay with intercalations of brownish-grey horizontal to low-angle cross-stratified, very fine-grained feldspathic sandstones. The latter contain wood fragments and heavy minerals such as hematite and limonite. Intercalations of thin-bedded, yellowish-grey, non-fossiliferous carbonate mudstones (Figs. 5.8.4G, L), laminated carbonate mudstones (Fig. 5.8.11B-D) with microbial structures (relicts of algae or cyanobacterial pellets) are common.

10.6.2 *Interpretation*

The dark-grey fine-grained siliciclastics with intercalations of feldspathic sandstones probably represent a protected low energy bay/or shallow lagoonal setting. The intercalated fine-

grained limestones represent periods of reduced siliciclastic influx probably in connection with brief transgressive episodes.

10.6.3 Occurrence

Upper part of the Lower Siliciclastic Member of the Bidou Formation, and uppermost part of the Baghamshah Formation in the Ravar area.

10.7 Storm deposits

10.7.1 *Characteristic features*

These facies consist of shell beds, thin- to thick-bedded rudstones, grainstones, pack- to grainstones, pel-grainstones, calcareous sandstones, horizontal to low angle laminated mature subarkose/sublitharenite to quartz sandstones, and hummocky cross-laminated sandstones.

Shell beds: Shell beds are thick-laminated to very thin-bedded, poorly to well sorted (Fig. 10.7.1.1A, B), and mostly occur in the topmost part of coarsening-/shallowing-upward carbonate cycles (from marl, marly mudstone to mud- to wackestone). The shells are mainly disarticulated and consist of bivalves, and gastropods, which are often encrusted by serpulids.

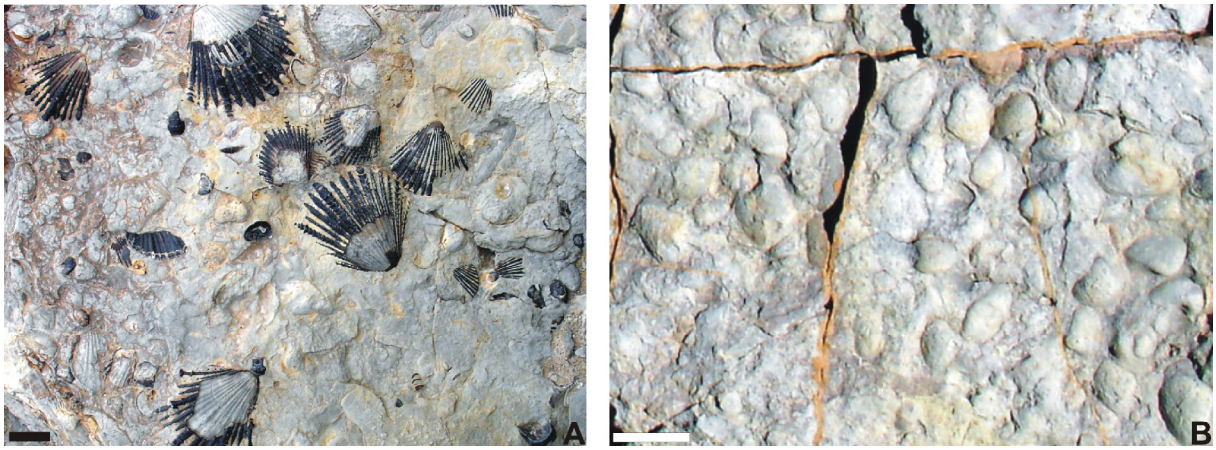

Fig. 10.7.1.1. Shell concentrations, middle to upper part of the Kamar-e-Mehdi Formation, Kamar-e-Mehdi area. (A) With poorly sorted disarticulated shells. (B) With well sorted shells. Black scale 10 mm, white scale 17.5 mm.

Rudstones: The skeletal grains are composed mostly of molluscan fragments, such as pectinids, oysters, gastropods, and some crinoids. The shell fragments are straight, curved, or rounded. The rounded grains are mainly covered by a thin micrite envelope (cortoid grains) or simple cortex. In most shell fragments, the original microstructure is not preserved but has been replaced by either sparry calcite or has been dissolved and the voids filled with sparite. However, in some samples, relicts of the shell have been preserved within the neomorphic sparry calcite, partly exhibiting irregular boundaries or sutured contacts between coarse sparry

grains and irregular anhedral inequigranular crystals within the shells (e.g., Fig. 5.8.12F-H; Fig. 5.8.13C-H).

- Thin- to medium-bedded rudstones (Fig. 10.7.1.2D): These rudstones are mainly sharp-based (Fig. 10.7.1.2A), and occasionally contain a bioclastic lag (Fig. 5.8.6E). The reworked shells are often graded (Fig. 5.8.6D). The individual beds are sometimes parallel laminated with wave rippled at top (Fig. 5.8.7E).

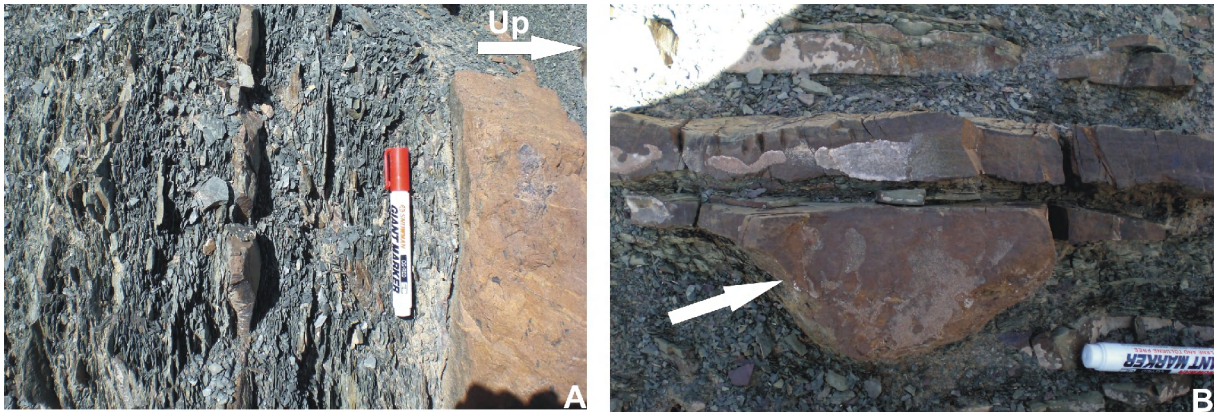

Fig. 10.7.1.2. (A) Intercalated light-brown, sharp-based, thin- to medium-bedded storm bed (rudstone) overlying shallow lagoonal fine-grained siliciclastic deposits of the uppermost part of the Mixed Siliciclastic-Carbonate Member, Bolboulieh area. (B) Gutter cast (arrowed), transitional zone between shallow lagoonal siliciclastic deposits of the Mixed Siliciclastic-Carbonate Member and lower deltafront deposits of the Upper Siliciclastic Member, Bolboulieh area.

- Thick-bedded rudstones (Fig. 10.7.1.2D): These are often poorly sorted with sharp, erosional base containing abundant silty clay, or sand sizes skeletal and non-skeletal grains filling the pore space between large shell fragments. In this facies some large bivalves are articulated (Fig. 10.7.1.2C, 5.8.11H).

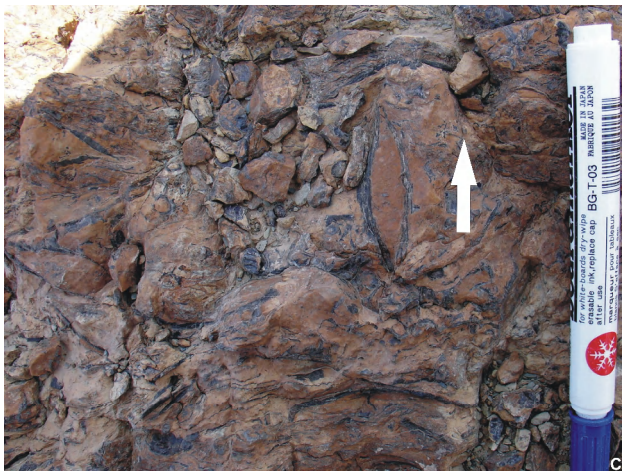

Fig. 10.7.1.2 (C) Thick-bedded, poorly sorted rudstone with sharp, erosional base, containing large articulated to disarticulated bivalve fragments. Arrow points to the top of the storm bed. Upper part of the Lower Siliciclastic Member, Mohamadshah area.

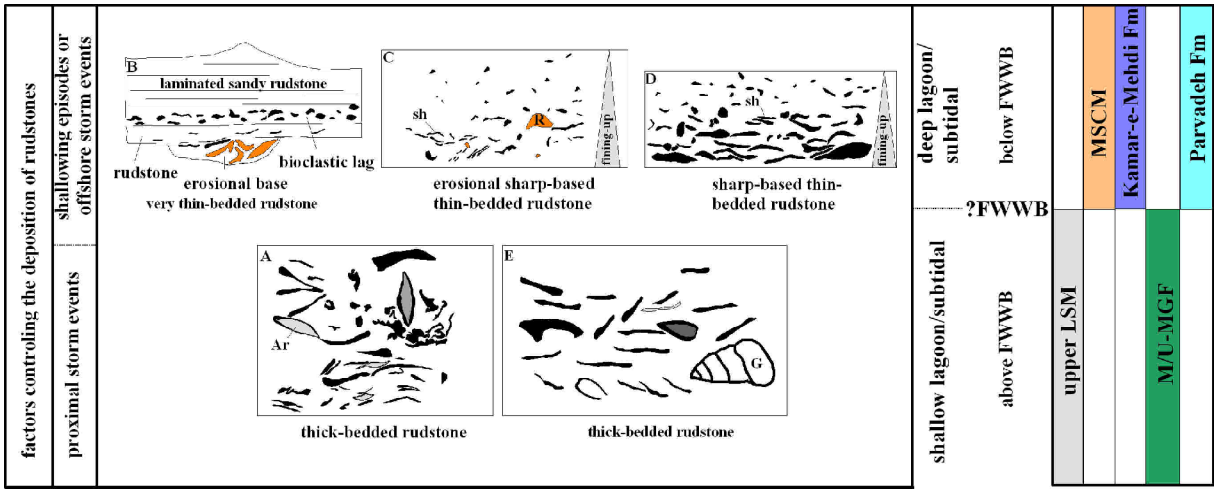

Fig. 10.7.1.2D. Various kind of rudstones which have been depositing by proximal to distal storm events. (A, E) Thick-bedded rudstone with poorly-sorted fabric, brief reworking (presence of articulated bivalves), and absence of grading or cross-bedding. (B-D) Rudstones with sharp base (D), bioclastic lag (B), reworked, often graded shells (C-D), and parallel laminated grainstone with wave-rippled top (B). Ar: articulated bivalves, Sh: shell fragments, R: rip-up clast, LSM: the Lower Siliciclastic Member, M/U-MGF: middle to upper part of the Magu Gypsum Formation, MSCM: the Mixed Siliciclastic-Carbonate Member, FWWB: fair-weather wave-base.

Grainstones: The sharp-based, cross-stratified, thin- to thick-bedded grainstones consist of spherical and or ellipsoidal ooids with a thin cortex and large nucleus (e.g. Fig. 5.1.5D-F) and some with a small nucleus (Fig. 5.8.11G). The nucleus is composed of quartz grains, intraclasts or skeletal grains. These microfacies also contain rounded intraclasts. Graded-bedding occurs (Fig. 5.2.4G). The cortex of the ooids consist mainly of very poorly or well developed radial laminae (Figs. 5.2.4B, 5.2.5A) and some concentric structures which partly to totally lost by micritization (Figs. 5.7.5H, 5.7.6A, 5.8.11G). Fig. 10.7.1.3A-B shows thin- to medium bedded storm-produced grainstone beds within the upper part of the Lower Siliciclastic Member.

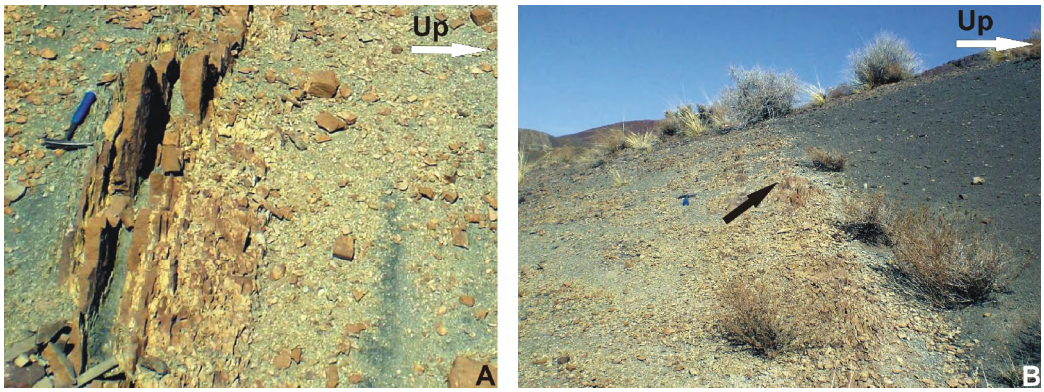

Fig. 10.7.1.3 (A, B) Intercalations of sharp-based oo-grainstones of storm origin within fine-grained siliciclastic bay deposits of the upper part of the Lower Siliciclastic Member in the Bolboulieh and Mohamadshah area.

Pack- to grainstone: The microfacies is characterized by abundant intraclasts and some molluscan, crinoid and bryozoan fragments,in a microspar cement (Fig. 5.4.4C-D).

Pel-grainstone: Medium- to thick-bedded grainstones composed of peloids (less than 100 µ in size) and a microsparry cement (Figs. 5.8.11B1, 10.7.1.3B) have been observed in the upper part of the Lower Siliciclastic Member.

Sharp-based sandstones: The horizontal to very low-angle cross-stratified sandstone beds are mostly mature with more than 95% quartz grains (Fig. 5.8.3B-C), but there are also subarkose or calcareous sandstones which overlie fine-grained siliciclastic or carbonate rocks with a sharp base (Fig. 10.7.1.4A).

Fig. 10.7.1.4. (A) Dolomitized calcareous sandstone with sharp base (white arrow) and hummocky cross-stratification overlying carbonate mudstone. Note rip-up clasts (black arrow), middle to upper part of the Kamar-e-Mehdi Formation in the Kamar-e-Mehdi area.

Hummocky cross-laminated sandstones: Light-brown medium-bedded hummocky cross-stratified poorly sorted, fine- to medium grained sandstones (Fig. 5.8.3F) occur within very shallow marine coarsening-/thickening upward successions.

10.7.2 *Interpretation*

The poorly to well sorted shell beds occur at the top of shallowing-/coarsening-upward cycles of the Kamar-e-Mehdi Formation. The sharp, flat base of the limestones formed during elevated water energy in form of storm-induced currents, whereas, the thick-bedded rudstones with erosional base (Fig. 10.7.1.2C) containing abundant large oysters and pectinids very likely have been produced by brief reworking events by storm waves. This facies exhibits a strongly disorganized fabric (see also FLÜGEL 2004). Based on FÜRSICH et al. (2003), these facies are characterized by a poorly sorted fabric, the presence of mud and silt in pore spaces, and the absence of sedimentary structures such as grading or cross-bedding, indicating lack of hydrodynamic sorting.

The thin-bedded rudstones with bioclastic lag and grading are interpreted to have been deposited by offshore storm flows under high energy conditions. According to FÜRSICH et al. (2003) the graded rudstones (Fig. 10.7.1.2D) are the result of gravity flows and low density turbidity currents generated by storm-induced currents (see also AIGNER 1985). Various skeletal and non-skeletal components in rudstones of very shallow marine origin (e.g., oysters, bivalves, large gastropods, cortoids, intraclasts) are evidence of offshore transport. According to BURCHETTE & WRIGHT (1992), rudstones composed of various skeletal grains, ooids, peloids and cortoids silmilarly represent a high-energy regime and were likely deposited by storms in a shallow subtidal environment. The rudstones of the Mixed Siliciclastic-Carbonate Member and the Magu Gypsum Formation (Fig. 5.4.4H), which have been deposited in subtidal/lagoonal environments experienced reworking and redeposition by storms (e.g., see Wilmsen et al. 2009). The sediments thus reflect varying degrees of storm influence depending on the water depth and bottom relief.

The well sorted grainstones with well-developed radial laminae were also deposited by storms in low-energy shallow subtidal settings or in an intertidal setting during high tide. The cross-stratified grainstones with superficial ooids probably formed in a very shallow, moderate to high water energy marine environments. Intraclasts and ooids with large nucleus can occur in intertidal, subtidal (by storms) and back reef environments (e.g., KHOSRO-TEHRANI 2007; ELF-AQUITAINE 1975).

A similar genesis is assumed for the pack- to grainstones and intra-oo-grainstones with faintly laminated graded grains.

Fig. 10.7.2 shows various kinds of grainstones in different siliciclastic, mixed siliciclastic-carbonate and carbonate rocks, respectively within the upper part of the Lower Siliciclastic Member, the Mixed Siliciclastic-Carbonate Member, the Kamar-e-Mehdi Formation, the Esfandiar Limestone Formation, and probably the Parvadeh Formation.

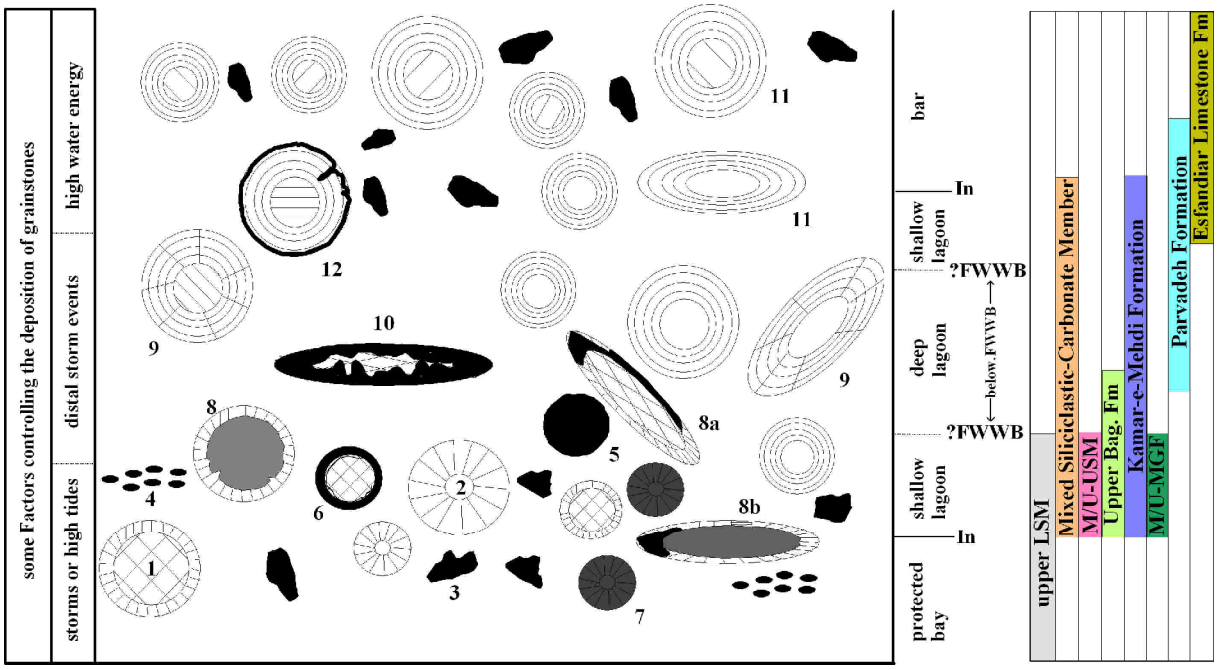

Fig. 10.7.2. Components and environments of grainstones. In: intertidal zone, FWWB: fair-weather wave-base, LSM: the Lower Siliciclastic Member, M/U-USM: middle to upper part of the Upper Siliciclastic Member, Bag.Fm: Baghamshah Formation, M/U-MGF: middle to upper part of the Magu Gypsum Formation. (1, 8) superficial ooid with calcareous and quartose nucleus, (2) ooid with radial laminae, (3) intraclast, (4) peloid, (5) perfectly micritized ooid, (7) faintly micritized ooid with radial laminae, (6, 8a, 8b, 12) partly to complete micritized cortex, (9) ooids with concentric to radial laminae, (10) cortoid, (11) concentric ooid.

- Intercalated hummocky cross-laminated sandstones within shallowing-upward cycles were probably also produced by storm waves. The cycles thus can be interpreted as oscillations of the relative sea-level within the storm-influenced shelf (see also EINSELE 1992).

- The mature quartz sandstones, subarkose or calcareous sandstones, which overlie fine-grained rocks with sharp-base within shallowing-upward cycles, are probably related to transgressive episodes with intermittent current activity. The sharp base of the sandstones is indicative of high flow velocities, reflecting storm-induced currents (HUNTER & CLIFTON 1982). According to LEITHOLD & BOURGEOIS (1984) low-angle cross-bedded sandstones may also reflect the migration of large bed forms with low amplitude. Rip-up clasts (Fig. 10.7.1.6A) in the lowermost part of the horizontal-laminated calcareous sandstones and thin-bedded rudstones (Fig. 10.7.1.2D), which overlie carbonate mudstones and silty clay in the Kamar-e-Mehdi Formation and Mixed Siliciclastic Member, imply erosion of underlying strata by storms in a lagoon/subtidal setting (see also Kelling & Mullin 1975; Walker 1985).

10.7.3 Occurrence

Upper part of the Lower Siliciclastic Member, middle to upper part of the Mixed Siliciclastic-Carbonate Member, Kamar-e-Mehdi Formation, uppermost part of the Baghamshah

Formation (Ravar and Doshakh areas), and middle to upper part of the Magu Gypsum Formation.

10.8 Beach deposits

10.8.1 *Characteristic features*

These facies are characterized by light-brown horizontal to unidirectionally very low-angle cross-laminated, medium-grained, mature subarkose sandstones (Figs. 5.6.4F). These facies occasionally contain recycled rounded heavy minerals such as zircon and rutile.

10.8.2 *Interpretation*

Heavy minerals are often concentrated in foreshore to backshore environments (e.g., EINSELE 1992), and since these sandstones conformably overlie channel inlet deposits of the upper part of the Baghamshah Formation, they are probably related to a beach setting. The sandstones are conformably overlain by bay deposits. According to Folk (1974) beach and bar environments are characterized by mature sandstones.

10.8.3 Occurrence

Upper part of the Baghamshah formation in the Ravar area.

10.9 Channel inlet deposits

10.9.1 *Characteristic features*

The well sorted, fine- to medium-grained subarkosic sandstones display uni- and bi-directional (herringbone) cross-stratification (Fig. 5.6.3G-H) with occasionally scours (Fig. 5.6.4D) at base, concretions (Fig. 5.6.4E), and sub-parallel to oscillation-crested ripples (Fig. 5.6.4C).

10.9.2 *Interpretation*

The herringbone cross-stratified sandstones with *Diplocraterion*/*Arenicolites* very likely correspond to high energy channel inlet deposits (e.g., SELLY 1996). These facies are overlain conformably by 15 m of horizontal-laminated beach (?backshore) sandstones. The small scours composed of conglomerate at the base of the cross-stratified sandstones are produced by erosion of the underlying sediment by currents (REINECK & SINGH 1973).

10.9.3 Occurrence

Upper part of the Baghamshah Formation in the Ravar area.

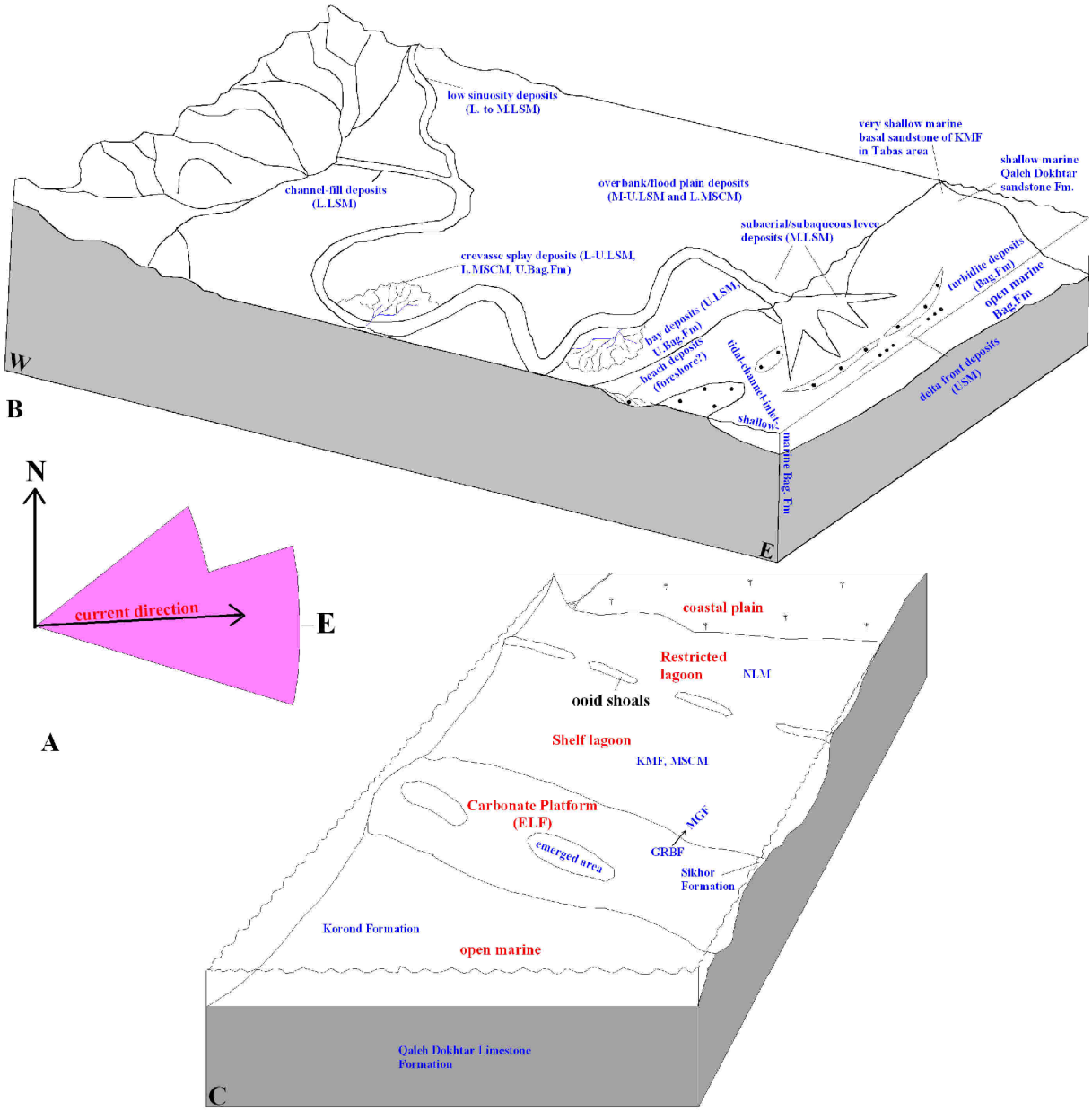

Fig. 10.1. (A) Rose diagram showing current direction of imbricated pebbles of the conglomerate and cross-laminated pebbly sandstones at the base of the Lower Siliciclastic Member at Bidou area. The current direction is mainly toward east (60%), and ENE (40%). (B-C) Different siliciclastic and carbonate sedimentary environments existing during the Late Jurassic in the western Tabas Block and eastern Lut Block. L: lower, M: middle, U: upper. LSM: Lower Siliciclastic Member, MSCM: Mixed Siliciclastic-Carbonate Member, USM: Upper Siliciclastic Member, KMF: Kamar-e-Mehdi Formation, MGF: Magu Gypsum Formation, Bag: Baghamshah Formation, NLM: Nar Limestone Member. ELF: Esfandiar Limestone Formation. GRBF: Garedu Red Bed Formation. For key of symbols see Fig. 5.8.16.

10.10 High-energy shallow marine deposits

10.10.1 *Characteristic features*

This facies is characterized by horizontal to unidirectional, low- to medium-angle planar cross-stratified, occasionally tabular cross-stratified (Figs. 5.3.2C), fine- to medium-grained, thin- to thick-bedded mainly feldspathic to calcareous sandstones with intercalated shell beds and bioturbated intervals (Figs. 5.6.2A-B, 5.8.3A). Some sandstones exhibit low-angle herringbone cross-lamination (Fig. 5.3.2D), a sharp base (Fig. 5.8.3D) and load casts (Fig. 5.8.3E) or ball and pillow structures (Fig. 5.3.2B) others exhibit an erosional lower surface. On these erosional surfaces prod casts, groove casts, and skip casts occur (Fig. 10.10.1A-C). Recognizable trace fossils are *Diplocraterion*/*Arenicolites* (Fig. 5.3.4B, 5.6.2C-D), *Gyrochorte* (Fig. 5.8.8A-B), and *Skolithos*. Petrographically, the sandstones occasionally contain intraclasts, shell fragments, ooids, crinoid ossicles, latter exhibiting in some cases syntaxial overgrowth of calcite (Fig. 5.3.5A-E).

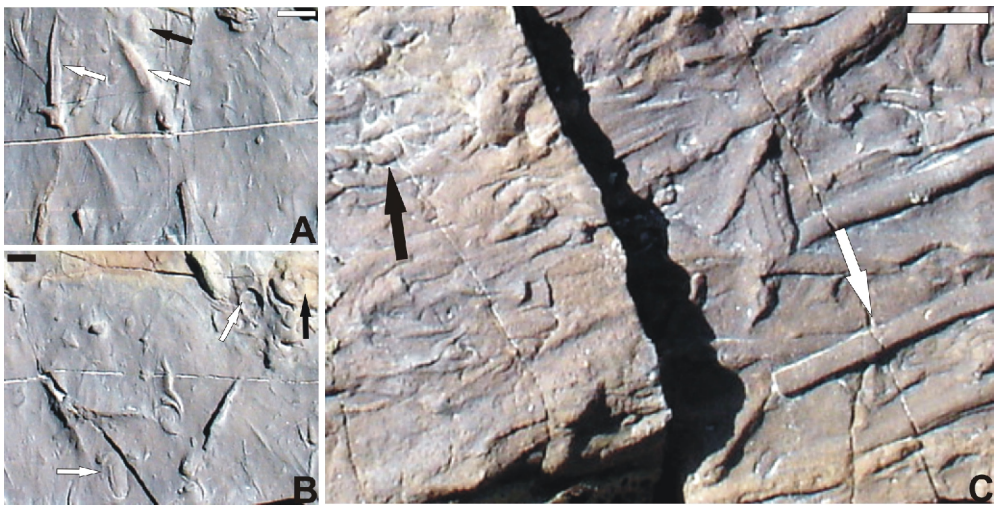

Fig. 10.10.1A-C. (A) Prod casts (white arrow) current directions is toward down the photo and very small load casts (black arrow). (B) Skip casts (white arrows), and load casts (black arrow). (C) Groove cast showing current direction (white arrow), and probably current-modified burrow (black arrow). Lower part of the Kamar-e-Mehdi Formation**,** Doshakh area.

10.10.2 ***Interpretation*** The low-angle cross-bedded sandstones may reflect the migration of large bed forms with low amplitude (LEITHOLD & BOURGEOIS 1984). The sharp base of sandstones is indicative of high flow velocities, reflecting storm-influenced currents (HUNTER & CLIFTON 1982). The intercalated shell beds (in the Ravar, Doshakh, and Kamar-e-Mehdi areas) with a silt to very fine-grained siliciclastic matrix point to reworking events. The low-angle herringbone cross-lamination in some beds represents tidal influence. The reworked skeletal to non-skeletal carbonate components of some sandstones (Tabas area) probably are

from neighbouring areas of shelf production, and the presence of trace fossils such as *Skolithos and Diplocraterion* /*Arenicolites* in the faintly bioturbated sandstones point to very shallow marine high-energy environments (e.g. FÜRSICH 1975; HÄNTZSCHEL, 1962, ELF-AQUITAINE 1975, SELLY 1996, FLÜGEL 2004). The sandstones with load cast and ball-and-pillow structures indicate rapid deposition. These sandstone beds lie above a hydroplastic mud layer, leading to unequal loading. According to EINSELE (1992), load casts and ball-and-pillow structures are not confined to any particular environment. They are known both in shallow water environments and deeper-water turbidites. Both structures point to mud sedimentation, interrupted by episodic deposition of sand by high-energy events. Groove casts should be equally common in very shallow water regions, they are produced by tools carried by the currents along a soft bottom (Fig. 10.10.2A). Prod and skip casts occur on the under surfaces of some sandstones of the Kamar-e-Mehdi Formation. According to DZULYNSKI & WALTON (1965), the asymmetrical prod marks are elongated semiconical to triangular depressions marks on the under surfaces of sandstone (Fig. 10.10.2A) with a shallow pointed upcurrent part and a deeper, broad down-current part. According to STOW (2005), prod and skip marks are formed when objects being carried by currents impact or scrape along the sediment surface. He stated grooves are oriented parallel to flow and with the V-shaped crenulations closing downstream.

10.10.3 Occurrence Upper part of the Hojedk and the Baghamshah formations in the Ravar area, and uppermost part of the Baghamshah Formation in the Abdoughi, Kamar-e-Mehdi and Doshakh areas. Lowermost part of the Kamar-e-Mehdi Formation in the Kamar-e-Mehdi, and Doshakh areas.

10.11 Lower shoreface to offshore siliciclastic deposits

10.11.1 *Characteristic features*

This facies association contains several coarsening-/thickening-upward cycles of poorly laminated silty clay (occasionally bioturbated), or silty marl at base, and very fine- to fine-grained, horizontal to very low-angle cross-stratified, sometimes hummocky cross-stratified, thick-laminated to medium-bedded sandstone beds at top. The latter also exhibit wave ripples (occasionally oscillation ripples) on bedding planes (e.g., Figs. 5.2.2A, 5.2.2E, 5.5.3D, 5.6.8C) and contain intercalations of bioturbated intervals (*Thalassinoides*, *Ophiomorpha, Rhizocorallium irregulare* and *Planolites*) (Figs. 5.7.4F-G, 5.7.5G).

10.11.2 *Interpretation*

The poorly laminated to bioturbated silty clay and occasionally silty marl represent low-energy conditions. Very likely they have been deposited in lower shoreface to offshore environments (Fig. 10.10.2A). The sandstones with wave ripples on top are probably tempestites formed above storm-wave base (e.g., DUKE et al. 1991). The hummocky cross-stratified sandstones often occur between fair weather wave base (FWWB) and storm wave base (SWB). The bioturbated structureless sandstones were likely deposited in lower shoreface to inner shelf environments (e.g. REINECK & SINGH 1980). WIGNALL & HALLAM (1996) described such bioturbated sandstones to have also been deposited in upper offshore environments. *Thalassinoides* is characteristic of shelf environments and indicates moderate to low water energy (FÜRSICH, 1975; HÄNTZSCHEL, 1962) (Fig. 10.10.2Af). *Ophiomorpha* is an indicator of high energy conditions in shallow-water environments (UCHMAN 1991, 1995; SCHLIRF 2003) and probably occurs in middle to upper shoreface (see Fig. 10.10.2A), whereas *Rhizocorallium irregulare* occurs mostly in low-energy shelf deposits (FÜRSICH, 1974).

10.11.3 Occurrence

Upper part of the Baghamshah Formation in the Abdoughi, Kamar-e-Mehdi and Doshakh areas, and very fine-grained siliciclastic rocks of the Mixed Siliciclastic-Carbonate Member of the Bidou Formation.

Fig. 10.10.2 (A) Very shallow to offshore marine siliciclastic environments of the upper part of the Hojedk (2), Baghamshah (1-4), and lowermost part of the Kamar-e-Mehdi formations (2). 1-4 refer to offshore to offshore transition zone (1), shallow to very shallow marine (2), channel-inlet deposits (3), and bay to lagoonal deposits (4) respectively. P: prod cast, G: groove cast, Es: transgressive surface, Ofs: flood plain deposits, ofl: Overbank/flood plain deposits overlie lagoonal deposits. Hm: hummocky cross-bedding, L: load cast, B.P: ball and pillow structure, C.s: calcareous sandstone, Q.s: quartz sandstone, In: intraclast, oi: ooid, cr: crinoid fragment, bi: bioclast, si: silt, m: marl, cl: clay, Pa: *Palaeophycus*, sh: shell debris, D: *Diplocraterion*, Pl: *Planolites*, Gy: *Gyrochorte*, Bi: bioturbation, Ta: *Thalassinoides*, Op: *Ophiomorpha*. Te: *Taenidium*, Sk: *Skolithos*. Rh: *Rhizocorallium,* a: shells, crinoid ossicles, and intraclasts transported by nearshore storms towards shoreline, b: a assemblages of feldspar (F), mostly angular heavy mineral (H.m), slate or shale (Lm), non-undolose/undolose monocrystalline quartz (black spots), polycrystalline quartz with >3 sub-grains (Qp>3c), and polycrystalline quartz with 2-3 sub-grains (Qp2-3) which have been transported by river to coastal areas. c: Skeletal and non-skeletal grains, which have been transported by currents from neighbouring carbonate producing areas. d: recycled, rounded mainly quartz or other siliciclastic or carbonate debris which probably were transported by longshore currents. e: trace fossils related to high water energy in very shallow marine setting. f: clay, marl, silt, very fine-grained calcareous sandstones, and trace fossils related to low to moderate water energy in a lower shoreface to offshore setting, Note also some trace fossils which are related to brief high-energy events. (B) Distribution of the skeletal and non-skeletal grains on a rimmed carbonate platform, modified from ELF-AQUITAINE (1975), SELLY (1996), and FLÜGEL (2004). For key of symbols see Fig. 5.8.16.

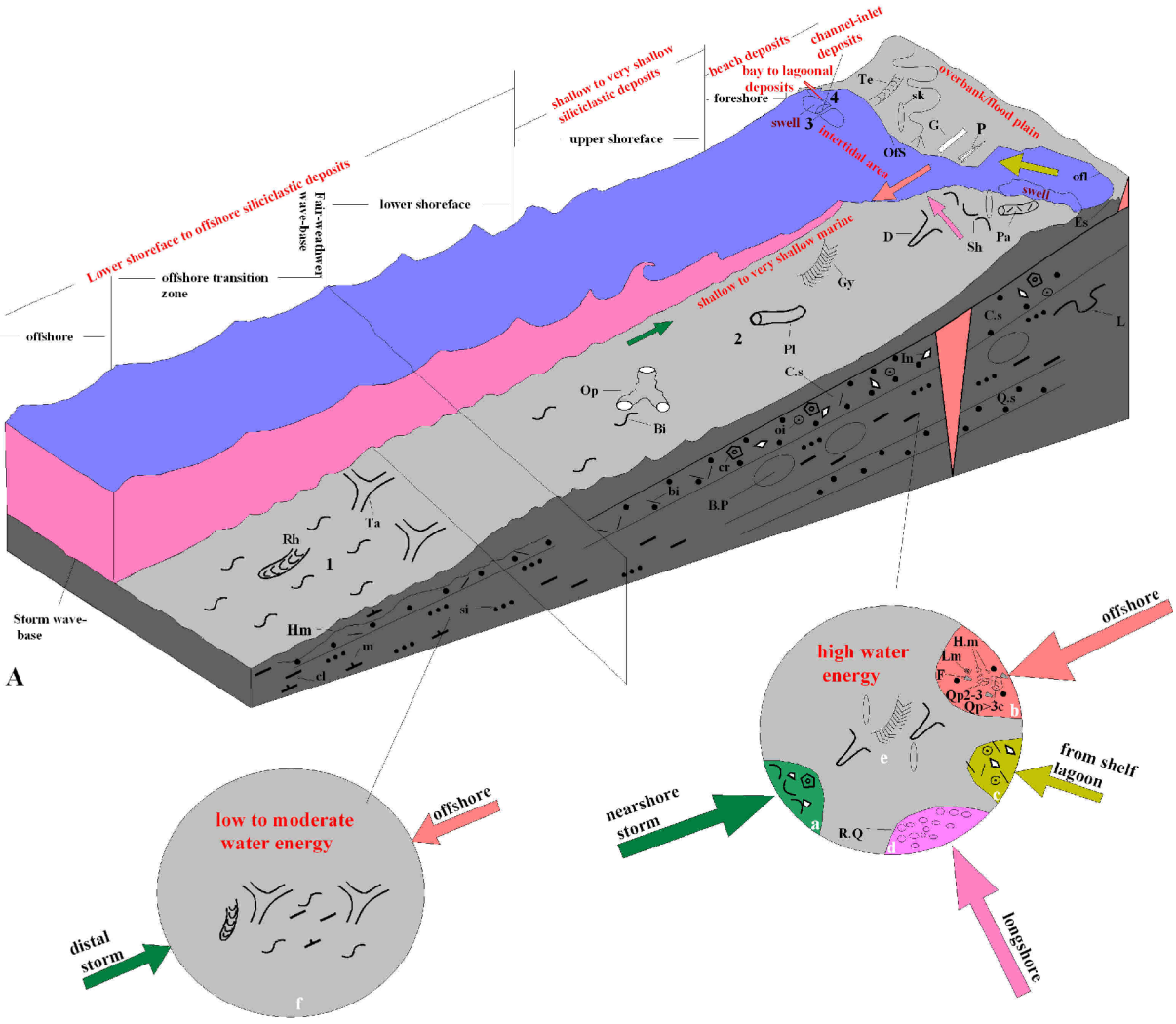
A
Lower shoreface to offshore siliciclastic deposits
offshore transition zone
offshore
Fair-weather wave-base
lower shoreface
shallow to very shallow siliciclastic deposits
upper shoreface
foreshore
beach deposits
bay to lagoonal deposits
channel-inlet deposits
overbank/flood plain
swell
intertidal area
shallow to very shallow marine
Storm wave-base
Rh
Ta
Hm
cl
m
si
Op
Bi
Pl
Gy
D
Sh
Pa
Es
C.s
L
Q.s
In
oi
cr
bi
B.P
Te
sk
G
P
OfS
ofl
high water energy
low to moderate water energy
offshore
nearshore storm
distal storm
from shelf lagoon
longshore
H.m
Lm
F
Qp2-3
Qp>3c
R.Q
a
b
c
d
e
f

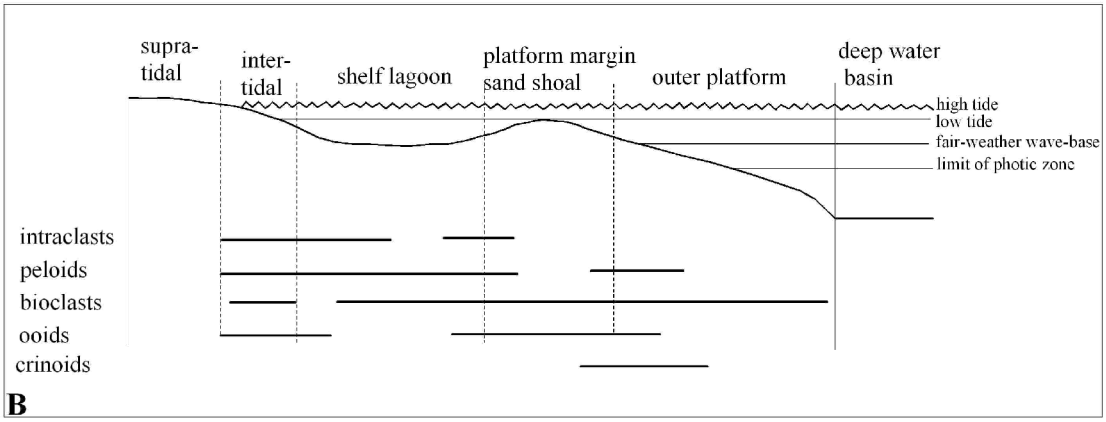
supra-tidal
inter-tidal
shelf lagoon
platform margin sand shoal
outer platform
deep water basin
high tide
low tide
fair-weather wave-base
limit of photic zone
intraclasts
peloids
bioclasts
ooids
crinoids
B

10.12 Low energy, intertidal to supratidal deposits (sabkha)

10.12.1 *Characteristic features*

This facies association consists of mainly red to brown silty clay to gypsiferous silty clay (Fig. 10.12B) with intercalations of laminated evaporate-carbonate bindstone (Fig. 10.12A), pure mudstone to dolomitic mudstone, and thickly laminated- to medium-bedded gypsum (Fig. 10.12C). The bindstone consists of alternating micrite and gypsum layers, and some mudstones contain a few thin horizontal laminae and also voids which are infilled with secondary opaque minerals (Fig. 5.8.11B-D). In gypsum beds often enterolithic folds (Fig. 5.4.2C), and occasionally nodular/chicken-wire texture occur (Figs. 10.12C-D). Large crystal of gypsum (Fig. 10.12B) have also been observed in silty clay beds.

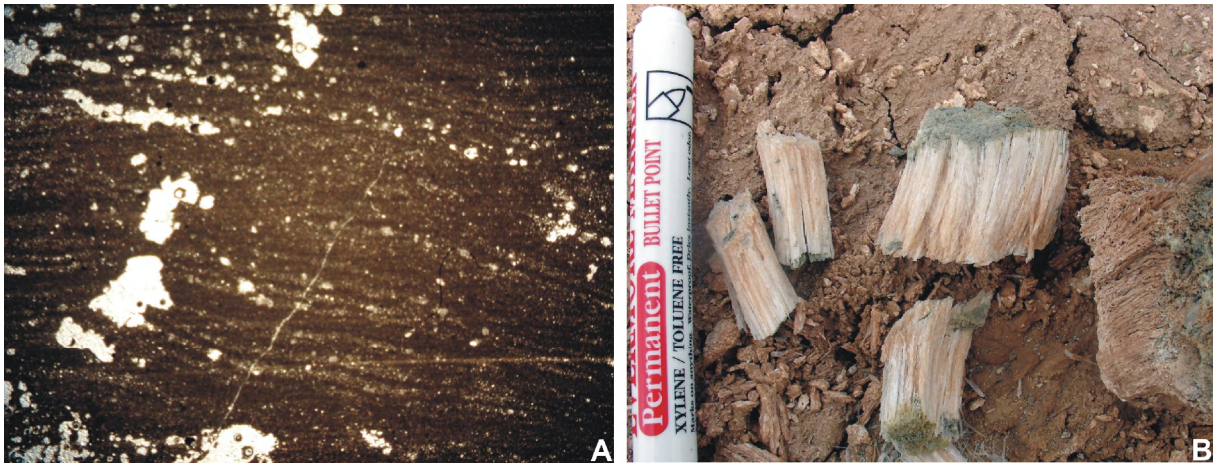

Fig. 10.12 (A) Laminated evaporate-carbonate bindstone with fenestral fabrics. (B) Large crystals of fibrous gypsum within red to brown silty clay.

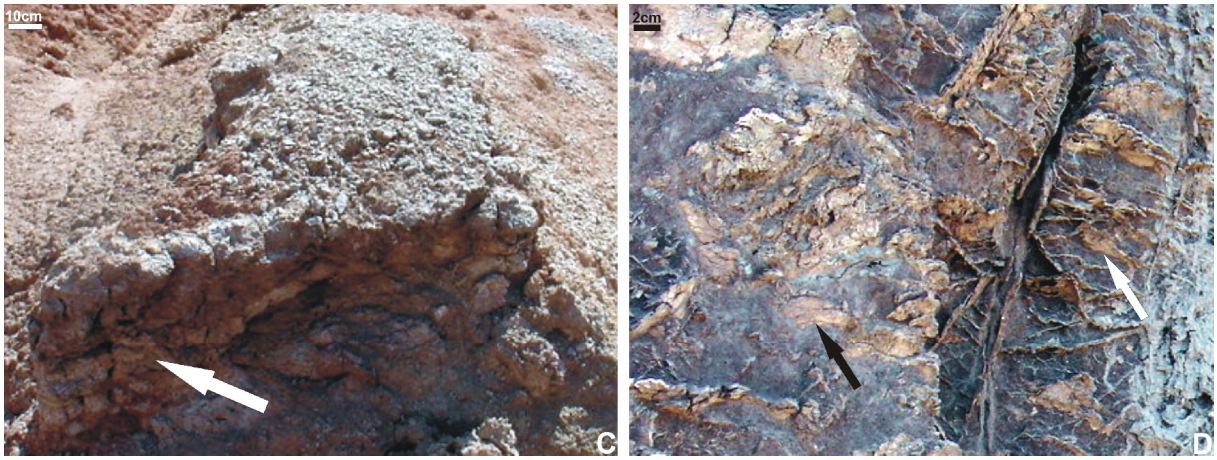

Fig. 10.12 (C) Nodular, and folded thin-bedded gypsum beds within red silty clay. (D) Silty clay with abundant gypsum veins (white arrow), and nodular gypsums (black arrow).

10.12.2 ***Interpretation***

The red to brown fine-grained siliciclastic rocks indicate low energy conditions and have been deposited on coastal plain and in shallow lagoons. The bindstones (probably with fenestral fabric), mudstones, dolomitic mudstones, and intercalated layers of gypsum/anhydrite very likely suggest low-energy inter- and supratidal conditions (sabkha) related to an arid climate. Vesicular mudstone is very likely formed on tidal flats under low energy conditions. The nodular/chicken-wire texture, enterolithic folds in gypsum/anhydrites, and large crystals of gypsum often occur in supratidal setting (ALSHARHAN & WHITTLE 1995, EINSELE 1992, FLÜGEL 2004). The former probably resulted from incomplete early cementation of anhydrite/gypsum beds.

10.12.3 Occurrence Mainly lower to middle and uppermost part of the Magu Gypsum Formation in the Qoleh Nar, Echellon, and Ravar areas.

10.13 Low-energy restricted shallow lagoonal deposits

10.13.1 ***Characteristic features***

This facies association is characterized by marl, thickly laminated to very thick-bedded mudstone or silty mudstone, faintly laminated bindstone, mudstone with gypsum needles (e.g., Fig. 5.3.7B, E, F), bio-wackestone, crustacean coprolite wackestone/packstone, silty dolomitic mudstone (Fig. 5.3.7H) with shell fragments of *Radulopecten tipperi*, clast-supported calcareous breccias, and anhydrite/gypsum.

10.13.1.1 Mudstones or silty mudstone: This facies type consists of pure very fine-grained micrite. The carbonate mud was possibly derived from mechanical or biological erosion. This microfacies occasionally contains silt, clay (Fig. 5.1.5B) and a few foraminifers (Fig. 5.1.4F) or shell fragments such as ostracods (Fig. 5.1.4B, 5.4.3C).

10.13.1.2 Laminated bindstone: The facies is characterized by very fine-grained micrite. The carbonate mud was possibly produced by mechanical or biological erosion (Fig. 5.1.4E, G, 5.4.3B, 5.8.11E).

10.13.1.3 Mudstone with gypsum needles: This facies is characterized by very fine-grained micrite with microbial structures, the latter are probably relicts of algae or cyanobacterial pellets. The microfacies contains some gypsum needles (Figs. 5.1.4A, 5.3.7E) and occasionally ostracod debris (Fig. 5.3.7F).

10.13.1.4 Silty dolomitic mudstone: This facies type is characterized by silty carbonate mudstone containing subhedral- to well-formed secondary dolomite rhombs which exhibit an

idiotopic porphyrotopic texture. The microfacies occasionally contains relicts of crinoid debris (Fig. 5.3.7H).

10.13.1.5 Crustacean coprolite wackestone/packstone: This facies consists of crustacean coprolites of the Parafavreina-type in a peloidal wackestone matrix (Fig. 5.4.3D-E).

10.13.1.6 Clast-supported calcareous breccias: They consist of angular fragments of the Nar Limestone Member which are cemented by microspar. In the matrix also occur white spots of gypsum, silt, and sand-sized debris (Fig. 10.13.1.6A).

Fig. 10.13.1.6A. Clast-supported calcareous breccias in the lower part of the Magu Gypsum Formation of the Echellon and Qoleh Nar area.

10.13.1.7: Anhydrite/gypsum bed: This facies type is characterized by several decameters of thick, white to light-green, mostly regular, horizontal, thickly laminated, thick-bedded anhydrite/gypsum beds (Fig. 10.13.1.7B, C).

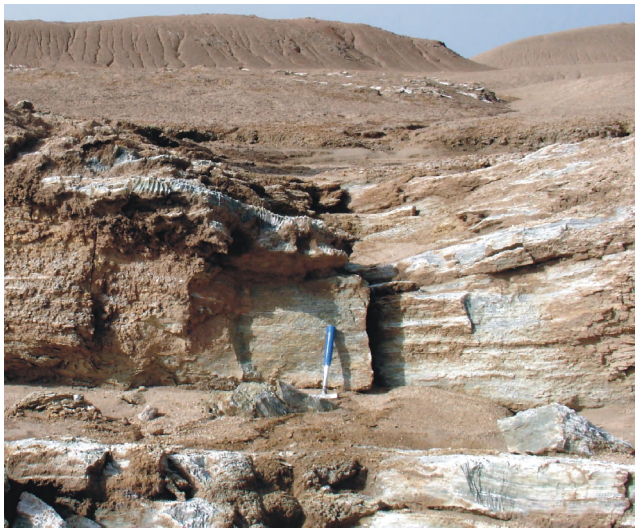

Fig. 10.13.1.7B. Note white to light-green thick-bedded laminated anhydrite beds.

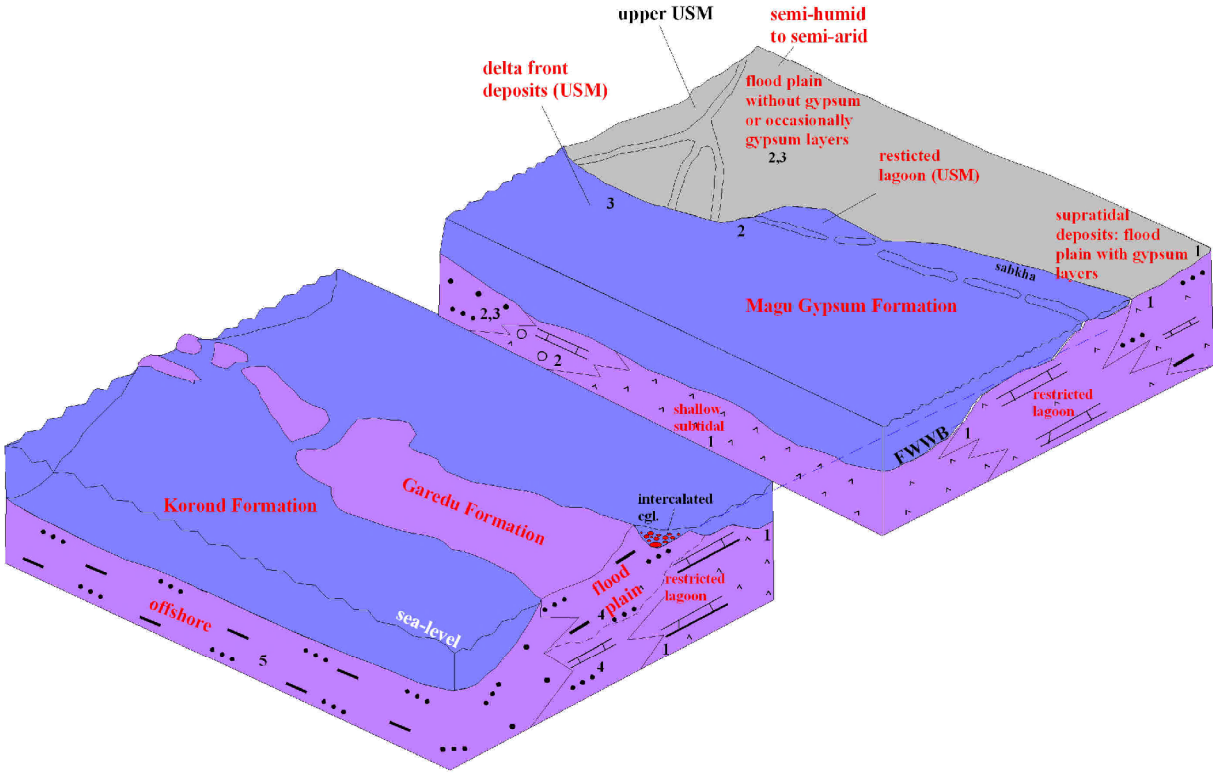

Fig. 10.13.1.7C. Sedimentary environments of the Magu Gypsum Formation, Upper Siliciclastic Member (USM) of the Bidou Formation, and of the Garedu- and Korond formations. 1-5 refer to Echellon (1), Bidou (2), Mohamadshah-Bolboulieh (3), Garedu (4) and Korond (5) areas respectively. For key of symbols see Fig. 5.8.16.

10.13.2 *Interpretation*

Faintly laminated bindstones, mudstones with gypsum needles, bio-wackestones, and silty dolomitic mudstones have been deposited in a restricted, low energy peritidal setting. The Parafavreina wackestone represents low-energy, restricted lagoonal setting (see also WILMSEN et al. 2009). However, since in these facies often benthic agglutinated larger foraminifera such as *Everticyclammina* and ostracods occur, they most likely were deposited in marine environments, probably shallow lagoonal/subtidal settings. The breccias may represent collapse breccias of early cemented limestone beds where evaporates were dissolved away. This may have happened in connection with the Late-Cimmerian movements. The evaporate beds with primary parallel lamination formed subaqueously in relatively deep parts of the basin, but also in marginal shallow-water areas. In the Echellon area, this facies type conformably overlies rudstone beds of storm-origin. The latter also occur within, and on top of the anhydrite beds.

10.13.3 Occurrence Upper part of the Nar Limestone Member of the Qoleh Nar and Echellon areas and upper part of the Mixed Siliciclastic-Carbonate Member of the Bidou and

Mohamadshah area, middle part of the Upper Siliciclastic Member in the Bidou area, and middle to upper part of the Magu Gypsum Formation in the Echellon, Qoleh Nar, and Ravar areas.

10.14 Deep subtidal/lagoonal deposits

10.14.1 *Characteristic features*

The sediments of the deep subtidal/shelf lagoon (Fig. 10.14) are mainly composed of marl, marly mudstone, silty mudstone arranged in irregular coarsening- and thickening-upward cycles. They contain intercalations of bio-wackestone/floatstone, intra-cortoid-bio-wackestone/floatstone, silty to sandy bio-wackestone/floatstone, onco-floatstone/packstone, and also bioturbated intervals. This facies association mainly contains macrofossils such as bivalves, oysters, gastropods, brachiopods, sponges, echinoderms, corals encrusted with *Serpula* (*Darsoserpula*), bryozoans (see Chapter 7 for details), and benthic foraminifers. Non-skeletal grains consist of cortoids, oncoids, intraclasts, ooids, and peloids.

10.14.1.1 Bio-wackestone/floatstone: This microfacies (e.g., Fig. 5.6.9D, E) contains shell fragments of crinoid, bryozoan and gastropod origin.

10.14.1.2 Intra-cortoid-bio-wackestone/floatstone: The facies consists of coated skeletal grains (mainly shell fragments) set within a micritic matrix. This facies has occasionally endured recrystallisation (neomorphism) leading to production of sparry calcite. Both shell moulds and thin micrite rims on the margins of the shells occur (e.g., Fig. 5.8.14A-C).

10.14.1.3 Silty to sandy bio-wackestone/floatstone: This facies contains microbioclasts, oyster and shell fragments, echinoid spines, crinoid debris and silt to sand-sized detrital grains, which float in a micritic matrix (e.g., Fig. 5.3.7D).

10.14.1.4 Silty to sandy oo-pel-wackestone/floatstone: This facies consists of non-sketetal grains such as peloids, ooids and silt- to sand-sized detrital grains and bioclasts of oysters, foraminifera, and crinoids floating in a micritic matrix (Fig. 5.3.7A).

10.14.2 *Interpretation*

The marl and silty mudstone reflect low to intermediate energy condition and probably were deposited on the inner shelf in a lagoonal or protected zone (e.g., FÜRSICH et al. 2003). The intercalated partly silty or sandy wackestones and floatstones indicate also a low-energy regime below the fair-weather wave-base (FWWB). The presence of crinoids, echinoderms and corals point to a fully marine environment. The oncoid floatstones/packstones and, silty bio-floatstones probably have been deposited below the fair-weather wave-base under low to moderate water energy. The presence of brachiopods in some carbonates points to a fully

marine environment, and serpulid-encrusted shell fragments indicate low rates of sedimentation. The intraclasts record rip-up phenomena thus pointing to erosion of previous deposits by storms. According to ELF-AQUITAINE (1975), intraclasts may form in back reefs and in intermediate to shallow subtidal settings (SELLY 1994). The cyanobacteria of the intra-cortoid-bio-wacke- to floatstones may have grown in shallow subtidal environments. Cortoid grains form in shallow- and deep-marine as well as in terrestrial and lacustrine environments.

10.14.3 Occurrence

Upper part of the Baghamshah Formation and Kamar-e-Mehdi Formation in the Kamar-e-Mehdi, Doshakh, Echellon, and Ravar areas and Mixed Siliciclastic-Carbonate Member of the Bidou Formation in the Bidou and Mohamadshah areas.

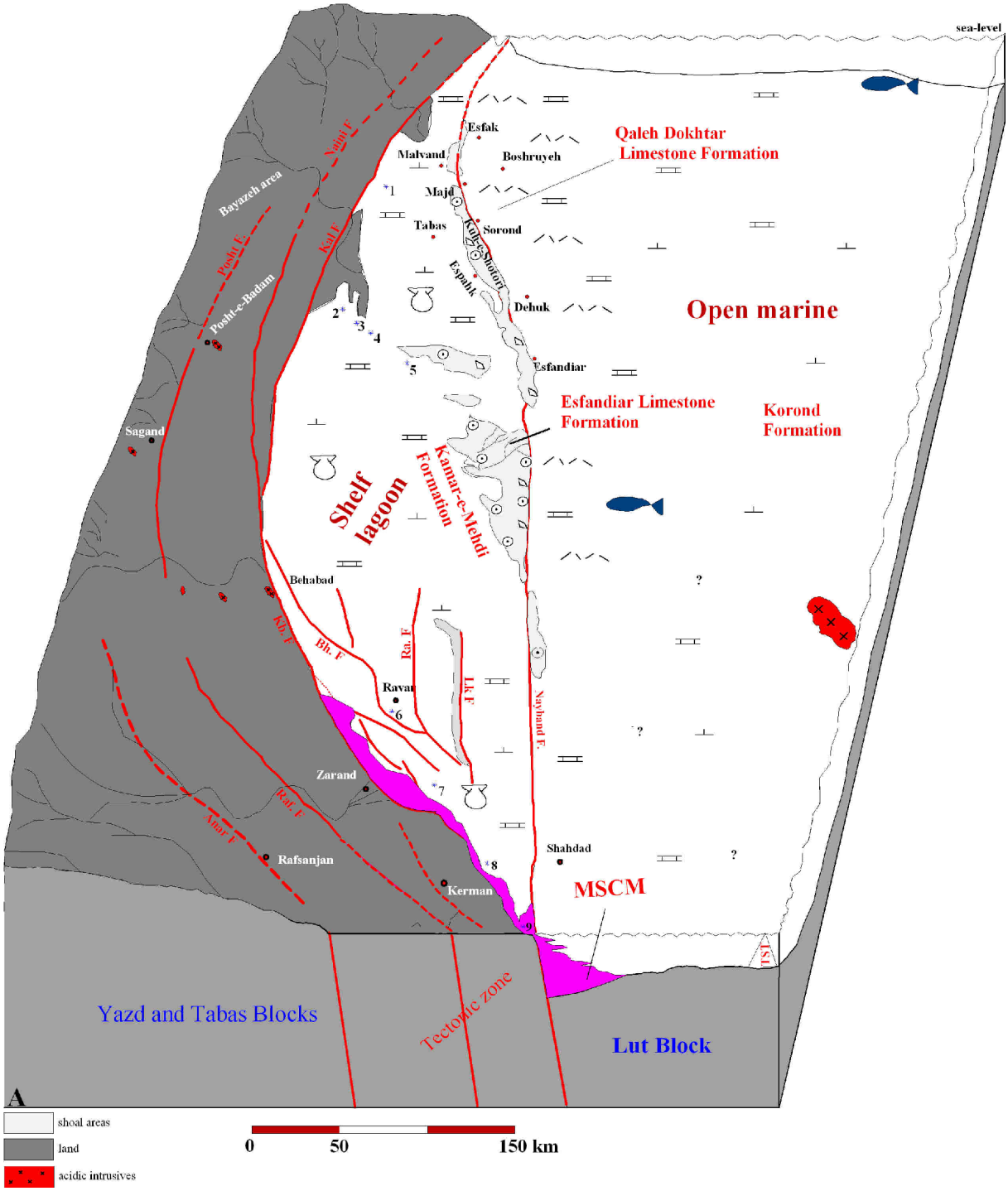

Fig. 10.14. Callovian-Oxfordian palaeogeography of east-central Iran. (A) 1-9 refer to Echellon (1), Doshakh (2), Kamar-e-Mehdi (3), Qoleh Nar (4), Abdoughi (5), Ravar (6), Bidou (7), Mohamadshah (8), and Bolboulieh (9) areas respectively, MSCM: Mixed Siliciclastic Carbonate Member. Major strike-slip or reverse faults of central and eastern Iran. Faults: Kal: Kalmard, Posht: Posht-e-Badam, Raf: Rafsanjan, Kb: Kuh Banan, Bh: Behabad, Ra: Ravar, Lk: Lakar Kuh, Red circle: city. For key of symbols see Fig. 5.8.16.

10.15 Patch reefs

10.15.1 *Characteristic features*

The small oyster *Nanogyra nana* formed small up to 2.5 meter-thick patch reefs in association with corals, sclerosponges (*Neuropora*), and calcisponges intercalated between marly mudstones, mud- to wackestones. Rarely sponges are the dominant reef-builder (for details see Chapter 7).

10.15.2 *Interpretation*

The presence of stenohaline corals indicates euhaline conditions (for detail see Chapter 7).

10.15.3 Occurrence

In the Kamar-e-Mehdi Formation of the Kamar-e-Mehdi, Doshakh, and Echellon areas, and in the Echellon Member SW of Tabas (FÜRSICH et al. 2003; WILMSEN et al. 2009).

10.16 Carbonate platform margin deposits

10.16.1 *Characteristic features*

This facies association is characterized by less than one meter to several decameters thick, packages of limestones with large-scale planar and occasionally trough cross-bedded, ooids are mostly well-sorted, spherical (Figs. 5.3.6C, 5.7.5H) and some ellipsoidal (Figs. 5.7.6H, 5.8.12C), with a small nucleus and thick cortex, and or a thin cortex and large nucleus (Figs. 5.3.5F, 5.3.6A) consisting of smooth and regular laminae formed as successive concentric coatings around the nucleus. Occasionally, the well developed concentric laminae have been partly (Figs. 5.3.6B, 5.8.12E) or completely lost by micritization (Fig. 5.8.12D), probably due to microbial action (ADAMS et al., 1998). The cement surrounding the grains is sparite or microsparite. Occasionally syntaxial echinoderm overgrowth calcite cements occur (Fig. 5.8.12D). The nuclei consist mostly of skeletal or non-skeletal carbonate grains, of silt- or sand-sized detrital grains. These sediments developed on the gently westward inclined hanging wall dip-slope of the shelf lagoon of the Kamar-e-Mehdi Formation and consist of oo-grainstones, bioconglomerates, and shell beds. (see FÜRSICH et al. 2003 for detail).

10.16 2 *Interpretation*

Well-sorted oo-grainstones (Figs. 5.7.5H, 5.7.6A) usually form under a high energy conditions on shoals. According to FLÜGEL (2004), the ooids occur in intertidal and shallow subtidal marine environments of wave-agitated regions of the seas.

According to FÜRSICH et al. (2003), the ooids on the margin of the Esfandiar Platform were piled up to form well-sorted and winnowed grainstone shoals with variable amounts of

bioclasts. Very shallow water is also suggested by the vadose fabric indicating early cementation.

10.16.3 Occurrence

Esfandiar Limestone Formation of the Shotori Mountain and probably the Parvadeh Formation.

11 Source rocks, palaeogeography and tectonic context

On the basis of the composition of sandstones and heavy mineral analysis, pre-existing sedimentary, low to upper rank metamorphic and plutonic rocks of the Kalmard, Posht-e-Badam, Sagand, Bayazeh, and Zarand-Kerman areas (Fig. 11.1.1) west of the study area are very likely the source rocks for the siliciclastic-carbonate rocks of the Middle to Upper Jurassic rocks in the western to southern area of the Tabas Block.

11.1 Source rocks and tectonic context

Pre-existing sedimentary rocks are the main source of the basal conglomerate of the Lower Siliciclastic Member of the Bidou and of the Parvadeh Formation in the Kerman-Ravar area. In the Bolboulieh, Mohamadshah and Bidou areas, this conglomerate is of non-marine origin (see Chapters 9, 10). In contrast, the time-equivalent conglomerate in the Ravar area has been deposited in a very shallow marine setting (Figs. 5.6.2F, 5.6.7C) as is evidenced by fossils in the matrix. The thickness of the conglomerate decreases from several meters in the Kerman-Zarand area to less than one metre in the Ravar area (about 37 km from Kerman-Zarand). This conglomerate is the expression of tectonic activities in the Central-East Iranian Microcontinent, the so-called Mid-Cimmerian Movements (see also FÜRSICH 2009). These tectonic movements were mainly block movements causing uplift of the plutonic-metamorphic rocks of the Posht-e-Badam, Bayazeh, Sagand areas and of the Pre-Cambrian, Ordovician-Triassic rocks of the Kalmard Block (see also AGHANABATI 2004) and subsidence in most parts of the Tabas and Ravar areas. ESE of the Kerman-Zarand area (Bolboulieh, Mohamadshah, Bidou sections), also a local uplift has been created by the Mid-Cimmerian Movements. This is documented by several decameters of channel-fill conglomerates, sandstones, and silt of the Lower Siliciclastic Member of the Bidou Formation, which overlie the shallow marine sediments of the Hojedk Formation. This succession has been deposited in a non-marine setting, while in the Tabas-Ravar area, the coarsening- and shallowing-upward cycles of the Hojedk Formation are followed by a partly shallow marine, partly fluvial conglomerate of the mixed siliciclastic-carbonate Parvadeh Formation.

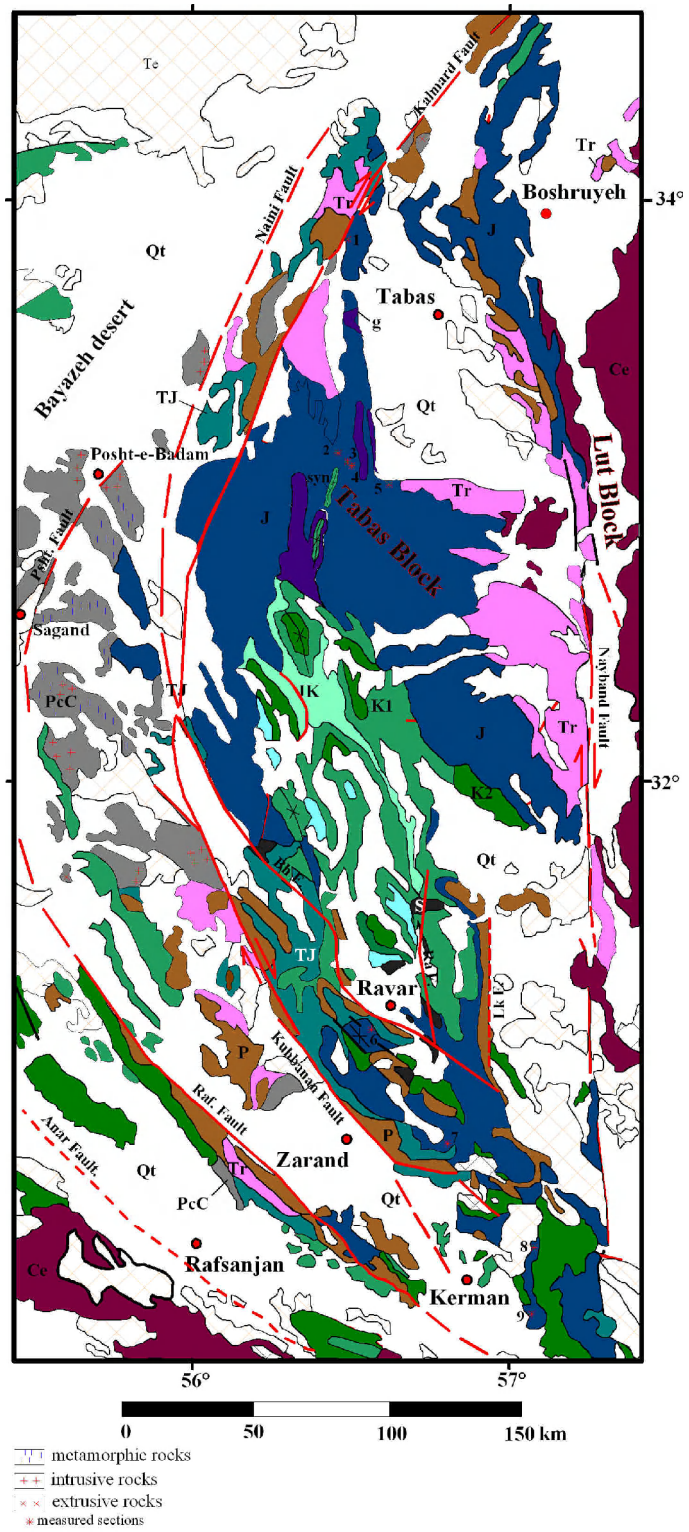

Fig. 11.1.1. Geological sketch map of the Tabas Block and adjacent areas. 1 to 9 refer to the Echellon, Doshakh, Kamar-e-Mehdi, Qoleh Nar, Abdoughi, Ravar, Bidou, Mohamadshah, and Bolboulieh sections, respectively. Qt: Quaternary, Te: Tertiary, Ce: Cenozoic, K1: Lower Cretaceous, K2: Upper Cretaceous, JK: Upper Jurassic-Lower Cretaceous, J: Jurassic, TJ: Upper Triassic-Lower Jurassic, Tr: Triassic, P: Paleozoic, PcC: Precambrian-Cambrian, g: evaporite, S: salt, syn: syncline, Psht: Posht-e-Badam, Raf: Rafsanjan, Ra: Ravar, Bh: Behabad, Lk: Lakar Kuh. Red dots: city.

According to SEYED-EMAMI & ALAVI-NAINI (1990), the facies differentiation and differential subsidence in several sedimentary and structural units such as the Lut, Tabas, and Yazd blocks, took place in connection with the "mid"-Bajocian Mid-Cimmerian tectonic movements. According to FÜRSICH et al. (2003) and WILMSEN et al. (2009), the Bajocian Mid-Cimmerian tectonic movements were followed, in the Bathonian to Callovian, by rapid subsidence (Parvadeh Formation) and the deposition of the thick and uniform silty to sandy shelf sequence of the Baghamshah Formation. Local renewed tectonic activities in the (Early) Callovian (e.g., in the Shotori Mountains) caused uplift, erosion, and progradation at the base of the Callovian-Oxfordian/Kimmeridgian Kamar-e-Mehdi Formation/Esfandiar Limestone Formation, and in Late Oxfordian-Late Kimmeridgian/Tithonian (siliciclastic-evaporiic rocks of the Garedu Group) in the northern and western Tabas Block (see also SEYED-EMAMI et al. 2005). The three major crustal domains, from east to west, the Lut Block, Tabas Block and the Yazd Block (e.g., ALAVI 1991), are separated by a series of intersecting regional-scale faults (Fig. 3.1). The Tabas and Yazd blocks are separated by a nearly 600 kilometer long, arcuate and structurally complex belt composed of variably deformed and fault-bound rocks. This belt is herein named the Kashmar-Kerman Tectonic Zone (Fig. 11.1.2B). In total, within the Central East Iranian Microcontinent three first-order fault systems occur, a north-trending system (Nayband and Nehbandan faults), a northeast directed system (the Poshteh-Badam, Kalmard, and Naini faults), and a northwest directed system (the Kuhbanan, Anar, Rafsanjan, and Behabad faults). The northeast and northwest directed systems dominate the western half of the CEIM which also includes the Kashmar-Kerman Tectonic Zone. A combination of strike-slip (right lateral) and reverse (thrust) movements associated with these faults has generated a complex pattern of regional deformation involving crustal shortening, horizontal block rotation and localized uplift (see also JACKSON & MCKENZIE, 1984). The present-day location of the CEIM is assumed to have been reached by means of a post Triassic 135° counterclockwise rotation (ALAVI et al. 1997). This reconstruction is based on few palaeomagnetic data obtained at localities of the Yazd, Tabas and Lut blocks of east-central Iran (SOFFEL et al. 1996).

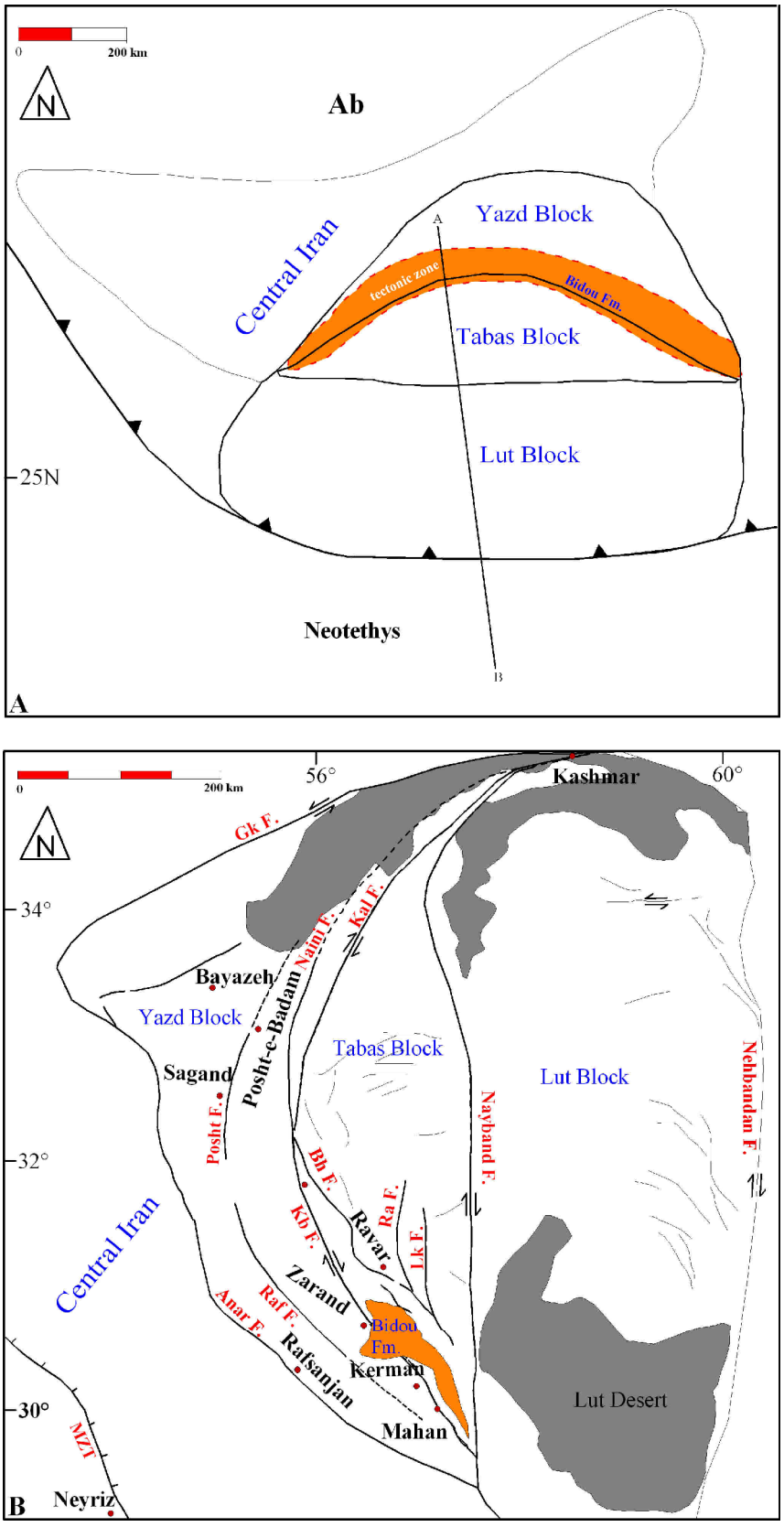

Fig. 11.1.2. (A) The central Iran and Central-East Iranian Microcontinent consists of the Yazd, Tabas, and Lut blocks shown here in a pre-rotational position (modified after WILMSEN et al. 2009). Shown is also the assumed original distribution of the Bidou Formation. Ab: Alborz, Fm: Formation, tectonic zone: composed of Behabad, Kuh Banan, Kalmard, and Naini faults. (B) Major strike-slip or reverse faults of east-central Iran. Faults: GK: Great Kavir, Kal: Kalmard, Posht: Posht-e-Badam, Raf: Rafsanjan, Kb: Kuh Banan, Bh: Behabad, Ra: Ravar, Lk: Lakar Kuh, MZT: Main Zagros thrust, grey colour: desert, Red circle: city.

According to WALKER & JACKSON (2004), structural, geodetic and seismological studies suggest that most of these measured palaeomagnetic rotations are connected to the Neogene tectonic evolution and that block-rotation acted as a main deformation mechanism connected to the strike-slip faults which bounded the crustal blocks. The present-day right lateral strain across eastern Iran has been measured by GPS at ~16 mm/yr (VERNANT et al. 2004a).

The late Cenozoic strain on the eastern Iranian faults appears to be focused on the eastern margin of the Dasht-e Lut, where bedrock offsets of ~70 km occur along the Sistan shear zone (WALKER & JACKSON 2004). If the distribution of cumulative right lateral shear is indicative of the present-day situation, the strike-slip faults to the east of the Dasht-e Lut may accommodate the major part of the relative motion between central Iran and Afghanistan (see TIRRUL et al. (1983) and ALLEN et al. (2006). North of 34°N, the right lateral shear is turned into left lateral faults (Fig. 11.1.2B) which are thought to rotate clockwise about vertical axes (JACKSON & MCKENZIE, 1984; WALKER & JACKSON 2004). It is likely that the transition from N-S right lateral faulting in the south to E-W left lateral faults in the north is influenced by pre-existing structural weaknesses (ALLEN et al. 2006). The change in style of faulting also highlights how slip on strike-slip faults may accommodate crustal shortening in ways that may not have an obviously direct relationship with the overall convergence vector. Both right lateral and left lateral sets of faults in eastern Iran perform the same job in facilitating crustal shortening in Iran by accommodating right lateral shear along the eastern border of the country.

As the siliciclastic-carbonate deposits of the Bidou Formation (Fig. 11.1.2B) occur in the tectonic zone (e.g., between the Behabad, Kuhbanan, and ?Rafsanjan faults) of the eastern Yazd Block (Kashmar-Kerman tectonic zone), and as this formation stratigraphically grades into the Magu Group (Figs. 4.1, 6.8.1), it is very likely that prior to rotation of the blocks (probably Middle Jurassic to Early Cretaceous), rocks equivalent of the Bidou Formation may have occurred along the tectonic zone between the Yazd and Tabas blocks (Figs. 11.1.2A, 11.1.3). However, from the Cretaceous onwards most of the Bidou Formation has been removed by a combination of strike-slip (right lateral) and reverse (thrust) movements of the Kashmar-Kerman tectonic zone which were associated with crustal shortening and counterclockwise block-rotation (see discussion above).

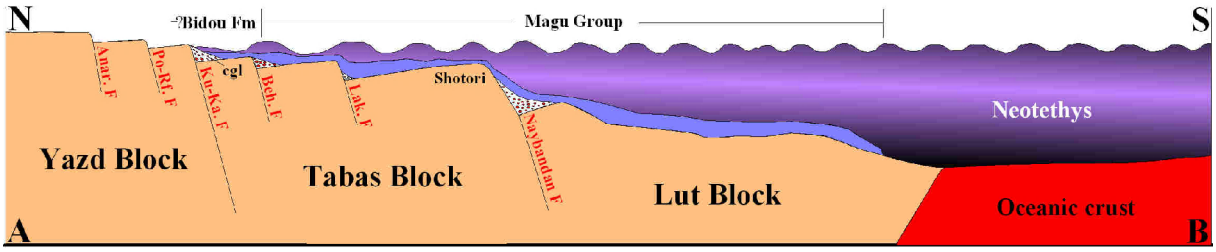

Fig. 11.1.3. N-S cross-section (A, B) through the CEIM with Middle to Upper Jurassic strata in pre-rotation. F: Fault, Fm: Formation, Po-Rf: Posht-e-Badam-Rafsanjan, Ku-Ka: Kuh Banan-Kalmard, Beh: Behabad, Lak: Lakar Kuh, cgl: conglomerate. For position of cross-section see Fig. 11.1.2A.

According to TIRRUL et al. (1983) (Fig. 11.1.4A), the right-lateral nature of the Nehbandan fault system (NHF) in the eastern part of the CEIM has been established on the basis of displaced geologic units as young as Quaternary alluvial fans. Further west, the Nayband fault is also dextral, as demonstrated by the geometry of a Quaternary pull-apart basin midway along its length and other associated structures (KLUYVER et al. 1978). The Kuhbanan fault is interpreted to be right-slip on the basis of its orientation with respect to nearby folds, although it is recognized that probably there has been considerable reverse-slip on this fault. The sense of shear on the Dehshir fault is indicated by the offset of the Baft-Nain "coloured melange" belt (HUBER 1977).

The three western dextral faults are approximately radially arranged about the northeast corner of the Arabian Shield. The Great Kavir fault (Fig. 11.1.2B) displays the opposite sense of displacement (MOHAJER-ASHJAI et al. 1975). These fault patterns are closely analogous to the deformation expected for the indentation of a semi-infinite rigid-plastic body by a rigid wedge according to slip-line theory (TAPPONNIER & MOLNAR 1976, MOLNAR & TAPPONNIER 1977, see Fig. 11.1.4B). The counterclockwise rotation of the system corresponds to the model. The similarity between the fault pattern and slip-line model suggests that the model is applicable in this area and therefore that the dominant mode of Neogene deformation can be approximated by plane strain. According to WALKER & JACKSON (2004), the geomorphology of the Deh Shir, Anar, and Great Kavir strike-slip faults in central Iran suggest that although little shortening is accommodated across this region, they might still be active, and hence capable of producing earthquakes. Based on BERBERIAN (1981), although central and eastern Iran are composed of various tectonic blocks, once separated by minor ocean basins that started to close in the Cretaceous (MCCALL 1996), much of the broader collision zone did not start to deform until the mid-Miocene or even later (DEWEY et al. 1986). In addition, a major reorganization of deformation appears to have occurred in many parts of the Arabia-Eurasia collision zone between 3 and 7 Ma ago (see ALLEN et al. 2004). and one might expect that the

present-day configuration of active faulting in eastern Iran dates from roughly this time (ALLEN et al., 2004). However, considering the model (Fig. 11.1.4B) presented by TAPPONNIER & MOLNAR (1976) and according to TIRRUL et al. (1983), the offset and renewed activity of the old faults such as the Kuhbanan, Kalmard, Posht-e-Badam and other reverse (thrust) or strike slip faults took place after collision of the Iran Plate and Arabian Plate. The counterclockwise block-rotation movements would then have occurred after the Cretaceous. Therefore, during the Middle to Upper Jurassic the Mid-Cimmeridgian movements were mainly block movements producing different sedimentary environments, whereas from the Cretaceous to the Cenozoic, the renewed activity of the faults was mainly destructive, in particular along the Kashmar-Kerman tectonic zone where the Bidou Formation had been deposited. According to FÜRSICH et al. (2009) and WILMSEN et al. (2009a), the Iran Plate was tectonically active throughout the Mesozoic, and this tectonic instability also governed the Jurassic sedimentation pattern. Prominent examples are the Mid- and Late Cimmerian tectonic events in the mid-Bajocian and Late Jurassic-earliest Cretaceous, which are documented by conspicuous inter-regional, in part angular unconformities across the Iran Plate.

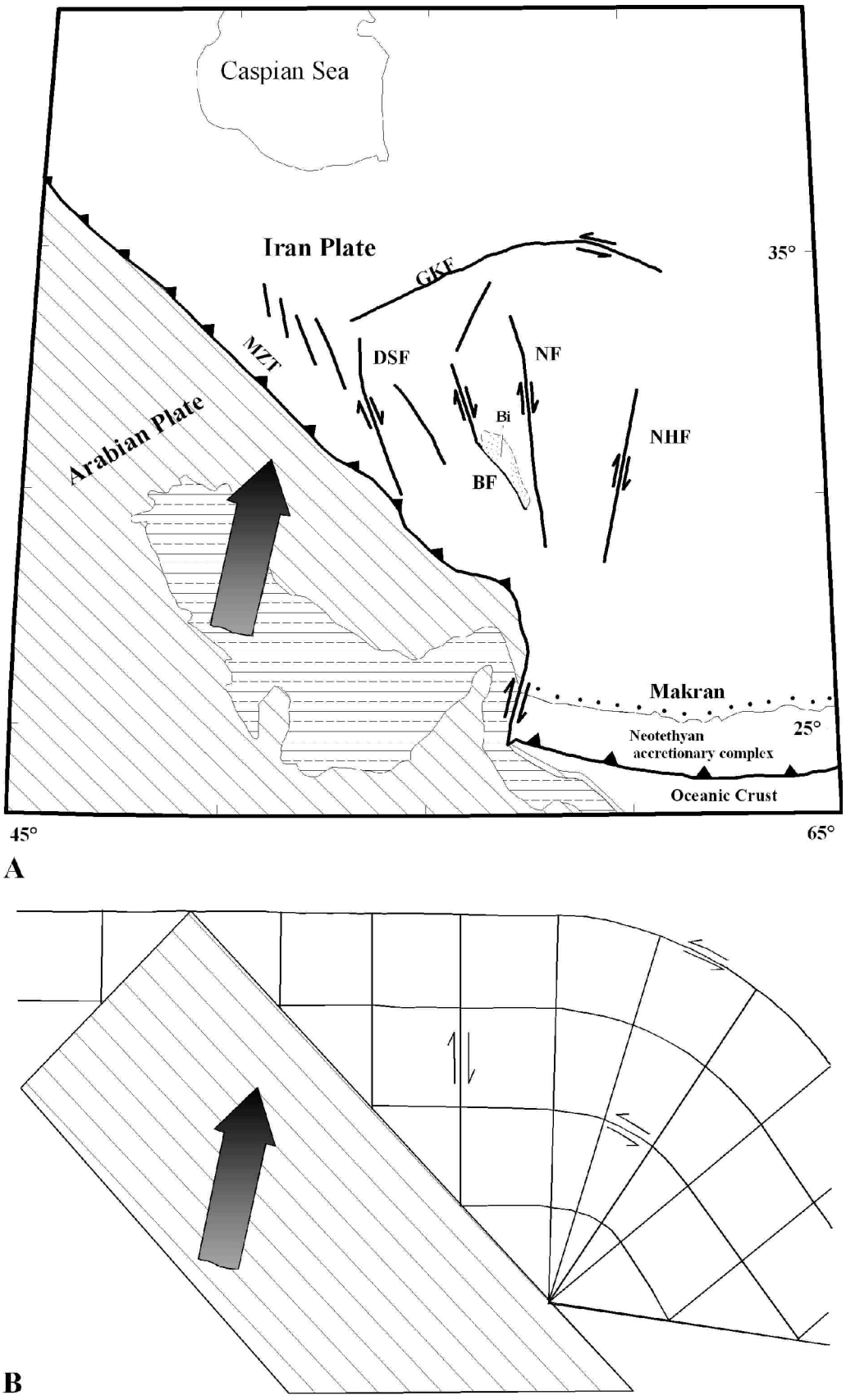

Fig. 11.1.4. A. Major strike-slip faults of central and eastern Iran. BF: Kuh Banan fault, DSF: Deh Shir fault, GKF: Great Kavir fault, MZT: Main Zagros thrust, NF: Nayband fault, NHF: Nehbandan fault system. B. Slip-line field produced by plane indentation of a semi-infinite rigid-plastic media by a triangular die (TAPPONNIER & MOLNAR 1976).

During the Jurassic, the Bidou Formation and the Magu Group (WILMSEN et al. 2009) of the Central-east Iranian Microcontinent (CEIM) run more or less parallel to the main Neotethys suture zone. This position is also documented by the presence of volcanic, intrusive (e.g., Shah-Kuh granite), and metamorphic rocks in the eastern part of the present-day Lut Block of Middle to Late Jurassic age, near the present-day Sistan Suture Zone, and by a magmatic arc (ESMAEILY et al. 2007, WILMSEN et al. 2009a). This part of the Lut Block is also analogous to the suture zone at Neyriz (see also SHAHABPOUR 2005). The Shah-Kuh granite and volcanic and metamorphic rocks were very likely produced by convergence between the Arabian and Iranian plates before rotation of the CEIM. In fact, this condition was responsible for the magmatic activity, metamorphism, and folded sedimentary rocks at the eastern margin of the Lut Block. WILMSEN et al. (2009) placed the CEIM, which consists of three N to S oriented structural units (Fig. 11.1.5), i.e., Yazd, Tabas, and Lut blocks, in the Callovian-Late Jurassic in a pre-rotational position, roughly parallel to the Neotethys subduction zone, with the Lut Block in a back-arc setting close to an inferred volcanic arc.

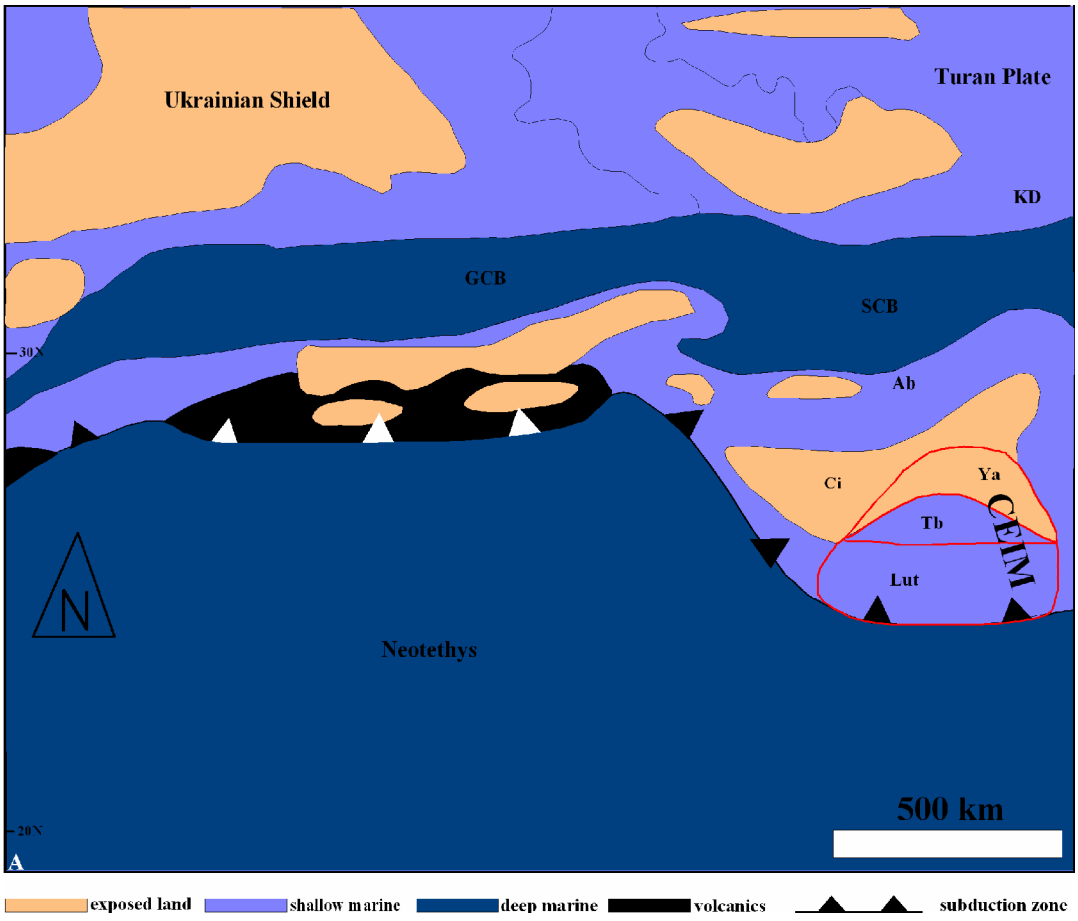

Fig. 11.1.5. Callovian-Late Jurassic palaeogeography of Iran (after WILMSEN et al. 2009). The Lut, Tabas, and Yazd blocks are shown in assumed Jurassic orientation. Ab Alborz, Bi Binalud Mountains, Ci Central Iran, GCB Greater Caucasus Basin, KB Kashafrud Basin, KD Koppeh Dagh, SCB South Caspian Basin.

According to STÖCKLIN et al. (1972), rocks of Jurassic age are most widespread among the pre-Tertiary formations of the Lut Block. Extensive outcrops occur on the northern Lut Block (STÖCKLIN & NABAVI 1971, see also WILMSEN et al. 2003, 2009). In the central Lut Block, Lower Jurassic rocks are conformably overlain by a limestone unit containing a Middle Jurassic fauna. West of Meighan (north of the Shahkuh granite) strongly nodular limestones overlie the shale-sandstone sequence with probably conformable contact. Fossils are rather abundant and include solitary and colonial corals, gastropods, and bivalves. Among the latter, K. SEYED-EMAMI identified *Chlamys (Radulopecten) tipperi*, ?*Ceratomya concentrica*, and *Lima* sp. (=*Plagiostoma*). Very likely, the Middle to Upper Jurassic strata of the Lut Block were mostly deposited in a marine setting (WILMSEN et al. 2003, 2009). STÖCKLIN et al. (1965, 1972), suspected that the rigidity of the Tabas and the Lut blocks was a consequence of consolidation of the pre-Jurassic substratum by strong folding in the Late Triassic revealed, for example, in the Shotori Range by a marked unconformity at the base of the Jurassic. In the southern part of the Lut Block, at Kuh-e-Shisheh and at Kuh-e-Abdullahi, the Middle to Upper Jurassic strata are directly overlain by Upper Cretaceous (Maastrichtian) conglomerate and limestone with a gentle but distinct angular unconformity. At Rakhneh, Aptian Orbitolina limestone overlaps both the Jurassic shales and the Shah Kuh granite. In some places, and particularly towards the eastern border fault (Nehbandan Fault), the Jurassic shale-sandstone complex becomes slightly metamorphic, the shales changing to phyllitic slates and the sandstones to hard quartzites.

Pre-existing sedimentary rocks

The siliciclastic-carbonate rocks of the Middle-Upper Jurassic rocks of the western Tabas Block which were deposited during these tectonic events consist of conglomerates, breccias, arkoses, subarkoses, sublitharenites, litharenites, quartzarenitic calcareous sandstones, and locally pebbly sandstones (Chapter 9, Table 3) and limestones. According to LEWIS & MCCONCHIE (1994) rock fragments, feldspars, and heavy minerals in arenites are very useful for provenance interpretations. The roundness of grains may indicate whether they came directly from the ultimate source (the original igneous or metamorphic rock) or from an immediate source comprising a sedimentary rock that derived its minerals from the ultimate source. According to CASCALHO & FRADIQUE (2007), the hydraulic behaviour of heavy minerals also can help in interpreting their distribution patterns within the dynamic sedimentary regime. Heavy mineral grains with lower mobility tend to remain relatively close to their input sources and these grains exhibit high angularity in river sediments. Therefore, it

is very likely that most of the heavy minerals with high angularity in the Lower Siliciclastic Member were deposited close to their input source and transported by rivers. For instance, the acidic intrusive rocks of the Zarand area (VAHDATI-DANESHMAND 1995), which has been uplifted by the Kuhbanan fault, may be one area producing the heavy minerals such as monazite and hornblende in the fluvial deposits of the Bidou Formation. According to MANGE & MAURER (1992) a heavy mineral assemblage containing only ultrastable minerals is more likely to be found in recycled rather than in first-cycle sediments. In the study area, higher percentages of ultrastable heavy minerals (zircon) only occur in the uppermost part of the Hojedk Formation which probably represents recycled sediments. In the following, some origins are suggested for the siliciclastic-carbonate rocks of the Bidou and Magu Group.

- Components of oligomict conglomerates of the Bidou and Parvadeh formations, and of intraformational monomict conglomerate and breccia of the Magu Gypsum Formation.
- Sandstone fragments (e.g., Fig. 5.8.9E) in the lowermost part of the Lower Siliciclastic Member.
- Rounded, non-undulose quartz minerals of the Baghamshah Formation (e.g., Figs. 5.7.5A, F, 5.6.7B, 5.6.8C). Based on BLATT & CHRISTIE (1963) non-undulatory quartz is uncommon in plutonic rocks, schists, and gneisses, whereas mature sedimentary rocks are characterized by high percentages of non-undulatory quartz.
- Quartz in the form of overgrowths (e.g., at the base of the Kamar-e-Mehdi Formation; Fig. 5.3.3B).
- Altered rounded feldspars e.g., in the middle to upper part of the Bidou Formation (e.g., Fig. 5.8.10G-H).
- Shale in the Lower Siliciclastic Member of the Bidou Formation (e.g., Fig. 5.7.5A) and at the base of the Kamar-e-Mehdi Formation.
- Rounded zircons (e.g., Fig. 9.6.4F), mostly at the top of the Hojedk Formation.
- Extrabasinal carbonate grains, mostly in the Mixed Siliciclastic-Carbonate and Upper Siliciclastic members of the Bidou Formation (e.g., Fig. 5.8.10E) but also at the base of the Kamar-e-Mehdi and Magu Gypsum formations.
- According to LEWIS & MCCONCHIE (1994), hematite and limonite (e.g., Fig. 9.6.3E-F) are common weathering and diagenetic alteration products of iron-bearing minerals. Chert (e.g., Fig. 5.6.7B) is probably a product of diagenetic (or pedogenic) silicification of mud, carbonate, or other material but can also form as a primary precipitate. Chert-rich arenitic frameworks are characteristic in some recycled orogenic suites (DICKINSON & SUCZEK 1979).

Low-grade metamorphic rocks

Slate (e.g., Fig. 5.8.10D), chlorite (e.g., Fig. 9.6.3H), muscovite, and a few biotite grains (e.g., Fig. 9.6.4C, E), mostly in the Lower Siliciclastic Member of the Bidou Formation and some at the base of the Kamar-e-Mehdi Formation.

Acidic plutonic rocks

- Undulose- and polycrystalline quartz grains (crystal boundaries are straight; e.g., Fig. 5.8.9F) mostly in the conglomerate and sandstones at the Lower Siliciclastic Member of the Bidou Formation and at the base of the Kamar-e-Mehdi Formation.
- Apatite (e.g., Fig. 9.6.2E-F).
- Hornblende (e.g., Fig. 9.6.3A-B).
- Zircon (angular) and magnetite (Fig. 9.6.3E), mainly in the Bidou Formation (see also CASCALHO & FRADIQUE 2007). Magnetite can also be produced by diagenetic processes but does not occur under normal weathering conditions. For example, according to MACCONCHIE (1987), diagenetic reactions between siderite and hematite can produce magnetite in banded iron formations.
- Polycrystalline quartz grains. Based on FOLK (1974) and BLATT et al. (1980), polycrystalline quartz grains composed of 3 or more crystals with straight to slightly curved intercrystalline boundaries indicate an origin from plutonic igneous rocks.

Pegmatites

- the heavy minerals monazite, tourmaline, and muscovite occur mainly in different parts of the Bidou Formation.

Intermediate to basic rocks

Enstatite, augite and rutile in sandstones, e.g., in the Lower Siliciclastic Member of the Bidou Formation in the Bolboulieh area, and at the base of the Kamar-e-Mehdi Formation in the Tabas area.

Middle to upper rank metamorphic rocks

- Epidote, magnetite, zircon, and polycrystalline quartz grains in which crystals are elongated in a preferred direction, e.g., uppermost part of the Hojedk Formation.
- Quartzite fragments (Fig. 5.7.5B) and polycrystalline quartz grains, in which sub-grains exhibit sutured boundaries, occur mainly in the lowermost part of the Lower Siliciclastic

Member of the Bidou Formation (see also PETTIJOHN 1975; ADAMS et al. 1984). The polycrystalline quartz grains are composed of elongated crystals and exhibit irregular to crenulated intercrystal boundaries. They indicate an origin from metamorphic source rocks (see also BLATT et al. 1980; ASIEDU et al. 2000).

- Sandstones consisting of monocrystalline quartz grains showing strong undulatory extinction also suggest metamorphic source rocks (BASU 1985).

These different sources are likely to be Pre-Cambrian, Ordovician-Triassic rocks of the Kalmard Block, west of the Kerman-Zarand area, the Yazd Block (see WILMSEN et al. 2009), and the plutonic-metamorphic rocks of the Bayazeh, Sagand areas and the Posht-e-Badam Complex (HAGHIPOUR & PELISSIER 1977). The latter consists of a diverse assemblage of mainly dark-coloured, medium-grade metamorphic rocks that are exposed to the west of the Posht-e-Badam Fault. A variable association of schists, gneisses, amphibolites and marbles comprise the bulk of the Posht-e-Badam Complex, which is severely disrupted by the intrusion of granitoid plutons. Another possible source is the Chapedony Complex that consists of a variety of highest grade metamorphic rocks (gneisses and associated migmatites) in the region. They are viewed as the oldest exposed Precambrian basement in central Iran (HAGHIPOUR 1974, STÖCKLIN 1974).

To evaluate the relative importance of plutonic and metamorphic rocks as quartz sources, polycrystalline quartz, non-undulatory, and undulatory monocrystalline quartz has been plotted in a double-triangular diagram (11.1.6A-B) following the technique of BASU et al. (1975) and TORTOSA et al. (1991). The results differ dramatically ranging from a medium to high rank metamorphic to a granitic source. However, the low-grade metamorphic components in the sandstones of the Bidou Formation and the Magu Group do not show up in the diagram. BLATT & CHRISTIE (1963) have shown empirically that undulatory quartz should be less stable than non-undulatory quartz. Similarly, polycrystalline quartz will break down and produce monocrystalline quartz. Consequently, the longer the effective residence time of a population of quartz in the sedimentary mill, the more the position of that population will move to the left corner of the diagram (Fig. 11.1.6A-B).

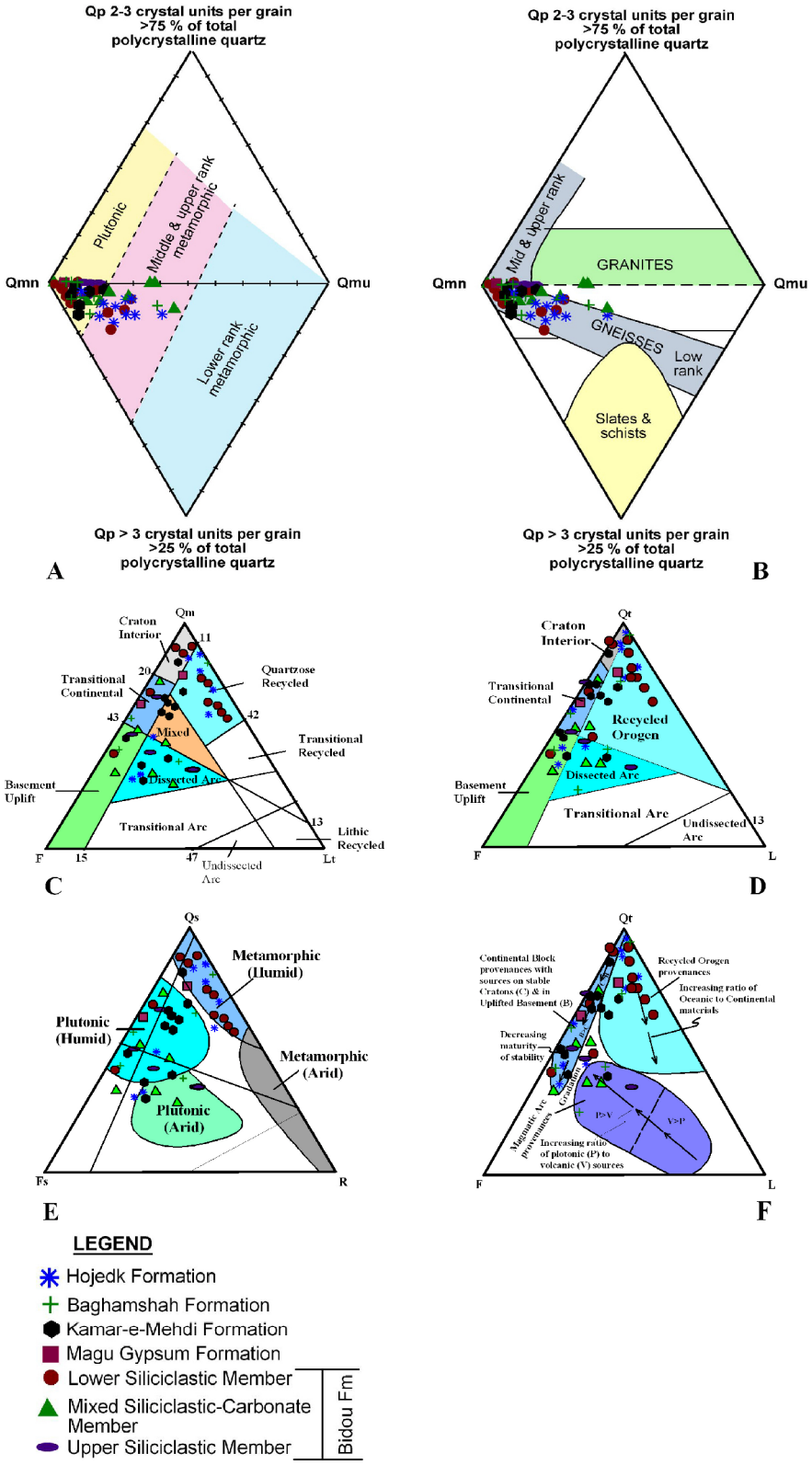

Fig. 11.1.6. (A-B) Varietal quartz diamond plots to discriminate sand from different types of crystalline rocks on the basis of the extinction pattern and polycrystallinity of quartz grains. Qmn: non-undulosity monocrystalline quartz grains; Qmu: high-undulosity monocrystalline quartz grains; Qp2-3: coarse-grained polycrystalline quartz grains; Qp>3: polycrystalline quartz grains with more than 3 sub-grains. Sandstones of the western and southern Tabas Block are compared with provenance fields after BASU et al. (1975) and TORTOSA et al. (1991). (C-D, F) QmFLt (C), QtFL (D, F) ternary diagrams for the studied sandstones of the western and southern Tabas Block (after DICKINSON et al. 1983, 1985). (E) The effect of source rocks on the composition of the studied sandstones using the diagram of SUTTNER et al. (1981).

Accordingly, the monocrystalline and polycrystalline quartz of the Magu Group and the Bidou Formation imply a mixed origin from plutonic and medium- to high-grade metamorphic rocks in the mentioned diagram.

In the Qm-F-Lt and Qt-F-L ternary diagrams (Fig. 11.1.6C-D, F) of DICKINSON et al. (1983), most point counting data from the Lower Siliciclastic Member and the top of the Hojedk Formation plot in the recycled orogen (Quartzose recycled) area of the diagram. The sandstones in this area can be explained by the Mid-Cimmerian Movements, which created a moderate to high relief in a semi-arid to sub-humid climate (Fig. 11.2.3A-B, see also Chapter 9, Table 2). This resulted in the exposure and erosion of the sedimentary cover of the Kalmard Block, WSW of the Zarand-Kerman area, and of low-grade metamorphic rocks and deep-seated igneous and metamorphic rocks of the Posht-e-Badam, Bayazeh, and Sagand areas. Braided and meandering rivers transported the sediments from the source rocks mainly west of the Kalmard and Kuh Banan faults to the site of deposition. This is the origin of the non-marine conglomerate ESE of the Kerman-Zarand area, of the marine and non-marine conglomerate of the Ravar-Tabas area, of the non-marine feldspathic and lithic sandstones in the lowermost part of the Lower Siliciclastic Member, and of floodplain and levee deposits of the upper part of the Lower Siliciclastic Member of the Bidou Formation.

The sandstones (arkoses to subarkoses and calcareous sandstones) at the base of the Kamar-e-Mehdi Formation occur mainly in the mixed area of the diagram of DICKINSON et al. (1983) (Fig. 11.1.6C) between the Quartzose recycled and Transitional continental areas, and some in the Basement uplift area of the diagram. In the Qt-F-L diagram (Fig. 11.1.6D) equivalent rocks, e.g., of the Mixed Siliciclastic-Carbonate Member, mainly occur in the same position. These sandstones can be interpreted by rapid relative sea-level fall in the Kerman-Zarand area, which resulted in the deposition of fluvial sandstones, of silty clay at the base of the Mixed Siliciclastic-Carbonate Member of the Bidou Formation, and of fluvial sediments at the base of the Kamar-e-Mehdi Formation in the Ravar and Abdoughi areas. In the area from Abdoughi to Doshakh and Echellon, marine calcareous sandstones were deposited at the base of the Kamar-e-Mehdi Formation by this process (see also FÜRSICH et al. 2003a). The tectonic setting of the Upper Siliciclastic Member of the Bidou Formation and the Baghamshah Formation is not clear from the diagrams. However, two samples from the Magu Gypsum Formation plotted in the Recycled orogen (Quartzose recycled) and Transitional continental areas of the diagrams of DICKINSON et al. (1983). Recycled orogenic conglomerates or sandstones have not been observed at the base of the Magu Gypsum Formation in the Echellon, Qoleh Nar and Ravar areas, because the rocks of the formation started to form

during a slow sea level fall. However, the tectonic activity locally increased towards the top. The presence of a lenticular monomict conglomerate (see Chapter 9.3) in a very shallow marine or occasionally non-marine setting represents local uplift, not only in the Echellon and Ravar area , but also in the lower part of the Upper Siliciclastic Member of the Bidou Formation in the Bidou area. In total, the boundary between the Kamar-e-Mehdi and Magu Gypsum formations is an erosional surface, and the boundary between the Mixed Siliciclastic-Carbonate Member and the Upper Siliciclastic Member of the Bidou Formation is gradual to sharp. The latter (sharp base) can be seen in the Bidou area where very shallow marine sediments of the Upper Siliciclastic Member overlie the limestones of the Mixed Siliciclastic-Carbonate Member.

Finally, some sandstone samples of the Lower Siliciclastic Member, the Kamar-e-Mehdi Formation, and the Hojedk Formation plotted in the Craton interior of the diagram. As pointed out by DICKINSON et al. (1983), sandstones plotting in the craton field are mature sandstones derived from relatively low-lying granitoid and gneissic sources, supplemented by recycled sands from associated platforms or passive margins.

In the study area, arkoses and subarkoses are the most abundant rock type, whereas sublitharenites, litharenites, calcareous sandstones, quartzarenites and pebbly sandstones are less common in the Middle to Upper Jurassic strata. As argued above, the feldspathic sandstones, especially of the Lower Siliciclastic Member are expression of the Mid-Cimmerian Movements. These sandstones were very likely deposited when the rate of sediment supply was too rapid for chemical destruction of the feldspars, and chemical weathering was restricted. According to LEWIS & MCCONCHIE (1994), recycled feldspathic sandstones are produced when poorly indurated feldspathic sediments are tectonically uplifted either in an arid climatic setting where chemical weathering is inhibited or where transport and deposition are very rapid. These feldspars are typically altered. They state that litharenites are also deposited during times of orogenic activity, and that physical weathering processes are as effective as chemical weathering in destroying rock fragments.

11.2 Palaeogeography

After the Bajocian Mid-Cimmerian tectonic event, the channel-fill and low sinuosity river sediments of the lower part of the Lower Siliciclastic Member were deposited along the present-day Kerman-Kashmar tectonic zone (Fig. 11.1.2B, see also 11.2.1A in pre-rotation position). These siliciclastic sediments laterally decrease in size and thickness from the northern margin (in pre-rotation position) of the Tabas Block towards the Lut Block.

However, with a slowly rising sea level and onset of landward migration of the shoreline, the marine siliciclastic Qaleh Dokhtar Sandstone Formation has been deposited with sharp erosional contact on the Hojedk Formation in the northern Lut Block (e.g., WILMSEN et al. 2003, 2009). With increasing depth of the basin due to a rapid sea level rise, the siliciclastic deposits turned into the mixed siliciclastic-carbonate facies of the Parvadeh Formation. The latter formation overlies the Hojedk Formation on the Tabas Bock (Fig. 11.2.1A). According to WILMSEN et al. (2003, 2009), the sediments of the Qaleh Dokhtar Sandstone Formation have been deposited in a marine setting. They state that this cross-bedded, fine- to medium-grained marine sandstone only occurs at the type locality west of Boshruyeh. In the western part of the present-day Lut Block (southern part of the Lut Block in pre-rotation position, roughly parallel to the Neotethys subduction zone), this formation is mostly covered by younger rocks (mainly Cenozoic volcanics) and is not exposed. The upper part of the Qaleh Dokhtar Sandstone Formation should, therefore, be equivalent to the transgression of the Parvadeh Formation onto the Tabas Block. The presence of calcareous sandstones, well-sorted oo-grainstones with mostly superficial ooids, and also onco-floatstones and rudstones in the Parvadeh Formation indicate high-energy bar, and shallow to deep subtidal settings, respectively (Fig.11.2.1A). The formation records distinct deepening at the top and is overlain conformably by offshore marine siliciclastic sediments of the Baghamshah Formation.

On the Lut Block, the Baghamshah Formation was deposited in open marine, and middle outer shelf to upper slope environments (e.g., turbidite deposits of the Lakar Kuh area). According to KLUYVER et al. (1983), in the Lakar Kuh quadrangle the formation can be subdivided into several informal members: a lower marl member, followed by a distal turbidite member, then a proximal turbidite member, a middle sandstone member and finally an upper red bed member. This subdivision, which holds up for the area west of Lakar Kuh, where a complete section is found, is partly found also east of Chehel Payeh and especially to the north in the Naybandan Quadrangle (KLUYVER et al. 1978). In the Ravar area of the Tabas Block, the Baghamshah Formation consists of offshore to very shallow marine, channel inlet, beach, and bay deposits. In the Abdoughi area, the formation often indicates open marine/offshore to very shallow siliciclastic deposits, but toward the Kamar-e-Mehdi, Doshakh, and Echellon areas of the Tabas Block (Fig. 2.1), carbonates such as onco-floatstone, well-sorted oo-grainstone containing ooids with radial laminae, and bio-wackestone are increasingly intercalated within the siliciclastic deposits towards the top of the formation representing shallow, partly protected subtidal settings. Apparently, the depth of the basin decreased from the Lut Block, where the Baghamshah Formation consists of mainly

open marine and middle outer shelf to upper slope deposits, towards the Tabas Block (Fig. 11.2.1B).

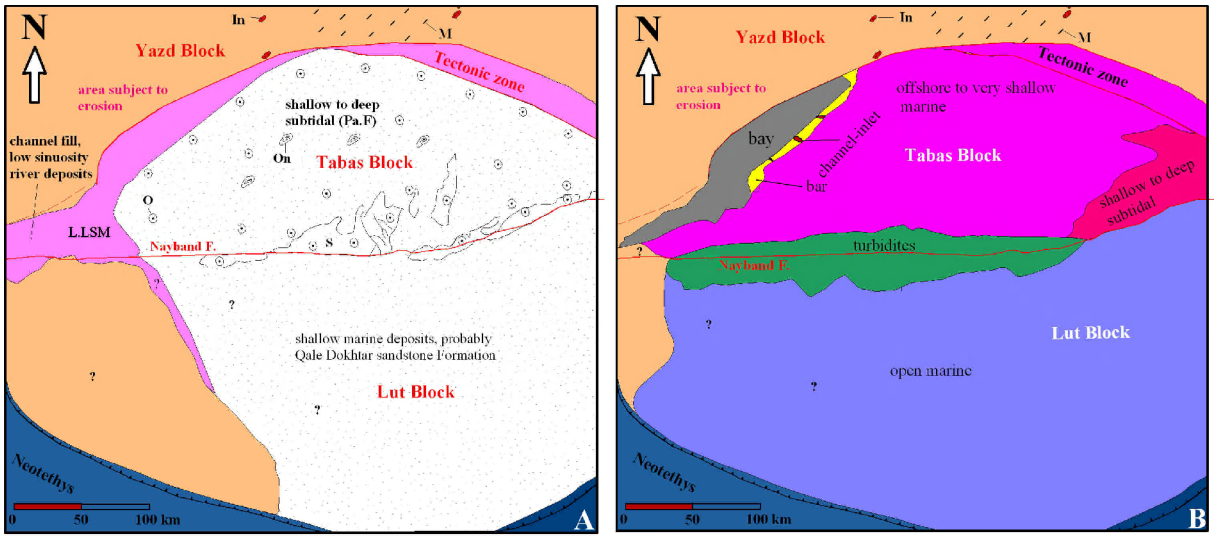

Fig. 11.2.1 (A) Palaeogeographic map of the Late Bajocian-Bathonian siliciclastic-carbonate system of Central East Iranian Microcontinent (CEIM). Note pre-rotation position of the lower part of the Lower Siliciclastic Member (L.LSM) within the tectonic zone, Pa.F: Parvadeh Formation. In: acidic intrusive source, M: metamorphic source, O: ooids, On: oncoids, S: swell. (B) Palaeogeographic map of the Callovian siliciclastic-carbonate system of the CEIM.

The uppermost part of the Baghamshah Formation is overlain by rocks of alluvial plain origin in the Ravar-Abdoughi area, and by muddy intertidal to very shallow, and shallow marine siliciclastic-carbonate deposits of the Kamar-e-Mehdi Formation in the Kamar-e-Mehdi, Doshakh, and Echellon areas. According to FÜRSICH et al. (2003a) on the northeastern part of the present-day Tabas Block, a fluvio-deltaic clastic wedge existed below the Esfandiar Limestone and Qaleh Dokhtar Limestone formations, the so-called Sikhor Formation (Fig. 11.2.2A, pre-rotation position). It overlies, with erosional surface, the Baghamshah Formation at the type locality Sikhor in the southern Shotori Mountains. Fluvial conglomerates of the Kuh-e-Neygu Member deeply cut into the Baghamshah Formation, followed by fluvial fining-upward cycles and flood-plain fines with pedogenic overprint (caliche nodules, calcrete layers). The latter deposits indicate an erosional surface at the top of the Baghamshah Formation around Majd (see Fig. 2.1).

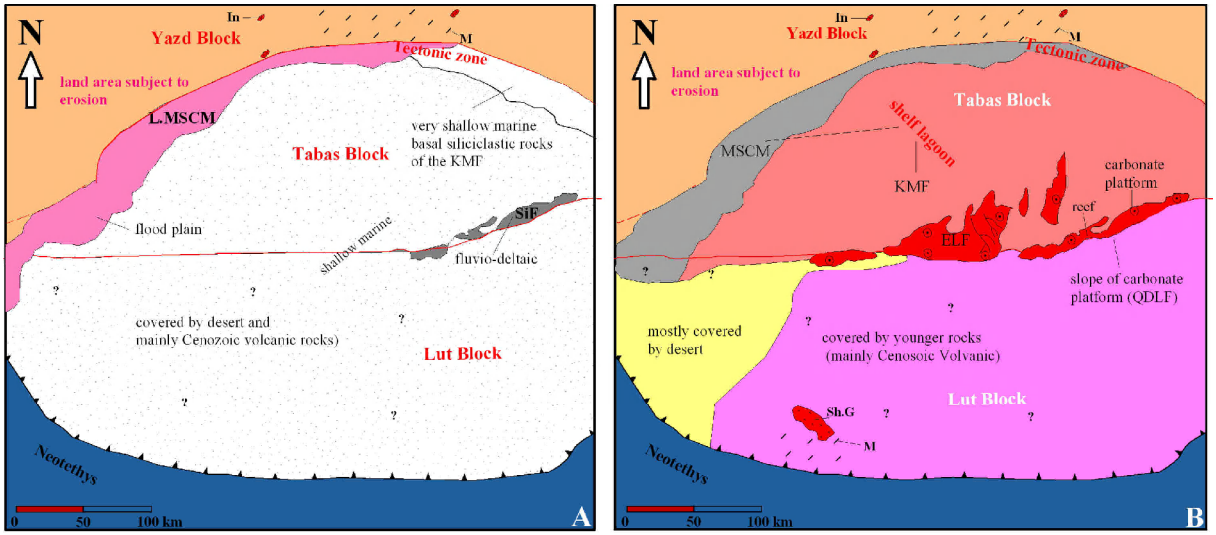

Fig. 11.2.2. (A) Palaeogeographic map of the basal siliciclastic rocks of the Mixed Siliciclastic-Carbonate Member and the Kamar-e-Mehdi Formation of the CEIM. Note pre-rotation position of the lower part of the Mixed Siliciclastic-Carbonate Member (L.MSCM) within the tectonic zone, SiF: Sikhor Formation, KMF: Kamar-e-Mehdi Formation. In: acidic intrusive source, M: metamorphic source. (B) Palaeogeographic map of the Oxfordian to Lower Kimmeridgian carbonates, and siliciclastic-carbonate system of the Kamar-e-Mehdi Formation, and the Mixed Siliciclastic-Carbonate Member. KMF: Kamar-e-Mehdi Formation, ELF: Esfandiar Limestone Formation (carbonate platform), QDLF: Qaleh Dokhtar Limestone Formation (slope of carbonate platform), Sh.G: Shah Kuh granite.

Based on STÖCKLIN et al. (1972), rocks of Jurassic age are most widespread among the pre-Tertiary formations of the Lut Block. Extensive outcrops exist in the northern Lut Block (STÖCKLIN and NABAVI 1971). In the central Lut Block they seem to belong, with few exceptions, to the Lower Jurassic which are conformably overlain by Middle to upper Middle Jurassic to lower Upper Jurassic rocks. At Qolleha-ye-Maaden (3o km from ESE of the Shah Kuh granite), well-bedded limestones with a marble-like appearance contain distinct fragments of corals, echinoids, and crinoids. This limestone has been tentatively assigned to the Upper Jurassic by STÖCKLIN et al. (1972).

The Kamar-e-Mehdi Formation in the Tabas Block can be traced from Kalshaneh in the north (WILMSEN et al. 2009, and see Fig. 2.1) to around Ravar in the south, with a N-S extension of about 360 km and E-W extension of 50 to 100 km. This formation occurs between the present-day Yazd Block in the west and the Esfandiar Limestone Formation characterizing the eastern margin of the northern Tabas Block from Honu in the north to south of the type area at Kuh-e-Esfandiar (FÜRSICH et al. 2003a, 2003b; WILMSEN et al. 2009). The large-scale carbonate system of the Esfandiar Subgroup, consists of a western shallow to deep shelf lagoon (Kamar-e-Mehdi Formation,), carbonate platform (Esfandiar Limestone Formation) with an eastern slope and basinal area (Qaleh Dokhtar Limestone and Korond formations (see Figs. 10.14A, 11.2.2B). These subgroups of the Callovian-Late Jurassic carbonate system

(e.g., WILMSEN et al. 2009) are placed in a pre-rotational position, parallel to the Neotethys subduction zone in Fig. 11.1.5.

According to WILMSEN et al. (2003, 2009), the Esfandiar Limestone Formation occurs in a north-south-trending outcrop belt close to the eastern margin of the Tabas Block (Shotori Swell). The age of the Esfandiar Limestone Formation is Early Callovian-(?Early) Kimmeridgian (STÖCKLIN et al. 1965; FÜRSICH et al. 2003b; BAGI & TASLI 2007). This carbonate platform mainly consists of well-bedded oo-grainstones and rudstones at the margin and carbonate mudstone and peloidal wackestone in the central part of the platform. The carbonate muds of the platform were exported into shelf-lagoon as suspended material, episodically accompanied by skeletal grains and intraclasts in the form of tempestites (e.g., FÜRSICH et al. 2003; WILMSEN et al. 2009), At the junction of the Tabas and Lut blocks, the platform sediments of the Esfandiar Limestone Formation interfinger with slope sediments of the up to 400 m-thick Qaleh Dokhtar Limestone Formation. It consists of bedded, dark-grey and often sharp-based, oolitic-bioclastic limestones, between which thicker packages of marl and marly limestone are intercalated. The formation also contains sponge/microbial patch reefs, channelized limestone conglomerates, and boulder beds with platform-derived biota. The marly intercalations contain abundant ammonites and the trace fossils *Zoophycus*. The age of the Qaleh Dokhtar Limestone Formation is Middle Callovian-Late Oxfordian (SCHAIRER et al. 2000, 2003). FÜRSICH et al. (2003b) presented a detailed microfacies analysis. The Qaleh Dokhtar Limestone Formation represents platform-derived allochthonites (graded allodapic limestones, debris- and mud-flow deposits, olistostromes) and autochthonous sediments such as peri-platform muds settling from suspension.

Reduced input of siliciclastic material led to deposition of low energy carbonate-silt interbeds in the uppermost part of the Baghamshah Formation. Transgressive carbonate or siliciclastic-carbonate deposits of the Esfandiar subgroup such as the Qaleh Dokhtar, Esfandiar, and Kamar-e-Mehdi formations, and the Mixed Siliciclastic-Carbonate Member of the Bidou Formation overlie the Baghamshah Formation and the Lower Siliciclastic Member in the present-day Kerman-Bidou area. Carbonate material was exported from the carbonate platform of the Esfandiar Limestone Formation at the eastern margin of the present-day Tabas Block both towards the east (Qaleh Dokhtar Formation in the Lut Block) and west (Kamar-e-Mehdi Formation, Mixed Siliciclastic-Carbonate Member of the Tabas Block). Probably, the small-scale coarsening-upward carbonate sequences of the Kamar-e-Mehdi Formation were produced by transport of carbonate grains from the platform (shell debris, ooids, intraclasts, and peloids) into the low-energy fine-grained carbonate sediments of the shelf lagoon by

storms. The thin siliciclastic interbeds, which are commonly formed in the Kamar-e-Mehdi Formation are very likely derived from the Yazd Block in the west, which at that time underwent erosion. Based on WILMSEN et al. (2009), the repetitive lithologies (cycles) and uniform depositional environment of the Kamar-e-Mehdi Formation suggest equilibrium conditions between sedimentation and accommodation space for a considerable period of the time (Callovian-Oxfordian). The shelf-lagoonal accumulation rates of the Kamar-e-Mehdi Formation are twice as high as those of the Esfandiar Platform (ca. 80 m/myr; FÜRSICH et al. 2003a). The mean accumulation rates of 150 m/myr and the mean thickness (3 m) of the ubiquitous lagoonal carbonate cycles of the Kamar-e-Mehdi Formation relate these high-frequency cycles to the ~20-kyr precession signal of the Milankovitch orbital frequencies (WILMSEN et al. 2009). The accumulation rate of the Kamar-e-Mehdi Formation also is much higher than in the Mixed Siliciclastic-Carbonate Member at the western margin of the Tabas Block. According to WILMSEN et al. (2009) a significant amount of sediment was also produced within the shelf-lagoon by the macrobenthic communities. With onset of sea level fall, the shallow lagoonal (restricted) fine-grained carbonate, marl, and gypsum deposits of the Nar Limestone Member were deposited. In the Tabas area, this formation is overlain by low-energy inter- and supratidal (sabkha) sediments (Magu Gypsum Formation) related to an arid climate (see Chapter 10). Towards the Bidou-Kerman area, the latter laterally turn into semi-humid to semi-arid flood plain to delta front deposits of the Upper Siliciclastic Member of the Bidou Formation. According to WILMSEN et al. (2009), in the Shotori Mountains at the eastern margin of the Tabas Block, an equivalent formation (Garedu Red Bed Formation) unconformably overlies the Esfandiar Limestone Formation.

In total, most samples from the Middle-Upper Jurassic rocks suggest a high to moderate elevation of the source area, and indicate a semi-arid, arid and Mediterranean to sub-humid climate (see also Fig. 11.2.3A-B and Chapter 9, Table 2). According to WELTJE et al. (1998), the composition of sand-sized detritus supplied to a sedimentary system is determined by the nature of the parent rocks, by the climate and the physiographic conditions in the source area. For the purpose of illustrating the climatic-physiographic controls on sediment composition, a broad tripartite subdivision of climate (C), relief (R), and weathering index (Iw) was considered (Chapter 9, Table 2).

Based on the diagram of SUTTNER et al. (1981) (Fig. 11.1.6E), most samples of the Lower Siliciclastic Members and top part of the Hojedk Formation plot

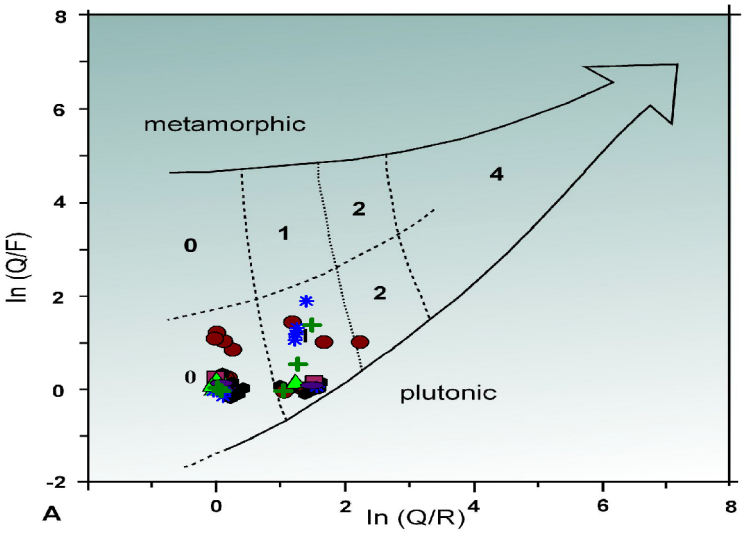

	Climatic-physiography conditions		Physiography (relief) High (mountains) 0	Moderate (hills) 1	Low (plains) 2
Climate (rainfall)	(Semi) Arid and mediterranean	0	0	0	0
	Sub-humid	1	0	1	2
	Humid	2	0	2	4

Fig. 11.2.3. (A) Log-ratio plot after WELTJE et al. (1998). Q: quartz, F: feldspar, R: rock fragments. (B) Fields 1-4 refer to the semi-quantitative weathering indices defined on the basis of relief and climate as indicated in the Table. For symbols see Fig. 11.1.1.

in the metamorphic (humid) field, the others mostly plot in the plutonic (humid) area. Climate is an important initial determinant of the composition of the first-cycle sand (SUTTNER et al. 1981). The diagram (Fig. 11.1.6E) is defined for first-cycle sediments but the effect of recycling and long distance transport can shift the data on the diagram towards humid conditions. This particular diagram can discriminate only sources of metamorphic and plutonic rocks (humid or arid climates) and does not discriminate between different tectonic settings. However, west of the Kerman to Tabas area (e.g., Kalmard, Posht-e-Badam, Bayazeh, and Sagand areas), the pre-existing rocks, composed of sedimentary, plutonic, and metamorphic rocks of first-cycle condition, produced the components of the sedimentary conglomerate and sandstones at the base of the Bidou Formation. This result is also supported

by the heavy mineral composition and higher angularity in the Lower Siliciclastic Member, because a heavy mineral assemblage consisting of only ultrastable minerals such as zircon, rutile and tourmaline is more likely in recycled sediments such as the uppermost part of the Hojedk Formation, rather than in first-cycle sediments e.g., the Lower Siliciclastic Member. According to SUTTNER et al. (1981), a single sedimentary cycle begins with derivation of detritus from a lithified parent rock and ends with lithification of the derived detritus. Sediment in temporary residence on a bar or on a floodplain, even if it lasts for thousands of years but is not buried and lithified is not considered to have passed through a second cycle.

Conclusions

(1) In the Bolboulieh and Ravar areas, the uppermost part of the Hojedk Formation corresponds to very shallow marine high-energy environments partly representing lower shoreface conditions.

(2) The basal conglomerate of the Parvadeh and Lower Siliciclastic Member of the Bidou Formation, which is related to Bajocian Mid-Cimmerian tectonic movements is a key bed. Lithostratigraphically, the Lower Siliciclastic, Mixed Siliciclastic-Carbonate, and Upper Siliciclastic members of the Bidou Formation are equivalents of the Parvadeh, Baghamshah, Kamar-e-Mehdi, and Magu Gypsum formations of the Magu Group.

(3) The Lower Siliciclastic Member consists of fluvial channel-fill, overbank/flood plain, and associated deposits. In the upper part of the member, siliciclastic deposits were mainly deposited in bay environments, and the intercalated carbonate rocks have been produced by storm-induced currents in a shallow marine setting.

(4) The lower part of the Mixed Siliciclastic-Carbonate Member was deposited in interchannel areas such as overbank/flood plain environments, and the middle to upper part of the member mostly in a deep subtidal/lagoonal to peritidal setting. In the latter also some storm beds occur.

(5) The Upper Siliciclastic Member indicates deltaic, and peritidal environments.

(6) In the Ravar area, the lower part of the Parvadeh Formation is of shallow marine origin. Towards the top gradual deepening occurred similarly to the situation on the northern Tabas Block.

(7) The sediments of the Baghamshah Formation have been deposited in a range of environments such as bays, beach, channel inlet, swells, lower shoreface to offshore, open shelf and deeper marine settings (east of the Lakar Kuh fault).

(8) In the Ravar and Abdoughi areas, the basal siliciclastic rocks of the Kamar-e-Mehdi Formation are of non-marine origin, probably representing fluvial or river-dominated delta deposits. In contrast, from the Kamar-e-Mehdi to the Echellon area, the siliciclastic rocks have been deposited in a marine setting. Most of the fine-grained carbonate rocks such as mudstones, wackestones, floatstone and marls, have been deposited in a deep, low energy shelf lagoon. Laminated bindstones, mudstones with gypsum needles, silty dolomitic mudstones, and gypsum beds indicate a restricted, low energy peritidal setting under semi-arid to arid climatic conditions and frequent hypersalinity. The grainstones, packstones and rudstones are probably the product of storm events, and indicate sediment export off the Esfandiar Platform situated in the east (WILMSEN et al. 2009).

(9) The Nar Limestone Member represents a peritidal setting, probably a restricted quiet water lagoonal environment.

(10) The Magu Gypsum Formation has been deposited in low energy, intertidal to supratidal (sabkha), and low-energy restricted shallow lagoonal environments, in which occasionally intercalations of storm beds occurred.

(11) The Magu Gypsum Formation of the Ravar area is assigned a Late Kimmeridgian to Late Berriasian age based on the dasycladacean green alga ?*Clypeina jurassica*. In the Qoleh Nar area, the Magu Gypsum Formation is followed with unconformable contact by Lower Cretaceous sediments. The latter are Late Hauterivian to Barremian in age based on the presence of the foraminifers *Torremiroella* sp. and *Vercorsella* sp. Therefore, the age of the Magu Gypsum Formation is considered to range from the Late Kimmeridgian to the Late Berriasian-?Valanginian.

(12) The boundary between the Hojedk Formation and the Lower Siliciclastic Member of the Bidou Formation in the Bolboulieh and Mohamadshah area, and the Parvadeh Formation in the Ravar area, is an unconformity. The contacts between the Lower Siliciclastic, Mixed Siliciclastic-Carbonate, and Upper Siliciclastic members of the Bidou Formation are conformable and mostly gradual to sharp. The boundary between the Parvadeh and the Baghamshah formations is conformable and sharp. In the Ravar and Abdoughi areas, the Kamar-e-Mehdi Formation overlies the Baghamshah Formation with unconformable contact. Towards Kamar-e-Mehdi, Doshakh and probably Echellon, an erosional surface occurs between the two formations. Finally, the boundary between the Magu Gypsum Formation and the Kamar-e-Mehdi Formation (Nar Limestone Member) is an erosional surface.

(13) Thirty-nine macroinvertebrate taxa, belonging to 26 bivalve, four gastropod, one ammonite, one brachiopod, one echinoid, two sponge, two coral, and two serpulid taxa have been identified and figured from Middle to Upper Jurassic rocks of the Bidou Formation and the Magu Group. The macrofauna has been used to determine the palaeoenvironment of the studied sections. For instance, the presence of stenohaline groups such as ammonites and brachiopods of the Baghamshah Formation indicate a fully marine environment. In the Kamar-e-Mehdi Formation, low sedimentation rates can be inferred from the predominance of abundant epifaunal cemented oysters such as *Nanogyra nana* and *Actinostreon gregareum* and encrusters such as the serpulids *Serpula* (*Cycloserpula*) and *Serpula* (*Dorsoserpula*).

(14) Ten ichnotaxa, belonging to ten ichnogenera, have been taxonomically described and figured from the Middle to Upper Jurassic rocks of the Bidou Formation and the Magu Group.

(15) In the study area, arkoses and subarkoses are the most abundant rock type, whereas sublitharenites, litharenites, calcareous sandstones, quartzarenites, and pebbly sandstones are less common in the Middle to Upper Jurassic strata. The feldspathic sandstones of the Lower Siliciclastic Member have been deposited as result of the Mid-Cimmerian Movements. These sandstones were very likely deposited very rapidly restricting the time for chemical destruction of the feldspars.

(16) Carbonate grains in the Kamar-e-Mehdi and Magu Gypsum formations are usually intrabasinal and are composed of peloids, ooids, cortoids, intraclasts, and bioclasts.

(17) In the Bolboulieh, Mohamadshah, and Bidou sections the size of the siliciclastic grains in the Bidou Formation varies from medium- to very coarse-grained in the lower, and from very fine to fine-grained in the upper part of fining-upward cycles. Texturally, the sandstones are mostly immature, poorly sorted, and the grains are mainly angular. In the Upper Siliciclastic Member of the Bidou area also mature, well sorted, subangular to subrounded calcareous sandstones occur, which contain intrabasinal carbonate grains such as intraclasts, superficial, concentric or radial ooids, echinoid spines, and algal fragments (?dasycladaceans).

(18) Apart from their major constituents, the sandstones of the Hojedk and Bidou formations contain a suite of opaque and transparent heavy minerals consisting of zircon, tourmaline, rutile, monazite, apatite, hornblende, antophyllite, enstatite, biotite, epidote, siderite, chlorite, hematite, magnetite, limonite, and pyrite in different percentages.

(19) Most of heavy minerals with higher angularity occur in the Lower Siliciclastic Member of the Bidou Formation and were probably deposited close to their source area.

(20) In the study area, higher percentages of ultrastable heavy minerals (zircon) only occur in the uppermost part of the Hojedk Formation and probably represent recycled sediments.

(21) According to the diagrams of BASU et al. (1975) and TORTOSA et al. (1991), the monocrystalline and polycrystalline quartz grains of the Magu Group and the Bidou Formation imply a mixed origin from plutonic and medium- to high-grade metamorphic rocks. Based on the diagram of SUTTNER et al. (1981), most samples of the Lower Siliciclastic Member and of the top part of the Hojedk Formation plot in the metamorphic (humid) field, the others mostly plot in the plutonic (humid) area.

(22) According to the diagram of WELTJE et al. (1998), most samples from the Middle-Upper Jurassic rocks suggest a moderate to high elevation of the source area, and indicate a semi-arid and mediterranean to sub-humid climate.

(23) In the Qt-F-L ternary diagrams of DICKINSON et al. (1983), most point counting data from the Lower Siliciclastic Member and the top of the Hojedk Formation plot in the recycled orogen (Quartzose recycled) area of the diagram. The sandstones in this area can be interpreted as being derived from the Mid-Cimmerian Movements

(24) The composition of sandstones and heavy mineral analysis point to pre-existing sedimentary, low, middle to upper rank metamorphic, and plutonic rocks of the Kalmard, Posht-e-Badam, Bayazeh, and Zarand-Kerman areas as the source rocks for siliciclastic-carbonate rocks of the Middle to Upper Jurassic rocks in the western to southern area of the Tabas Block.

(25) Quite likely, before rotation of the blocks (probably during the Middle Jurassic to Lower Cretaceous), equivalent rocks of the Bidou Formation occurred along the tectonic zone between the Yazd and the Tabas blocks. However, from the Cretaceous onwards, most of the Bidou Formation has been removed by a combination of strike-slip (right lateral) and reverse (thrust) movements of the Kashmar-Kerman tectonic zone, which were associated with crustal shortening and counterclockwise block-rotation.

(26) The offset and renewed activity of old faults such as the Kuhbanan, Kalmard, Posht-e-Badam and other reverse (thrust) or strike slip faults are related to post-collision movements between the Iran Plate and the Arabian Plate. Roughly, these counterclockwise block-rotation movements occurred after the Cretaceous. During the Middle to Upper Jurassic, the tectonic activities were vertical movements producing the sedimentary pattern in the CEIM. In contrast, from the Cretaceous to the Cenozoic, the movements of faults were mainly destructive, in particular along the Kashmar-Kerman tectonic zone where the Bidou Formation occurred.

13 Acknowledgments

I wish to express my deep gratitude to Prof. F. T. FÜRSICH, FG Paläoumwelt of the Geozentrum Nordbayern, Erlangen-Nürnberg University, for his supervision, fruitful discussions, scientific and linguistic corrections, critical review, and constructive comments on the manuscript. I am very grateful to him for his kindness and hospitality and for providing many facilities during the progress of my thesis. I also appreciate the kindness of his wife toward my family during our stay in Germany.

I would like to extend my thanks to Prof. Dr. M. WILMSEN for useful discussions and comments on the manuscript. Many thanks to Dr. B. NIEBUHR (SARAH) for her help during my stay in Würzburg. Also, special thanks go to Dr. MICHAEL HEINZE, Geozentrum Nordbayern, Erlangen-Nürnberg University, for his help, kindness, and hospitality during the progress of my thesis.

I would like to thank Dr. F. HOLZFÖRSTER then Würzburg University, for his help to identify the heavy minerals in the laboratory in Würzburg. I am very grateful to him because he taught me about the separation of heavy minerals of my specimens.

Many thanks to H. SCHÖNIG, Würzburg University, who carried out the photographic work. Special thanks also to Miss VAKIL, the Geological Survey of Iran, and Karbalaee-Hasan who kindly prepared my thin-sections.

I would like to express my deep gratitude to all the staff members and colleagues of the FG Paläoumwelt, Erlangen University, for their valuable help.

Financial support of part of my stay in Germany by CDC organization is gratefully acknowledged.

I also wish to acknowledge the Head of Geological Survey of Iran (Eng. KOREHEE), Assistants Dr. GHASEMI, Dr. J. TAHERI and Dr. MAJIDIFARD, Head of the Stratigraphic Group in the Geological Survey of Iran, for their help to complete my thesis in Germany.

Last, my deepest gratitude and respect go to my wife, for her love, support, encouragement and understanding throughout this toil. Many thanks go to my parents and my family for all their kindness.

Thanks again to all of them.

Masoud Zamani Pedram

14 References

ADAMS, A. E., MACKENZIE, W. S. & GUILFORD, C. 1984. Atlas of sedimentary rocks under the microscope. - 104 pp., Harlow (Longman).

ADAMS, A. E. & MACKENZIE, W. S. 1998. A colour atlas of carbonate sediments and rocks under the microscope. - 180 pp., London (Manson).

AGHANABATI, A. 1977. Etude géologique de la région de Kalmard (W. Tabas). - Geological Survey of Iran, Report No. 35: 230 pp.

AGHANABATI, A. 1998. Jurassic stratigraphy of Iran. - Vls. 1-2: 746 pp., Tehran (Geological Survey of Iran) (in Farsi).

AGHANABATI, A. 2004. Geology of Iran. - 257 pp., Tehran (Geological Survey of Iran) (In Farsi).

AGHANABATI, A. & REZAEE, A. 2009. Correlation of lithostratigraphic units of Iran in major structural and sedimentary basins. - National Geoscience Database of Iran **6:** 1-6.

AIGNER, T. 1985. Storm Depositional Systems. - 174 pp. Berlin, Heidelberg, New York (Springer).

ALAVI, M. 1991. Sedimentary and structural characteristics of the Paleo-Tethys remnants in northeastern Iran. – Geological Society of America Bulletin **103**: 983-992.

ALAVI, M., VAZIRI, H., SEYED-EMAMI, K. & LASEMI, Y. 1997. The Triassic and associated rocks of the Nakhlak and Aghdarband areas in central and northern Iran as remnants of the southern Turan active continental margin. - Geological Society of America Bulletin **109**: 1563-1575.

ALLEN J.R.L. 1984. Sedimentary structures - their character and physical basis, Developments in Sedimentology, 30: 1256pp., Elsevier, Amsterdam.

ALLEN, M., JACKSON, J. & WALKER, R. 2004. Late Cenozoic reorganization of the Arabia-Eurasia collision and the comparison of short-term and long-term deformation rates. - Tectonics **23**: 16 pp., TC2008, doi:10.1029/2003TC001530.

ALLEN, M.B., WALKER, R., JACKSON, J., TALEBIAN, M. & GHASSEMI, M.R. 2006. Contrasting styles of convergence in the Arabia-Eurasia collision: Why escape tectonics does not occur in Iran. - Geological Society of America Special Paper **409**: 579-589.

ALONSO-AZCÁRATEA, J., ALFREDO, A., BARRENECHEAB, J., LÓPEZ-GÓMEZC, F., LUQUEB, K., & RODAS, M. 1997. Palaeogeographical significance of clay mineral assemblages in the Permian and Triassic sediments of the SE Iberian Ranges, eastern Spain. - Palaeogeography, Palaeoclimatology, Palaeoecology **136**: 309- 330.

AMIREH, B.S. 1997. Sedimentology and palaeogeography of the regressive-transgressive Kurnub Group (Early Cretaceous) of Jordan. – Sedimentary Geology **112:** 69–88.

ARRIBAS, J. & TORTOSA, A. 2003. Detrital modes in sedimenticlastic sands from low-order streams in the Iberian Range, Spain: The potential for sand generation by different sedimentary rocks. - Sedimentary Geology **159**: 275-303.

ASIEDU, D.K., SUZUI, S. & SHIBATA, T. 2000. Provenance of sandstones from the Lower Cretaceous Sasayama Group, inner zone of southwest Japan. - Sedimentary Geology **131**: 9–24.

AZHDARI, A. 2004. Geological map and report of Robat-e-Khan, on scale of 1:100000. – Tehran (Geological Survey of Iran).

BASU, A., YOUNG, S.W., SUTTNER, L.J., JAMES, W.C. & MACK, G.H. 1975. Reevaluation of the use of undulatory extinction and polycrystallinity in detrital quartz for provenance interpretation. – Journal of Sedimentary Petrology **45**: 873-882.

BASU, A., 1985. Reading provenance from detrital quartz. - In: ZUFFA, G.G. (ed.), Provenance of Arenites: 231–249, Dordrecht (Reidel).

BAGI, H. & TASLI, K. 2007. Paleoenvironmental analysis and biostratigraphy of the Upper Jurassic Esfandiar Formation (East-Central Iran). Neues Jahrbuch für Geologie und Paläontologie, **243**: 101-111.

BAGHERI, S. 2008. Anticlockwise rotation of the Central-East Iranian Microcontinent and the Eurasian-Indian collision. – 33ed International Geological Congress Oslo 2008, Abstract.

BERBERIAN, M. 1981. Towards a paleogeography and tectonic evaluation of Iran. - Canadian Journal of Earth Sciences **18**: 210-265.

BENTON, M. J. & HARPER, D.A.T. 1997. Basic Palaeontology. – 342 pp., Harlow (Addison Wesley Longman).

BLATT, H. & CHRISTIE, J.M. 1963. Undulatory extinction in quartz of igneous and metamorphic rocks and its significance in provenance studies of sedimentary rocks. - Journal of Sedimentary Petrology **33**: 559–579.

BLATT, H., MIDDLETON, F. & MURRAY, R. 1980. Origin of sedimentary rocks (second edition). – 782 pp., Englewood Cliffs, New Jersey (Prentice-Hall).

BOSWELL, P.G.H. 1933. On the mineralogy of sedimentary rocks. – 393 pp., London (Murby & Co.).

BOUCOT, A.J., BRACE, W. & DEMAR, R. 1958. Distribution of brachiopod and pelecypod shells by currents. – Journal of Sedimetary Petrology **28**: 321-332.

BROMLEY, R.G. 1996. Trace fossils: Biology, Taphonomy and Applications (2ed edition). – 361 pp., London (Unwin Hyman).

BROENNIMANN, P., ZANINETTI, L., BOZORGNIA, F., DASHTI, G.R. & MOSHTAGHIAN, A. 1971. Lithostratigraphy and foraminifera of the Triassic Naiband Formation, Iran. - Revue de Micropaléontologie **14**: 7-16.

BURCHETTE, T.P. & WRIGHT, V.P. 1992. Carbonate ramp depositional systems. - Sedimentary Geology **79:** 3–57.

CAVAZZA, W., ZUFFA, G.G., CAMPORESI, C. & FERRETTI, C. 1993. Sedimentary recycling in a temperate climate drainage basin (Senio River, north-central Italy): composition of source rock, soil profiles, and fluvial deposits. - In: JOHNSSON, M.J. & BASU, A. (eds.), Processes Controlling the Composition of Clastic Sediments. - Geological Society of America Special Paper **284:** 247–261.

CASCALHO, J. & FRADIQUE, C. 2007. The source and hydraulic sorting of heavy minerals on the northern Portuguese continental margin. – Developments in Sedimentology **58**: 75-110.

COE, A.L. & CHURCH, K.D. 2003. Sequence stratigraphy and sea-level change. – In: COE, A. L., BOSENCE, D.W.J., CHURCH, K.D., FLINT, S.S., HOWELL, J.A. & WILSON, R.C.L.

(eds.), The sedimentary record of sea-level change. - 288 pp., Cambridge (Cambridge University Press).

COMPTON, R.R. 1962. Manual of field geology. – 108 pp., New York (Wiley).

COLLINSON, J.D., 1996. Alluvial sediments. In: READING, H.G. (ed.), Sedimentary environments: process, facies and stratigraphy, - 37-82, Oxford (Blackwell Science).

COLEMAN, M. & GAGLIANOS, M. 1965. Sedimentary structures: Mississippi River deltaic plain. - In: MIDDLETON, G.V (ed.), Primary Sedimentary Structures and their Hydrodynamic Interpretation. - Society Economic Paleontologists and Mineralogists, Special Publication **12**: 113-148.

CRIMES, T. P., GOLDRING, R., HOMEWOOD, P., STUIJVENBERG, J. V. & WINKLER, W. 1981.Trace fossil assemblages of deep-sea fan deposites, Gurnigel and Schlieren flysch (Cretaceous-Eocene), Switzerland. - Eclogae Geologicae Helvetiae 74: 953-995.

DEVISMES, P. 1978. Photographic atlas of detrital minerals. - Mémoires du Bureau de recherches géologiques et minières **95**: 1-203.

DEWEY, J.F., HEMPTON, M.R., KIDD, W.S.F., SAROGLU, F. & ENGOR, A.M.C.S. 1986. Shortening of continental lithosphere: The neotectonics of eastern Anatolia, a young collision zone. - Geological Society, Special Publications **19**: 3–36.

DICKINSON, W.R. & SUCZEK, C. 1979. Plate tectonics and sandstone compositions. – Bulletin of the American Association of Petroleum Geologists **63**: 2164-2182.

DICKINSON, W.R., BEARD, L.S., BRAKENRIDGE, G.R., ERJAVEC, J.L., FERGUSON, R.C., INMAN, K.F., KNEPP, R.A., LINDBERG, F.A. & RYBERG, P.T. 1983. Provenance of North American Phanerozoic sandstones in relation to tectonic setting. - Geological Society of America Bulletin **94**: 222-235.

DICKINSON, W.R. 1985. Interpreting provenance relations from detrital modes of sandstones. - In: Zuffa, G.G. (ed.), Provenance of arenites: 333-362, Dordrecht (Reidel Co).

DOUGLAS, J.A. 1929. A marine Triassic fauna from eastern Persia. - Quarterly Journal of the Geological Society, London **85**: 624-650.

DUNHAM, R.J. 1962. Classification of carbonate rocks according to depositional texture. - In: HAM, W.E. (ed.), Classification of carbonate rocks. - American Association of Petroleum Geologists, Memoir **1**: 108–121.

DUKE, W.L., ARNOTT, R.W.C., & CHEEL, R.J. 1991. Shelf sandstones and hummocky cross stratification: New insights on stormy debate. - Geology **19**: 625-628.

DZULYNSKI, S., WALTON, E.K. 1965. Sedimentary features of flysch and greywackes. Developments in sedimentology, Amsterdam, Elsevier **7**: 1-274

EFTEKHAR-NEZHAD, J., HUSHMAND-ZADEH, A., NABAVI, M.H., STÖCKLIN, J., TATEVOSSIAN, SH. & ZAHEDI, M. 1971. Explanatory text of the Boshruyeh Quadrangle Map 1: 250000. - Geological Survey of Iran **J7**: 1-50.

EINSELE, G. 1992. Sedimentary Basins: Evolutions, Facies, and Sediment Budget. - 628 pp. Berlin (Springer).

ELF-AQUITAINE 1975. Essai de caractérisation sédimentologique des dépôts carbonatés Eléments d'analyse. - 173 pp., Pau (Centre de Recherche de Boussens et Pau).

EMBRY, A.F. & KLOVAN, J.E. 1972. Absolute water depth limits of Late Devonian paleoecological zones. - Geologische Rundschau **61**: 672-686.

EMERY, D. & MYERS, K.J. 1996. Historical perspective in sequence stratigraphy. – 297 pp., Oxford (Blackwell Sciences).

ESMAEILY, D., BOUCHEZ, J.L. & SIQUEIRA, R. 2007. Magnetic fabrics and microstructures of the Jurassic Shah-Kuh granite pluton (Lut Block, Eastern Iran) and geodynamic inference. - Tectonophysics **439**:149–170.

FARROW, G.E. 1966. Bathymetric zonation of Jurassic trace fossils from the coast of Yorkshire, England. - Palaeogeography, Palaeoclimatology, Palaeoecology **2**:103-151.

FARRELL, K.M. 1987. Sedimentology and facies architecture of overbank deposits of the Mississippi River, False River Region, Louisiana. – In: ETHRIDGE, F.G., FLORES, R.M & HARVEY, M.D. (eds), Recent developments in fluvial geology. – SEPM Special Publications **39**: 111-120, Tulsa.

FILLION, D. & PICKERILL, R.K. 1990. Ichnology of the Upper Cambrian? to Lower Ordovician Bell Island and Waban groups of eastern Newfoundland, Canada. – Palaeontographica Canadiana **7**: 1–119.

FIELDING, C.R. 1984. Upper delta plain lacustrine and fluviolacustrine facies from the Westphalian of the Durham coalfield, NE England. - Sedimentology **31**: 547–567.

FLÜGEL, E. 2004. Microfacies of Carbonate Rocks. Analysis, Interpretation and Application. – 976 pp., Berlin, Heidelberg, New York (Springer).

FOLK, R.L. 1951. Stages of textural maturity in sedimentary rocks. – Journal of Sedimentary Petrology **21**: 127-130.

FOLK, R.L. 1959. Practical petrographic classification of limestones. - Bulletin of the American Association of Petroleum Geologists **43**: 1-38.

FOLK, R.L. 1974. Petrology of sedimentary rocks, second edition. – 182 pp., Austin, Texas (Hemphill Press).

FREY, R.W 1975. The study of trace fossils: A synthesis of principles, problems, and procedures in ichnology. – 562 pp. Berlin, Heidelberg, New York (Springer).

FREY R.W., CURRAN, A.H. & PEMBERTON, G.S. 1984. Tracemaking activities of crabs and their environmental significance: the ichnogenus *Psilonichnus*. – Journal of Paleontology **58**: 511-528.

FÜRSICH, F.T. 1973a. A revision of the trace fossils *Spongeliomorpha*, *Ophiomorpha* and *Thalassinoides*. - Neues Jahrbuch für Geologie und Paläontologie, Monatshefte 1973: 136-156.

FÜRSICH, F.T. 1973b. *Thalassinoides* and the origin of nodular limestone in the Corallian Beds (Upper Jurassic) of Southern England. - Neues Jahrbuch für Geologie und Paläontologie, Monatshefte 1973: 136-156.

FÜRSICH, F.T. 1974a. Ichnogenus *Rhizocorallium.* - Paläontologische Zeitschrift **48**: 16–28.

FÜRSICH, F.T. 1974b. On *Diplocraterion* TORELL 1870 and the significance of morphological features in vertical, spreiten-bearing, U-shaped trace fossils. - Journal of Paleontology **48**: 952–954.

FÜRSICH, F.T. 1975. Trace fossils as environmental indicators in the Corallian of England and Normandy. – Lethaia **8**: 151-172.

FÜRSICH, F.T. 1982. Rhythmic bedding and shell bed formation in the Upper Jurassic of East Greenland. - In EINSELE, G., & SEILACHER, A. (eds.), Cyclic and Event Stratification: 209-222, Berlin (Springer).

FÜRSICH, F. T. 1998. Environmental distribution of trace fossils in the Jurassic of Kachchh (western India). - Facies **39**: 243-272.

FÜRSICH, F.T. & HEINBERG, C. 1983. Sedimentology, biostratigraphy, and palaeoecology of an Upper Jurassic offshore sand bar complex. - Bulletin of the Geological Society of Denmark **32**: 67-95.

FÜRSICH, F.T. & MAYR, H. 1981: Non-marine *Rhizocorallium* (trace fossil) from the Upper Freshwater Molasse (Upper Miocene) of southern Germany. - Neues Jahrbuch für Geologie und Paläontologie, Monatshefte **1981**: 321–333.

FÜRSICH, F.T. & WERNER, W. 1986. Benthic associations and their environmental significance in the Lusitanian Basin (Upper Jurassic, Portugal). - Neues Jahrbuch für Geologie und Paläontologie, Abhandlungen **172**: 136-156.

FÜRSICH, F.T. & WERNER, W. 1991. PALAEOECOLOGY OF CORALLINE SPONGE-CORAL MEADOWS FROM THE UPPER JURASSIC OF PORTUGAL. - PALÄONTOLOGISCHE. ZEITSCHRIFT **65**: 35-69.

FÜRSICH, F.T., WILMSEN, M., SEYED-EMAMI, K., SCHAIRER, G. & MAJIDIFARD, M.R. 2003a. Platform-basin transect of a Middle to Late Jurassic large-scale carbonate platform system (Shotori Mountains, Tabas area, east-central Iran). - Facies **48**: 171-198.

FÜRSICH F.T., WILMSEN M., SEYED-EMAMI, K., MAJIDIFARD, M.R. 2003b. Evidence of synsedimentary tectonics in the northern Tabas Block, east-central Iran: the Callovian (Middle Jurassic) Sikhor Formation. - Facies **48**:151–170.

FÜRSICH, F.T., OSCHMANN, W., PANDEY, D.K., JAITLY, A.K., SINGH, I.B. & LIU, C. 2004. Palaeoecology of middle to lower Upper Jurassic macrofauna of the Kachchh Basin, western India. - Journal of the Palaeontological Society of India **49**: 1-26.

FÜRSICH, F.T., WILMSEN, M., SEYED-EMAMI, K. & MAJIDIFARD, M.R. 2005. The Upper Shemshak Formation (Toarcian-Aalenian) of the eastern Alborz (Iran): Biota and palaeoenvironments during a transgressive-regressive cycle. - Facies **51**: 365-384.

FÜRSICH, F.T., WILMSEN, M., SEYED-EMAMI, K. & MAJIDIFARD, M.R. 2009. The Mid-Cimmerian tectonic event (Bajocian) in the Alborz Mountains, Northern Iran: evidence of the break-up unconformity of the South Caspian Basin. – In: BRUNET, M. F., WILMSEN, M. & GRANATH, J. W. (eds.), South Caspian to Central Iran basins. - Geological Society London, Special Publications **312**: 189-203.

GERDES, G., DUNAJTSCHIK-PIEWAK, R., RIEGE, H., TAHER, A.G., KRUMBEIN, W.E. & REINECK, H.E. 1994. Structural diversity of biogenic carbonate particles in microbial mats. - Sedimentology **41**: 1273–1284.

HAGHIPOUR, A., MS. 1974. Etude géologique de la région de Biabanak-Bafq (Iran Central); pétrologie et tectonique du socle Precambrien et de sa couverture. – 403 pp., These, Universite Scientifique et Medicale de Grenoble.

HAGHIPOUR, A. & PELISSIER, G. 1977. Geology of the Saghand Sector. - In: HAGHIPOUR, A., VALEH, N., PELISSIER, G., & DAVOUDZADEH, M. (eds.), Explanatory Text of the Ardekan Quadrangle Map. - H8: 10-68, Geological Survey of Iran (Tehran).

HAJ MOLA ALI, A. 1995. Geological map and report of Ravar - on scale of 1:100000, Geological Survey of Iran (Tehran).

HEINBERG, C. 1973. The internal structure of the trace fossils *Gyrochorte* and *Curvolithus*. - Lethaia **6**: 227-238.

HOLZAPFEL, S. 1998. Palökologie benthischer Faunengemeinschaften und Taxonomie der Bivalven im Jura von Südtunesien. - Beringeria **22**: 1-199.

HOTTINGER, L. 1971. Larger foraminifera of the Mediterranean Jurassic and their stratigraphic use. - Annales Institute of Geology of Hungary (Budapest) **54**: 497-504.

HUBER, H. 1977. Geological map of Iran, sheets no. 1-6, 1:1000,000 scale, with explanatory notes: Tehran (National Oil Company of Iran, Exploration and Production Affairs).

HUBER, H. & STÖCKLIN, J. 1954. Hodjedk Coal Geology: Iran Oil Corporation. - Geological Survey of Iran, Report **4:** 1–133.

HUCKRIEDE, R., KÜRSTEN, M. & VENZLAFF, H. 1962. Zur Geologie des Gebietes zwischen Kerman und Saghand (Iran). - Geologisches Jahrbuch **51**: 1-197.

HÄNTZSCHEL, W. 1962. Trace fossils and Problematica. - In MOORE, R. & TEICHERT, C. (eds.), Treatise on Invertebrate Paleonotology: 245 pp. Boulder (Geological Society of America) & Lawrence (University of Kansas Press).

HÄNTZSCHEL, W. 1975. Trace fossils and Problematica. - In: TEICHERT, C. (ed.), Treatise of Invertebrate Paleontology (2ed edition), part W, Miscellanea: 269 pp., Boulder (Geological Society of America), and Lawrence (University of Kansas Press).

HEER, O. 1876-1877. Flora fossilis Helvetiae. Die vorweltliche Flora der Schweiz. – 182 pp., Zürich (J. Wüster & Co.).

HUNTER, R.E. & CLIFTON, H.E.V. 1982. Cyclic deposits and hummocky cross-stratification of probable storm origin in Upper Cretaceous rocks of the Cape Sebastian area, southwestern Oregon. – Journal of Sedimentary Petrology **52**: 127–144.

INGERSOLL, R.V., BULLARD, T.F., FORD, R.L., GRIMM, J.P., PICKLE, J.D. & SARES, S.W. 1984. The effect of grain size on detrital modes: a test of the Gazzi-Dickinson point-counting method. - Journal of Sedimentary Petrology **54**: 103-116.

JACKSON, J. & MCKENZIE, D. 1984. Active tectonics of the Alpine-Himalayan Belt between western Turkey and Pakistan. - Geophysical Journal of the Royal Astronomical Society **77**: 185–264.

KALANTARI, A. 1969. Foraminifera from the Middle Jurassic-Cretaceous successions of Koppet-Dagh region N.E. Iran. - National Iranian Oil Company Geological Laboratories, Publication **3**: 1-298.

KARIMI-BAVANDPUR, A. 2002. Geological map and report of Tabas, on scale of 1:100000. - Geological Survey of Iran (Tehran).

KAZMIERCZAK, J., COLEMAN, M.L., GRUSZCZYNSKI, M. & KEMPE, S. 1996. Cyanobacterial key to the genesis of micritic and peloidal limestones in ancient seas. - Acta Palaeontologica Polonica **41**: 319–338.

KELLING, G. & MULLIN, P.R. 1975. Graded limestones and limestone-quartzite couplets: Possible storm deposits from the Moroccan Carboniferous. - Sedimentary Geology **13**: 161–190.

KHOSRO-TEHRANI, KH. 2007: Microfacies. – 496 pp., Tehran (University of Tehran).

KLUYVER, H.M., TIRRUL, R., CHANCE, P.N., JOHNS, G.W. & MEIXNER, H.M. 1978. Explanatory text of the Naybandan Quadrangle Map. - Geological Survey of Iran **J8**: 1-143.

KLUYVER, H. M., TIRRUL, L., CHANCE, P.N., JOHNS G.W. & MEIXNER, H.M. 1983. Explanatory text of the Naybandan Quadrangle Map. 1:250000. - Geological Survey of Iran (Geological of Quadrangle) **J8**: 1-143.

LEWIS, DOUGLAS, W. & MCCONCHIE, D. 1994. Analytical Sedimentology. – 197 pp., New York (Chapman & Hall).

LEITHHOLD, E.L. & BOURGEOIS, J. 1984. Characteristics of coarse-grained sequences deposited in nearshore, wave-dominated environments - examples from the Miocene of southwest Oregon. - Sedimentology **31**: 749–775.

LOEBLICH, A.R., & TAPPEN, JR.H. 1988. Foraminiferal genera and their classification (2 vls.). – 868 pp., New York (Van Nostrand Reinhold Company).

MACEACHERN, J.A., BANN, K.L., PEMBERTON, S.G. & GINGRAS, M.K. 2007. The ichnofacies paradigm: High-resolution paleoenvironmental interpretation. SEPM Short Course Note **52**: 308 pp.

MANGE, M.A. & MAURER, F.W. 1992. Heavy minerals in colour. – 147 pp., London (Chapman).

MCKEE, E.D. 1966. Significance of climbing-ripple structure. - US Geological Survey Professional Paper **550**D: D94-103.

MCCALL, G.J.H. 1996. The inner Mesozoic to Eocene ocean of south and central Iran and associated microcontinents. - Geotectonics 29: 490 – 499.

MCCONCHIE, D.M., WARD, J.B., MCCANN, J.H. & LEWIS, D.W. 1979. A Mössbauer investigation of glauconite and its geological significance. - Clays & Clay Minerals **27:** 339-348.

MCCONCHIE, D.M. 1987. The geology and geochemistry of the Joffre and Whaleback Shale members of the Brockman Iron Formation, western Australia. - In: APPEL, P. & LABERGE, G. (eds.), Precambrian iron formations: 541-601, Athens (Theophrastus Publications).

MIALL, A. D. 1985. Architectural-element analysis: a new method of facies analysis applied to fluvial deposits. - Earth Science Review **22**: 261-308.

MOHAJER-ASHJAI, A., BEHZADI, H. & BERBERIAN, M. 1975. Reflections on the rigidity of the Lut Block and recent crustal deformation in eastern Iran. - Tectonophysics **25**: 281-301.

MOLNAR, P. & TAPPONNIER, P. 1977. Relation of the tectonics of eastern China to the India-Eurasia collision: Application of slip-line field theory to large-scale continental tectonics. - Geology **5**: 212-216.

MURRAY, J.W. 1991. Ecology and palaeoecology of benthic foraminifera. - 397 pp., Harlow (Longman Scientific and Technical).

NABAVI, M.H. & TATEVOSSIAN, SH. 1966. Geology of the Seh Qaleh area (south-Ferdows, East Iran). - Geological Survey of Iran **30**: 1-33.

PETTIJOHN, F.J., 1975. Sedimentary rocks, 3d ed..- 628 pp., New York (Harper & Row).

PETTIJOHN, F.J., POTTER, P.E., & Siever, R. 1972. Sand and Sandstone. – 618 pp., New York (Springer).

PETTIJOHN, F.J., POTTER, P.E. & SIEVER, R. 1987. Sand and sandstone. – 553 pp., New York (Springer).

PEMBERTON, S.G. & FREY, R.W. 1982. Trace fossil nomenclature and the *Planolites-Palaeophycus* dilemma. - Journal of Paleontology **56**: 843-881.

PICKERILL, R.K. & HURST, J.M. 1983. Sedimentary facies, depositional environments and faunal associations of the Lower Llandovery (Silurian) Beech Hill Cove Formation, Arisaig, Nova Scotia. - Canadian Journal of Earth Sciences **20**:1761–1779.

POLYANSKY, B.V. 1984. Genesis and correlation of Triassic–Jurassic coal–bearing formations of the Caucasus–Pamirs Zone of the Alpine–Himalayan Belt.- Comptes Rendus, Congres International de Stratigraphie et de Geologie du Carbonifere **9**: 385-388.

POTTER, P.E. & PETTIJOHN, F.J. 1977. Paleocurrents and basin analysis. – 420 pp., Berlin (Springer).

REINECK, H.E. & SINGH, I.B. 1973. Depositional sedimentary environments. – 439 pp., Heidelberg (Springer).

REINECK, H.E. & SINGH, I.B. 1980. Lower shoreface to inner shelf environments. - In: Reineck, H.E. & Singh, I.B. (eds.), Depositional sedimentary environments, 2ud ed., Berlin (Springer).

RUTTNER, A., NABAVI, M.H. & HAJIAN, J. 1968. Geology of the Shirgesht area (Tabas area, East Iran). - Geological Survey of Iran, Report **4**: 1-133.

SAHANDI, M.R. 1991. Geological map and report of Robat-e-Khan, on scale of 1:250000. with explanatory text. - Tehran (Geological Survey of Iran).

SAIDI, A., BRUNET, M.F. & RICOU, L.E. 1997. Continental accretion of the Iran Block to Eurasia as seen from Late Paleozoic to Early Cretaceous subsidence curve. - Geodinamica Acta **10**: 189-208.

SAYFOURI, S. 2007. Analysis of Middle Jurassic strata in Ravar-Kerman area. - 191 pp., Tehran (Research Institute For Earth Sciences, Geological Survey of Iran).

SCHAIRER, G., FÜRSICH, T., WILMSEM, M., SEYED-EMAMI, K.A., MAJIDIFARD, M.R. 2003. Stratigraphy and ammonite fauna of Upper Jurassic basinal sediments at the eastern margin of the Tabas Block (East-Central Iran). - Geobios **36**: 195-222.

SCHAIRER, G., SEYED-EMAMI, K., FÜRSICH, T., SENOWBARI-DARYAN, B., AGHANABATI, A. & MAJIDIFARD, M.R. 2000. Stratigraphy, facies analysis and ammonite fauna of the Qal eh Dokhtar Formation (Middle-Upper Jurassic) at the type locality west of Boshrouyeh (east central Iran). - Neues Jahrbuch für Geologie und Paläontologie, Abhandlungen **216:** 35-66.

SCHLIRF, M. 2003. The palaeoecologic significance of Late Jurassic trace fossils from the Boulonnais, N France. – Acta Geologica Polonica **53**: 123-142.

SDZUY, K. & MONNINGR, W. 1985. Neue Modelle des Jakobstabes.- Neues Jahrbuch für Geologie und Paläontologie, Monatshefte 1985, 300-320.

Seilacher, A. 1967. Bathymetry of trace Fossils. - Marine Geology, **5**:413-428.

Selley, R.C., 1996. Ancient Sedimentary Environments and Their Subsurface Diagnosis. - 4th edition, Chapmann Hall, London, pp. 300, Seltzer, G.O., Baker, P., Cross.

SENGÖR, A.M.C. 1990. A new model for the late Palaeozoic-Mesozoic tectonic evolution of Iran and its implications for Oman. - In: ROBERTSON, A.H.F., SEARLE, M.P. & RIES, A.C. (eds.), The geology and tectonics of the Oman region. - Geological Society of London, Special Publication **49**: 797-831.

SENGÖR, A.M.C., ALTINER, D., CIN, A., USTAÖMER, T. & HSÜ, K.J. 1988. Origin and assembly of the Tethysides orogenic collage at the expense of Gondwana Land. - Geological Society of London, Special Publication **37**: 119-181.

SEPTFONTAINE, M. 1981. Les foraminifères imperforés des milieux de plate-forme au Mésozoïque: détermination pratique, interprétation phylogénétique et utilisation biostratigraphique. - Revue de Micropaléontologie **23**: 169-206.

SEYED-EMAMI, K. 1971a. A summary of the Triassic in Iran. - Geological Survey of Iran, Report **20**: 41-53.

SEYED-EMAMI, K. 1971b. A new species of *Distichites* (Ammonoidea) from the Upper Triassic Nayband Formation of the Zefreh area (Central Iran). - Neues Jahrbuch für Geologie und Paläontologie, Monatshefte 1971: 734-744.

SEYED-EMAMI, K. & ALAVI-NAINI, M. 1990. Bajocian stage in Iran. - Memorie decriptive della carta geologica d'Italia **40**: 215-221.

SEYED-EMAMI, K., 1999. New informations on the evaporitic Ravar formation and the stratigraphic position of the Middle and Upper Jurassic strata in the Kerman-Ravar area (Central Iran). – Faculty of Engineering University of Tehran **33**: 81-95.

SEYED-EMAMI, K., SCHAIRER, G. & AGHANABATI, S.A. 1997. Ammoniten aus der Baghamshah Formation (Callov, Mittlerer Jura) NW Tabas (Zentraliran). - Mitteilungen der Bayerischen Staatssammlung für Paläontologie und. historische Geologie **37**: 27-40.

SEYED-EMAMI, K. & FÜRSICH, F.T. & SCHAIRER, G. 2001. Lithostratigraphy, ammonite faunas and palaeoenvironments of Middle Jurassic strata in north and Central Iran. - Newsletters on Stratigraphy **38**: 163-184.

SEYED-EMAMI, K., SCHAIRER, G. & AGHANABATI, S.A. 1998. BULLATIMORPHITES aus dem Oberbathon (Mittlerer Jura) SW Tabas (Zentraliran). - Mitteilungen der Bayerischen Staatssammlung für Paläontologie und historische Geologie **38**: 121-134

SEYED-EMAMI, K., SCHAIRER, G., FÜRSICH, F.T., WILMSEN, M. & MAJIDIFARD, M.R. 2002. Reineckeiidae (Ammonoidea) from the Callovian (Middle Jurassic) of the Shotori Range (East-central Iran). - Neues Jahrbuch für Geologie und Paläontologie, Monatshefte 2002: 184-192.

SEYED-EMAMI, K., FÜRSICH, F.T., WILMSEN, M., SCHAIRER, G., & MAJIDIFARD, M.R. 2004. Jurassic (Toarcian to Bajocian) ammonites from the Lut Block, east-central Iran. - Acta Geologica Polonica **54**: 77-94.

SEYED-EMAMI, K., FÜRSICH, F.T. & WILMSEN, M. 2005. New evidence on the lithostratigraphy of the Jurassic System in the northern Tabas Block, East-Central Iran). - Earth Science **57**: 78-97.

SHAIKHOLESLAMI, M.R. 1999. Geological map and report of Halvan, on scale of 1:100000, Tehran (Geological Survey of Iran).

SHAHABPOUR, J. 2005. Tectonic evolution of the orogenic belt in the region located between Kerman and Neyriz. - Journal of Asian Earth Sciences **24**: 405–417.

SOFFEL, H. & FÖRSTER, H. 1984. Polar wander path of the Central East Iran microplate including new results. – Neues Jahrbuch für Geologie und Paläontologie, Abhandlungen **168**: 165-172.

SOFFEL, H., DAVOUDZADEH, M., ROLF, C. & SCHIMDT, S. 1996. New paleomagnetic data from Central Iran and a Triassic paleoreconstruction. - Geologische Rundschau **85**: 293-302.

STÖCKLIN, J. 1961. Lagoonal formation and salt domes in East Iran. - Bulletin of the Iranian Petroleum Institute **3**: 29-46.

STÖCKLIN, J. 1968. Structural history and tectonics of Iran; a review. – Bulletin of American Association of Petroleum Geologists **52**:1229-1258.

STÖCKLIN, J. 1974. Possible ancient continental margins in Iran. - In: BURK, C. & DRAKE, C. (eds.), The geology of continental margins: 873-887, Berlin (Springer).

STÖCKLIN, J., EFTEKHAR-NEZHAD, J. & HUSHMANDZADEH, A. 1965. Geology of the Shotori Range (Tabas area, East Iran). - Geological Survey of Iran **3**: 1-69.

STÖCKLIN, J. & NABAVI, M.H. 1971. Boshruyeh Quadrangle map, scale 1: 250000 with explanatory text. - 50 pp., Tehran (Geological Survey of Iran).

STÖCKLIN, J., EFTEKHAR-NEZHAD, J. & HUSHMAND-ZADEH, A. 1972. Central Lut Reconnaissace East Iran. - Geological Survey of Iran, Report **22**: 1-62.

STÖCKLIN, J. & SETUDEHNIA, A. 1991. Stratigraphic Lexicon of Iran. – GSI **18**: 376 pp., Tehran (Geological Survey of Iran).

STOW, D.A.V. 2005. Sedimentary rocks in the field. A colour Guide. – 320 pp., London (Manson).

SUTTNER, L.J.A. & BASU, A. 1981. Climate and the origin of quartz arenites. - Journal of Sedimentary Petrology **51**: 1235–1246.

TAKIN, M. 1972. Iranian geology and continental drift in the Middle East. - Nature **235**: 147-150.

TAPPONNIER, P. & MOLNAR, P. 1976. Slip-line field theory and large-scale continental tectonics. – Nature **264**: 319-324.

TIRRUL, R., BELL, I.R., GRIFFIS, R.J. & CAMP, V.E. 1983. The Sistan suture zone of eastern Iran. - Geological Society of America Bulletin **94**: 134–150.

TORTOSA, A., PALOMARES, M. & ARRIBAS, J. 1991. Quartz grain types in Holocene deposits from the Spanish Central System: some problems in provenance analysis. - In: MORTON, A.C., TODD, S.P. & HAUGHTON, P.D.W. (eds.), Developments in Sedimentary Provenance Studies. - Geological Society of London, Special Publication **57**: 47– 54.

TUCKER, M.E. 1981. Sedimentary petrology: An introduction. - 252 pp., London (Blackwell Scientific Publications).

TUCKER, M.E. 1991. Sedimentary petrology: An introduction to the origin of sedimentary rocks. – 260 pp., Oxford (Blackwell Scientific).

UCHMAN, A. 1991. "Shallow water" trace fossils in Palaeogene flysch of the southern part of the Magura Nappe, Polish Outer Carpathians. – Annals of the Geological Society of Poland **61**: 61-75.

UCHMAN, A. 1992. Ichnogenus *Rhizocorallium* in the Paleogene Flysch (Outer Western Carpathians, Poland). - Geologica Carpathica **43**: 57–60.

UCHMAN, A. 1995. Taxonomy and palaeoecology of flysch trace fossils: The Marnoso-arenacea Formation and associated facies (Miocene), Northern Apennines, Italy. - Beringeria **15**: 1-115.

UCHMAN, A. & DEMIRCAN, H. 1999. Trace fossils of Miocene deep-sea fan fringe deposits from the Cingöz Formation, southern Turkey. Annals of the Geological Society of Poland **69**: 125-153.

VAHDATI-DANESHMAND, F. 1995. Geological map and report of Zarand, on scale of 1:100000. - Tehran (Geological Survey of Iran).

VERNANT, F., P., NILFOROUSHAN, F., HATZFELD, D., ABBASSI, M.R., VIGNY, C., MASSON, F., NANKALI, H., MARTINOD, J., ASHTIANI, A., BAYER, A., TAVAKOLI, F. & CHÉRY, J. 2004. Present-day crustal deformation and plate kinematics in the Middle East constrained by GPS measuraments in Iran and northern Oman. - Geophysical Journal International **157**: 381-398.

WALKER, R.G. 1985. Geological evidence for storm transportation and deposition on ancient shelf sands and sandstone reservoirs. - In: TILLMAN, R.W., SWIFT, D.J.P. & WALKER, R.G. (eds.), Shelf sands and sandstone reservoirs. - Society of Economic Palaeontologists and Mineralogists, Short Course Notes **13:** 243-302.

WALKER, R.G. & CANT, D.J. 1984. Sandy fluvial systems. – In: WALKER, R.G. (ed.), Facies models: 71-90, Toronto, Ontario (Geological Society of Canada).

WALKER, R. & JACKSON, J. 2004. Active tectonics and Late Cenozoic strain distribution in central and eastern Iran. - Tectonics **23**: 1-24.

WELTJE, G.J., MEIJER, X.D. & DE BOER, P.L. 1998. Stratigraphic inversion of siliciclastic basin fills: A note on the distinction between supply signals resulting from tectonic and climatic forcing. - Basin Research **10**: 129–153.

WENTWORTH, C.K. 1922. A scale of grade and class terms for classifying sediments. - Journal of Geology **30**: 377-392.

WETZEL, A. 1981. Ökologische und stratigraphische Bedeutung biogener Gefüge in quartären Sedimenten am NW-Afrikanischen Kontinentalhang. - Meteor-Forschungsergebnisse. Reihe C, Geologie und Geophysik **34**: 1–47.

WETZEL, A. 1983. Biogenic sediment structures in a modern upwelling region: northwestern African continental margin. - In: THIEDE, J. & SUESS, E. (eds.), Coastal upwelling - Its sediment record, Part B: Sedimentary records of ancient coastal upwelling: 123-144, New York (Plenum Press).

WETZEL, A. & UCHMAN, A., 1998. Biogenic sedimentary structures in mudrocks - an overview. - In: SCHIEBER, J., ZIMMERLE, W. & SETHI, P. (eds.), Shales and mudrocks. – Vol. **1**: 351-369, Stuttgart (Schweizerbart).

WETZEL, A., BLECHSCHMIDT, I., UCHMAN, A. & MATTER, A. 2007. A highly diverse ichnofauna in late Triassic deep-sea fan deposits of Oman. – Palaios **22**: 567-576.

WIGNALL, P.B. & HALLAM, A. 1996. Facies change and the end-Permian mass extinction in SE Sichuan, China. - Palaios **11**: 587– 596

WILMSEN, M., FÜRSICH, F.T., & SEYED-EMAMI, K. 2003. Revised lithostratigraphy of the Middle and Upper Jurassic Magu Group of the northern Tabas Block, east-central Iran. - Newsletters on Stratigraphy **39**:143–156.

WILMSEN, M., FÜRSICH, F.T., SEYED-EMAMI, K. & MAJIDIFARD, M.R. 2009a. An overview of the lithostratigraphy and facies development of the Jurassic System on the Tabas Block, east-central Iran. In: BRUNET, M.F., WILMSEN, M. & GRANATH, J. (eds.), South Caspian to Central Iran basins. - Geological Society of London Special Publication **312**: 323–344.

WILMSEN, M., FÜRSICH, F.T., SEYED-EMAMI, K., MAJIDIFARD, M.R. & ZAMANI-PEDRAM, M. 2009b: Facies analysis of a large-scale Jurassic shelf-lagoon: the Kamar-e-Mehdi Formation of east-central Iran. - Facies **56**: 59-87.

WILSON, J.L. 1975. Carbonate facies in geologic history. – 471 pp., New York (Springer).

ZUFFA, G.G. 1980. Hybrid arenites: their composition and classification. - Journal of Sedimentary Petrology **50**: 21–29.

Publikationen

SHAHIDI, A. & ZAMANI PEDRAM, M. (1996). *Geological map of Dehbid area*, Scale 1:100,000, Geological Survey of Iran.

JAFARIAN, M.B. & ZAMANI PEDRAM, M. 1997. *Geological map of Malayer area,* Scale 1:100,000, Geologyical Survey of Iran.

ZAMANI PEDRAM, M., HOSSAINI, H. & JAFARIAN, M. B. 1998. *Geological map of Qom area*, Scale 1:100,000, Geological Survey of Iran.

SHEIKHOLESLAMI, M.R. & ZAMANI PEDRAM, M. 1999. *Geological map of Halvan area*, Scale 1:100,000, Geological Survey of Iran.

ZAMANI PEDRAM, M., HOSSAINI, H., JALALI, A. & JAFARIAN, M.B. 2001. *Geological map of Gorgan area*, Scale 1:100,000, Geological Survey of Iran.

ZAMANI PEDRAM, M. 2002: *Petrological studies of the voclanic rocks in the south and west Huz- e- Soltan Lake, Qom area*. - Unpublished M. Sc. Thesis, Islamic Azad University, Iran: 210 pp., Tehran.

ZAMANI PEDRAM, M. 2002. *Petrology and geochemistry in the volcanic rocks in the north of Qom sheet*. - 21th Symposium on Geoscience, Tehran, Iran.

ZAMANI PEDRAM, M., KARIMI, A., HOSSAINI, H. & JAFARIAN, M.B. 2003. *Geological map of Aliabad area*, Scale 1:100,000, Geological Survey of Iran.

ZAMANI PEDRAM, M., EMAMI, M.H. & LOTFI, M. 2003. *Petrographical and geochemical evidences for magma mixing in volcanic rocks around the Hoz-e- Soltan lake*. - 22th Symposium on Geoscience, Tehran, Iran.

ZAMANI PEDRAM, M., KARIMI, H.R., HOSSAINI, H., JAFARIAN, M.B. & GHASEMI, M.R. 2005. *Tectonic and structural geology of Gorgan and Aliabad*. - 23th Symposium on Geoscience, Tehran, Iran.

WILMSEN, M., FÜRSICH, F.T., SEYED-EMAMI, K. S., MAJIDIFARD, M. R. & ZAMANI PEDRAM, M. 2010. Facies analysis of a large-scale Jurassic shelf-lagoon: the Kamar-e-Mehdi Formation of east-central Iran. – Facies **56**: 59-87.